Development of Appropriately Tailored Adsorbents for Effective Defluoridation of Water

THESIS

Submitted in partial fulfilment

of the requirements for the degree of

DOCTOR OF PHILOSOPHY

By

BARATHI M

ID No: 2012PHXF529H

Under the Supervision of

Prof. N. Rajesh

BIRLA INSTITUTE OF TECHNOLOGY AND SCIENCE, PILANI

HYDERABAD CAMPUS

2016

BIRLA INSTITUTE OF TECHNOLOGY & SCIENCE, PILANI
HYDERABAD CAMPUS

CERTIFICATE

This is to certify that the thesis entitled "**Development of Appropriately Tailored Adsorbents for Effective Defluoridation of Water**" submitted by **BARATHI M, ID. No. 2012PHXF529H** for the award of Ph. D. degree of the Institute embodies the original work done by him under my supervision.

Signature in full of the supervisor : _____

Name in capital block letters : **N. RAJESH**

Designation : **Professor, Department of Chemistry**

Date :

DEDICATED
TO
MY FAMILY

ACKNOWLEDGMENT

At the outset, I would like to thank the Almighty for giving me the strength to do the research work with good health.

My heart-felt gratitude to **Prof. V. S. Rao,** Acting Vice-Chancellor and Director (BITS-Pilani, Hyderabad Campus), for permitting me to carry out my research work in the campus.

My deep sense of gratitude to **Prof. B. N. Jain,** former Vice Chancellor (BITS, Pilani), for permitting me to carry out my doctoral work in the institute.

I wish to express my sincere gratitude and heartfelt thanks to my guide **Prof. N. Rajesh**, Department of Chemistry. He has been actively involved in my work and has always been available to discuss with me to improve my research work in a prominence manner. I am very grateful for his immense knowledge, patience, friendly approach, motivation, enthusiasm, and helping nature, that taken together, make him a great mentor. My research work would not have been completed without him.

I am also obliged to **Prof. Vidya Rajesh,** Associate Dean**,** Academic Research Division, (ARD) BITS-Pilani, Hyderabad campus, for her co-operation, involvement and encouragement at every stage of this research work.

I am grateful to **Prof. Suman Kapur,** Dean, IPCD, **Prof. P. Yogeeswari,** Associate Dean, SRCD, BITS-Pilani, Hyderabad campus for the valuable support.

I sincerely acknowledge **Prof. K.V.G Chandrasekhar** and **Prof. Jayanty Subbalakshmi,** Doctoral Advisory committee members for their constant encouragement and valuable suggestions.

My sincere thanks and respectful regards to **Prof. K. Sumithra** (Former Head) and **Dr. Anupam Bhattacharya,** Head, Department of Chemistry, BITS-Pilani Hyderabad campus, for providing me with all the necessary laboratory facilities and encouragement at various stages of my research work. I also thank the Doctoral Research Committee (DRC) convener, **Dr. Balaji Gopalan**, **Prof. R. Krishnan, Dr. G. Ramakrishnan,** and all DRC members for their support and encouragement.

I wish to express my thanks to all the faculty of Department of Chemistry, for their support and encouragement, time, interest, helpful comments, to carry out this research

work. I also thank all technicians in chemistry department as well as Central Analytical Laboratory for their co-operation.

I am very grateful to **Prof. S. S. Deshmukh,** Associate Dean, Student Welfare Division, BITS Pilani, Hyderabad Campus for his valuable support towards completing my PhD work successfully.

I deeply acknowledge the funding sources **Department of Science and Technology (DST)**, New Delhi, India and **Birla Institute of Technology and Science (BITS Pilani), Hyderabad campus** for making my PhD work possible.

Words are inadequate to express my thanks to my senior **Dr. A. Santhana Krishnakumar,** Department of Chemistry, National Sun Yat-sen University, Kaohsiung City, Taiwan, for his valuable help and support, constant encouragement to finish my PhD work completely. He always treated me as his own brother. Many thanks to you Anna.

I am thankful to **Mr. H. N. Nagesh, Mr. Srinivasarao Singireddi, Mr. P. Ravikiran, Mr. A. Mahesh, Mr. Yadhagiri**, Department of Chemistry, BITS Pilani Hyderabad campus and **Dr. Rajesh Kannan, Mr. D. N. Prasad, Mr. Krishna, Mr. Subba Rao,** Department of Physics, BITS Pilani Hyderabad campus and **Mr. Santhosh,** Department of Pharmacy, BITS Pilani Hyderabad campus and **Mr. Muthu Kumar,** Department of Computer Science, BITS Pilani Hyderabad campus for their primary help to fulfill my research work.

I want to thank my research group, my lab mates, (**Dr. S. Kalidhasan, Ms. Shivani Sharma, Ms. Manasi, Mr. Jagadeesh kodali and Ms. Satvika Talasila**) and all my friends in and out of the department for their support and making the last few years an exciting and memorable experience.

I am grateful to my friend **Mr. P. Sennu**, PhD student, Chonnam National University, South Korea for his constant support and help at various stages in my research work.

I would like to acknowledge **Central Electrochemical Research Institute** (CECRI) Karaikudi, India, **Indian Institute of Chemical Technology Hyderabad**, India, **Hyderabad Central University**, **Alagappa University**, Karaikudi, India and **Metrohm, India Limited**, **Sophisticated Analytical Instrumentation Facility**, Cochin, India, **Mrs.**

Park Jin Hee, Centre for the Development of Fine Chemicals at Chonnam National University, South Korea for their valuable assistance in characterization of adsorbent.

Last and Foremost, I want to thank my brother (**Mr. M. Tamil Selvan**) and my parents, for their love and care, faith and support throughout my life.

I humbly dedicate this doctoral thesis to my Family.

Date: **Barathi M**

ABSTRACT

The accessibility to innocuous and clean water is an important global issue to be addressed in the new millennium. Challenges are copious and novel sustainable strategies are required to ease the universal problem of ground water pollution. Among the various threats, fluoride pollution to the ground water is quite alarming. Skeletal and dental fluorosis is the most common health problems associated with excess fluoride in drinking water. Several techniques such as precipitation, coagulation, oxidation, solvent extraction, evaporation, distillation, reverse osmosis, ion exchange and electro dialysis are reported for fluoride removal. Considering the gravity of the problem, and to surmount some of the inadequacies in the existing methods it is imperative to develop effective adsorbents with removal efficiency in the permissible limit (1.0-1.5 mg L^{-1}).

In this regard, a variety of adsorbents such as cellulose, Amberlite XAD 1180 resin and graphene oxide were explored for defluoridation.The first chapter presented in the thesis deals with a novel microwave assisted preparation of Al-Zr impregnated cellulose adsorbent and its application for defluoridation. The proposed method involves the impregnation of Al-Zr in cellulose matrix wherein fluoride ion from aqueous medium interacts with the cellulose hydroxyl groups as well as cationic Zr and Al hydroxides. The facile preparation of the adsorbent was accomplished by microwave-assisted synthesis. The adsorbent prior and subsequent to the adsorption of fluoride was characterized comprehensively using Fourier transform infrared spectroscopy (FT-IR), Energy dispersive X-ray spectrometry (EDX) and X-ray diffraction (XRD) studies. Hydrogen bonding and electrostatic interactions support the adsorption mechanism. Various adsorption isotherm models, kinetics and thermodynamics were studied in detail. Pseudo second order kinetics supports the adsorption data. The adsorbent exhibits excellent adsorption up to 5 mg L^{-1} fluoride with an adsorption capacity of 5.76 mg g^{-1} at pH 5.0 and shows good potential towards practical application.

The second method illustrates the utility of an ultrasound assisted methodology involving the impregnation of zirconium in a cellulose matrix and application for fluoride removal

in aqueous solutions. Fluoride from aqueous solution interacts with the cellulose hydroxyl groups and the cationic zirconium hydroxide. Ultrasonication ensures a green and quick alternative to the conventional time intensive method of preparation. The effectiveness of this process was confirmed by comprehensive characterization of zirconium impregnated cellulose (ZrIC) adsorbent using Fourier transform infrared spectroscopy (FT-IR), Energy dispersive X-ray spectrometry (EDX) and X-ray diffraction (XRD) studies. The study of various adsorption isotherm models, kinetics and thermodynamics of the interaction validated the method. The adsorbent removes fluoride with an adsorption capacity of 4.95 mg g^{-1} at pH 5.0.

The fourth chapter of the thesis deals with potential application of aluminum hydroxide impregnated macroporous polymeric resin (Amberlite XAD 1180) as a sustainable option for defluoridation of water. The impregnation of aluminium hydroxide on to the residual vinyl groups (within the pores of the XAD1180 resin matrix) could be referred to as '*alumylation'*. The BET surface area of the $Al(OH)_3$ incorporated polymeric resin adsorbent was found to be 373.73 m^2g^{-1}. The adsorption of fluoride on the adsorbent was confirmed by FT-IR, PXRD and EDS analysis. Various characterization techniques supported the adsorption of fluoride through electrostatic, ion exchange and hydrogen bonding mechanism. The robust polymeric resin adsorbent exhibits an adsorption capacity of 36.37 mg g^{-1} at pH 7.0. The q_{max} was found to be 31.27 mg g^{-1} for drinking water. The second order kinetics and the exothermic, spontaneous adsorption are other characteristic features associated with this method. A sample volume of 1500 mL on a laboratory scale column containing 5.0 mg L^{-1} of fluoride could be treated effectively.

Graphene oxide has emerged as an attractive member of carbon family in the same view of its high surface area and presence of various functional groups (hydroxyl, epoxy groups and carboxylic). The fifth chapter in the thesis deals with preparation of novel aluminium oxy hydroxide [Al-O(OH)] modified graphene oxide by chemical precipitation method and its application for fluoride removal in real water samples. The presence of aluminium oxy hydroxide on the surface of graphene oxide was also confirmed by XRD analysis. Furthermore, XPS analysis reveals that a distinct Al 2p transition was observed at 74.7eV, characteristic of Al-O(OH) or pseudoboehmite. The zero-point charge of GO-Al-O(OH) adsorbent was found to be 7.54. The

thermodynamically feasible adsorption is supported by the pseudo second order kinetics and a high Langmuir maximum adsorption capacity (51.42 mg g^{-1}) for GO-Al-O(OH) adsorbent. The leached aluminum content in aqueous solution is very less (3.0-5.0 ppb) even at different initial fluoride concentrations in the pH range of 7.0-8.0 and is less than 200 ppb in pH 5.0 - 6.0 range. Furthermore, 2.0 L of 5.0 mg L^{-1} fluoride ion solution could be removed using 2.0 g of the adsorbent. The regeneration of the adsorbent was done using ammonium hydroxide. The applicability of this material was also tested in water samples collected from different places at Nalgonda district, Telangana. The fluoridated water can be treated either in a simple bucket system or packed column prototype. The leaching of aluminium in the residual water is negligible.

Keywords: Adsorption, Fluoride, Cellulose, Al-Zr Hydroxides, Aluminium oxyhydroxide, Zirconium oxychloride, Microwave assisted synthesis, Ultrasonication, Co-precipitation, Amberlite XAD-1180, Graphene oxide (GO), Ultrasonication, Regeneration, Adsorption isotherm, Adsorption kinetics, and Thermodynamics,

TABLE OF CONTENTS

	Page No.
Certificate	i
Dedications	ii
Acknowledgements	iii
Abstract	vi
Table of contents	ix
List of abbreviations and symbols	xiii
List of Figures	xv
List of Tables	xix

Chapter 1

1. Introduction

1.1.Chemistry of fluoride	1
1.1.1. Occurrence, Sources and exposure of Fluoride to human beings	1
1.1.2. Health impacts of fluoride	4
1.2.Methods available for defluoridation	5
1.2.1. Adsorption	5
1.3.Recent literature review	6
1.3.1. Metal and Metal Hydroxides	6
1.3.2. Ion-Exchange Resins	9
1.3.3. Bio-polymer based Materials	10
1.3.4. Carbonaceous Materials	13
1.4.Fluoride adsorption mechanism	15
1.5.Scope and objectives of work	17
References	19

Chapter 2

2. Materials and Method

2.1.Chemicals and reagents	24
2.2.Physico-chemical Characterization Instruments	24
2.3.Calorimetric studies and energy efficiency calculations	26
2.4. Preparation of Stock solution	26
2.5.Analysis of fluoride concentration	26
2.6.Batch Adsorption Studies	27
2.7.Adsorption Isotherm	27
2.7.1. Langmuir Isotherm	28
2.7.2. Freundlich Isotherm	28
2.7.3. Dubinin–Radushkevich (D-R) isotherm	29
2.7.4. Redlich and Peterson (R-P) isotherm	29
2.7.5. Elovich isotherm	30

2.7.6. Temkin Isotherm 30
2.8. Adsorption kinetics 30
2.9. Adsorption Thermodynamics 32
References 33

Chapter 3

3. Al(III) and Zr(IV) impregnated onto the surface of Cellulose biopolymer matrix for the removal of fluoride in aqueous solutions

3.1.Abstract 34

3.2.Microwave assisted preparation of Al (III) and Zr (IV) impregnated Cellulose biopolymer adsorbent for defluoridation 35

3.2.1. Introduction 36
3.2.2. Experimental Section 36
(i) Adsorbent Preparation 36
(ii) Adsorption Studies 36
(iii) Column Study 36
3.2.3. Results and Discussion 37
(i) Characterization of the adsorbent 37
(ii) Amount of adsorbent 44
(iii) Effect of pH 45
(iv) Mechanism of interaction of Al-Zr impregnated cellulose with fluoride 48
(v) Adsorption Isotherm and Kinetic studies 51
(vi) Adsorption Thermodynamics 55
3.2.4. Conclusions 56

3.3.*Ultrasonication Assisted Preparation of Zr(IV) Ions Onto the Cellulose Biopolymer for the Facile Defluoridation of Water* 57

3.3.1. Introduction 57
3.3.2. Experimental section 58
(i) Adsorbent Preparation 58
(ii) Adsorption procedure 59
3.3.3. Results and Discussion 59
(i) Characterization 59
(ii) Mechanism of interaction of Zr impregnated cellulose with fluoride 63
a. Calorimetric studies and energy efficiency 63
b. Role of ultrasonication 64
c. Comparison of ultrasonication and conventional method of Adsorbent preparation 67
(iii) Optimization of pH 67
(iv) Amount of adsorbent 68

(v) Adsorption Isotherm and Kinetic studies 68
(vi) Adsorption Thermodynamics 72
3.3.4. Conclusions 73
References 74

Chapter 4

4. Aluminium hydroxide impregnated macroreticular aromatic polymeric resin as a sustainable option for defluoridation

4.1.1. Introduction 77
4.1.2. Experimental Section 78
(i) Preparation of Aluminum hydroxide impregnated polymeric resin adsorbent 78
(ii) Adsorption studies through batch experiments 78
(iii) Column Study 79
4.1.3. Results and Discussion 79
(i) Characterization of the adsorbent 79
(ii) Mechanism for interaction between Al $(OH)_3$ and the resin 91
(iii) Effect of pH 93
(iv) Adsorption Isotherm studies 94
(v) Adsorption kinetic studies 98
(vi) Adsorption Thermodynamics 100
(vii) Preliminary column studies 102
4.1.4. Conclusions 103
References 104

Chapter 5

5. Preparation and characterization of Graphene oxide-Aluminium oxyhydroxide adsorbent for the effective defluloridation of water

5.1.1. Introduction 106
5.1.2. Experimental Section 107
(i) Preparation of Graphene oxide from graphite 107
(ii) Preparation of [Al-O(OH)] incorporated graphene oxide 108
(iii) Adsorption studies through batch experiments 108
(iv) Column Study 108
5.1.3. Results and Discussion 109
(i) Characterization of the adsorbent 109
a. Electronic (UV-Visible)spectroscopy 109
b. FT-IR Spectrum Analysis 110
c. FT-Raman spectrum Analysis 110
d. Powder XRD Analysis 112
e. SEM & EDS Analysis 115
f. XPS Analysis 119

(ii) Probable Mechanism 122
(iii) Effect of pH 124
(iv) Adsorption Isotherm studies 125
(v) Adsorption kinetic and thermodynamic studies 129
(vi) Application to field study 131
a. Bulk synthesis 131
b. Application to real water samples and Prototype development 132
5.1.4. Conclusions 137
References 138

Chapter 6

6. Summary and Conclusion

6.1.Summary and conclusion 141
6.2.Scope of the Future work 143

List of Publications 144
Abstract presented in conferences 145
Brief biography of the supervisor 145
Brief biography of the candidate 146

LIST OF ABBREVIATIONS

AA	Activated Alumina
AC	Activated Carbon
ACF	Activated Carbon Fibers
ACNTs	Aligned Carbon Nanotubes
AER	Anion Exchange Resin
AIAA	Alum Impregnated Activated Alumina
AIC	Akaike's Information Criterion statistical methodology
AlZrIC	Al-Zr Impregnated Cellulose
AIC	Akaike's Information Criterion statistical methodology
b	Langmuir Constant
BC	Bituminous Coal
BET	Brunauer-Emmett-Teller
BJH	Barrett-Joyner-Halenda
CCB	Carboxylated Chitosan Beads
CCS	Chitosan Coated Silica
CNF	Carbon Nano Fibers
CNTs	Carbon Nanotubes
COCA	Copper Oxide Coated Alumina
CR	Chelating resin
DC	Defluoridation Capacity
DLS	Dynamic Light Scattering
DMF	Dimethyl Formamide
DNA	Deoxyribonucleic Acid
DVB	Styrene–divinylbenzene
EDAX	Energy-dispersive X-ray spectroscopy
EDS	Energy Dispersive Spectroscopy
FC	Fine Coke

FT-IR	Fourier transform infrared spectroscopy
GAC	Granular Activated Carbon
GO-Al-O(OH)	Graphene oxide Aluminium Oxyhydroxide
HIACMO	Hydrated Iron (III)-Aluminium(III)-Chromium(III) ternary Mixed Oxide
ICP-AES	Inductively coupled atomic emission spectrometry
JCPDS	Joint Committee of Powder Diffraction Standards
K_F	Freundlich constant (adsorption capacity)
K_c	Equilibrium Constant
k_{int}	Intra-particle diffusion constant
LN	Lignite
MGA	Metallurgical Grade Alumina
MW	Microwave Irradiation
n	Adsorption Intensity
NABL	National Accredited Board for Laboratories
PCCB	Protonated as well as Carboxylated Chitosan Beads
PCB	Protonated Chitosan Beads
PSDVB	Poly-Styrene divinylbenzene
PXRD	Powder X-Ray Diffraction
PZC	Point of Zero charge
q_o	Maximum Adsorption capacity
R	Universal Gas Constant
R_L	Dimensionless Constant
SEM	Scanning Electronic Microscope
t	Time
THA	Thermally treated Hydrated Alumina
UHA	Untreated Hydrated Alumina
USEPA	United States Environmental protection agency
XPS	X-Ray Photoelectron Spectroscopy
ZrIC	Zr-Impregnated Cellulose

LIST OF FIGURES

Figure No.	Caption	Page No.
1.1	A schematic illustration for the diverse sources of fluoride in the environment	2
1.2	Maximum adsorption capacities of fluoride sorption into different metal hydroxide based materials	7
1.3	Structure of cellulose biopolymer	13
1.4	Fluoride adsorption mechanism	16
3.1	FT-IR spectrum of cellulose biopolymer (A) and Al/Zr impregnated cellulose adsorbent (B)	38
3.2	FT-IR spectrum of Al/Zr impregnated cellulose adsorbent (A) and the fluoride adsorbed (B)	38
3.3	SEM images of Cellulose biopolymer (A) Al/ZrIC bio adsorbent (B) and fluoride ion adsorbed (C) on the adsorbent	39
3.4a	EDX Figures of Cellulose biopolymer	40
3.4b	EDX Figures of Al/ZrIC bio adsorbent	41
3.4c	EDX Figures of Al/ZrIC bio adsorbent after fluoride ion adsorbed ion the adsorbent surface	42
3.6	XRD pattern of Cellulose biopolymer (A) Al/ZrIC biopolymer adsorbent (B) after fluoride ion adsorption on the adsorbent (C)	44
3.6a	Point of zero charge for the Al-Zr Impregnated Cellulose biopolymeradsorbent	45
3.6b	Effect of pH on the adsorption of fluoride	46
3.7a	The schematic diagram shows the interaction of metal ions with cellulose biopolymer surface	49
3.7b	Schematic diagram of the interaction of fluoride with Al/ZrIC biopolymer adsorbent surface	50
3.8	(a) Langmuir isotherm (b) Freundlich isotherm (c) D-R isotherm	

	(d) Temkin isotherm (e) Elovich isotherm (f) R-P isotherm	53
3.9	(a) Pseudo first order kinetic plot (b) Pseudo second order kinetic plot (c) Plot of q_t versus square root of time (d) Variation of lnK with temperature	54
3.10	Schematic diagram of ultrasonic horn	58
3.11	FT-IR spectrum of Zr impregnated cellulose adsorbent (A) and the fluoride adsorbed (B)	60
3.12	EDX spectrum of the fluoride ion adsorbed onto Zr impregnated cellulose surface	61
3.13	XRD pattern of (A) cellulose (B) ZrIC biopolymer adsorbent (C) After fluoride ion adsorption on the adsorbent	63
3.14	Schematic diagram depicting the interaction of fluoride ion with Zr impregnated cellulose biopolymer surface	66
3.15	(A) Langmuir isotherm (B) Freundlich isotherm (C) D-R isotherm (D) Temkin isotherm	69
3.16	(A) Effect of time on adsorption (B) Pseudo first order kinetic plot (C) Pseudo second order kinetic plot (D) Plot of q_t versus square root of time (E) Variation of lnK with temperature	71
4.1	FT-IR spectrum of XAD 1180 polymeric resin (A) and Aluminum hydroxide impregnated macroporous polymeric resin adsorbent (B) and the fluoride adsorbed (C)	80
4.2	Schematic diagram depicting the interaction of fluoride with Aluminum hydroxide impregnated macroporous polymeric resin adsorbent	82
4.3	SEM images of aluminum hydroxide impregnated macroporous polymeric resin adsorbent (A) and fluoride ion adsorbed (B) onto the adsorbent surface	83
4.4	Optical images of adsorbent (Spot test reagent added) (E) and fluoride adsorbed onto adsorbent (F)	83
4.5a	EDS spectrum of aluminum hydroxide impregnated macroporous polymeric resin adsorbent	84

4.5b	EDS spectrum of aluminum hydroxide impregnated macroporous polymeric resin adsorbent after fluoride ion adsorbed onto the adsorbent surface	85
4.6	XRD pattern of Aluminum hydroxide impregnated macroporous polymeric resin adsorbent (A) and after fluoride ion adsorption (B)	86
4.7a	N_2 adsorption-desorption isotherm plot of $Al(OH)_3$ impregnated macroporous polymeric adsorbent (C)	88
4.7b	BET isotherm plot of $Al(OH)_3$ impregnated macroporous polymeric adsorbent (C)	89
4.7c	BJH distribution curve of $Al(OH)_3$ impregnated macroporous polymeric adsorbent (C)	90
4.8	Proposed mechanism for preparation of aluminum hydroxide impregnated macroporous polymeric resin adsorbent	92
4.9	Zero point charge of the adsorbent and Impact of pH towards the F^- ion adsorption	94
4.10	Non-linear Langmuir and Freundlich Isotherm plots obtained at pH 3.0 (A), pH 7.0 (B) and pH 7.0 (C, Tap water)	96
4.11	Plot of q_t against t at different fluoride concentrations (A and B) and Plot of q_t against $t^{1/2}$ at different fluoride concentrations (C and D)	99
4.12	Variation of $\ln K_c$ with 1/T	101
4.13	Plot of C_t/C_0 against the sample volume	101
5.1A	UV-Vis spectrum of graphene oxide	109
5.1B	FT-IR spectra of synthesized GO (a), GO-Al-O(OH) adsorbent before (b) and after fluoride ion adsorption (c)	111
5.1C	Raman spectra of synthesized GO (a), GO-Al-O(OH) adsorbent before (b) and after fluoride ion adsorption (c)	111
5.1D	XRD spectra of synthesized GO (a), GO-Al-O(OH) adsorbent before (b) and after fluoride ion adsorption (c)	113
5.2	SEM images of GO (a), Aluminium oxy hydroxide incorporated GO (b) and after adsorption of fluoride (c) at different magnifications	114
5.3a	EDS spectra of prepared graphene oxide	116

5.3b	EDS spectra of Aluminium oxyhydroxide incorporated graphene oxide adsorbent	117
5.3c	EDS spectra of Al-O(OH) incorporated graphene oxide adsorbent surface after adsorption of fluoride	118
5.4	A) Total survey of XPS spectra B) C1s spectrum C) O 1s spectrum of graphite (a), prepared GO (b), GO-Al-O-(OH) adsorbent (c) and after adsorption fluoride (d). D) Al 2p spectrum of GO-Al-O-(OH) adsorbent (a) and fluoride adsorbed onto the adsorbent surface (b), F 1s spectrum of F^- ion adsorbed onto the adsorbent surface (c)	121
5.5	Preparation of GO and GO-Al-O-(OH) adsorbent and the possible mechanism towards the fluoride ion adsorption	123
5.6	Adsorption of fluoride ion influenced by pH and zero point charge onto the adsorbent surface	124
5.7	Isotherm models A) Langmuir plot B) Freundlich plot C) Temkin plot D) Redlich-peterson (R-P) plot E) Dubinin-Radushkevich (D-R) plot F) Plot of q_e Vs C_e	126
5.8	Kinetic plots obtained from the A) pseudo first-order equation B) pseudo second-order equation C) Intra-particle diffusion kinetics equation with 5.0 mg/L and 10.0 mg/L F^- ion concentrations D) Van't Hoff isotherm plot obtained for the adsorption of F^- ion onto GO-Al-O-(OH) adsorbent surface	130
5.9	A simple water purification filter system (A) packed with GO-Al-O-(OH) adsorbent (B)	132
5.10	A simple bucket system (A) with GO-Al-O-(OH) adsorbent (B) for defluoridation of water	134
5.11	A prototype model column packed with GO-Al-O-(OH) adsorbent	135

LIST OF TABLES

Table No.	Description	Page No.
1.1	Fluoride concentration levels in different districts in India in 2010	3
1.2	Health impacts of fluoride at different fluoride concentrations	4
1.3	Technologies available for defluoridation of drinking water	5
1.4	Maximum adsorption capacity of modified chitosan biopolymer	12
3.1	Adsorption isotherm parameters	52
3.2	Kinetic parameters and intra-particle rate constant for fluoride ion adsorption	52
3.3	Thermodynamic parameters for adsorption of fluoride ion onto Al-ZrIC adsorbent surface at different temperatures	56
3.4	Adsorption isotherm parameters	70
3.5	Kinetic parameters and intra-particle rate constant for fluoride ion adsorption	70
3.6	Thermodynamic parameters ΔH°, ΔS° and ΔG° and E_a for adsorption of fluoride at various temperatures	72
4.1	Adsorption isotherm parameters	97
4.2	Kinetic parameters and intra-particle rate constant for fluoride ion adsorption	99
4.3	Thermodynamic parameters for adsorption of fluoride ion at different temperatures	102
5.1	Elemental composition of various atoms present on the adsorbent surface	120
5.2	Isotherm parameters for the adsorption of fluoride	128
5.3	Kinetic parameters for the adsorption of fluoride onto Al-O (OH) incorporated graphene oxide	128
5.4	Adsorption thermodynamic parameters	131
5.5	Defluoridation results of collected real water samples with GO-Al-O(OH) adsorbent at ambient pH conditions	133

5.6 Defluoridation results of samples collected from simple bucket and prototype column system at ambient pH conditions 136
6.1 Summary of methods 143

CHAPTER 1

1. Introduction

Safe and clean drinking water for every human being is a primary need.[1] The availability of pure water is limited due to the rapid increase in population, industrialization, agricultural activities, and other geological and environmental changes.[2,3] Over the years, water pollution has emerged as a serious problem worldwide. A variety of organic, inorganic and biological contaminants affect the overall aquatic conditions and ecosystem.[4]

Fluoride is one of the major contaminants widely dispersed either naturally in the ground water caused by the solvent action of water on the rocks and the soil[5,6] or by industrial effluents released from aluminum and steel production, glass and semiconductor manufacturing, fertilizer and electroplating industries.[7] Wastewater emanating from electronic, toothpaste and insecticide manufacturing plants could also result in the contamination of ground water with fluoride.[8] Fluoride is required at low concentration limits (0.8 – 1.0 mg L^{-1}) in drinking water.[9] However, the excessive intake of fluoride would lead to skeletal and dental fluorosis.[10] The risk of fluorosis due to fluoride contaminated ground water is prevalent in many countries of Asia, America, Africa and Europe.[11] Hence, the contamination of groundwater due to fluoride is an important problem to be addressed. The challenges are manifold and it is imperative to develop effective methodologies for fluoride remediation. An overview of the chemistry of fluoride, health impacts and methods available for defluoridation are presented in the following sections.

1.1. Chemistry of Fluoride

1.1.1. Occurrence, Sources and exposure of fluoride to human beings

Fluorine is a greenish diatomic gas and belongs to the halogen group (VII A). It is the most electronegative element[12] and is not encountered in nature in the elemental form. It is present as fluoride in the environment which is about 0.06– 0.09% of the earth's crust.[13] Fluorine is quite reactive and is found naturally as CaF_2. It reaches the soil through weathering of rocks, precipitation and waste run off. The fluoride occurs notably as sellaite, fluorspar (CaF_2), Cryolite (Na_3AlF_6) and Fluorapatite ($Ca_5(PO_4)_3F$). Fluoride is an important constituent in minerals like topaz, fluorite, fluorapatite, cryolite,

phosphorite, etc.[14,15] Due to the small size and high electronegativity, fluoride behaves as a hard Lewis base. Hence, it has great tendency to behave as ligand by forming different organic and inorganic compounds in soil, rocks, air, plants and animals.[16,17] The possible sources of existence of fluoride in the environment is shown in Figure 1.1.

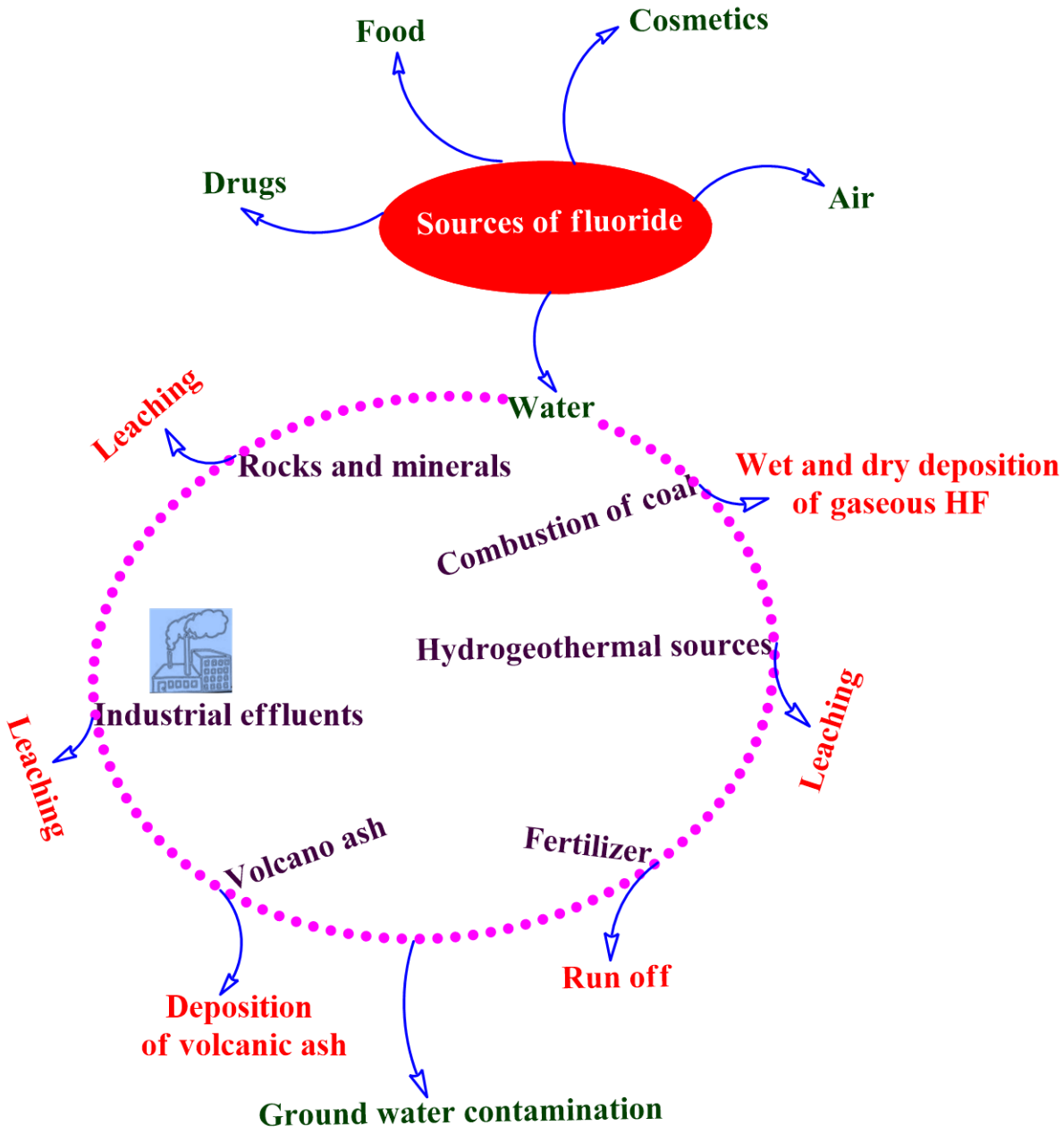

Figure 1.1. A schematic illustration for the diverse sources of fluoride in the environment[17]

The problem of excessive fluoride concentrations in drinking water is a global concern and more than 20 developed and developing nations are affected by endemic fluorosis.[18,19,20] The alarming problems associated with endemic fluorosis is prevalent in India, [21] China, [22] Rift Valley countries in Africa and Sri Lanka.[23] Due to a variety of factors, the fluoride concentrations in groundwater range from under 1.0 mg L^{-1} to more than 35.0 mg L^{-1}.[24] In India, fluoride was first observed in drinking water in the Nellore district of Andhra Pradesh in 1937.[19] It has been observed that fluorosis is prevalent in 17 states of India especially in Rajasthan, Madhya Pradesh, Andhra Pradesh, Telangana, Tamil Nadu, Gujarat, and Uttar Pradesh (Table 1.1).[8]

Table 1.1. Fluoride concentration levels in different districts in India in 2010[8]

States	Representative Districts	Range of F^- ion (mg L^{-1})
Andhra Pradesh/Telangana	Adilabad, Anantpur, Chittoor, Guntur, Hyderabad, Karimnagar, Krishna, Medak, and Nalgonda	1.8-8.4
Chhattisgarh	Bastar, Bilaspur, Dantewada, Janjgir-Champa, Jashpur, Kanker, Korba, Raipur	1.5-2.7
Haryana	Bhiwani, Faridabad, Gurgaon, Hissar, Jhajjar, Mahendragarh, Panipat, Rewari	1.5-17.0
Madhya Pradesh	Bhind, Chhatarpur, Chhindwara, Harda, Jabalpur,Jhabua, Khargaon, Mandsaur, Rajgarh, Satna, Seoni	1.5-10.7
Rajasthan	Ajmer, Alwar, Banaswara, Barmer, Bharatpur, Bhilwara, Bikaner, Bundi, Chittaurgarh, Churu, Dausa, Dhaulpur, Dungarpur, Ganganagar, Hanumangarh, Jaisalmer, Jalor, Jhunjhunun, Jodhpur, Nagaur	1.54-11.3
Tamilnadu	Coimbatore, Dharmapuri, Dindigul, Erode, Karur, Krishnagiri, Namakkal, Sivaganga, Theni, Thiruvannamalai, Tiruchirapally,Vellore	1.5-3.8
Uttar Pradesh	Agra, Aligarh, Firozabad, Jaunpur, Kannauj, Mainpuri, Mathura	1.5-3.11
West Bengal	Bankura, Bardhaman, Birbhum, Dakshindinajpur, Malda, Nadia, Purulia	1.5-9.1

1.1.2. Health impacts of fluoride

Fluoride has beneficial and detrimental effects and it is dependent on the concentration levels in drinking water. Health effects[25,26] of fluoride with respect to varying fluoride concentrations in drinking water are summarized in Table 1.2. At low levels, it helps in the normal mineralization of bones and formation of dental enamel.[18] However, excessive intake results slowly in the progressive crippling scourge which is commonly known as fluorosis. Skeletal and dental fluorosis[10] are the common problems associated with excess fluoride in drinking water. In addition to fluorosis, high fluoride concentration can also lead to adverse effects including cancer, digestive and nervous disorders, low hemoglobin levels, reduced immunity, urinary tract and respiratory problems.[26,27] Based on the severe effects on human health by fluoride contaminated ground water, U.S. Environmental Protection Agency (USEPA)[28] has recommended 4.0 mg L^{-1} as maximum contaminant level for fluoride in drinking water while WHO limits[29] are within the range 1.0–1.5 mg L^{-1}. This limit has been set as maximum 1.0 mg L^{-1} in Indian standards.[30] Higher fluoride can also lead to osteoporosis, brittle bones and thyroid disorders.[31]There are a few reports that excess fluoride could interfere with DNA synthesis[32] and carbohydrate metabolism.[32] The ingestion of excess fluoride would also result in the formation of hydrofluoric acid in the stomach causing gastrointestinal irritation.[33]

Table 1.2. Health impact with different fluoride concentrations[26]

F^- ion Concentration (mg L^{-1})	**Effects on human health**
Less than1.0	Quite safe
1.0-3.0	Dental fluorosis
3.0-4.0	Stiff and brittle bones and joints
4.0-6.0 and above	Deformities in knee and hip bones leading to paralysis

1.2. Methods available for defluoridation

1.2.1. Adsorption

The main advantages and disadvantages of various defluoridation methods are discussed in Table 1.3. A variety of defluoridation techniques such as precipitation-coagulation,[34-36] Ion-exchange,[37-40] Adsorption,[41] Membrane techniques (Reverse osmosis, nanofiltration, dialysis and electrodialysis)[42-45] and electrolytic defluoridation[46] have proved to be quite efficient to maintain fluoride levels within the permissible limits in drinking water.

Table 1.3. Technologies available for defluoridation of drinking water[8,42]

Techniques	Advantages	Disadvantages
Precipitation-Coagulation	Established and widely used at the community level.	Low treatment efficiency of~70% (Not effective at high fluoride contamination); Requirement of large dosage of aluminum sulfate (700-1200 mg L^{-1}). Adverse health effects of excess dissolved aluminum leaching in the treated water; Requirement of skilled manpower.
Ion-Exchange	Removes fluoride up to 90-95%; Retains the taste and color of treated water.	Presence of sulfate, phosphate, bicarbonate, etc. can reduce effectiveness; Relatively higher cost; Treated water has lower pH and higher chloride.
Adsorption	High efficiency; Cost effective.	Process is dependent on pH; Presence of sulfate, phosphate, bicarbonate, etc. can compete with fluoride; Regeneration is required; Disposal of fluoride-laden material is an issue.
Membrane process	Removes fluoride up to 90-95%; Retains the taste and color of treated water.	Presence of sulfate, phosphate, bicarbonate, etc. can compete with fluoride; Relatively higher cost; Treated water has lower pH and higher chloride.
Electro-Dialysis	Excellent removal No chemicals required No waste generation.	High capital cost and high operational cost Vital nutrients and other essential ions also removed together with fluoride

Nevertheless, considering the cost factor and design simplicity, adsorption is considered to be a more viable option for defluoridation. Essentially, this is a solid phase extraction methodology that would be well suited for diverse field applications. The well-known Nalgonda technique [47] which involves the use of lime and alum for fluoride adsorption has been in vogue. But, there are some drawbacks associated with this process. The leaching of excess aluminum with increase in ground water pH is a major concern. Activated alumina, activated carbon, activated alumina-coated silica gel, calcite, activated coconut shell carbon-activated fly ash, magnesia, tricalcium phosphate, bone charcoal are different adsorbent materials reported in the literature.[8,43] The most commonly used adsorbents are activated alumina[48] and activated carbon.[49] The diverse adsorbents reported recently for fluoride removal are reviewed in detail in the following sections.

1.3. Recent Literature review for defluoridation

1.3.1. Metal and Metal hydroxides

Generally, trivalent or tetravalent metal oxides and hydroxides (referred commonly as hydrous oxides or oxyhydroxides) such as Al, Mn, Fe, Zr, Ti, Ce and La are used to remove anionic and cationic contaminants effectively from water.[50] The small size of fluoride, high electronegativity and its behavior as a hard base also makes it compatible with the above metal ions. In addition to this, most of the metal oxides and hydroxides are have PZC (zero point pH) above pH 7.0 which favors the fluoride adsorption in natural water. Typical examples are granulated ferric hydroxide[51] pH 7.5-8.0, γ-alumina[52] pH 8.0 and activated alumina[53] pH 8.25). Many metal oxide and hydroxides have shown a very good adsorption capacity towards fluoride (Figure 1.2.).

Wajima et al. has reported a gel-like titanium hydroxide-derived adsorbent from titanium oxysulfate, $TiO(SO_4)$ for defluoridation.[54] Granular ferric hydroxide[51] was tested in batch and small column for the potential adsorption of fluoride. Activated and ordinary quick lime were also reported as an effective adsorbents for fluoride removal from aqueous solutions.[55] The Langmuir adsorption capacity of activated quick lime was found to be 16.67 mg g^{-1} for fluoride. Pumice stone[56] modified with peroxide/$MgCl_2$ and nanohydroxyapatite[57] have been reported to sequester fluoride with good efficacy.

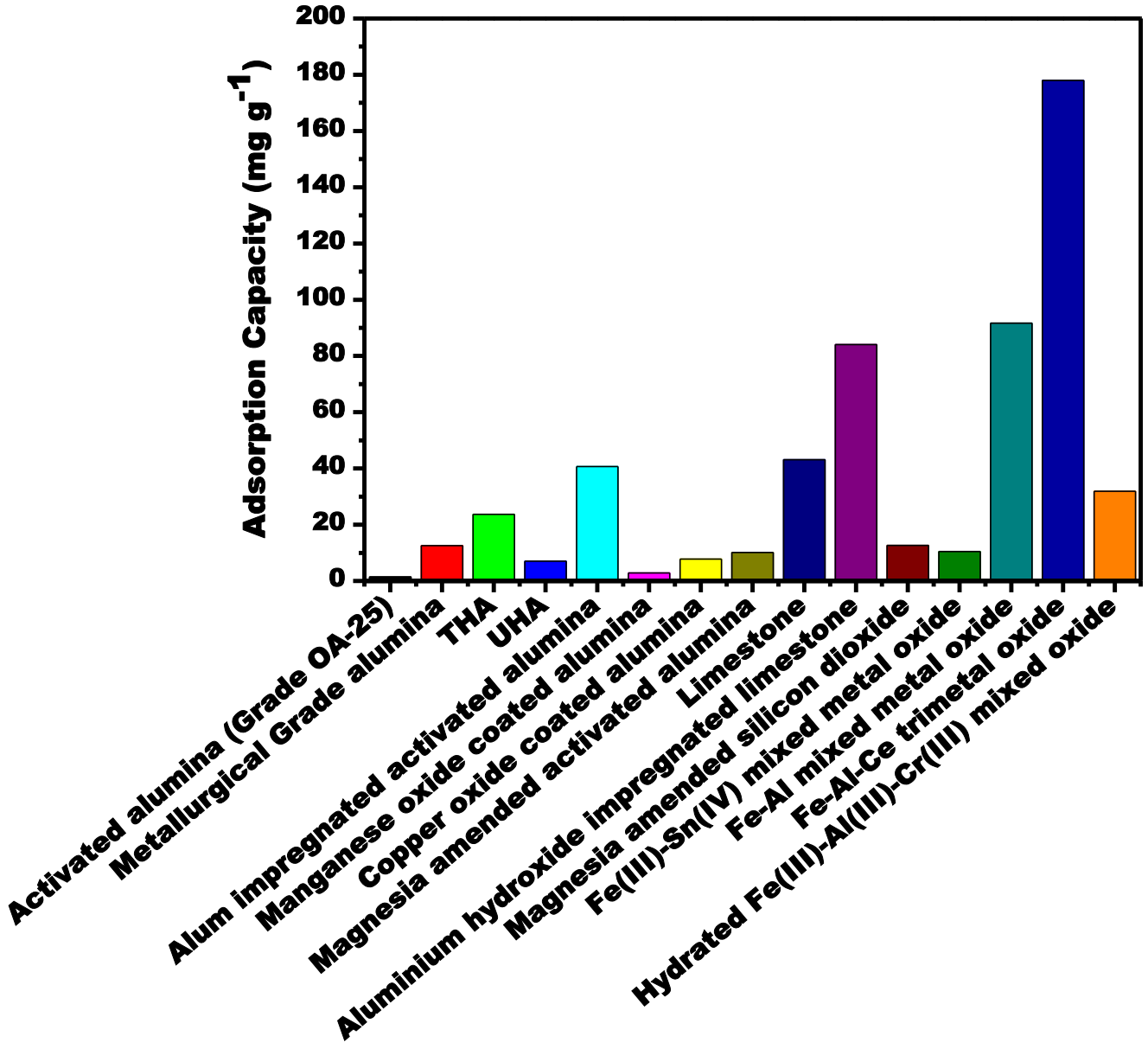

Figure 1.2. Maximum adsorption capacities of fluoride sorption into different metal hydroxide based materials[17]

Among all the oxides and hydroxides of the metals, activated alumina is one of the versatile and well known adsorbents for removing fluoride due to high affinity and selectivity. However, pH of the treated water and the leaching of excess aluminum is one concern that needs to be addressed in this methodology. The high surface area of activated alumina obtained from a distribution of micro and macropores is produced by thermal degradation of aluminium hydroxide.[58,59] The adsorption capacity of activated alumina also depends on the structure of alumina. γ-Al_2O_3 has ten times more adsorption capacity than α-Al_2O_3 and it shows that adsorption of fluoride varies with the structure of the alumina.[60] The selectivity of different anions on activated alumina[61] follows the order as below in pH range 5.5-8.5.

$OH^- > AsO_4^- > Si(OH)_3O^- > HSeO_3^- > F^- > SO_4^{2-} > CrO_4^{2-} >> HCO_3^- > Cl^- > NO_3^- > Br^- > I^-$

Recently, different forms of alumina such as Untreated hydrated alumina (UHA) and thermally treated hydrated alumina (THA)[62], amorphous[63] $Al(OH)_3$, gibbsite or alumina (Al_2O_3),[63] activated alumina (AA) (Grade OA-25),[64] metallurgical grade alumina (MGA),[65] Sand like AlOOH nanoarchitecture (SANA)[66] and electrospun alumina fibres[67] were also reported as good adsorbents for the adsorption of fluoride from aqueous solutions. The adsorption data fitted well to the Freundlich isotherm model with a minimum capacity of 23.7 mg F^-g^{-1} and 7.0 mg F^-g^{-1} for THA and UHA, respectively.[63] Langmuir maximum adsorption capacity of MGA for fluoride was found to be 12.57 mg g^{-1}.[66]

In order to enhance the adsorption capacity of activated alumina, many researchers explored the utility of modified alumina surface by different metal ions or with mixed metal ion mixtures. The copper oxide coated alumina (COCA),[68] La(III)-Y(III) impregnated to alumina[69] and alum impregnated activated alumina (AIAA)[70] were reported recently for maximum adsorption of fluoride. Lanthanum hydroxide supported on alumina[71] was also reported for defluoridation from aqueous solution. Ion exchange between anion and hydroxide group on the adsorbent surface is the plausible mechanism towards fluoride adsorption onto the adsorbent surface. The selectivity of removal onto the modified alumina adsorbent was found to be in the order: fluoride > phosphate > arsenate > selenite. Fluoride is superficially adsorbed by surface precipitation not by simple adsorption onto alum impregnated activated alumina adsorbent as evident from

the Energy-dispersive X-ray spectroscopy (EDAX) analysis.[70] Recent literature reveals that mixed metal oxides have good potential for the removal of fluoride from aqueous solutions. The maximum adsorption capacity of prepared Al-Ce hybrid,[72] Fe-Al-Ce trimetal oxide,[73] Mn-Ce oxide[74] and Hydrated iron (III)-aluminium(III)-chromium(III) ternary mixed oxide (HIACMO)[75] adsorbents were found to be 91.4, 84.5, 79.5 and 31.88 mg g^{-1} respectively for fluoride removal from aqueous medium. Very recently, cerium loaded mesoporous zirconium phosphate,[76] hydrous Ce(IV)-Zr(IV) mixed oxide,[77] Fe-Mg-La triple-metal composite,[78] granular zirconium–iron oxide,[79] Fe-Ti oxide nano-adsorbents[80] were also reported for defluoridation with high adsorption capacity.

1.3.2. Ion-Exchange Resins

Ion exchange resins are another vital category of adsorbents used in the removal of anionic and cationic pollutants from drinking water.[42] Ion-exchange is a rapid, reversible stoichiometric process and when any ion leaves from the surface of the ion-exchange resin, it is replaced by another counter ion to maintain electro-neutrality. Ion-exchange resins have macromolecular and irregular matrix with a three dimensional network of hydrocarbon chain.[81] Generally, it is classified into two types namely cation and anion exchange resins. The cation exchange resins have negatively charged functional groups whereas the anion exchange resins are held by positively charged groups. Therefore the cation and anion exchange resins could exchange cations and anions respectively. However, the cation exchange resin can be impregnated with positively charged metal ions and have strong affinity towards anions.[82,83]

In most of the anion exchange materials, the anion exchange capacity decreases in the following order and it shows low affinity for fluoride ions as compared to the other anions.[83,84]

Citrate > SO_4^{2-} > oxalate > I^- > NO_3^- > CrO_4^{2-} > Br^- > SCN^- > Cl^- >formate > acetate > F^-

Thus, a strongly basic anion exchange resin could adsorb NO_3^-, Br^-, and SO_4^{2-} effectively, but not Cl^- and F^- ions.[84] However, a strongly basic ion-exchange resin which contains quaternary ammonium functional groups is used for defluoridation in drinking water.

The exchange of chloride ions favors the adsorption of fluoride as shown below

$$M\text{-}NR_3^+ Cl^- + F^- \rightarrow M\text{-}NR_3^+ F^- + Cl^-$$

Over the years, the most widely used polymeric sorbents[85] are styrene–divinyl benzene (DVB) copolymers for removal of heavy metals and it is mainly attributed to their hydrophobic nature, physical and chemical stability. These are generally referred as Amberlite XAD resins[86] and have surface area in the range 300-800 m^2g^{-1} with pore volume and average pore diameter between 0.9-1.5 cm^3g^{-1} and 4-9 nm respectively.[85,86] Styrene–divinylbenzene (DVB) copolymers have acquired great interest for developing tailored adsorbents in defluoridation of water.[82-84] Chelating resin (CR) and anion exchange resin (AER),[87] Metal (III)-loaded Amberlite resin,[83] Al-Amberlite resin,[82] Ion exchange fibre,[88] Zr immobilized resin,[89] Al-chelating porous anion exchanger[90] have proved their efficacy of fluoride removal in aqueous solutions. Lopez et al. observed the order of selectivity on Amberlite IRA-410 anionic resin as sulfate > chloride > bicarbonate > hydroxide > fluoride.[91] In a similar manner, the adsorption capacity of fluoride for different metal (III)-loaded Amberlite200 resin[83] follows the trend La(III) $\geq$ Ce(III) > Y(III) > Fe(III) = Al(III). Solangi et al. has reported thiourea modified Amberlite XAD-4 resin[92] for defluoridation of water in aqueous solution with 90% fluoride removability from a 10 mL solution containing 16 mg L^{-1} where as the unmodified resin removes only 30% at pH 7.0. This high adsorption capacity of fluoride is attributed to the hydrogen bonding between the amide groups in thiourea and fluoride. Functionalized polymeric resins also possess distinct advantages and recently, iminodiacetic acid functionalized cation exchange resin and amine functionalized copolymeric resins were reported for fluoride adsorption.[93] More recently, Ca-Zr-polyvinyl alcohol composite was reported at wide pH range with high adsorption capacity (12.72 mg g^{-1}) for defluoridation of water.[94]

1.3.3. Bio-Polymer based materials

In the past few years, biopolymer based materials have gained attention as an effective adsorbent in water treatment because of their relative abundance, low cost, good stability and chemical reactivity, biodegradability and availability of adequate functional groups. Among the various bio-adsorbents, chitin, chitosan-derivatives[95,96] have significant adsorption ability for the removal of fluoride from aqueous solution. Several researchers

focused on the modification of chitosan surface by the impregnation or incorporation of suitable metal ions for enhancing fluoride adsorption in accordance with the recent literature reports. For example, chitin, chitosan and lanthanum incorporated chitosan (20% La-chitosan),[97] magnesia-chitosan,[98] La incorporated chitosan beads and flakes, [99,100] aluminum and neodymium-modified chitosan[101,102] were reported recently for the enhanced defluoridation of water. Metal ions modified with chitosan show higher affinity and adsorption capacity towards fluoride as compared to native chitin and chitosan biopolymer. The adsorption capacity of various metal ions modified chitosan biopolymer is given in Table 1.4.Viswanathan et al. have developed multifunctional chitosan beads[103] (viz., $-NH_3^+$ and -COOH groups) for defluoridation involving protonation and carboxylation mechanisms. The protonated as well as carboxylated chitosan beads (PCCB) showed higher defluoridation capacity (DC) (1800 mg kg^{-1}) as compared to Protonated chitosan beads (PCB, 1664 mg kg^{-1}) and carboxylated chitosan beads (CCB,1385 mg kg^{-1}) whereas unmodified chitosan beads shows only 52 mg kg^{-1} adsorption capacity.[97] Hydrogen bonding is responsible for fluoride removal by PCB. In order to effectively utilize both hydroxyl and amino groups of chitosan, carboxylation followed by chelation of amino groups with different metal ions (La, Zr and Fe) were adopted to enhance the adsorption of fluoride. La-CCB,[104] Zr-CCB[105] and Fe-CCB[106] shows a maximum adsorption capacity of 4711, 4850 and 4230 mg kg^{-1} respectively where as carboxylated chitosan beads displayed only 1385 mg kg^{-1}. The metal ion modified CCB surface involves both adsorption and complexation mechanism. Chitosan modified with several composites such as Hydrotalcite/chitosan,[107] Chitosan coated silica (CCS),[108] Ti-Al binary metal oxide supported chitosan beads,[109] zirconium (IV) tungstophosphate,[110] magnetic-chitosan[111] and nanohydroxyapatite-chitin composite[112] have also been prepared and evaluated for their ability in defluoridation. Besides chitosan, other biosorbents such as β-Cyclotextrin,[113] cellulose,[114,115] algal[116] and fungal biomass[117] have also been studied for defluoridation of water. For example, the most commonly available algal Spirogyra IO2 was used as an adsorbent for the removal of fluoride in aqueous solution by Mohan et al.[115] Most recently, β-Cyclotextrin modified hydrous zirconium oxide[113] was synthesized and shows high adsorption capacity (31.45 mg g^{-1}) for fluoride.

Table 1.4. Maximum adsorption capacity of chitosan based materials

Sl.No	Adsorbent	Adsorption capacity	Reference
1.	Chitosan	52 mg kg^{-1}	97
2.	magnesia-chitosan	4440 mg kg^{-1}	98
3.	La incorporated chitosan beads	4.7 mg g^{-1}	99
4.	Aluminum modified chitosan	1.73 mg g^{-1}	100
5.	Neodymium-modified chitosan	22.380 mg g^{-1}	101
6.	Carboxylated chitosan beads	1385 mg kg^{-1}	102
7.	La-Carboxylated chitosan beads	4711 mg kg^{-1}	104
8.	Zr-Carboxylated chitosan beads	4850 mg kg^{-1}	105
9.	Fe-Carboxylated chitosan beads	4230 mg kg^{-1}	106
10.	Hydrotalcite/chitosan	1255 mg kg^{-1}	107
11.	Chitosan coated silica	44.40 mg g^{-1}	108
12.	Ti-Al binary metal oxide supported chitosan	2.22 mg g^{-1}	109
13.	Zirconium (IV) tungstophosphate	2025-2142 mg kg^{-1}	110
14.	Magnetic-chitosan	22.49 mg g^{-1}	111
15.	Nanohydroxyapatite-chitin composite	2840 mg kg^{-1}	112

But, cellulose biopolymer (Figure 1.3) has acquired considerable importance in recent years for the removal of dyes, boron and arsenic from aqueous solutions due to its natural abundance and biodegradability.[118-120] Cellulose (Figure 1.3) is a natural polysaccharide endowed with inter and intramolecular hydrogen bonding and good stability.[121] It is a linear polymer of β-(1,4)-D glucopyranose units and each glucose unit has three hydroxyl groups.[120] Anirudhan et al have used cellulose grafted epichlorohydrin functionalized polyethylenimine (Cell-g-E/PEI) graft copolymer[122] as an adsorbent for the removal and recovery of phosphate ions in aqueous solutions. The same group of researchers have also used iron(III)-coordinated amine-modified poly(glycidylmethacrylate)-grafted densified cellulose for defluoridation of water.[123] Zr(IV) impregnated collagen fiber[114] is yet another novel adsorbent reported for defluoridation with an adsorption capacity of 2.29

mmol g^{-1} at pH 5.5. Moving forward, the modified cellulose biopolymers with suitable metal ions could pave way to remediate fluoride in field applications.

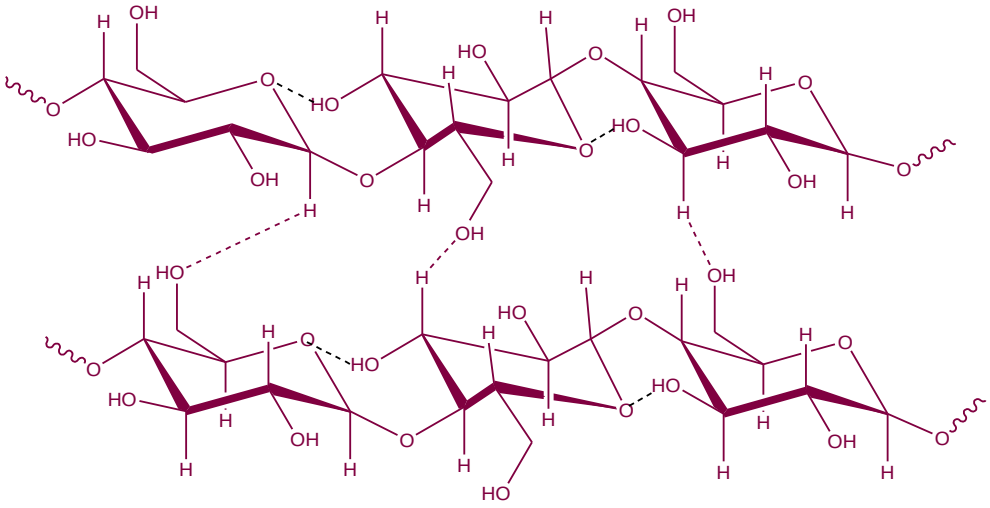

Figure 1.3. Structure of cellulose biopolymer

Cellulose sourced waste materials have also been utilized for defluoridation of water. For instance, Al and Fe loaded tea waste material was reported recently as a low cost material for the removal of fluoride and it shows a good fluoride adsorption capacity (18.52 mg g^{-1}).[124] Tea waste supported hydrous aluminium oxide[125] has also been reported to have an adsorption capacity of 42.14 mg g^{-1} in the pH range 4.0-9.0.

1.3.4. Carbonaceous materials

Carbonaceous materials such as activated carbon, graphite, carbon nanotubes, graphene and graphene oxide have emerged as new promising materials for defluoridation of water. Activated carbon[126] (AC) have been widely studied as an effective adsorbent for water treatment to remove a wide range of pollutants due to its relatively lower cost and ready availability, high surface area (500-1500 m^2g^{-1}), microporosity and presence of diverse functional groups on its surface. In view of its low zero point charge (pH 1.6-3.5),[127] it has poor adsorption capacity towards anionic pollutants. The adsorption capacity of activated carbon towards anionic pollutants is dependent on the pore size distribution because the adsorption process mainly occurs in the pores of the adsorbent.

Therefore, the amount of fluoride adsorbed increased with the specific surface area in several carbonaceous materials.[128] In contrast, the adsorption of fluoride on bone char does not depend on specific surface area since fluoride is adsorbed chemically by ligand exchange and not physically adsorbed on its surface.[129] Keseva et al reported the application of regenerated bone char for defluoridation of water.[130] The maximum adsorption capacity and highest percentage of fluoride removal was obtained as 0.75 mg g^{-1} and 70.64% respectively. Granular activated carbon (GAC) coated with manganese oxides was also used for fluoride removal from aqueous solution.[131] Defluoridation of groundwater using Assam coal and other coal based adsorbents such as lignite (LN), fine coke (FC), and bituminous coal (BC) were also evaluated for fluoride removal.[132,133]

Daifullah et al. reported that the structure of activated carbon can be modified by steam pyrolysis of rice straw followed by oxidation using HNO_3, H_2O_2, and $KMnO_4$. The material obtained by $KMnO_4$ oxidation gave the highest fluoride adsorption and ligand exchange was postulated as the mechanism for fluoride adorption.[134] Janardhana et.al prepared zirconium impregnated activated charcoal in order to increase the fluoride adsorption capacity. The adsorption capacity of Zr-impregnated activated charcoal was 3-5 times higher than that of unmodified activated charcoal and it shows maximum fluoride uptake followed by coconut shell and ground nut shell charcoals. This material was found to effective to in treating 6 liters of water to bring the fluoride concentration levels to permissible limits.[135]

Various grades of graphite[136] have also proved as an adsorbent for defluoridation and the Langmuir maximum adsorption capacity was found to be 3.13 mg g^{-1} for the graphite having 818 m^2g^{-1} surface area. Gupta et al. reported Aluminium impregnated onto a new micronanohierarchal web (MiNaHiWe) consisting of activated carbon fibers (ACF) and carbon nanofibers (CNF) for the removal of fluoride from wastewater.[137] Very recently, Jin et al. prepared an amorphous Alumina-modified Expanded Graphite (Al_2O_3/EG) composite[138] through a facile method followed by thermal treatment and tested for defluoridation of water. The Al_2O_3/EG adsorbent shows 1.18 mg g^{-1} fluoride adsorption capacity with a removal efficiency of 94.4%.

In recent years, carbon nanotubes (CNTs) have gained prominence for a wide range of applications. It is attributed to their high surface area, small size and high mechanical

strength. Li et al. have explored the possibility of Al_2O_3/CNTs for the efficacy of fluoride adsorption in aqueous solution.[139] The maximum fluoride adsorption was found to be in the pH range of 5.0-9.0. The adsorbent shows 13.5 times higher fluoride adsorption capacity than that of activated carbon (AC-300) and four fold higher than that of γ-Al_2O_3 at 12 mg L^{-1} equilibrium fluoride concentration. Aligned carbon nanotubes (ACNTs) is as a novel carbon material prepared by catalytic decomposition of xylene using ferrocene as catalyst and modified ACNTs with Al (III) were also evaluated as novel material for defluoridation.[140,141]

In the carbon family, graphene is yet another emerging carbon material which is hexagonal, sp^2-hybridized with one-atom-thick layer structure.[85,142] Graphene oxide, the oxidized form has high surface area and various functional groups (hydroxyl, epoxy groups and carboxylic).[143,144] Graphene[145] has proved to be an effective adsorbent for the adsorption of F^- ion in aqueous solution with an adsorption capacity of 17.65 mg g^{-1}. A novel metalloporphyrin grafted-graphene oxide[146] has been utilized as a sensor for F^- ion in aqueous solution and hence it is possible that suitable modification of graphene oxide could also assist in the adsorption of F^- ion with good adsorption capacity. The incorporation of Zr-hydroxide into graphene oxide can significantly increase the adsorption capacity of negatively charged ionic pollutants.[147,148] Furthermore, manganese oxide coated graphene oxide (MOGO) [149] studied recently for fluoride ion adsorption as a new hybrid material shows an adsorption capacity of 11.63 mg g^{-1}. Basic aluminum sulfate@ graphene hydrogel has been reported to possess an adsorption capacity of 33.4 mg g^{-1} at pH 7.2 towards F^- ion adsorption.[150]

1.4. Fluoride adsorption mechanism

The adsorption of fluoride onto the adsorbent surface involves the following probable interactions[42]

a. Van der Waals forces
b. Ion exchange
c. Hydrogen bonding
d. Ligand exchange
e. Chemical modification of the adsorbent surface.

The outer sphere surface complexations (ion exchange) are governed by weak physical adsorption and are quite non-specific to fluoride, whereas inner-sphere surface complexations (Hydrogen bonding) involve strong chemical adsorption specific to fluoride. The chemical modification involves both specific and non-specific adsorption.

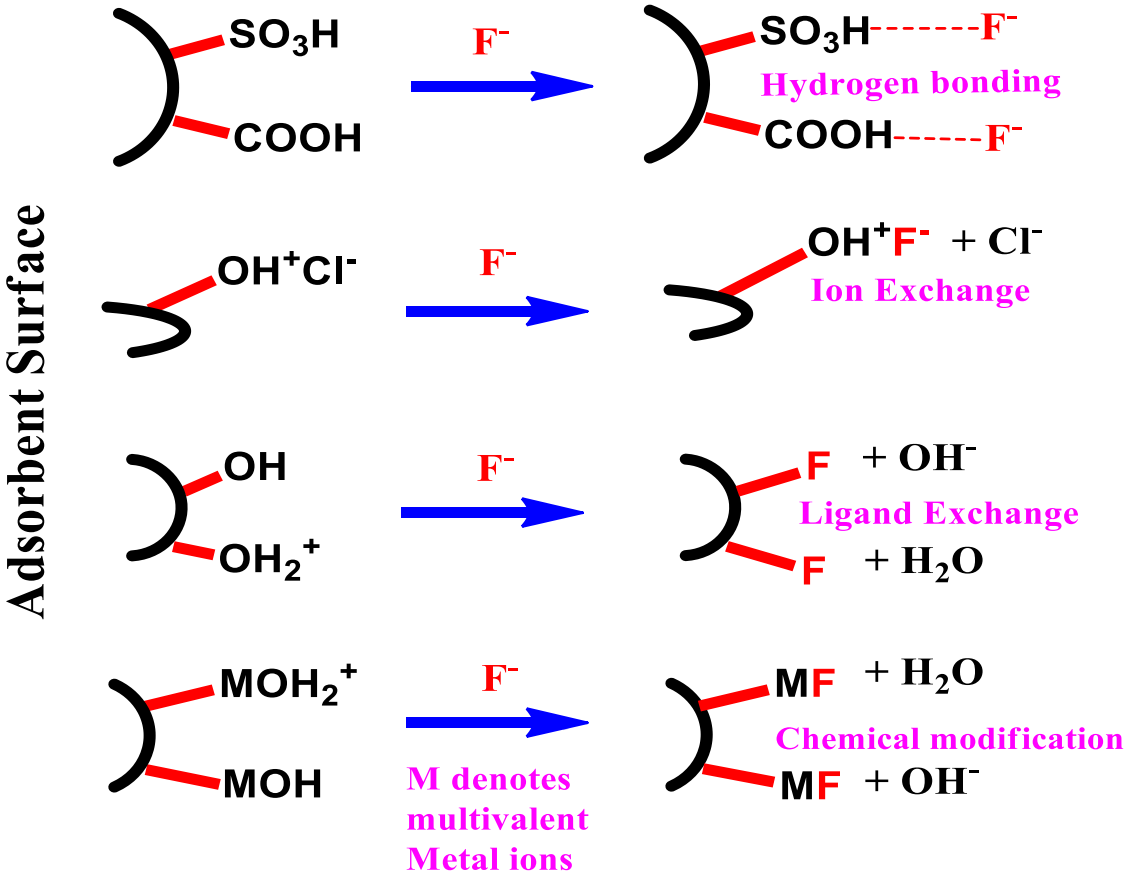

Figure 1.4. Fluoride adsorption mechanism[42]

Theoretically, there are four possible steps to explain the kinetics of fluoride adsorption as follows[151]

a. External mass transfer;
b. Intra particle or Pore diffusion
c. Adsorption at interior sites
d. Physical or chemical adsorption

1.5. Scope and Objective of the Work

A systematic survey of literature reveals that the impregnation of metal ions in a suitable matrix such as cellulose biopolymer, synthetic polystyrene divinyl benzene resins and graphene oxide have not been fully explored for their efficacy towards fluoride adsorption. The preparation of adsorbents using ultrasonication or microwave-assisted synthesis has also not yet been utilized as sustainable alternatives for removal of fluoride from drinking water. Hence, developing novel metal ion impregnated adsorbents were explored with a view to enhance the adsorption capacity as well as column scale up towards fluoride adsorption. The regeneration of the adsorbents with environmentally benign (green) reagents is also the emphasized in these studies. The application of these sorbents for removal of fluoride ions from drinking water samples and taking it to the field application for real water samples were examined.

Solid phase extraction (SPE) involves the distribution of fluoride ions between the liquid and solid phase effectively by adsorption of fluoride on the surface. The impregnation of metal ions in the matrix would enhance the adsorption of fluoride ions from drinking water. The small size of fluoride, high electronegativity and behavior as a hard base makes it compatible with hard metal ions such as aluminium and zirconium. Taking advantage of the fact that fluoride can complex effectively with these metal ions, biodegradable polymers and economically viable adsorbent materials (Cellulose biopolymer, Synthetic polystyrene divinyl benzene resin and graphene oxide) were explored for the effective detoxification of fluoride. Furthermore, the prepared adsorbents were tested in batch and column studies for adsorption of fluoride. The work presented in the following chapters deals with the development of the following:-

1. A novel Al and Zr impregnated cellulose adsorbent prepared using ultrasonication and microwave irradiation for the facile defluoridation of water.
2. Aluminium hydroxide impregnated macroreticular aromatic polymeric resin as a sustainable option for defluoridation
3. Graphene oxide–aluminium oxyhydroxide interaction and its application for the effective adsorption of fluoride

Various adsorption parameters such as pH, adsorbent dosage, isotherm studies, kinetics, thermodynamic parameters, aqueous phase volume, interfering ions and column studies were investigated in detail. The modified adsorbents were characterized thoroughly using BET surface area analysis, FT-IR spectroscopy, SEM, EDX, XRD and XPS studies. The concentration of metal ions (Al^{3+} and Zr^{4+}) leached into the aqueous phase after adsorption (detectable if any) was checked using ICP-AES.

Chapter 3 The proposed method involves the impregnation of Al and Zr in cellulose matrix wherein fluoride ion from aqueous medium interacts with the cellulose hydroxyl groups as well as cationic Zr and Al hydroxides. The facile preparation of the adsorbent was accomplished by microwave and ultrasound assisted synthesis. The preparation, characterization, mechanistic aspects and application to defluoridation of water are discussed in detail.

Chapter 4 This chapter explains in detail the preparation, characterization, mechanistic aspects of aluminium hydroxide impregnated macroreticular aromatic polymeric resin and its application for the removal of fluoride in aqueous solution.

Chapter 5 A novel aluminium oxy hydroxide [Al–O(OH)] modified graphene oxide was prepared by a chemical precipitation method. The Al^{3+} modified graphene oxide adsorbent was characterized using FT-IR, FT-Raman and SEM-EDS, XRD and XPS studies. The prepared (GO–Al–O(OH) adsorbent was tested for the effective defluoridation of water.

Chapter 6 This chapter presents the overall summary and important conclusions.

References

1. Kanaujia, S.; Singh, B.; Singh, S. K. *Journal of Geoscience and Environment Protection*, **2015**, 3, 1.
2. Tchobanoglous, G; Franklin, L. B. Wastewater Engineering: Treatment, Disposal and Reuse; McGraw Hill, Inc.: New York, **1991**.
3. Nemerow, N.; Dasgupta, A. Industrial and Hazardous Waste Treatment, Van Nostrand Reinhold: New York, **1991**.
4. Laws, E. A. Aquatic Pollution: An Introductory Text, 3rd ed.; John Wiley & Sons: New York, **2000**.
5. Amini, M.; Mueller, K.; Abbaspour, K. C.; Rosenberg, T.; Afyuni, M.; Moller, K. N.; Sarr M.; Johnson, C. A. *Environ. Sci. Technol.* **2008**, 42, 3662.
6. Tekle-Haimanot, R.; Melaku, Z.; Kloos, H.; Reimann, S.; Fantye, W.; Zerihun L.; Bajorvatn, K. *Sci. Total Environ.* **2006**, 367, 182.
7. Liao, X.; Shi, B. *Environ. Sci. Technol.* **2005,** 39, 4628.
8. Jagtap, S.; Yenkie, M.K.; Labhsetwar, N.; Rayalu, S. *Chem. Rev.* **2012**, 112, 2454.
9. WHO, Fluoride and oral health. Report of a WHO expert committee on oral health status and fluoride use, WHO Technical Report Series, No. 846; Geneva, **1994**.
10. Yadugiri, V. T. *Curr. Sci.* **2011**, 100, 1475.
11. Rajiv Gandhi National Drinking Water Mission (RGNDWM), Prevention and control of fluorosis in India, **1993**.
12. Pauling, I. The nature of chemical bond, Cornell University press Ithaca, New York, 3rd edn, **1960**.
13. Fawell, J.; Bailey, K.; Chilton, J.; Dahi, E. Fewtrell L.; Magara, Y. Fluoride in drinking water, World Health Organisation, IWA Publishing, London, UK, **2006**, 5.
14. Meenakshi, S.; Garg, V. K.; Kavita, Renuka, Malik, A. *J. Haz. Mater. B* **2004**, 106, 85.
15. Singh, R.; Maheshwari, R. C. *Ind. J. Environ. Protec.* **2001**, 21, 983.
16. Brindha, K.; Elango, L. Fluoride in Groundwater: Causes, Implications and Mitigation Measures. In: Monroy, S.D. (Ed.), Fluoride Properties, Applications and Environmental Management, **2011**, 111-136.
17. Vithanage, M.; Bhattacharya, P. *Environ Chem Lett.* **2015**, 13, 131.
18. Bell, M.C.; Ludwig, T.G. The supply of fluoride to man: ingestion from water, in: Fluorides and Human Health, WHO Monograph Series 59, World Health Organization, Geneva, **1970**.
19. Ayoob, S.; Gupta, A. K. *Crit. Rev. Environ. Sci. Technol.* **2006**, 36, 433.
20. Smet, J.; Frencken, J.E. Fluoride in drinking water. Symposium on Endemic Fluorosis in Developing Countries: Causes, Effects and Possible Solutions, NIPG-TNO, Liden, Sweden, **1990**; Chapter 6, p 51.
21. Agarwal, M.; Rai, K.; Shrivastav, R.; Dass, S. *J. Clean Prod.* **2003**, 11, 439.
22. Wang, W.; Li, R.; Tan, J.; Luo, K.; Yang, L.; Li, H.; Li, Y. *Fluoride* **2002**, 35, 122.
23. Dissanayake, C. B. *Int. J. Environ. Stud.* **1991**, 19, 195.
24. Fluorine and fluorides, Environmental Health Criteria, 36, IPCS International Programme on Chemical Safety, **1984**.
25. Murray, J. J. A history of water fluoridation, *Br. Dent. J.* **1973**, 134, pp.250–254, 299–302, 347–350.
26. Meenakshi, S.; Maheshwari, R.C. *J. Hazard. Mater. B* **2006**, 137, 456.

27. Fawell, J.; Bailey, K.; Chilton, E.; Dahi, E.; Fewtrell, L.; Magara, Y. Fluoride in Drinking Water, World Health Organization, IWA Publishing, UK, **2006**.
28. United State Environmental Pollution Agency (USEPA), National primary drinking water standards, EPA/816-F/03/016, **2003**.
29. Na, C. K.; Park, H.J. *J. Hazard. Mater.* **2010**, 183, 512.
30. Bureau of Indian Standards IS 10500.1991.
31. Sujana, M. G.; Pradhan, H. K.; Anand, S. *J. Hazard. Mater.* **2009**, 161, 120.
32. Zhou, Y.; Yu, C.; Shan, Y. *Sep. Purif. Technol.* **2004**, 36, 89.
33. Islam, M.; Patel, R. K. *Chem. Eng. J.* **2011**, 169, 68.
34. John, D.J.; Stolenberg, C. Water treatment. Handbook of drinking water quality standards and controls; Van Nostrand Reinhold: New York, **1958**; pp 407-490.
35. Reardon, E. J.; Wang, Y. *Environ. Sci. Technol.* **2000**, 34, 3247.
36. Saha, S. *Water Res.* **1993**, 27, 1347.
37. Sujana, M. G.; Soma, G.; Vasumathi, N.; Anand, S. *J. Fluorine Chem.* **2009**, 130, 749.
38. Lopez, M.; Coca, J.; Rosal, R.; Garcia, R.; Sastre, H. *J. Ind. Chem.* **1992**, 20, 109.
39. Singh, G.; Kumar, B.; Sen, P.K.; Majumdar, *J. Water Environ. Res.* **1999**, 71, 36.
40. Ku, Y.; Chiou, H.M.; Wang, W. *Sep. Sci. Technol.* **2002**, 37, 89
41. Loganathan, P.; Vigneswaran, S.; Kandasamy, J.; Naidu, R. *J. Hazard. Mater.* **2013**, 248–249, 1.
42. Ndiaye, P. I.; Moulin, P.; Dominguez, L.; Millet, J. C.; Charbit, F. *Desalination* **2005**, 173, 25.
43. Diawara, C. K., *Sep. Purif. Rev.* **2008**, 37, 303.
44. Alkan, E.; Kir, E.; Oksuz, L. *Sep. Purif. Technol.* **2008**, 61, 455.
45. Tor, A. *J. Hazard. Mater.* **2007**, 141, 814.
46. Mameri, N.; Lounici, H.; Belhocine, D.; Grib, H.; Piron, D. L.; Yahiat, Y. *Sep. Purif. Technol*. **2001**, 24, 113.
47. Nawlakhe, W. G.; Paramasivam, R. *Curr. Sci.* **1993**, 65, 743.
48. Bishop, P. L.; Sansoucy, G. *J. AWWA* **1978**, 70, 554.
49. Mckee, R.; Johnston, W.S. *Ind. J. Environ. Health.* **1999**, 41, 53.
50. Zhou, Y.; Haynes, R.J. *Crit. Rev. Environ. Sci. Technol.* **2011**, 40, 909.
51. Kumar, E.; Bhatnagar, A.; Minkyu, J.; Jung, W.; Lee, S.; Kim, S.; Lee, G.; Song, H.; Choi, J.; Yang, J.; Jeon, B. *Water Res.* **2009**, 43, 490.
52. Ku, Y.; Chiou, H. *Water Air Soil Pollut.* **2002**, 133, 349.
53. Maliyekkal, S. M.; Sharma, A. K.; Philip, L. *Water Res.* **2006**, 40, 3497.
54. Wajima, T.; Umeta, Y.; Narita, S.; Sugawara, K. *Desalination* **2009**, 249, 323.
55. Islam, M.; Patel, R. K. *J. Hazard. Mater.* **2007**, 143, 303.
56. Viswanathan, N.; Meenakshi, S. *J. Hazard. Mater.* **2010**, 176, 459.
57. Alagamuthu, G.; Rajan, M. *Chem. Eng. J.* **2010**, 158, 451.
58. Li, Y. H.; Wang, S.; Cao, A.; Zhao, D.; Zhang, X.; Xu, C.; Luan, Z.; Ruan, D.; Liang, J.; Wu, D.; Wei, B. *Chem. Phys. Lett.* **2001**, 350, 412.
59. Chubar, N. Physico-chemical treatment of micropollutants: adsorption and ion exchange, in: Virkutyte, J.; Varma, R. S.; Jegatheesan, V. Eds.), Treatment of Micropollutants in Water and Wastewater, IWA publishing, London, 2010, pp. 165–203.

60. Li, Y. H.; Wang, S.; Cao, A.; Zhao, D.; Zhang, X.; Xu, C.; Luan, Z.; Ruan, D.; Liang, J.; Wu, D.; Wei, B. *Chem. Phys. Lett.* **2001**, 350, 412.
61. Johnston, R.; Heijnen, H. Safe Water Technology for Arsenic Removal. Report; World Health Organization (WHO): Geneva, Switzerland, 2002.
62. Shimelis, B.; Zewge, F.; Chandravanshi, B.S. *Bull. Chem. Soc.* Ethiopia **2006**, 20, 17.
63. Farrah, H.; Slavek, J.; Pickering, W.F. *Aust. J. Soil Res.* **1987**, 25, 55.
64. Ghorai, S.; Pant, K. K. *Chem. Eng. J.* **2004**, 98, 165.
65. Pietrelli, L. *Anal. Chim.* **2005**, 95, 303.
66. Saha, G.; Maliyekkal, S. M.; Sabumon, P. C.; Pradeep, T. *J. Environ. Chem. Eng.* **2015**, 3, 1303.
67. Mahapatra, A.; Mishra, B. G.; Hota, G. *Ind. Eng. Chem. Res.* **2013**, 52, 1554.
68. Bansiwal, A.; Pillewan, P.; Biniwale, R. B.; Rayalu, S. S. *Microporous Mesoporous Mater.* **2010**, 129, 54.
69. Wasay, S. A.; Tokunaga, S.; Park, S. W. *Sep. Sci. Technol.* **1996**, 31, 1501.
70. Tripathy, S. S.; Bersillon, J. -L.; Gopal, K. *Sep. Purif. Technol.* **2006**, 50, 310.
71. Puri, B.K.; Balani, S. *J. Environ. Sci. Health Part A: Toxic/Hazardous Subst. Environ. Eng.* **2000**, 35, 109.
72. Liu, H.; Deng, S.; Li, Z.; Yu, G.; Huang, J. *J. Hazard. Mater.* **2010**, 179, 424.
73. Wu, X.; Zhang, Y.; Dou, X.; Yang, M. *Chemosphere* **2007**, 69, 1758.
74. Deng, S.; Liu, H.; Zhou, W.; Huang, J.; Yu, G. *J. Hazard. Mater.* **2011**, 186, 1360.
75. Biswas, K.; Gupta, K.; Goswami, A.; Ghosh, U.C. *Desalination* **2010**, 255, 44.
76. Dash, S.; Sahu, M. K.; Sahu, E.; Patel, R. K. *New J. Chem.*, **2015**, 39, 7300.
77. Ghosh, A.; Chakrabarti, S.; Biswas, K.; Ghosh, U.C. *Appl. Surf. Sci.* **2014**, 307, 665.
78. Y. Yu, L. Yu, J. Paul Chen, *Chem. Eng. J.* **2015**, 262, 839.
79. Dou, X.; Zhang, Y.; Wang, H.; Wang, T.; Wang, Y. *Water Research* **2011**, 45, 3571.
80. Chen, L.; He, B.-Y.; He, S.; Wang, T.-J.; Su, C.-L.; Jin, Y. *Powder Technology* **2012**, 227, 3.
81. Helferich, F. Ion Exchange, Dover Publication Inc., USA, **1995**
82. Ku, Y.; Chiou, H.; Wang, W. *Sep. Sci. Technol.* **2002**, 37, 89.
83. Luo, F.; Inoue, K. *Solvent Extract. Ion Exch.* **2004**, 22, 305.
84. Vaaramma, K.; Lehto, J. Desalination **2003**, 155, 157.
85. Kumar, A.S.K. PhD Thesis, **2014**, BITS-Pilani Hyderabad, India.
86. SivaKesavaRaju, CH. PhD Thesis, **2006,** IIT Madras, India.
87. Meenakshi, S.; Viswanathan, N. *J. Colloid Interface Sci.* **2007**, 308, 438.
88. Ruixia, L.; Jinlong, G.; Hongxiao, T. *J. Colloid Interface Sci.* **2002**, 248, 268.
89. Mizuki, H.; Ito, Y.; Samatya, S. Harada, H.; Kawakita H.; Uezu, K. *Solvent Extraction and Ion Exchange* 2011, 29:1, 146.
90. Popat, K.M.; Anand, P.S.; Dasare, B.D. *React. Polym.* **1994**, 23, 23.
91. Lopez, M.; Coca, J.; Rosal, R.; Garcia, R.; Sastre, H. *J. Ind. Chem.* **1992**, 20, 109.
92. Solangi, I.B.; Memon, S.; Bhanger, M.I. *J. Hazard. Mater.* **2010**, 176, 186.
93. Prabhu, S.M.; Meenakshi, S. Desalin. *Water Treat.* **2014**, 52 (13–15), 2527.
94. Bhandari, R.; Janardhana, C. *Desalination and Water Treatment* **2016**, 57, 9437.
95. Jagtap, S.; Thakre, D.; Wanjari, S.; Kamble, S.; Labhsetwar, N.; Rayalu, S. J. *Colloid Interface Sci.* **2009**, 332, 280.
96. Davila-Rodriguez, J.L.; Escobar-Barrios, V.A.; Shirai, K.; Rangel-Mendez, J.R. *J. Fluorine Chem.* **2009**, 130, 718.

97. Kamble, S.P.; Jagtap, S.; Labhsetwar, N.K.; Thakare, D.; Godfrey, S.; Devotta, S.; Rayalu, S.S. *Chem. Eng. J.* **2007**, 129, 173.
98. Sundaram, C.S.; Viswanathan, N.; Meenakshi, S. *J. Hazard. Mater.* **2009**, 163, 618.
99. S. Jagtap, M.K. Yenkie, S. Das, S. Rayalu, *Desalination* **2011**, 273, 267.
100. Bansiwal, A.; Thakre, D.; Labhshetwar, N.; Meshram, S.; Rayalu, *S. Colloids Surf. B: Biointerfaces* **2009**, 74, 216.
101. Swain, S.K.; Dey, R.K.; Islam, M.; Patel, R.K.; Jha, U.; Patnaik, T.; Airoldi, C. *Sep. Sci. Technol.* **2009**, 44, 2096.
102. Meng, F.; Zhang, L.; Ma, D.; Wang, M. *J. Hazard. Mater.* **2009**, 165, 454.
103. Viswanathan, N.; Sairam Sundaram, C.; Meenakshi, S. *J. Hazard. Mater.* **2009**, 167, 325.
104. Viswanathan, N.; Meenakshi, S. *J. Colloid Interface Sci.* **2008**, 322, 375.
105. Viswanathan, N.; Meenakshi, S. *Colloids Surf. B: Biointerfaces* 2009, 72, 88.
106. Viswanathan, N.; Meenakshi, S. *J. Fluorine Chem.* **2008**, 129, 503.
107. Viswanathan, N.; Meenakshi, S. *Appl. Clay Sci.* **2010**, 48, 607.
108. Vijaya, Y.; Krishnaiah, A. *E-J. Chem.* **2009**, 6, 713.
109. Thakre, D.; Jagtap, S.; Sakhare, N.; Labhsetwar, N.; Meshram, S.; Rayalu, S. *Chem. Eng. J.* **2010**, 158, 315.
110. Viswanathan, N.; Meenakshi, S. *J. Hazard. Mater.***2010**, 176, 459.
111. Ma, W.; Ya, F.-Q.; Han, M.; Wang, R. *J. Hazard. Mater.* **2007**, 143, 296.
112. Sundaram, C.S.; Viswanathan, N.; Meenakshi, S. *J. Hazard. Mater.***2009**, 172, 147.
113. Saha, I.; Ghosh, A.; Nandi, D.; Gupta, K.; Chatterjee, D.; Ghosh, U.C. *Chem. Eng. J.* 2015, 263, 220.
114. Liao, X.-P.; Shi, B. *Environ. Sci. Technol.* **2005**, 39, 4628.
115. Mandal, S.; Mayadevi, S. *Chemosphere* **2008**, 72, 995.
116. Mohan, S.V.; Ramanaiah, S.V.; Rajkumar, B.; Sarma, P.N. *J. Hazard. Mater.***2007**, 141, 465.
117. Ramanaiah, S.V.; Venkata Mohan, S.; Sarma, P.N. *Ecol. Eng.* **2007**, 31, 47.
118. Bouzaida, I.; Rammah, M.B. *Mat. Sci. Eng. C* **2002**, 21, 151.
119. Liu, R.; Ma, W.; Jia, C.Y.; Wang, L.; Li, H.Y. Desalination **2007**, 207, 257.
120. Guo, X.; Chen, F. *Environ. Sci. Technol.* **2005**, 39, 6808.
121. Klemm, D.; Heublein, B.; Fink, H.P.; Bohn, A. *Angew. Chem. Int. Ed.* **2005**, 44, 3358.
122. Anirudhan, T. S.; Rauf, T. A.; Rejeena, S. R. *Desalination* **2012**, 285, 277.
123. Anirudhan, T. S.; Suchitra, P.S. *Ind. Eng. Chem. Res.***2010**, 49, 12254.
124. Cai, H.m.; Chen, G.j.; Peng, C.y.; Zhang, Z.z.; Dong, Y.y.; Shang, G.z.; Zhu, X.h.; Gao, H.j.; Wan, X.c. *Appl. Surf. Sci* **2015**, 328, 34.
125. H. Cai, G. Chen,C. Peng, L. Xu, X. Zhu, Z. Zhang, Y. Dong, G. Shang, F. Ke, H. Gao and X. Wan. *RSC Adv.* **2015**, 5, 101819.
126. Yin, C.Y.; Aroua, M. K.; Daud, W. M. A. W. *Sep. Purif. Technol.* 2007, 52, 403.
127. Mahmudov, R.; Huang, C. P. *Sep. Purif. Technol.* **2010**, 70, 329.
128. Abe, I.; Iwasaki, S.; Tokimoto, T.; Kawasaki, N.; Nakamura, T.; Tanada, S. *J. Colloid Interface Sci.* 2004, 275, 35.
129. Bhargava, D. S.; Killedar, D. *J. Water Res.***1992**, 26, 781.
130. Kaseva, M. E. *J. Water Health* 2006, 4, 139.

131. Ma, Y.; Wang, S.-G.; Fan, M.; Gong, W.-X.; Gao, B.-Y. *J. Hazard. Mater.* **2009**, 168, 1140.
132. Borah, L.; Dey, N. C. *Indian J. Chem. Technol.* **2009**, 16, 361.
133. Sivasamy, A.; Singh, K. P.; Mohan, D.; Maruthamuthu, M. *J. Chem. Technol. Biotechnol.* **2001**, 76, 717.
134. Daifullah, A. A. M.; Yakout, S. M.; Elreefy, S. A. *J. Hazard. Mater.* **2007**, 147, 633.
135. Janardhana, C.; Nageswara Rao, G.; Sai Sathish, R.; Sunil Kumar, P.; Anil Kumar, V.; Vijay Madhav, M. *Indian J. Chem. Technol.* **2007**, 14, 350.
136. Karthikeyan, M.; Elango, K. P. *Indian J. Chem. Technol.* **2008**, 15, 525.
137. Gupta, A. K.; Deva, D.; Sharma, A.; Verma, N. *Ind. Eng. Chem. Res.* **2009**, 48, 9697.
138. Jin, H.; Ji, Z.; Yuan, J.; Li, J.; Liu, M. Xu, C.; Dong, J.; Hou, P.; Hou, S. *J. Alloy Compd.* **2015**, 620, 361.
139. Li, Y.-H. ; Wang, S.; Cao, A.; Zhao, D.; Zhang, X.; Xu, C.; Luan, Z.; Ruan, D.; Liang, J.; Wu, D.; Wei, B. *Chem. Phys. Lett.* **2001**, 350, 412.
140. Li, Y.-H.; Wang, S.; Zhang, X.; Wei, J.; Xu, C.; Luan, Z.; Wu, D. *Mater. Res. Bull.* **2003**, 38, 469.
141. Li, Y. H.; Wang, S.; Zhang, X.; Wei, J.; Xu, C.; Luan,; Wu, D.; Wei, B. *Environ. Technol.***2003**, 24, 391.
142. Rao, C. N. R.; Sood, A. K.; Subrahmanyam, K. S.; Govindaraj, A. *Angew. Chem. Int. Ed.* **2009,** 48, 7752.
143. Dreyer, D. R.; Park, S.; Bielawski C. W.; Ruoff, R. S. *Chem. Soc. Rev.* **2010**, 39, 228.
144. Subrahmanyam, K. S.; Vivekchand, S. R. C.; Govindaraj, A.; Rao, C. N. R. *J. Mater. Chem.* **2008**, 18, 1517.
145. Li, Y.; Zhang, P.; Du, Q.; Peng, X.; Liu, T.; Wang, Z.; Xia, Y.; Zhang, W.; Wang, K.; Zhu, H.; Wu, D. *J. Colloid Interface Sci.* **2011**, 363, 348.
146. Poursaberi, T.; Ganjali, M. R.; Hassanisadi, M. *Talanta* **2012**, 101, 128.
147. Luo, X.; Wang, C.; Wang, L.; Deng, F.; Luo, S.; Tu, X.; Au, C. *Chem. Eng. J.* **2013**, 220, 98.
148. Zong, E.; Wei, D.; Wan, H.; Zheng, S.; Xu, Z.; Zhu, D. *Chem. Eng. J.* **2013**, 221, 193.
149. Li, Y.; Du, Q.; Wang, J.; Liu, T.; Sun, J.; Wang, Y.; Wang, Z.; Xia, Y.; Xia, L.; *J. Fluorine Chem.* **2013**, 148, 67.
150. Chen, Y.; Zhang, Q.; Chen, L.; Bai, H.; Li, L. *J. Mater. Chem. A* **2013**, 1, 13101.
151. Fan, X.; Parker, D. J.; Smith, M. D.; *Water Res.* **2003**, 37, 4929.

CHAPTER 2

2. Materials and Methods

This chapter gives an outline of the materials used and the general experimental procedures for calculating the efficiency of ultrasonicator, instrumentation and the isotherms, kinetics and thermodynamics associated with the defluoridation.

2.1. Chemicals and Reagents

Analytical grade reagents were used for the fluoride adsorption studies. Cellulose, Sulfuric acid (H_2SO_4, 96.0%), hydrochloric acid (HCl, 35.0 %) and ethanol (CH_3CH_2OH, 95.0 %) was procured from Himedia laboratories, India. The macroporous polymeric resin (Amberlite XAD 1180, 1.4 cm^3/g pore volume, 500 m^2 g^{-1} surface area) and Graphite with a mean particle size (< 20 µm) were procured from Sigma Aldrich. Zirconium oxychloride octahydrate ($ZrOCl_2.8H_2O$), activated neutral alumina, Orthophosphoric acid (H_3PO_4, 85%), hydrogen peroxide (H_2O_2, 30 %), potassium permanganate ($KMnO_4$), aluminum sulfate hydrate ($Al_2(SO_4)_3.16H_2O$), Sodium hydroxide (NaOH) and sodium fluoride (NaF) were purchased from S.d.fine Chemicals, India. Total ionic strength adjustment buffer (TISAB II, HI4010-00) solution was obtained from Hanna instruments, USA. Nitric acid (HNO_3), sulfuric acid (H_2SO_4), hydrochloric acid (HCl), Hydrogen peroxide (H_2O_2) sodium hydroxide (NaOH), methanol and acetone, are procured from S.D. Fine Chemicals, Mumbai (India) and Merck (India) respectively.

2.2. Physico-chemical Characterization Instruments

The prepared adsorbent was characterized using various physico-chemical characterization techniques. A SHARP model 23-GT microwave oven procured from Cole-Parmer with a maximum power range 1600W was used in the preparation of the Al(III)-Zr(IV)-cellulose adsorbent. A probe sonicator (36” x 16” x 31”, Frontline, India model no FS-500) which uses ultrasonic (23 ± 3 KHz) signal in producing mechanical vibrations at tip of the probe was used in the preparation of the adsorbent. Stainless steel tips of diameter 6 mm was utilized for sonication and the sonicator was housed in a sound abating chamber. Orbital incubator shaker (Biotechnics, India) was used for equilibrating the adsorbents with various concentrations of fluoride. The pH of the aqueous medium was adjusted using appropriate amount of HCl/NaOH using an LI-127 pH meter (Elico,

India). The FT-IR spectra of the adsorbent was recorded by mixing 0.01 g of the sorbent with spectroscopy grade KBr and the spectra were recorded using a Jasco-4200 FT-IR spectrometer in the range 400‑4000 cm^{-1} at a resolution of 4 cm^{-1}. FT Raman spectra of the adsorbent were recorded using a thermo electron corporation Nexus 670 model spectrometer using an NdYAG laser excitation source. The electronic spectrum of graphene oxide was recorded using UV-visible spectrophotometer (Jasco model V 650). The XRD pattern of cellulose based adsorbents before and after adsorption of fluoride was recorded using a Panalytical X-ray X'Pert PRO spectrometer at a scan rate of 0.5^0 min^{-1} using Cu Kα radiation (1.54Å) provided with a secondary beam graphite monochromator. The X-ray diffraction (XRD) pattern of GO, GO-Al-O (OH) adsorbent before and after the adsorption of fluoride ion were obtained using a Bruker AXS D8 Advance XRD diffractometer with Cu Kα radiation source (λ = 1.5406 Å) source energized at 40 KV and 35 mA with step size and time of 0.020°and 65.6 s respectively. The samples were scanned at the rate 2.0° min^{-1} in the 2θ range 5° to 100°. The surface morphology of prepared adsorbent before and after fluoride adsorption was obtained using a JEOL Model JSM-6390LV and Hitachi S-520 scanning electron microscope along with the energy dispersive X-ray spectrum (JEOL Model JED – 2300). The surface area and porosity of the adsorbent was determined by N_2 adsorption−desorption isotherms measured at 77 K using a porosimeter analyzer (BELSORP MINI II model). The samples were degassed at 105 °C for 2 h at a vacuum pressure of 10^{-2} kPa. The Brunauer-Emmett-Teller (BET) and Barrett-Joyner-Halenda (BJH) models were used to measure the specific surface area of the $Al(OH)_3$ impregnated adsorbent in the range 0.0 – 1.0 relative pressure and the pore size distribution of the adsorbent by plotting dV_p / dr_p against r_p respectively. The particle size of the adsorbent was measured by DLS method using a Malvern nano-ZS particle size analyzer in the range 0.3 nm to 5 µm.Optical microscopy images of the modified resin before and after adsorption was obtained using an Olympus model CH20i microscope. XPS data of the adsorbent and the starting material were recorded using a VG Multilab 2000 spectrometer (Thermo VG Scientific, Southend-On-Sea, Essex, UK) in an ultra-high vacuum and an unmonochromatized Mg Kα (1253.6eV) X-ray source with a spherical section analyzer. Survey scans and core

peak data were acquired with pass energies of 50eV, respectively. The XPS spectrum calibration was done with hydrocarbon C 1s peak at a binding energy of 284.5eV.

2.3. Calorimetric studies and energy efficiency calculations

The energy efficiency was calculated using calorimetric methods. A known volume of the solvent (50 mL) was taken in the 100 mL beaker which was insulated and then subjected to ultrasonication for 5 min. The actual power (energy) dissipated in the liquid medium was calculated using the following equation, [1]

$$\text{Power } P = mC_P \frac{dT}{dt} \qquad (1)$$

Where C_p is the heat capacity of the solvent (C_p H_2O = 4.2 J g^{-1} K^{-1}, C_p, MeOH =2.14 J g^{-1}. K^{-1}), m is the mass of solvent (g), *dT* is the temperature difference and *dt* refers to the time in seconds. The % energy efficiency (E.E) and the power or acoustic intensity[2] can be calculated as follows:

$$E.E = \frac{\text{Power dissipated in the solvent medium}}{\text{Electric power supplied to the system}} \text{ X } 100 \qquad (2)$$

$$\text{Power intensity } (W/cm^2) = \frac{\text{Power dissipated into the solvent}}{\pi r^2} \qquad (3)$$

2.4. Preparation of Stock solution

Milli pore water (Elix 3 Millipore unit) was used in preparation of the stock solution of fluoride. A 1 L volume of 1000 mg L^{-1} stock solution of fluoride (2.210 g of NaF) was prepared using sodium fluoride (Merck, India) and stored in a polypropylene bottle. Thin disposable nitrile gloves were used to handle fluoride solutions. The working solutions of varying fluoride concentrations for the batch adsorption study were prepared by appropriate dilution.

2.5. Analysis of fluoride concentration

The concentration of fluoride was monitored using ion selective meter (Model No.98185 Hanna Instruments, USA) and a fluoride ion selective electrode (Model No. HI 4110, Hanna Instruments, USA). The ionic strength was adjusted using TISAB II buffer solutions (pH 5.0-5.5) before measuring the fluoride concentration. Fluoride ion selective electrode was calibrated using 1-100 mg L^{-1} of standard fluoride solutions to get a maximum slope between 90-110%. A Metrohm fluoride ion meter (ISE model no.

6.0502.150, Switzerland) along with pH meter (Metrohm 867 pH/ion analysis) was also utilized for monitoring the levels of fluoride before and after adsorption. The electrode was calibrated with standard solutions of fluoride. The total ionic strength was adjusted using (1:100) TISAB II (Total ion adjusting buffer) solutions to get an optimum pH (5.0–5.5) for measurement of fluoride concentration. The standard fluoride solutions of 1.0, 2.0 and 5.0 mg L^{-1} was used to calibrate the electrode. Before analyzing fluoride concentrations in aqueous solution, the fluoride ion selective electrode was calibrated to ensure that slope is obtained between 55-65 mV.

2.6. Batch Adsorption Studies

Batch adsorption studies were conducted by equilibrating for 120 min with 0.1 g of the prepared adsorbent with 100 mL of 5 mg L^{-1} fluoride ion solution at different initial pH levels (Varied from 3.0 to 9.0 by adding 0.1 mol L^{-1} of HCl and NaOH solution) and the F^- ion concentrations before and after adsorption was estimated in the aqueous solution by the ion selective electrode method. The amount of fluoride adsorbed (mg g^{-1}) onto the resin at equilibrium (q_e) was calculated as

$$q_e = \frac{(C_o - C_e)\ V}{W} \qquad (4)$$

Where C_o and C_e are the initial and equilibrium concentrations (mg L^{-1}) of fluoride, V is the aqueous volume (L) and W is the weight of the prepared adsorbent (g). The percentage of the fluoride adsorption onto the prepared adsorbent was estimated by the following expression as,

$$\%\ \text{of}\ F^- \text{ion Removal} = \frac{C_o - C_e}{C_0}\ X\ 100 \quad (5)$$

Where C_o = Initial F^- ion concentration (mg L^{-1}), C_e = Equilibrium F^- ion concentration (mg L^{-1}).

2.7. Adsorption Isotherm

At constant temperature, the relation between the concentration of fluoride and its ability to accumulate onto the adsorbent surface is generally called as an adsorption isotherm. A variety of empirical isotherm models were used to review the experimental fluoride adsorption data. The following linear isotherms have been widely employed in several adsorption studies and these isotherms give important parameters. However, the non-

linear Langmuir, Freundlich and Redlich-Peterson isotherm models were also studied using the Origin 9.0 software.

2.7.1. Langmuir Isotherm

The Langmuir isotherm model[3] is used to calculate the maximum adsorption capacity which is a measure of amount of the fluoride ion adsorbed per unit weight of the adsorbent. The main assumptions in this model include monolayer coverage and site equivalency with homogeneous surface uniformity. The maximum adsorption capacity was obtained by fitting the experimental data to the non-linear and linear Langmuir expression given as

$$q_e = \frac{q_m b C_e}{1 + bC_e} \qquad (6)$$

$$\frac{C_e}{q_e} = \frac{1}{q_m b} + \frac{C_e}{q_m} \qquad (7)$$

where C_e is the equilibrium concentration of the fluoride ion in mg L^{-1} q_e is the amount of fluoride ion adsorbed at equilibrium in mg g^{-1}, q_m is the maximum adsorption capacity in mg g^{-1}, and b is a constant (L mg^{-1}) that relates to the energy of adsorption. The Langmuir plot C_e/q_e against C_e gives the parameters q_o and the constant b respectively. Furthermore, a dimensionless parameter (R_L = 1 / 1 + b C_o) is used to link the energy of adsorption (b) for the Langmuir isotherm in describing the adsorption F ion onto adsorbent surface. Adsorption is irreversible if R_L is zero, while the value higher than 1 signifies unfavorable adsorption. Constructive adsorption is reflected in the value of R_L between 0 to1.[4]

2.7.2. Freundlich Isotherm

The non-linear and linear Freundlich isotherm can be expressed as[5]

$$q_e = K_F C_e^{1/n} \qquad (8)$$

$$\log q_e = \log K_F + \frac{1}{n} \log C_e \qquad (9)$$

In the above expression, the constants K_F and n are the adsorption capacity and the intensity respectively. The K_F and n values were obtained from the slope and intercept of the logarithmic plot of q_e vs C_e. The Freundlich constant n lies between 1-10 ($0.1 < 1/n < 1.0$) which shows the favourable[6] adsorption of fluoride. Generally, the smaller value of 1/n or higher values of n indicates the efficacy of fluoride adsorption onto the adsorbent

surface. The normal L-type (1/n < 1) and cooperative (1/*n* >1) Freundlich isotherm are depends on inverse of Freundlich constant.[6] Freundlich Isotherm explains about the nature of fluoride adsorption onto the heterogeneous adsorbent surface. Fluoride may be adsorbed due to physical (multilayer and cooperative)[7] or chemical (monolayer and L-type)[8] adsorption and it depends on the nature of adsorbate-adsorbent interactions.

2.7.3. Dubinin–Radushkevich (D-R) isotherm

The Dubinin–Radushkevich isotherm (D-R)[9] has similarity to Langmuir isotherm and it gives the adsorption energy and the nature of the adsorption mechanism involved in the interaction between fluoride ion and the prepared adsorbent surface. The D-R isotherm is expressed as

$$\ln q_e = \ln q_m - \beta\varepsilon^2 \qquad (10)$$

Where, q_m is the maximum adsorption capacity and the parameter β is a constant related as

$$\varepsilon = RT \ln\left[1 + \frac{1}{C_e}\right] \qquad (11)$$

In the above equation ε is called as Polanyi potential and the values of β and q_m for this adsorption system are acquired from the slope and intercept of the plot of lnq_e against ε^2. The adsorption energy, E can also be expressed as

$$E = -2\beta^{-0.5} \qquad (12)$$

The negative and positive value of E indicates that the interaction between the fluoride anion and prepared adsorbent is exothermic and endothermic respectively. Hence, this isotherm explains the favourable fluoride adsorption with various temperatures. Furthermore, the mean free energy value lying between 1-8 kJ mol^{-1} indicates physisorption and 8-16 kJ mol^{-1} reflects ion exchange adsorption.[10]

2.7.4. Redlich and Peterson (R-P) isotherm

The R–P isotherm yields an exponent g which could be correlated with the Langmuir model and in addition other constants A and B are also obtained. The R-P isotherm (non-linear) can be expressed as [11]

$$q_e = \frac{AC_e}{1 + BC_e^g} \qquad (13)$$

The above equation shows correspondence with the Langmuir model when g is unity. The corresponding R–P isotherm parameters g and B can be obtained from the linear expression

$$\ln \{A \left[\frac{C_e}{q_e}\right] - 1\} = g \ln C_e + \ln B \quad (14)$$

If the exponent g was found to be 1.0, the adsorption of fluoride can well be explained through the Langmuir isotherm model as well.

2.7.5. Elovich isotherm

The basis of Elovich model[12] isotherm is that the adsorption sites increase exponentially with adsorption, resulting in a multilayer adsorption. The multilayer adsorption governed by the Elovich model is given by the expression[13]

$$ln\frac{q_e}{C_e} = lnK_E q_m - \frac{q_e}{q_m} \quad (15)$$

Where K_E and q_m are characteristic equilibrium constant and the adsorption capacity. The Elovich isotherm parameters are obtained from the plot of $\ln(q_e/C_e)$ against q_e.

2.7.6.Temkin Isotherm

In this isotherm the heat of adsorption of all the molecules in the layer decreases linearly with surface coverage[14] due to adsorbent-adsorbate interactions with uniform distribution of binding energies until it reaches a maximum value.[14] The Tempkin and Pyzhev[15,16] model is represented by the equation,

$$q_e = B_1 \ln K_T + B_1 lnC_e \quad (16)$$

Values of B_1 and K_T were calculated from the plot of q_e against $\ln C_e$ where $RT/b = B_1$. From the slope and intercept of this plot, the variation of adsorption energy and the Temkin equilibrium constant can be calculated respectively.

2.8. Adsorption kinetics

A known weight of the prepared adsorbent was added to a known volume of different initial fluoride concentrations and constantly stirred. The initial pH of the solution was adjusted to 7.0. The fluoride ion concentrations in solution phase were measured at 1, 2, 5, 10, 15, 20, 30, 40, 50, 60 min time intervals. The adsorption kinetics was studied using the linear pseudo first order[17] and the second order rate equations[18]

$$\log(q_e - q_t) = logq_e - \frac{k_1 t}{2.303} \quad (17)$$

$$\frac{t}{q_t} = \frac{1}{k_2 q_e^2} + \frac{t}{q_t} \qquad (18)$$

Furthermore, the nonlinear pseudo-first and second order models were also used to evaluate the kinetics fluoride adsorption. The non-linearized form of the pseudo-first order equation[17] is generally expressed as

$$q_t = q_e(1 - e^{-K_1 t}) \qquad (19)$$

Where q_e and q_t refers to the adsorption capacity at equilibrium and at time t, respectively. and k_1 is the pseudo first order rate constant.

The pseudo-second order kinetic model[18] is represented as

$$q_t = \frac{k_2 q_e^2}{1 + k_2 q_e t} \qquad (20)$$

Herein, k_2 is the overall rate constant of pseudo-second order adsorption. In addition, Weber–Morris[19] intraparticle diffusion is used to ascertain whether intraparticle diffusion is the rate-determining step. The Weber-Morris intraparticle diffusion[19] equation also used to evaluate the adsorption kinetics and it can be expressed as

$$q_t = k_{int} t^{0.5} \qquad (21)$$

In this model, a plot of q_t versus $t^{0.5}$ would be linear and only if the plot passes through the origin then intraparticle diffusion is the only rate-limiting step.The plot was linear in fluoride adsorption process giving the intraparticle rate constant (k_{int}) and a non-zero intercept pointing to the fact that boundary layer phenomenon could also direct the adsorption of fluoride onto the prepared adsorbent surface. Therefore, the overall rate of adsorption of fluoride ion onto the prepared adsorbent surface could be influenced[20] by the following steps

(i) External mass transfer in which the fluoride ion is transported from the bulk solution to the adsorbent exterior surface.

(ii) Intraparticle or pore diffusion in which fluoride ions permeate to the interior of the adsorbent particles or in the pore and in the adsorbate along the pore walls

(iii)Fluoride ions diffuse within the particle and on the external surface. Hence, the overall adsorption rate could be controlled by surface or intraparticle diffusion.

A linear plot of q_t vs $\sqrt{t}$ with non-zero intercept signifies that the intraparticle diffusion is not the only rate limiting step.

2.9. Adsorption Thermodynamics

The adsorption of fluoride was tested at different temperatures to ascertain the spontaneity from the equilibrium constant (K) values. Adsorption free energy (ΔG^0), adsorption enthalpy (ΔH^0) and adsorption entropy (ΔS^0) were calculated from the classic Van't Hoff plot of lnK against 1/ T. The Van't Hoff equation is expressed as follows,[21,22]

$$\Delta G^o = -RT lnK_c \qquad (22)$$

$$lnK_c = \frac{-\Delta H^o}{RT} + \frac{\Delta S^o}{R} \qquad (23)$$

Where is R is universal gas constant ($JK^{-1}mol^{-1}$), T is the temperature (Kelvin) and K_c is the equilibrium constant obtained from the ratio of concentration of fluoride ion adsorbed on the prepared adsorbent to that in the solution. Also, the activation energy (E_a) required for favorable fluoride adsorption was obtained using the expression[23]

$$E_a = \Delta H^0_{ads} + RT \qquad (24)$$

The magnitude of ΔH^0 would reflect the adsorption mechanism. If physical adsorption occurs, then ΔH^0 is usually lower than 80 kJ mol^{-1}, while for chemical adsorption the value lies in the range 80 - 400 kJ mol^{-1}.[24]

References

1. Gogate, P. R.; Shirgaonkar, I. Z.; Sivakumar, M.; Senthilkumar, P.; Vichare, N. P.; Pandit, A. B. *AIChE J.* **2001**, 47, 2526.
2. Sun, Y. J.; Ma, G. P.; Ye, X. Q.; Kakuda, Y.; Meng, R. F. *Ultrason. Sonochem.* **2010**, 17, 654.
3. Langmuir, I. *J. Am. Chem. Soc.* **1918**, 40, 1361.
4. Sairam, S. C.; Viswanathan, N.; Meenakshi, S. *J. Hazard. Mater.* **2008**, 155, 206.
5. Freundlich, H. M. F. *Z. Phys. Chem.* **1906**, 57, 385.
6. Ru-Ling, T.; Feng-Chin, W.; *J. Hazard. Mater.* **2008**, 155, 277.
7. Garg, V. K.; Gupta, R.; Kumar, R.; Gupta, R. K. *Bioresour. Technol.,* **2004,** *92,* 79.
8. Selvi, K.; Pattabhi, S.; Kadirvelu, K. *Bioresour. Technol.* **2001,** *80,* 87.
9. Foo, K. Y.; Hameed, B. H. *Chem. Eng. J.* **2010**, 156, 2.
10. Srivastava, V.; Weng, C. H.; Singh, V. K.; Sharma, Y. C. *J. Chem. Eng. Data* **2011**, *56*, 1414.
11. Redlich, O.; Peterson, D. L.; *J. Phys. Chem.* **1959**, 63, 1024.
12. Elovich, S. Y.; Larinov, O. G. *Izv. Akad. Nauk. SSSR, Otd. Khim. Nauk* **1962,** *2,* 209.
13. Ncibi, M. C. J. Hazard. Mater. **2008**, 153, 207.
14. Nigussie, W.; Zewgeb, F.; Chandravanshib, B. S. *J. Hazard. Mater.* **2007**, 147, 954.
15. Tempkin, M. J.; Pyzhev, V. *Acta Physiochim. URSS* 1940, 12, 327.
16. Temkin, M. I. *Zh. Fiz. Chim*. **1941,** *15,* 296
17. Lagergren, S.; *K. Sven. Vetenskapsakad. Handl.* **1898**, 24, 1.
18. Ho, Y. S. *J. Hazard. Mater. B* **2006**, 136, 681.
19. Weber, W. J.; Morris, J. C. *J. Sanit. Eng. Div. Am. Soc. Civ. Eng.***1963**, 89, 3.
20. Mittal, A.; Kurup, L.; Mittal, J. *J. Hazard. Mater.* **2007**, 146, 243.
21. Thakre, D.; Rayalu, S.; Kawade, R.; Meshram, S.; Subrt, J.; Labhsetwar, N. *J. Hazard. Mater.* **2010**, 180, 122.
22. Khan, A. A.; Singh, R. P. *Colloid Surf.* **1987**, 24, 33.
23. Kumar, A. S. K.; Kalidhasan, S.; Vidya, R.; Rajesh, N. *Ind. Eng. Chem. Res.* **2012**, 51, 58.
24. Gubbuk, I. H. *J. Hazard. Mater.* 2011, 186, 416.

CHAPTER 3

3. Aluminum (III) and Zirconium (IV) impregnated onto the Cellulose Biopolymer matrix for the removal of fluoride in aqueous solutions

3.1. Abstract

This chapter deals the modification of cellulose biopolymer with aluminium (III) and zirconium (IV) metal ions using microwave and ultrasonic assisted methods of preparation for defluoridation of water. Due to their relative abundance, low cost, good stability and chemical reactivity, biodegradability and presence of different functional groups, biopolymer based adsorbents are quite useful for the defluoridation of water. Cellulose is a linear polymer of β – (1,4) –D- glucopyranose units and each glucose unit has three hydroxyl groups that could bond with Zr and Al metal ions.[1] It is a natural polysaccharide endowed with intramolecular hydrogen bonding and good stability.[2] The small size of fluoride, high electronegativity and its behavior as a hard base also makes it compatible with metal ions such as aluminium and zirconium. Taking advantage of this fact, cellulose biopolymer was explored as an effective matrix for impregnation of zirconium and aluminium through electrostatic interaction with the hydroxyl groups in cellulose. The hydrogen bonding interaction between the cellulose hydroxyl groups and fluoride also influences the adsorption of fluoride anion on the surface of the cellulose biopolymer. Herein, a novel and environmentally benign approach for defluoridation of water based is proposed based on microwave and ultrasonication assisted impregnation of Al (III) and Zr(IV) metal ions onto the cellulose biopolymer matrix.

The first part of this chapter deals with a microwave assisted preparation of Al (III) and Zr (IV) impregnated cellulose adsorbent for fluoride removal in aqueous solution. The adsorbent prior and subsequent to the adsorption of fluoride was characterized comprehensively using FT-IR, EDX and XRD studies. Various adsorption isotherm models, kinetics and thermodynamics were also studied in detail.

The second part of this chapter deals with a novel ultrasound assisted methodology involving the impregnation of zirconium in a cellulose matrix. The role of ultrasonication in the preparation of an adsorbent followed by characterization is also discussed in detail.

3.2. Microwave assisted preparation of Al (III) and Zr (IV) impregnated Cellulose Biopolymer adsorbent for defluoridation

3.2.1. Introduction

A variety of adsorbents have been reviewed for defluoridation.[3] Activated alumina is one of the versatile and well-known adsorbents for removing fluoride,[4] but the pH of the treated water and the leaching of excess aluminium is one concern that needs to be addressed in this methodology. Activated alumina and magnesia amended activated alumina[5] have been utilized for defluoridation with an adsorption capacity of 4.04 mg g^{-1} and 10 mg g^{-1} respectively. Alumina chitosan composite has been tested for defluoridation from villages with a defluoridation capacity of 3800 mg kg^{-1}.[6] Nano hydroxyapatite/chitosan composite,[7] magnesia/chitosan composite[8] are also known to exhibit good defluoridation capacity. Lanthanum impregnated carboxylated chitosan beads[9] have been studied for the removal of fluoride with an adsorption capacity of 4.7 mg g^{-1}. Similarly, zirconium tungstophosphate coated chitosan[10] has also proved to be equally effective for defluoridation. Alagamuthu and Rajan[11] have studied the removal efficiency of fluoride from a fluoride endemic area using zirconium impregnated cashew nut shell carbon. Zr(IV) impregnated collagen fiber[12] is yet another novel adsorbent reported for defluoridation with an adsorption capacity of 2.29 mmol/g at pH 5.5. Fe (III) coordinated amine modified PGMA grafted cellulose[13] and acidic alumina[14] have also proven to be effective for defluoridation.

Despite the varied methods for the removal of fluoride, there is still a growing need and demand for the development of more effective and simpler adsorbents with good removal efficiency. The objective of the present investigation is to develop a novel Al-Zr impregnated cellulose biopolymer adsorbent so as to bring down the concentration of fluoride to less than the stipulated toxic limit. The efforts channelized towards the development of this novel sorbent material by optimizing various analytical parameters are discussed at length.

3.2.2. Experimental Section

(i) Adsorbent Preparation

A known weight of cellulose biopolymer (2.0 g) was dispersed in the minimum amount (1-1.5 mL) of DMF. About 2.0 g of activated alumina and 1.0 g of zirconium oxychloride were added to the dispersed cellulose and stirred for 5-10 min to get a homogeneous mixture. It was subjected to microwave irradiation at 160W for 2 min with 30 sec alternating time interval, and washed with Millipore water. The Al-Zr impregnated biopolymer adsorbent was dried at 60 °C in a vaccum oven (Biotechnics, India) for 4 hours and further characterized analytically thoroughly through various techniques.

(ii) Adsorption Studies

The batch adsorption studies were conducted by equilibrating 0.3 g of the AlZrIC adsorbent material with 50 mL of 5 mg L^{-1} fluoride ion solution at pH 5.5 in an orbital incubator shaker (Biotechnics, India) for varying time intervals and the concentration of fluoride in the solution phase was estimated by the ion selective electrode method. The percentage of fluoride adsorbed increased with time with good removal efficiency at 60 min thereby bringing down the concentration to less than 1.0 mg L^{-1} level.

(iii) Column Study

The applicability of the Al-Zr impregnated cellulose adsorbent material on a laboratory scale was examined for the defluoridation of water from a larger sample volume using a glass column (2.5 cm diameter, 30 cm length) by packing 2.0g of the adsorbent. A known volume (300 mL) of tap water (original fluoride conc 0.6 mg L^{-1}) spiked with 3 mg L^{-1} fluoride ion was transferred to the column at a flow rate of 8 mL min^{-1} and the concentration of fluoride was measured in the emerging solution. The concentration of fluoride was found to be 0.72 mg L^{-1} signifying a fluoride removal efficiency of greater than 80%. The column could be re-used by desorption with 5ml of 1mol L^{-1} sodium hydroxide as sodium fluoride in the eluate.

3.2.3. Results and Discussion

(i) Characterization of the adsorbent

The FT-IR spectrum (Figure 3.1 and 3.2) shows characteristic peaks pertaining to the different functional groups in cellulose[15,16] and Al-ZrIC adsorbent. A strong peak at 3328 cm^{-1} is associated with O-H stretching and that at 2901 cm^{-1} is due to C-H stretching in the biopolymer. A strong peak at 901 cm^{-1} emanates from the C-O-C pyranose ring vibration.[15] The peak at 1643 cm^{-1} could be ascribed to the H-OH hydrogen bonding. The peaks characteristic of Al-ZrIC were observed at 787 cm^{-1}, 841cm^{-1}(Al-O stretching vibration and Zr-O-C vibration) and 1701cm^{-1} (formation of C=O by partial oxidation of cellulose) respectively.[17,18,19,20,21] The interaction of zirconium and aluminium with glycosidic linkage of the cellulose biopolymer is evident from the decrease in the peak intensity at 901 cm^{-1}. The O-H peak also shows some broadening after the adsorption of fluoride. The FT-IR spectrum (Figure 3.1 and 3.2) shows some distinct peaks for the various functional groups in Al-ZrIC bioadsorbent before and after fluoride adsorption. Significant changes occur after the adsorption of fluoride ion with the appearance of deformation peaks at 584 cm^{-1} and 567 cm^{-1} attributed to the adsorption of fluoride on the adsorbent surface.[22] Furthermore, new peak appears at 763 cm^{-1} and the peak intensity increases in the range 500-900 cm^{-1}. The hydrogen bonding interaction (–OH---F)[15,16] is evident from the peak at 763 cm^{-1} and the metal-fluoride interactions are dominant in the region 500-900 cm^{-1}.

The SEM images (Figure 3.3) clearly shows the structural and morphological changes in cellulose, Al/ZrIC adsorbent on and after fluoride adsorption. The EDX spectrum (Figure 3.4) confirms the presence of Al and Zr elemental peaks on the surface of the cellulose biopolymer and this indicates that Al and Zr were successfully loaded onto the cellulose matrix. The adsorption of fluoride on the surface of the Al/ZrIC adsorbent was ascertained from the EDX spectrum which shows the presence of fluorine along with the other major peaks such as C, O, Al and Zr respectively.

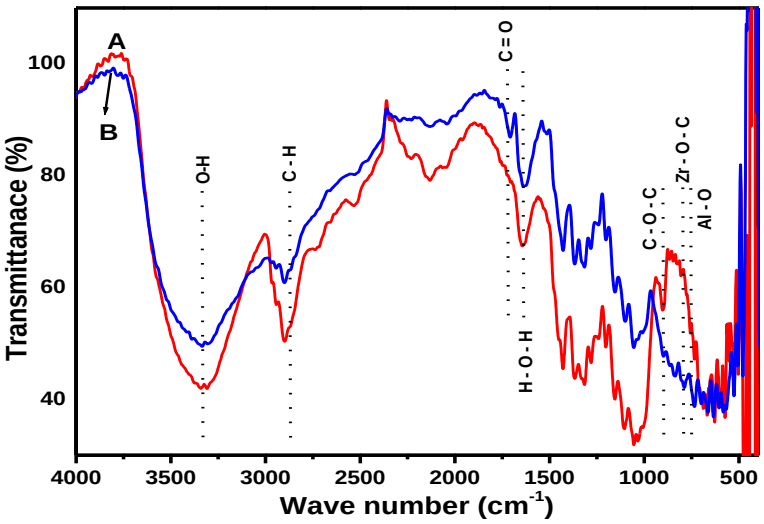

Figure 3.1. FT-IR spectrum of cellulose biopolymer (A) and Al/Zr impregnated cellulose adsorbent (B)

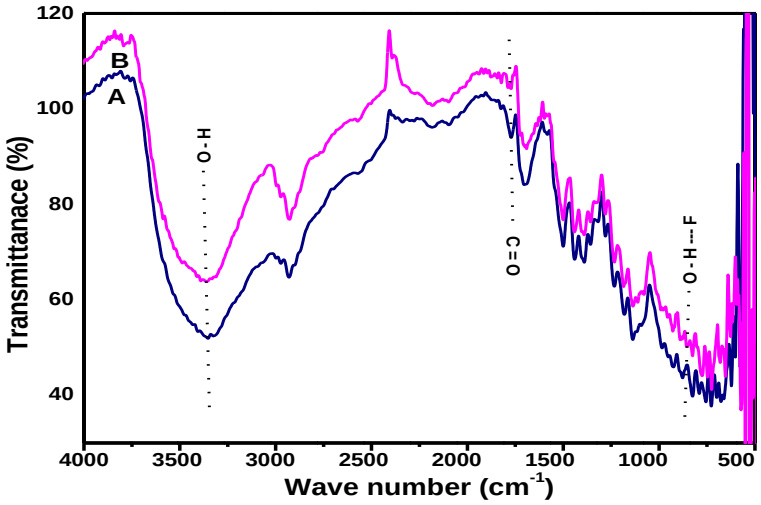

Figure 3.2. FT-IR spectrum of Al/Zr impregnated cellulose adsorbent (A) and the fluoride adsorbed (B)

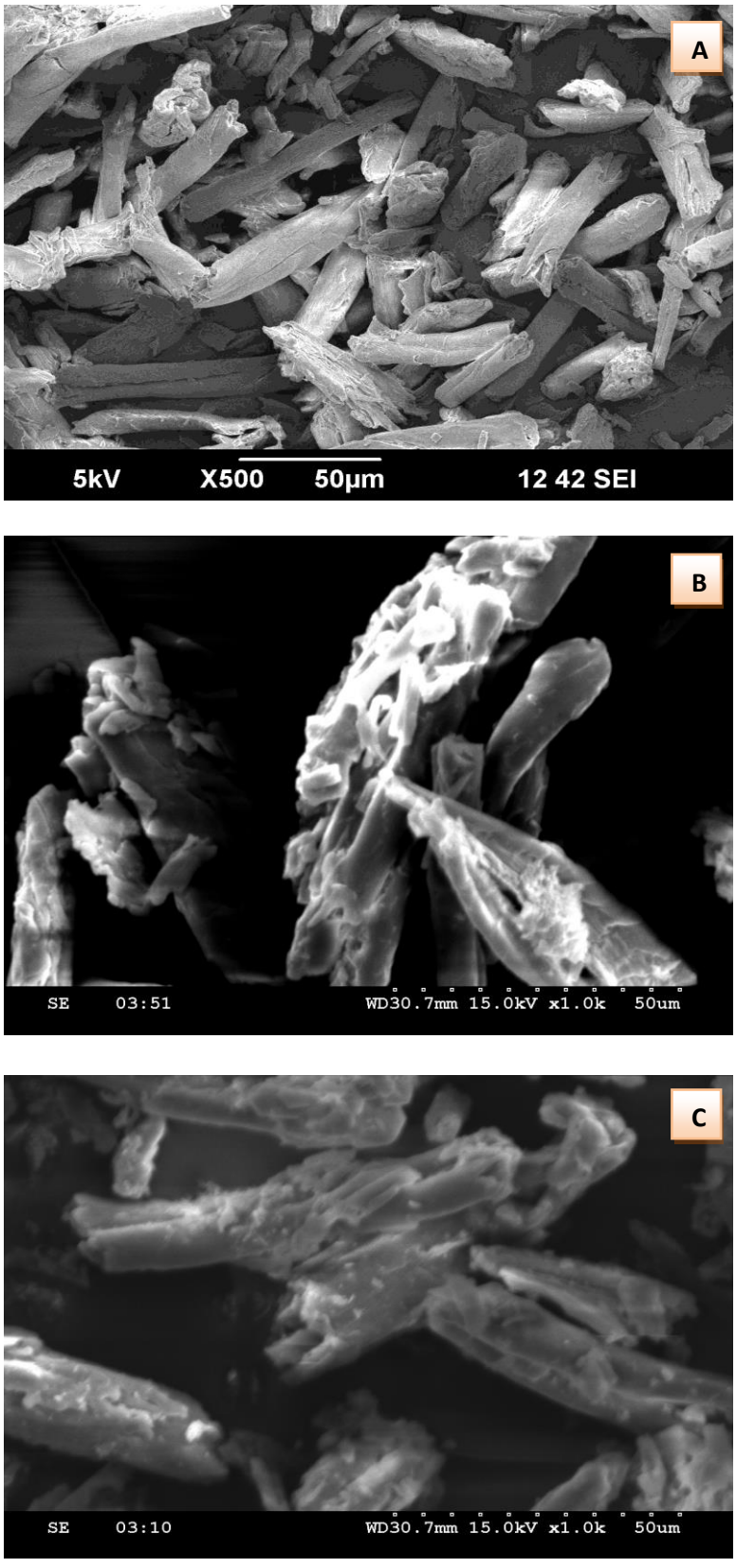

Figure 3.3. SEM images of Cellulose biopolymer (A) Al/ZrIC bio adsorbent (B) and fluoride ion adsorbed (C) on the adsorbent

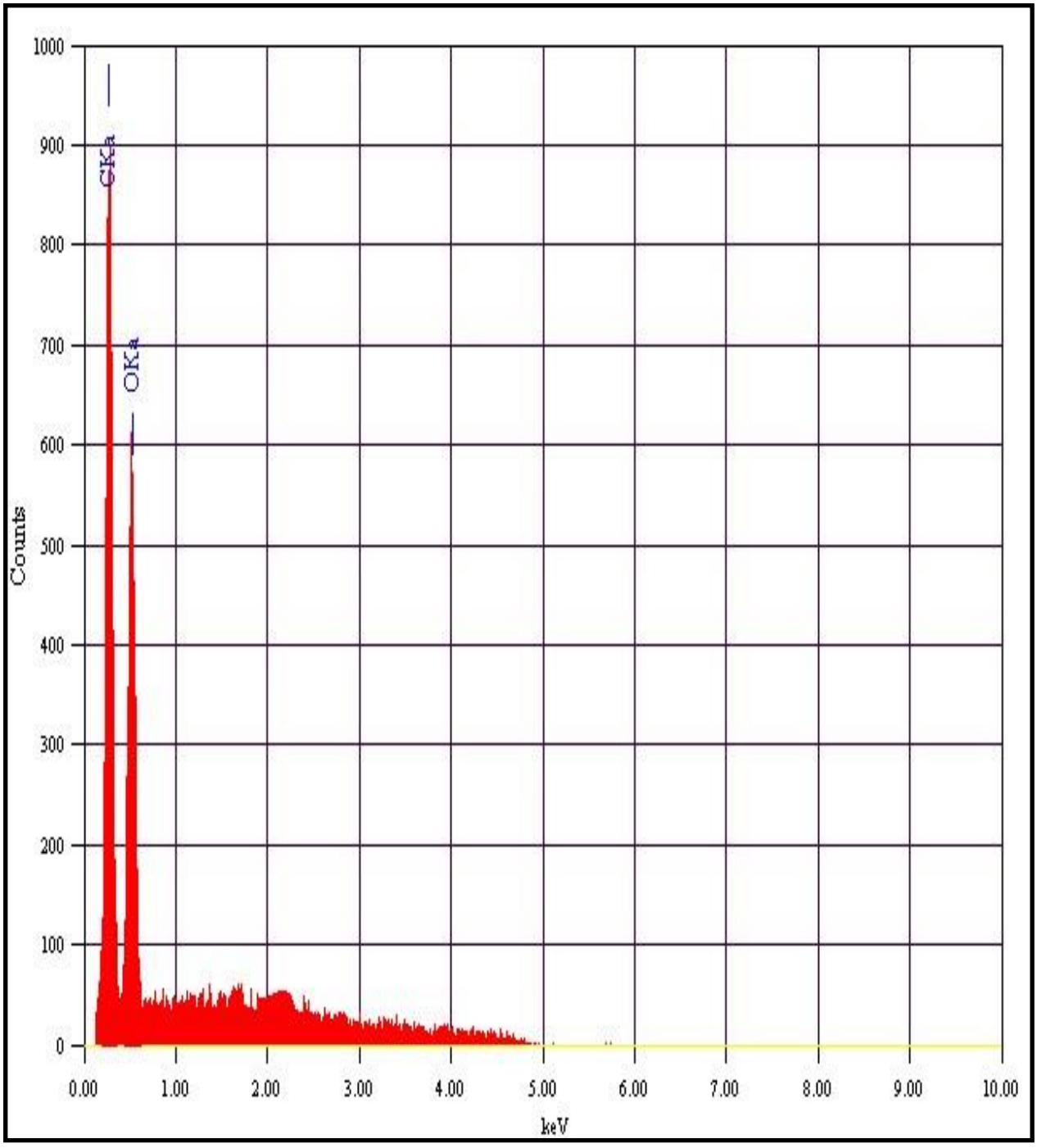

Figure 3.4a. EDX Figures of Cellulose biopolymer

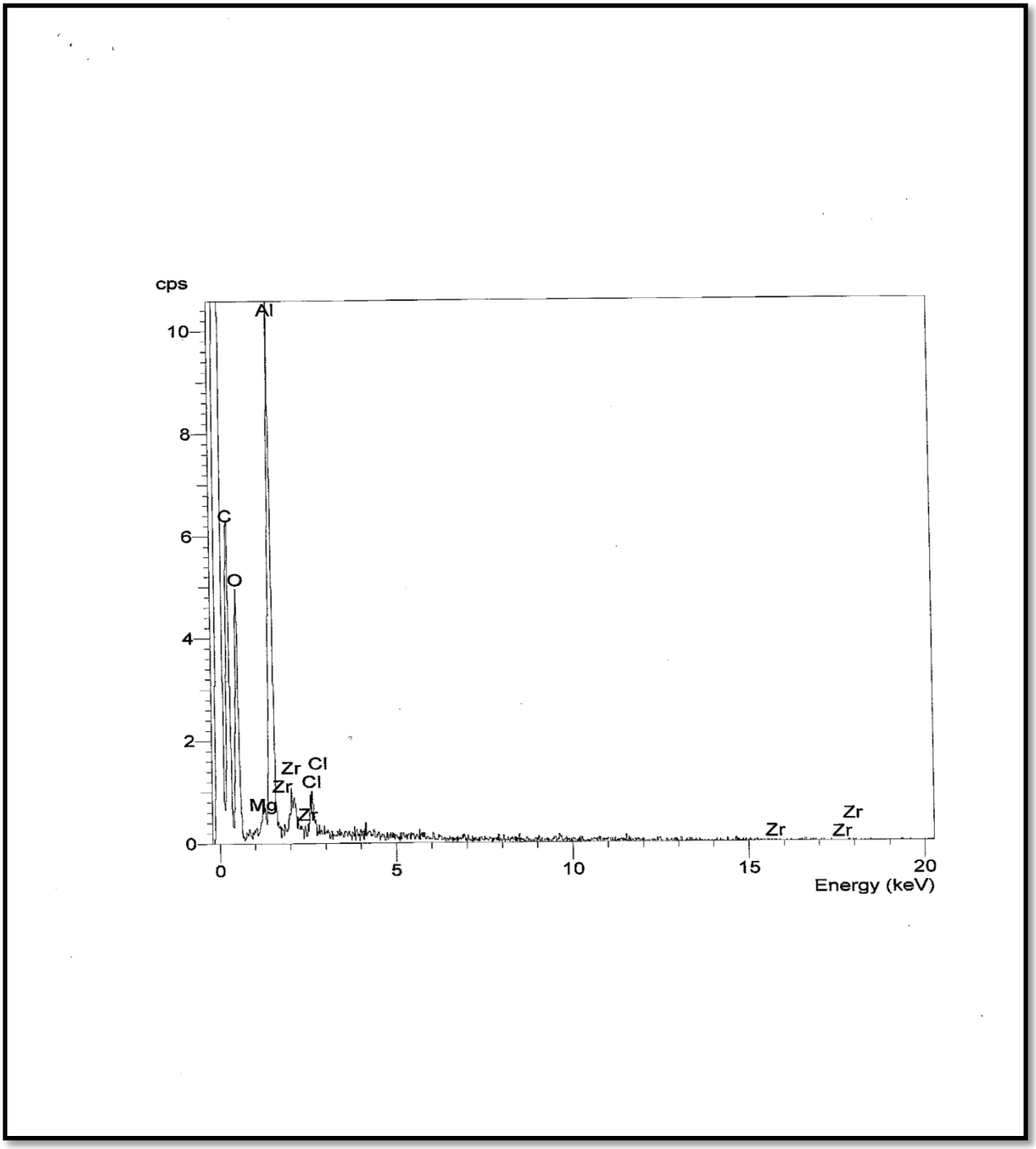

Figure 3.4b. EDX Figure of Al/ZrIC bio adsorbent

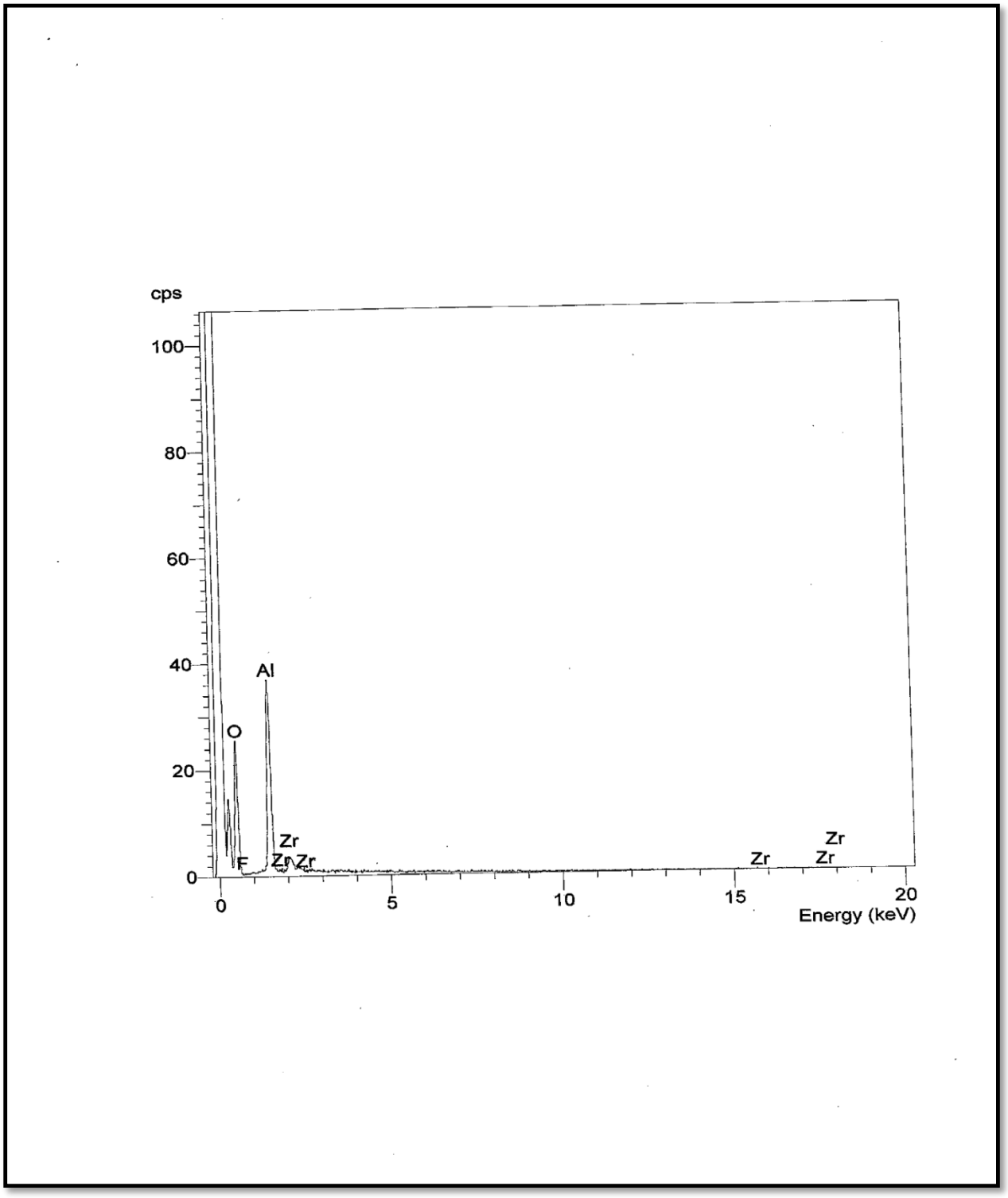

Figure 3.4c. EDX Figure of Al/ZrIC bio adsorbent after fluoride ion adsorbed on the adsorbent surface

The observed diffraction peaks (Figure 3.5a) for native cellulose[23] at 2θ = 14.78^0, 16.42^0, 22.8^0 and 34.57^0 correspond to the planes (-101), (101), (002) and (-231) respectively. These planes are associated with the d-spacing values 6.04, 5.39, 3.88, and 2.65 Å respectively (JCPDS No. 03-0289). After the impregnation of metal ions onto the cellulose matrix (Figure 3.5b), the above peaks are shifted corresponding to 2θ values 37.73^0, 37.70^0, 42.81^0, 46.08^0, and 67.53^0. The average crystallite size was calculated from the full width at half-maximum of the peak using Debye Scherrer's equation[23]

$$D = \frac{0.9\lambda}{\beta cos\theta} \qquad (25)$$

Where D is the average crystallite size in nm, λ is the characteristic wavelength of X-ray used (1.5406 Å), θ is the diffraction angle, and β is the angular width at intensity equal to half of the maximum peak intensity. The average crystallite size of cellulose biopolymer decreased from 8.048 to 1.06 µm due to the strong interaction of the interaction of metal ions with the glycosidic linkage of cellulose biopolymer which was also confirmed by FTIR spectra. The new sharp peaks corresponding to 2θ value 37.70^0 and 67.53^0 could be ascribed to aluminium oxide (JCPDS – 04-0877) and illustrates that the metal ions have been successfully impregnated onto cellulose biopolymer. Moreover, the peaks corresponding to 37.73^0 and 46.08^0 are assigned to the γ alumina phase.[24] After the fluoride adsorption, XRD pattern of AlZrIC biopolymer (Figure 3.5c) adsorbent shows peaks corresponding to 2θ values 37.65^0, 39.63^0, 42.64^0, 45.85, and 67.15^0. Herein, the average crystallite size of the cellulose biopolymer increased from 1.06 to 8.38 µm and this could be attributed to the hydrogen bonding interaction between the cellulose hydroxyl groups and fluoride.The new sharp peaks corresponding to 2θ value 37.65^0 and 39.61^0 indicates the presence of aluminium fluoride (JCPDS– pdf no.47-1659).The peaks at 42.64^0 and 45.85^0 are due the formation of zirconium oxy fluoride (JCPDS – pdf no.39-1216) and zirconium fluoride (JCPDS–pdf no.39-1217) on Al-Zr impregnated cellulose biopolymer adsorbent.

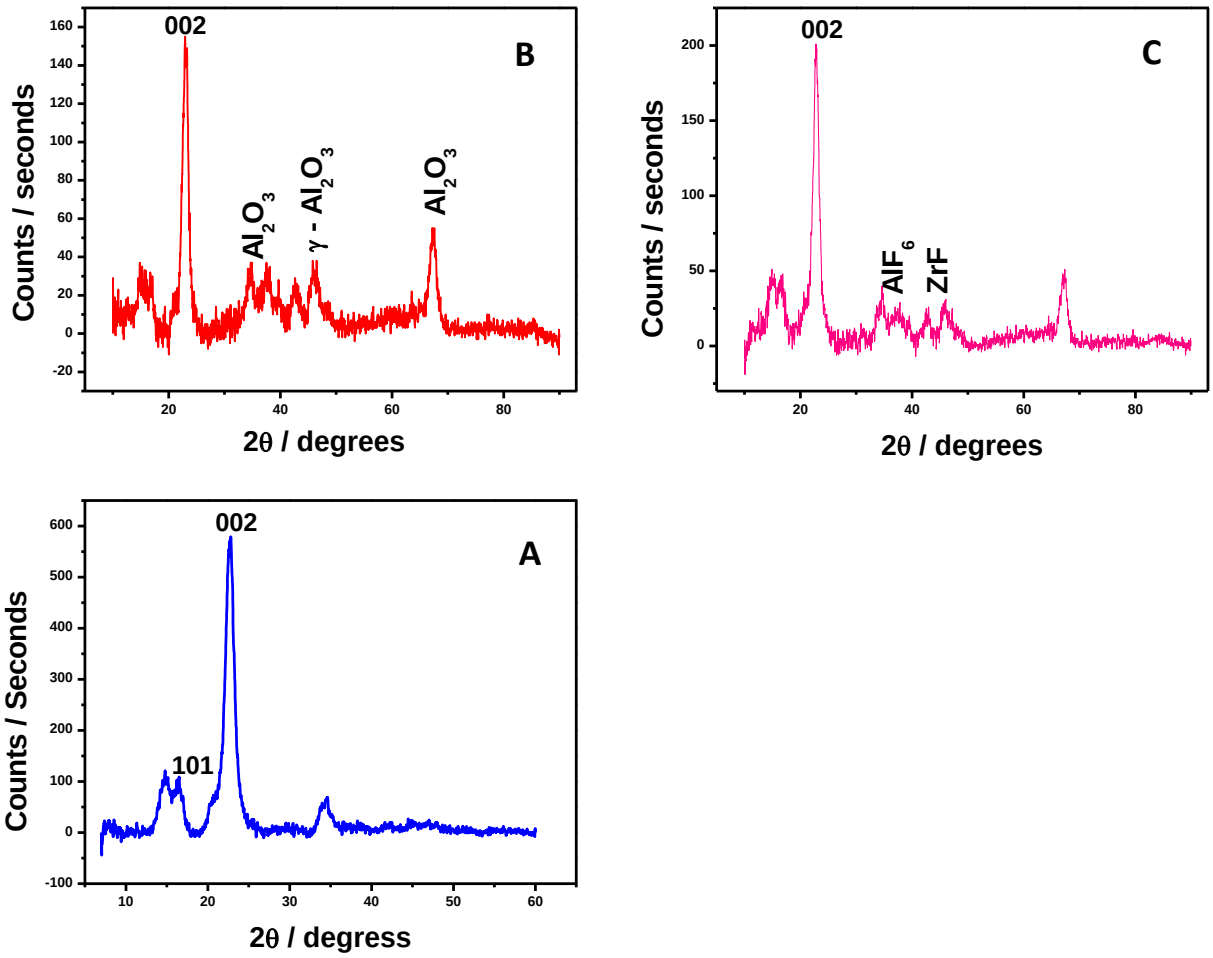

Figure 3.5. XRD pattern of Cellulose biopolymer (A) Al/ZrIC biopolymer adsorbent (B) after fluoride ion adsorption on the adsorbent (C)

(ii) Amount of Adsorbent

The amount of adsorbent used in the batch study with 5 mg L^{-1} fluoride was varied in the range 0.1-1.0 g. The removal of fluoride was effective in the range 0.3-0.5 g in 50 mL sample volume. The initial increase in adsorption is attributed to the strong electrostatic attraction between the fluoride anion and the Al/ZrIC biopolymer adsorbent. Beyond 0.3 g, there was no appreciable increase in the percentage adsorption, which indicates the saturation of the active adsorption sites.

(iii) Effect of pH

The effect of pH is important in the adsorption of fluoride. Due to the small size and high electronegativity, fluoride is solvated and the undissociated HF at very low pH can lead to a reduction in the removal efficiency of fluoride.[25] The pH at the point of zero charge (pH_{PZC}) of the adsorbent was determined by batch equilibration technique.[26,27] About 0.2g of Al-Zr adsorbent added to 50 ml of 0.1M KNO_3 solution and the initial pH was adjusted from 3.0 to 9.0 by the addition of 0.1mol/L HCl or NaOH. The experiments were carried out in a thermostat shaker at 25 ◦C for 24 h. After a time period of 24 hours, the final pH values of supernatant solutions were measured. The pH_{PZC} of the Al-Zr impregnated cellulose biopolymer adsorbent was determined from the plot of ΔpH [$pH_{initial} - pH_{final}$] versus $pH_{initial}$ (Figure 3.6a).

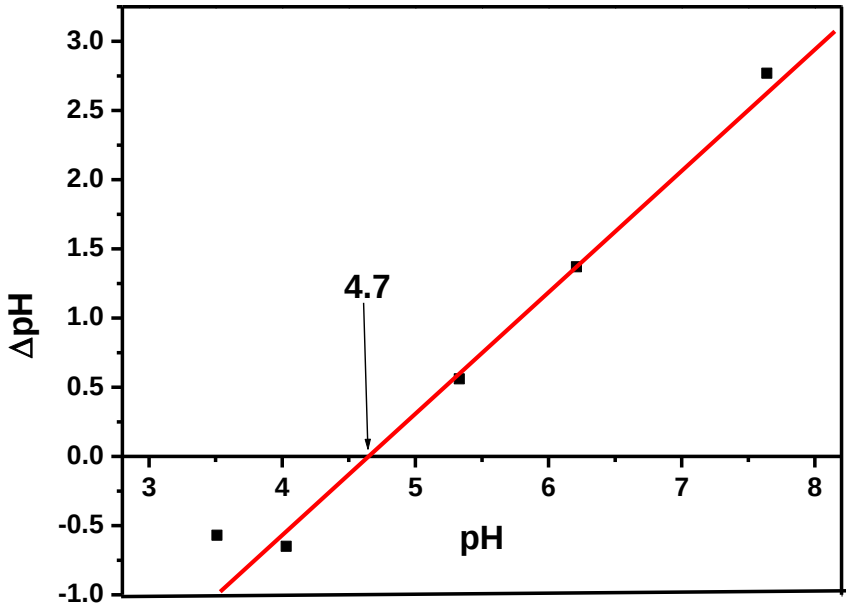

Figure 3.6a. Point of zero charge for the Al-Zr Impregnated Cellulose biopolymeradsorbent

The effect of solution pH on fluoride adsorption is presented in Figure 3.6b. The adsorption decreases to 46.37% at high pH values. In the pH range 2.5-3.5, Al and Zr cationic complexes interact with fluoride effectively. At pH < 4.0, the extent of fluoride adsorption increased but turbidity was observed in the aqueous phase attributed to the formation of HF and HF_2^- which interacts with Al and Zr metal ions effectively to form soluble metal fluorides.

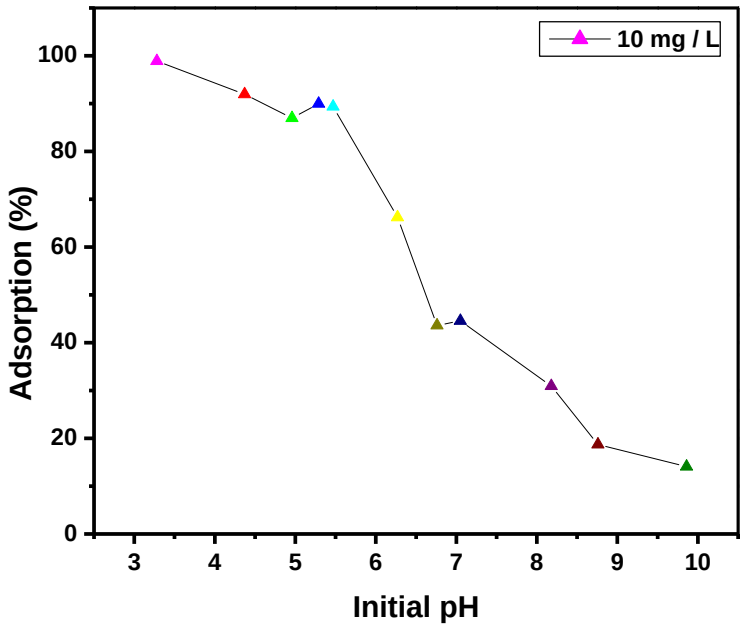

Figure 3.6b. Effect of pH on the adsorption of fluoride

It is well-known that $Al(OH)_3$ dissolves to form soluble species of aluminium at low or high pH conditions.[28] It is possible that $Al(OH)_3$ would yield soluble aluminates ($[Al(OH)_4]^-$) at sufficiently alkaline pH. The formation of these soluble Al species affects the effective interaction of the cationic hydroxides of aluminium and zirconium with fluoride. However, in the pH range 4.5-5.5, there is no turbidity in the aqueous solution that emerges after adsorption and this shows that Al and Zr cationic complexes strongly bind with the cellulose biopolymer and effectively interacts with fluoride. Indeed, in this

pH range, the concentration of fluoride remaining in the solution was found to be less than the permissible value of 1.0 mg L^{-1}. When pH < pHpzc the surface charge would be positive, and at pH > pHpzc, it would be negative. The results of the zero point of charge of the Al-Zr impregnated biopolymer adsorbent (pH_{PZC} = 4.7) was depicted in Figure 3.6a. This shows that at pH less than 4.7 the surface of the Al-ZrIC adsorbent is predominated by positive charges while at pH greater than 4.7 the surface is predominated by negative charges. Therefore, the protonized adsorbent surface favors the adsorption of fluoride, whereas above pHpzc, more of surface sites are negatively charged and the fluoride would be adsorbed to a lesser extent due to the repulsive interaction between F^- ions and negative adsorbent surface.

In a weakly acidic medium, the fluoride ion interacts with the positively charged hydroxyl groups present on the metal ions and the cellulose biopolymer composite surface as evidenced by the FT-IR study. According to Pearson's classification, fluoride is grouped as a hard base[29] while aluminium and zirconium are classified as hard acids respectively. Hence, there could be an effective interaction between the positively charged metal ion and negatively charged fluoride anion as shown below

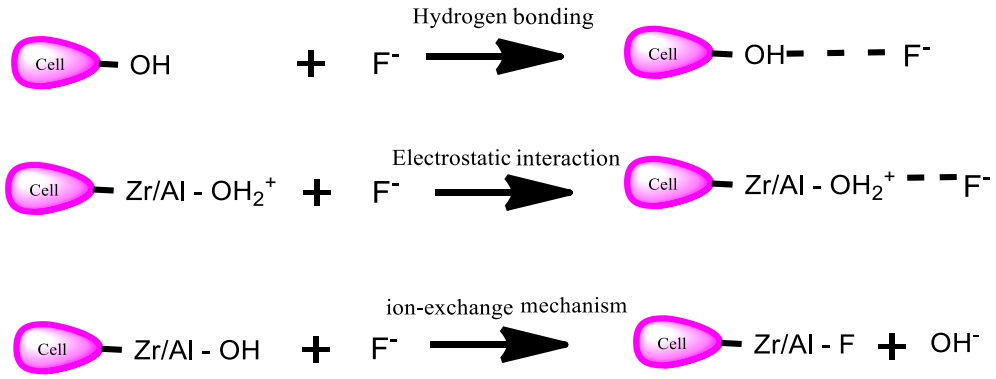

Beyond pH 5.5, there is a decrease in the percentage adsorption of fluoride. This could be attributed to the deprotonation of the surface hydroxyl groups in the Al-ZrIC adsorbent and similarly at higher pH, the competition of the hydroxide anion with the fluoride anion for the active adsorption sites could also lead to a reduction in the percentage adsorption of fluoride. Three replicate analyses yielded a reduction of fluoride in the aqueous solution to 0.6 ± 0.02 mg L^{-1}, which is appreciably less than the permissible limit.

(iv) Mechanism of interaction of Al-Zr impregnated cellulose with fluoride

Microwave-assisted preparation of the adsorbent ensures efficient dielectric heating and under microwave (MW) irradiation there is rapid energy transfer from the cellulose hydroxyl groups to neighboring molecules.[30] Further MW radiation also results in[31] lowering of Gibbs energy of activation thereby promoting the effective interaction of the cationic $Zr(OH)_2^{2+}$ and $Al(OH)_2^{+}$ hydroxides with the hydroxyl groups of cellulose. The mechanism of fluoride ion interaction with Al-Zr impregnated cellulose is shown in Figure 3.7. The metal ion interacts with the glycosidic linkage of cellulose in the form of a strong electrostatic attraction. In aqueous solution, aluminium and zirconium ions could exist as cationic hydroxides such as $Al(OH)_2^{+}$, $Zr(OH)_2^{2+}$etc and these species also interact with fluoride through electrostatic attractive forces. Furthermore, the hydrogen bonding interaction between the cellulose hydroxyl groups and fluoride would further reinforce the adsorption of fluoride anion on the surface of the Al-Zr biopolymer adsorbent.

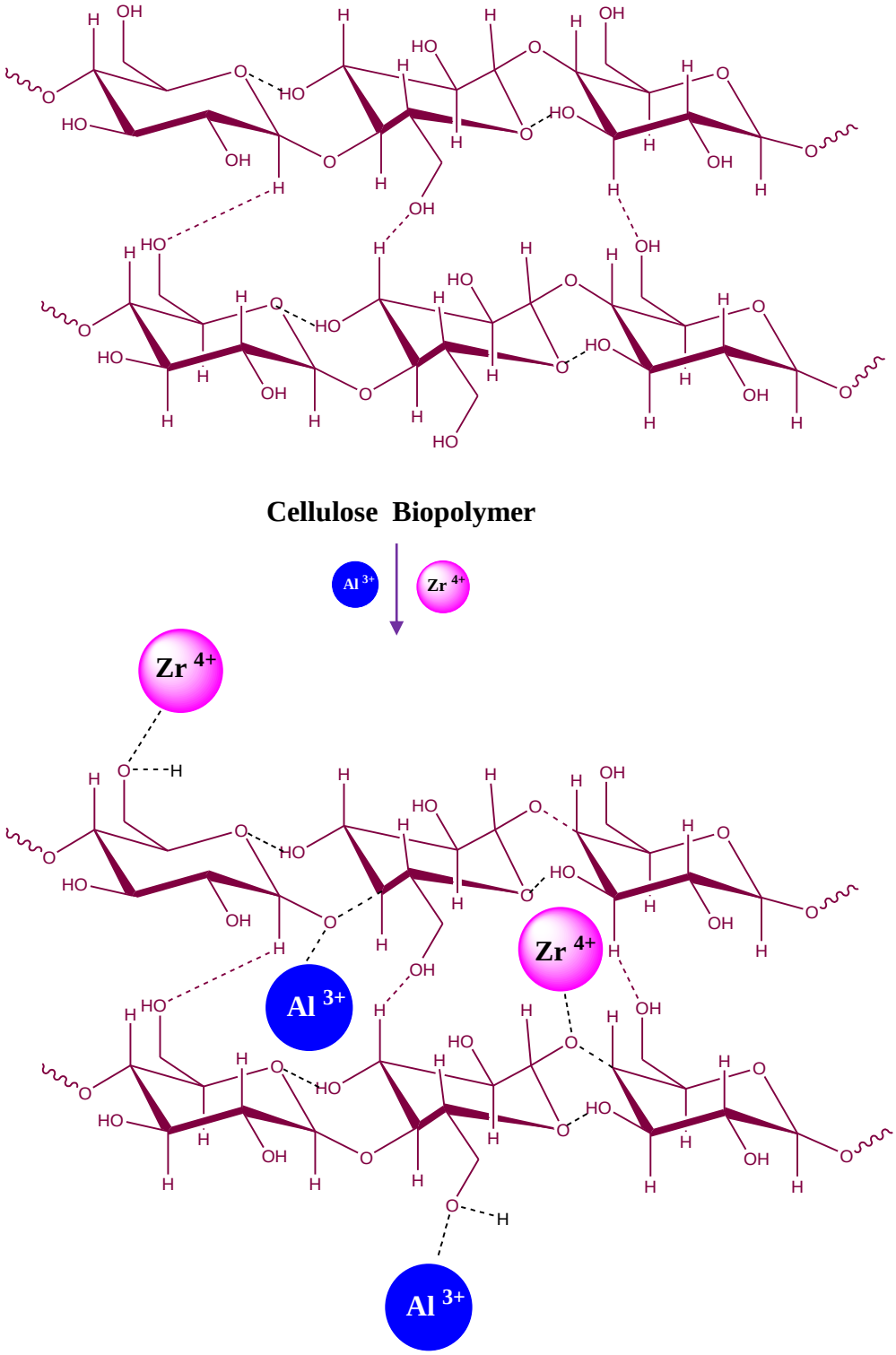

Figure 3.7a. The schematic diagram shows the interaction of metal ions with cellulose biopolymer surface

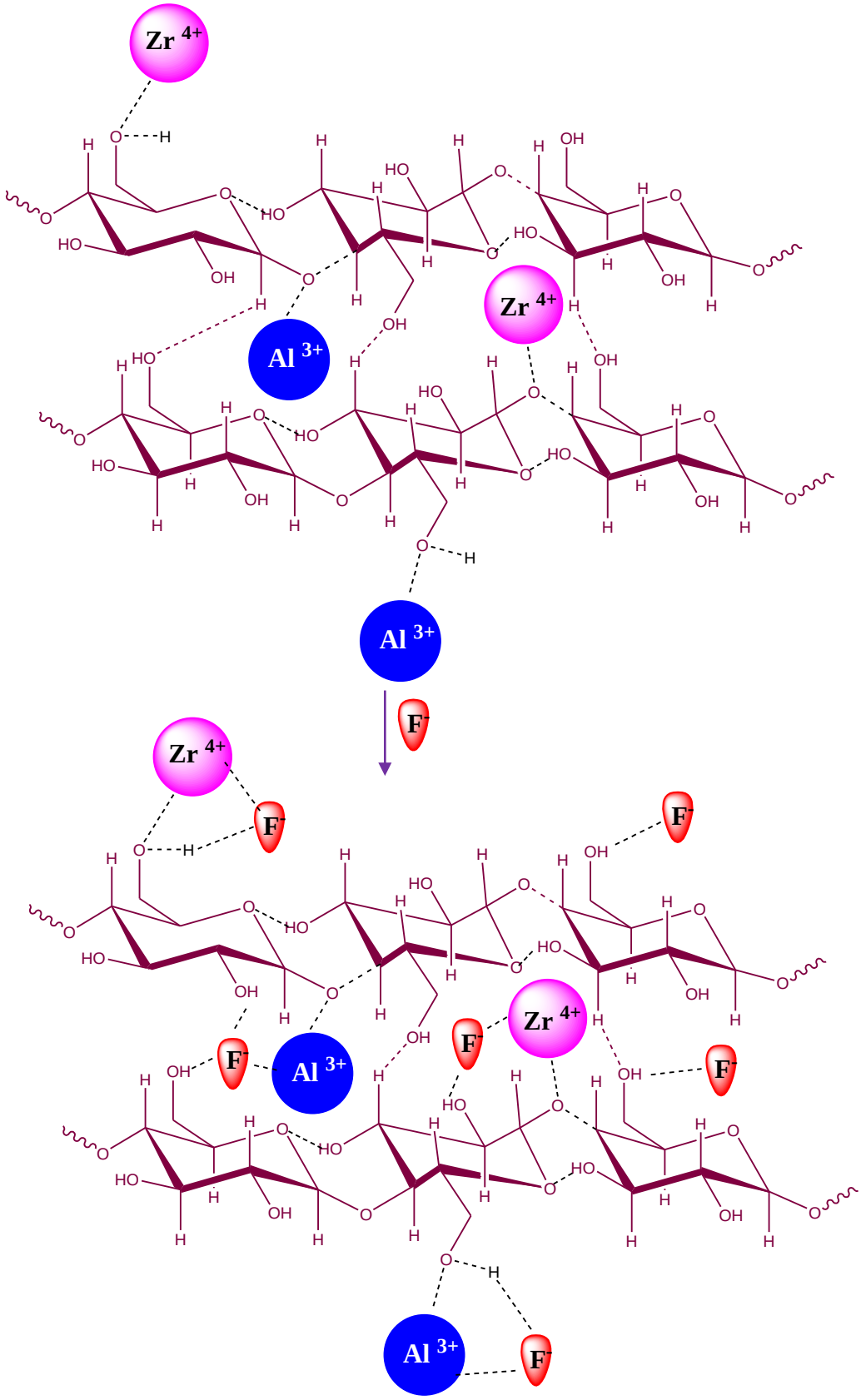

Figure 3.7b. Schematic diagram of the interaction of fluoride with Al/ZrIC biopolymer adsorbent surface.

(v) Adsorption Isotherm and Kinetic studies

Several isotherm studies were performed for the adsorption of fluoride onto Al-ZrIC adsorbent and those plots and parameters are given in a Figure 3.8 and Table 3.1. For instance, the Langmuir isotherm model[32] is used to calculate the maximum adsorption capacity which is a measure of amount of the fluoride ion adsorbed per unit weight of the adsorbent. The maximum adsorption capacity (q_o), the constant (b) and dimensionless parameter (R_L) were found to be 5.76 mg g^{-1}, 0.1643 and 0.4594 respectively. The Freundlich constant n lies between 1-10 ($0.1 < 1/n < 1.0$) and this shows the favourable[33] adsorption of fluoride onto Al/ZrIC biopolymer adsorbent surface.The Dubinin–Radushkevich isotherm (D-R)[34] has similarity to Langmuir isotherm and it gives the adsorption energy and the nature of the adsorption mechanism involved in the interaction between fluoride ion and the Al-Zr impregnated cellulose adsorbent surface.The adsorption energy, E can also be expressed as $-(2\beta)^{-0.5}$and the negative value of E (-1.059 kJ mol^{-1}) indicates that the interaction between the fluoride anion and metal ion impregnated biopolymer adsorbent is exothermic and hence adsorption is favoured at low temperature. As shown in Table 3.1 for the Tempkin isotherm, $R^2 > 0.94$, which is close to the value obtained in Langmuir model and this indicates the vital interaction between fluoride ion and Al-Zr biopolymer adsorbent surface. The value of b (kJ mol^{-1}) was found to be 2.076 which illustrate the electrostatic interaction between fluoride ion and Al-ZrIC biopolymer adsorbent.[35] The R–P isotherm yields an exponent g (1.13) which illustrates the fact that adsorption of fluoride can well be explained through the Langmuir isotherm model as well.[36]

Table 3.1. Adsorption isotherm parameters

Isotherm models	Parameters				
Langmuir	q_o (mg g^{-1})	b (L mg^{-1})	R_L	r^2	χ^2
	5.7696	0.1643	0.4594	0.93	0.0252
Freundlich	K_F (mg $^{1-1/n}$ g^{-1} $L^{1/n}$)	n	r^2	χ^2	
	0.9146	1.7135	0.96	0.0371	
Dubinin Radushkevich	q_m (mg g^{-1})	β (mol^2 kJ^{-2})	E (kJ mol^{-1})	r^2	χ^2
	3.222	0.4459	1.0589	0.85	1.0923
Temkin	K_T	B	r^2	b (kJ mol^{-1})	χ^2
	1.859	1.213	0.95	0.032	3.153
Elovich	q_m (mg g^{-1})	K_E	r^2	χ^2	
	3.153	0.351	0.84	0.1092	
Redlich-Peterson	g	A (L g^{-1})	r^2	χ^2	
	1.1316	0.9479	0.97	1.1236	

Table 3.2. Kinetic parameters and intra-particle rate constant for fluoride ion adsorption

Conc. of F^- ion (mg L^{-1})	q_e mg g^{-1}	Pseudo first order kinetic model			Pseudo second order kinetic model			Intraparticular diffusion model	
		k_1 min^{-1}	q_1 mg g^{-1}	R^2	k_2 g mg min^{-1}	q_2 mg g^{-1}	R^2	k_{int} g mg^{-1} $(min^{0.5})^{-1}$	R^2
3.81	0.6182	0.0371	0.0323	0.741	4.7894	0.6171	0.998	0.0109	0.733
4.91	0.7246	0.0202	0.6000	0.815	3.0974	0.7088	0.998	0.0086	0.809
6.92	0.7895	0.0217	0.0796	0.912	0.4728	0.999	0.998	0.0105	0.926

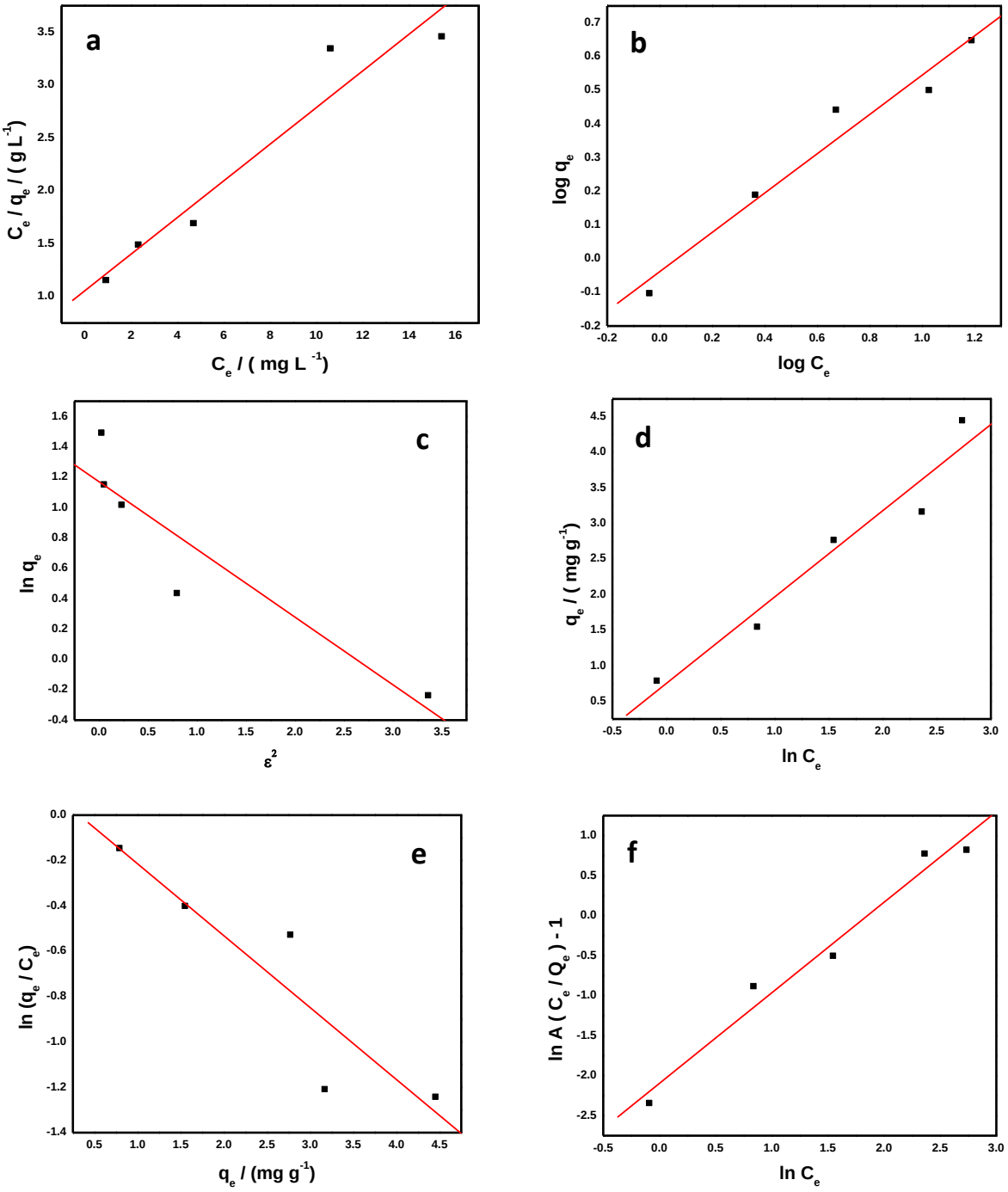

Figure 3.8. (a) Langmuir isotherm (b) Freundlich isotherm (c) D-R isotherm (d) Temkin isotherm (e) Elovich isotherm (f) R-P isotherm

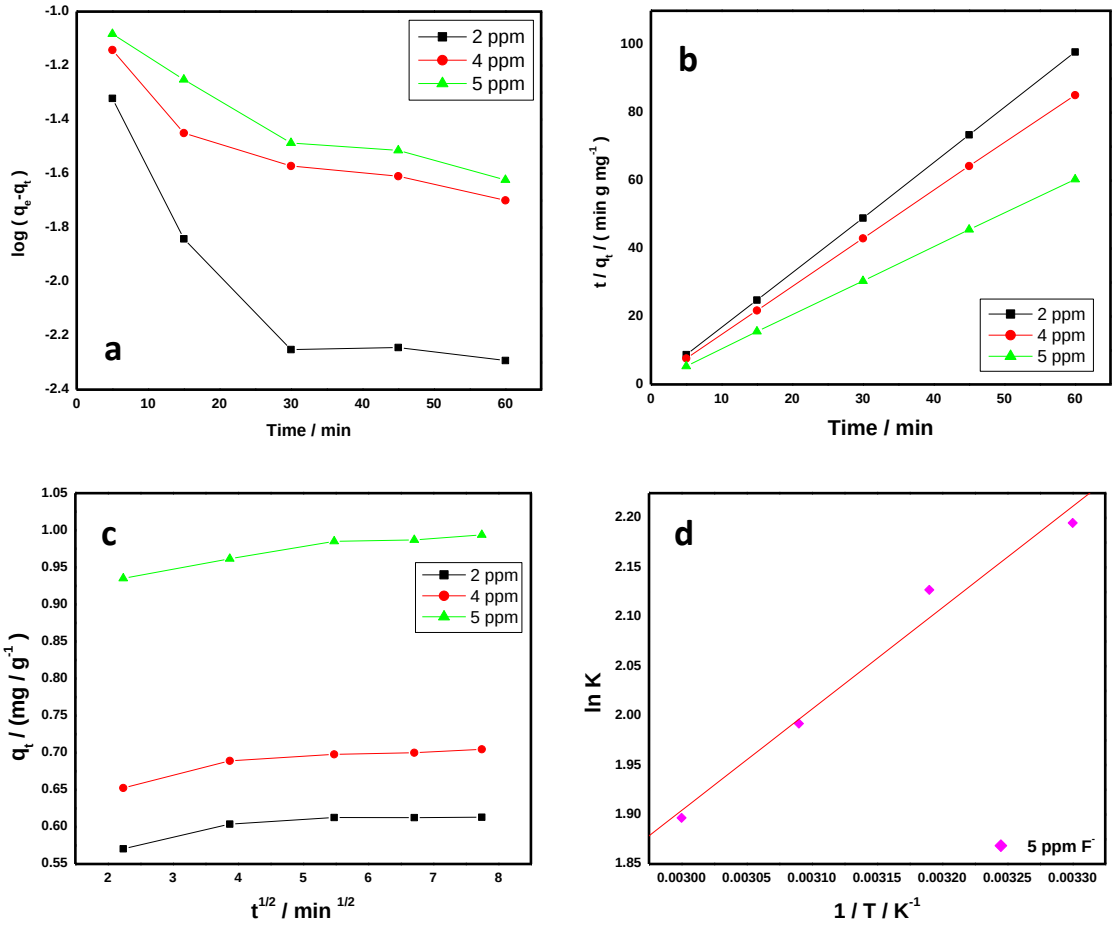

Figure 3.9. (a) Pseudo first order kinetic plot (b) Pseudo second order kinetic plot (c) Plot of q_t versus square root of time (d) Variation of lnK with temperature.

The kinetic and intra particle diffusion plots for varying fluoride concentrations are shown in Figure 3.9a-c and Table 3.2 lists the rate constants for different initial fluoride concentrations using the pseudo-first-order, pseudo-second-order and intra-particle diffusion models. The value of correlation coefficient R^2 for the pseudo-second-order adsorption model is very high (0.998) and therefore this model (Figure 3.9b) is more suitable to describe the adsorption kinetics of fluoride onto Al-ZrIC biopolymer adsorbent. Weber–Morris[37] intraparticle diffusion is used to ascertain whether intraparticle diffusion is the rate-determining step. In this model, a plot of q_t versus $t^{0.5}$ would be linear if and if the plot passes through the origin then intraparticle diffusion is the only rate-limiting step. In the present adsorption process, the plot is linear, the slope

gives the intraparticle rate constant k_{int}, and the non-zero intercept (Figure 3.9c) shows that diffusion is not the only phenomenon that controls the adsorption of the fluoride ion on the Al/ZrIC biopolymer adsorbent.[38] The overall rate of adsorption of fluoride ion on the surface of the metal ion impregnated cellulose adsorbent could be influenced[39] by a) external mass transfer when the fluoride ion is transported from the bulk solution to the external surface of the Al-Zr impregnated biopolymer adsorbent. b) intraparticle or pore diffusion, in which the adsorbate molecules permeate the interior of the adsorbent particles and c) adsorption at the interior sites of the Al-Zr impregnated cellulose adsorbent. Among these factors, the adsorption step happens relatively fast and hence it is assumed that it does not have considerable influence on the overall kinetics of adsorption. The overall adsorption rate could be controlled by surface or intraparticle diffusion.

(vi) Adsorption Thermodynamics

The novel adsorbent material was tested at varying temperatures to ascertain the spontaneity of the adsorption process. The equilibrium constant K is obtained from the ratio of concentration of fluoride ion adsorbed on the Al-ZrIC biopolymer adsorbent to that in the solution. The values of ΔH^0 and ΔS^0 were calculated from the lnK against 1/ T plot (Figure 3.9d) The spontaneity of adsorption process is ascertained from the Gibb's free energy values (Table 3.3) which are negative at the temperatures studied for 5 mg L^{-1} of fluoride.[40] The activation energy of adsorption (E_a) at various temperatures can be obtained from the relation[41] $E_a = \Delta H^0_{ads} + RT$ and for the present adsorption system, the average energy of activation was found to be -5.88 kJ mol^{-1} in accordance with the exothermic physical adsorption process. This fact could also be corroborated from the negative value of calculated ΔH^0 (-8.52 kJ mol^{-1}) and the magnitude of ΔH^0 would reflect the adsorption mechanism. If physical adsorption occurs, then ΔH^0 is usually lower than 80 kJ mol^{-1}, while for chemical adsorption the value lies[42] in the range 80 - 400 kJ mol^{-1}. The ΔS_{total} also depends on the entropy changes occurring due to the Al-Zr-cellulose as well as Al-Zr-cellulose---F interaction. This can be expressed as $\Delta S_{total} = f (\Delta S_{Al\text{-}Zr\text{-}cellulose}, \Delta S_{Al\text{-}Zr\text{-}cellulose\text{---}F})$. Since, entropy is categorized as an extensive thermodynamic property; the overall entropy change is hence reflected in the negative value obtained from the

summation of these entropy changes. The negative ΔS^0 (-9.75 J $mol^{-1}K^{-1}$) values also suggest decreased randomness at the Al-Zr cellulose adsorbent- solution interface.

Table 3.3. Thermodynamic parameters for adsorption of fluoride ion onto Al-ZrIC adsorbent surface at different temperatures

T/ K	ΔG^o / kJ mol^{-1}	ΔH^o / kJ mol^{-1}	ΔS^o / J K^{-1} mol^{-1}	E_a / kJ mol^{-1}
303	-5.53	-8.52	-9.73	-5.88
313	-5.53			
323	-5.34			
333	-5.25			

3.2.4. Conclusions

This work has demonstrated effective interaction between the Al-Zr impregnated cellulose biopolymer and fluoride ion. The novel Al-Zr impregnated cellulose adsorbent exhibits an adsorption capacity of 5.76 mg g^{-1} and the experimental data showed a good fit to the Freundlich and Langmuir isotherm models. The adsorption of fluoride is favored by the interaction of cationic aluminium and zirconium hydroxides through electrostatic, hydrogen bonding and complexation mechanism. The spontaneity of adsorption and second order kinetic model describes the adsorption process. A sample volume of 300 mL on a laboratory scale column containing 3.6 mg L^{-1} of fluoride could be brought down to less than the permissible limit of 1.0 mg L^{-1} . This is attainable at the natural pH prevailing in the water and hence the method could be tested very well for the field applications. Further studies are ongoing in our laboratory to accordingly modify the cellulose biopolymer by functionalizing and test the efficacy to a still higher sample volume.

3.3. Ultrasonication Assisted Preparation of Zr(IV) Ions Onto the Cellulose Biopolymer for the Facile Defluoridation of Water

3.3.1. Introduction

This chapter discusses the advantages of ultrasonication assisted preparation of Zr (IV) modified cellulose biopolymer adsorbent and utilization of this adsorbent for the defluoridation of water. The well-known Nalagonda technique[43] which involves the use of lime and alum for fluoride adsorption has been in vogue, nevertheless there are some drawbacks associated with this process. The leaching of excess aluminium with an increase in groundwater pH is a major concern. Activated alumina,[44] alumina impregnated carbon,[45] dispersed alumina in charcoal[46] and alumina-chitosan composite[47] are some of the alumina-based sorbents used for defluoridation. Magnesia-chitosan composite,[48] protonated chitosan beads,[49] waste phosphogypsum[50] and kaolinite[51] are some of the other effective adsorbents that have been explored. In view of the small size and high electronegativity of fluoride, it has good tendency to interact effectively with rare earth metals such as zirconium and lanthanum. Alginate entrapped Fe(III)-Zr(IV)[52] Zr(IV)-ethylene diamine,[53] zirconium impregnated activated charcoal[54] and zirconium impregnated collagen,[55] Zr(IV)-metalloporphyrin Fe_3O_4 [56] are some of the zirconium based sorbents reported for adsorption of fluoride. Since fluoride ion has a strong affinity towards multivalent metal ions including Al(III) and Zr(IV) metal ions[57] biodegradable polymers such as cellulose can be explored as an effective host matrix. Potentiometric sensor for fluoride based on the interaction with zirconium and cellulose has been reported.[58] Zr(IV) phosphate-cellulose acetate nano composite is known for its photocatalytic activity.[59]

The objective of the present work is to develop an ultrasound assisted preparation method for Zr impregnated cellulose biopolymer adsorbent thereby leading to its application for the adsorption of fluoride. The high pressure and acoustic cavitation leading to the collapse and formation of the bubbles[60] during ultrasonication ensures a quick, green and effective method in the preparation of the adsorbent compared to the conventional method of mixing-stirring for several hours. The shear forces associated with the acoustic cavitation[61] leads to an increase in surface area and ensures homogenous dispersion of the

zirconium oxychloride in the biopolymer through methanol medium. To the best of our knowledge, this is the first report on the use of ultrasonication in the preparation of Zr-impregnated cellulose sorbent for the adsorption of fluoride. The efforts leading to the application of this adsorbent material and the optimization of the experimental parameters are discussed in the following sections.

3.3.2 Experimental Section

(i) Adsorbent Preparation

The Zr (IV) Impregnated Cellulose biopolymer was prepared with cellulose as the starting material using ultrasonication. The schematic representation of ultrasonic horn is depicted in Figure 3.10. The cellulose biopolymer was washed with warm water, dried in an oven at 50 °C and 4.0 g of the biopolymer was dispersed in 30 mL methanol. 2.0 g of zirconium oxychloride was added cautiously to the cellulose solution. The mixture was sonicated for 20 min with a 5 min intermittent time interval and to ensure the completeness of the impregnation, the contents were stirred magnetically for an additional 10 min time duration. The mixture was centrifuged and the and solid adsorbent was filtered using Whatmann 42 filter paper and then dried for 2 h at 50 ^{0}C. The prepared ZrIC adsorbent was used for further adsorption studies.

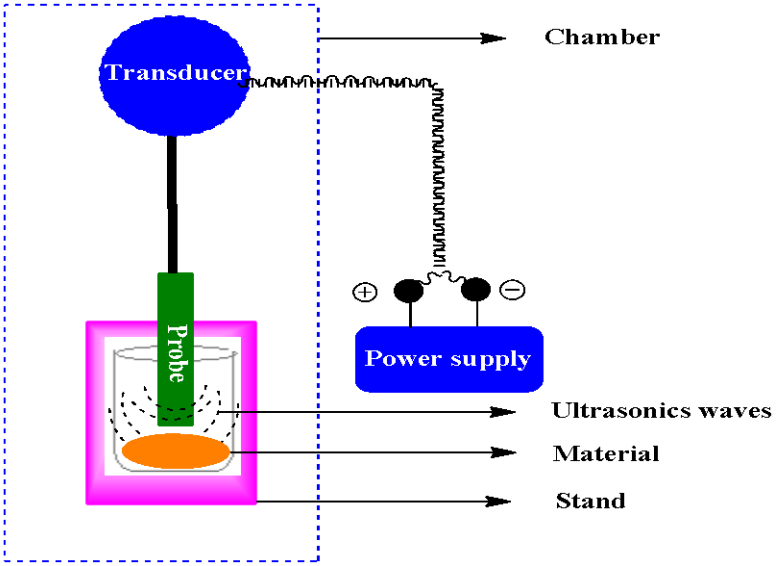

Figure 3.10. Schematic diagram of ultrasonic horn

(ii) Adsorption Procedure

Batch adsorption study was performed by equilibrating 0.5 g of the ZrIC adsorbent material with 50 mL of 5 mg L^{-1} fluoride solution at pH 5.0. The concentration of fluoride in the aqueous solution was estimated by the ion selective electrode method. The amount of fluoride adsorbed (mg g^{-1}) at equilibrium (q_e) is obtained from the corresponding difference between the initial (C_o) and equilibrium fluoride (C_e) concentrations.

3.3.3. Results and Discussion

(i) ***Characterization***

The FT-IR spectrum (Figure 3.11) of ZrIC adsorbent shows characteristic peaks corresponding to the O-H, C-H and C-O-C pyranose ring around 3330 cm^{-1}, 900 cm^{-1}, 2901 cm^{-1} respectively.[16,62] In addition, a peak at 514 cm^{-1} due to stretching vibrations[63] of Zr–O suggests that zirconium atoms are present on the surface of the cellulose biopolymer surface. The peaks characteristic of ZrIC were observed at 841cm^{-1} (Zr-O-C vibration) and 1710 cm^{-1}(due to partial oxidation of cellulose) respectively.[64,65] The sharpness in the O-H peak intensity after adsorption shows the interaction of zirconium as $Zr(OH)_2^{2+}$ with the surface hydroxyl groups of cellulose. Significant changes occur after the adsorption of fluoride ion with the appearance of deformation peak at 514 cm^{-1} and the peak intensity increased in the range 500-900 cm^{-1} attributed to the adsorption of fluoride on the adsorbent surface.

The EDX spectrum (Figure 3.12) confirms the presence of Zr and F elemental peaks on the surface of the cellulose biopolymer and this indicates that zirconium and fluoride are effectively anchored onto the cellulose matrix.

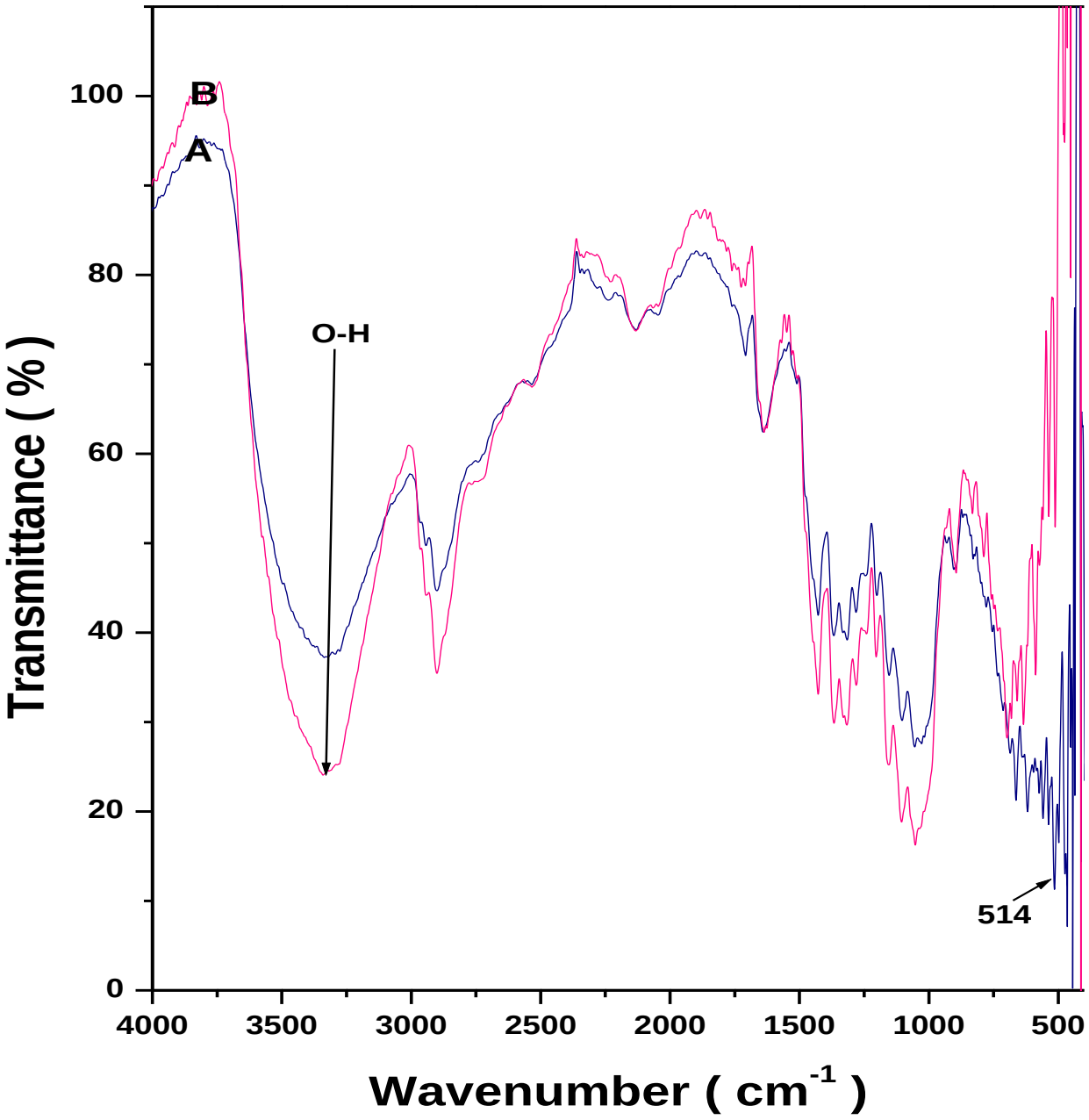

Figure 3.11. FT-IR spectrum of Zr impregnated cellulose adsorbent (A) and the fluoride adsorbed (B).

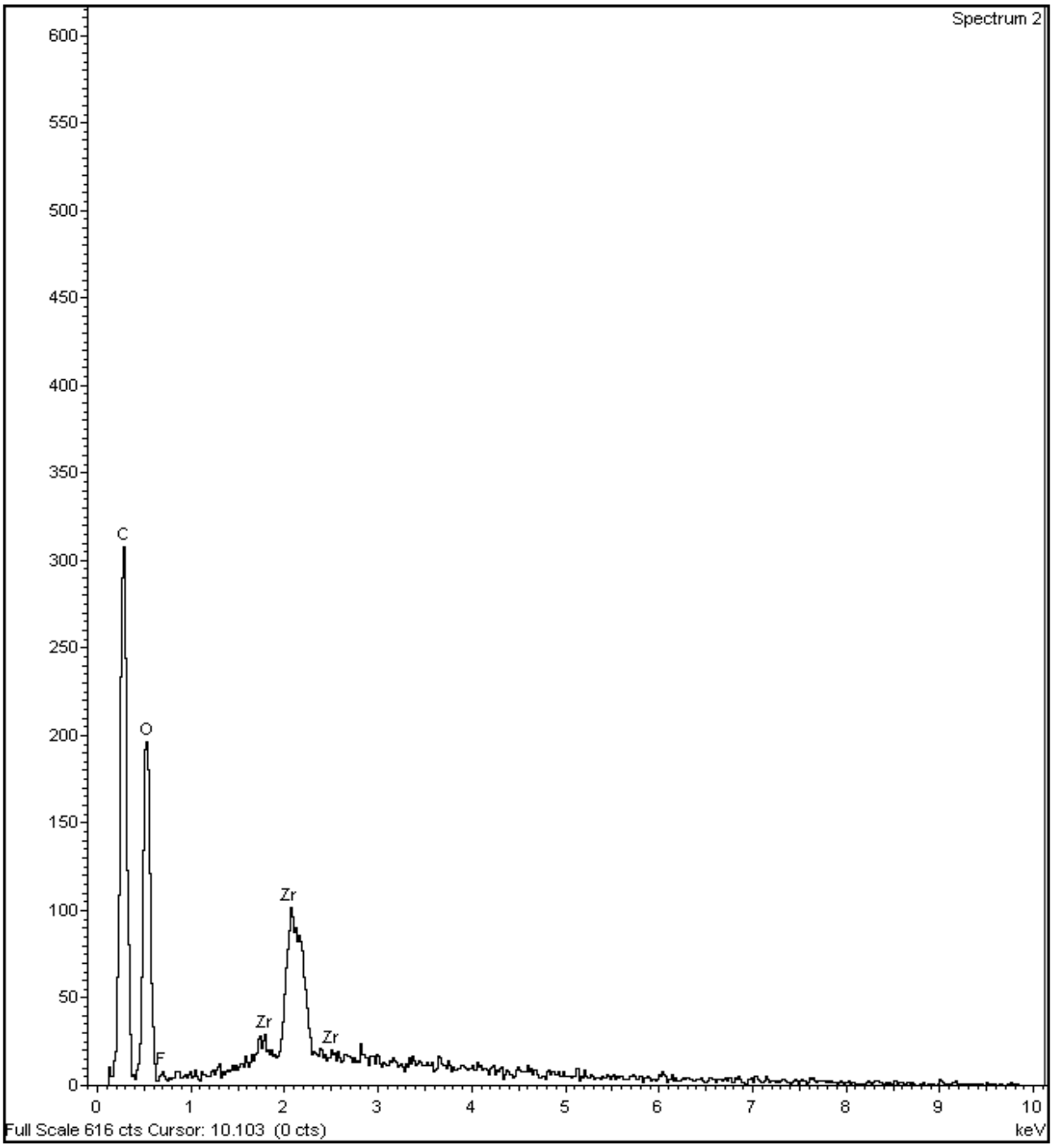

Figure 3.12. EDX spectrum of the fluoride ion adsorbed onto Zr impregnated cellulose surface.

The X-ray diffraction patterns of cellulose, Zr impregnated cellulose biopolymer and fluoride adsorbed biopolymer are given in Figure 3.13. The observed diffraction peaks for cellulose biopolymer[66] are at $2\theta = 14.65^0$, 16.42^0, 22.89^0 and 33.73^0 respectively. The ultrasonication treatment results in weakening the hydrogen bond between the cellulose biopolymer layers and leads to the formation of ZrO_2 nanoparticles. Further, it is also probable that the Zr metal ions could occupy the interlayer of cellulose biopolymer matrix during the ultrasonication. Two distinct peaks at $2\theta = 31.2^0$ and 59.3^0 of the Zr impregnated cellulose biopolymer could be indexed to the (0 1 1) and (3 1 1) reflections[67] of ZrO_2, respectively, which indicates that ZrO_2 nanoparticles were formed in the inter layers of cellulose or on the surface of cellulose biopolymer. The zirconium impregnated biopolymer also shows peaks characteristic of (101) and (002) planes[68] at 16.57^0 and 23.04^0 in addition to the other characteristic peaks of cellulose (JCPDS – pdf no.03-0289).

The average crystallite size of the Zr impregnated biopolymer adsorbent as calculated from Debye-Scherer equation ($d=0.9\ \lambda/\beta\cos\theta$) was found to be 12.4 nm and this is attributed to the interaction of zirconium with the hydroxyl and glycosidic linkages of cellulose. After adsorption of fluoride, XRD pattern of ZrIC biopolymer adsorbent shows peaks corresponding to 2θ values 14.72^0, 16.79^0, 23.10^0, and 34.63^0. The d spacing (3.8602 Å) of ZrIC (corresponding to 2θ value 23^0) reduces to 3.8494 Å due to the interaction of fluoride onto ZrIC adsorbent surface. The analysis of particle size distribution of the zirconium-impregnated adsorbent obtained by DLS method gave a peak maximum corresponding to 164 nm.

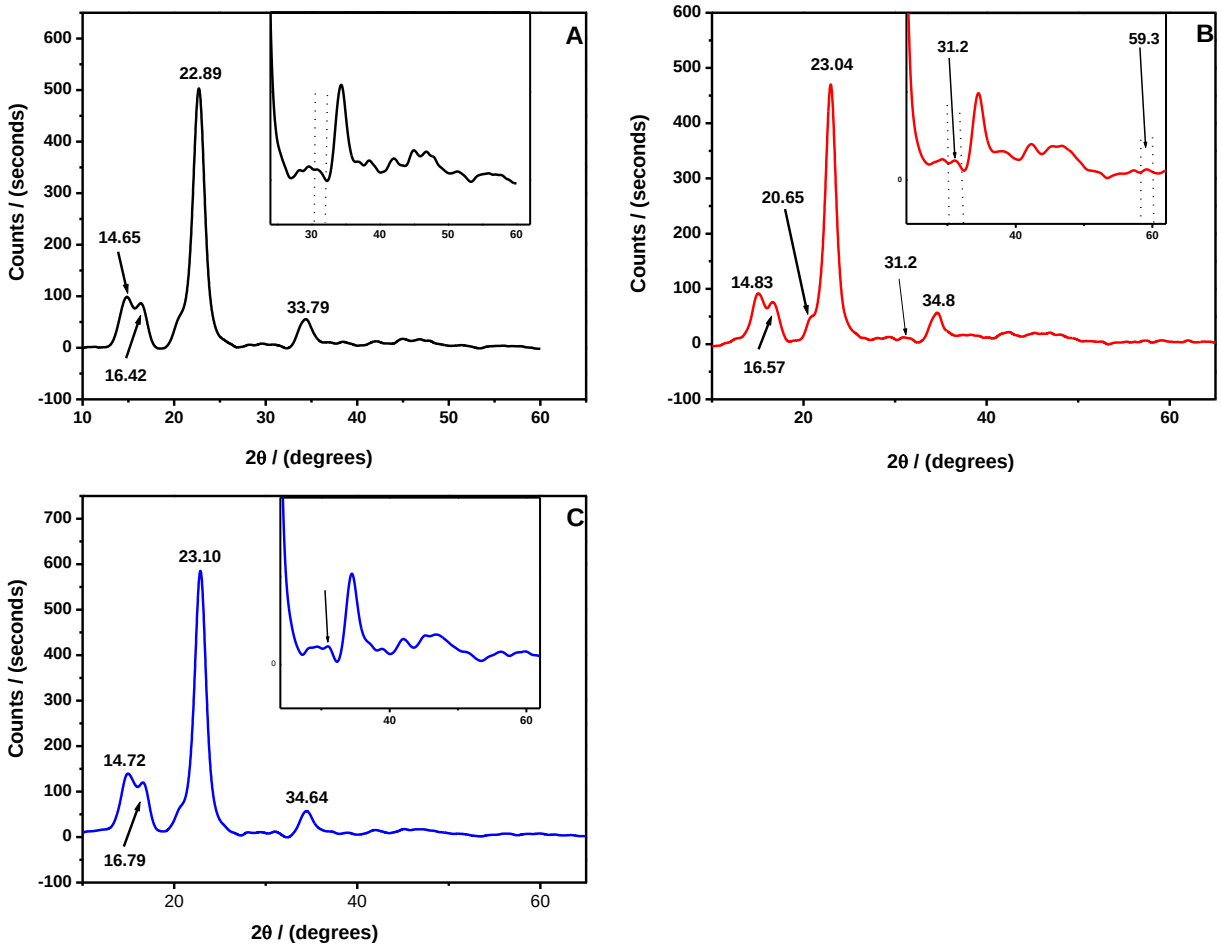

Figure 3.13. XRD pattern of (A) cellulose (B) ZrIC biopolymer adsorbent (C) After fluoride ion adsorption on the adsorbent

(ii) *Mechanism of interaction of Zr impregnated cellulose with fluoride*

a) Calorimetric studies and energy efficiency

With water as the solvent, the power dissipated was found to be 26.6 W. Since, the adsorbent was prepared in methanol medium, the power dissipated using this solvent was found to be 8.2 W. With water as the medium, the energy efficiency was found to be 5.32%. The energy efficiency in methanol medium was found to be 2.92%. The energy utilized during the acoustic cavitation was calculated as per the procedure reported earlier in the literature.[69] Since, the sonication was performed at a 5 min time interval over a period of 20 min, the power dissipated during the adsorbent preparation (with methanol

as the solvent) was found to be 17.520 kJ. The net energy supplied for the preparation of the adsorbent through sonochemical method was found to be 0.5888 kJ g^{-1}. This was obtained by dividing the power dissipated with the total quantity of ingredients used (23.754 g methanol + 4.0 g cellulose + 2.0 g $ZrOCl_2$).

b) Role of ultrasonication

The sonicator operates at a frequency 23 ± 3 kHz with a nominal output power of 500 W. The sonicator rod is made of stainless steel tip with 6 mm diameter. The operation of the horn is controlled by a microcontroller based double display timer. The widespread pores and hydrogen bonding network are vital towards understanding the diverse properties of the cellulose biopolymer.[69] During ultrasonication, the surface area increases due to cavitation effects onto the biopolymer surface. When ultrasound passes through a solvent medium, the liquid circulation and the related turbulence generates the formation and collapse of bubbles known as cavitation, thereby generating high temperature (around 10^4 K) and pressure (10^3 bars) inducing chemical and physical transformations.[70] Cavitation occurs at several locations simultaneously and generates high temperatures and pressures causing acoustic streaming, thereby introducing distinct energy input. Hence, it is quite probable that the hydroxyl radical could be generated due to the decomposition of methanol molecules and furthermore, pyrolysis can occur on the surface of cellulose biopolymer or zirconium oxychloride in the cavitation bubble. Cavitation processes could be classified as acoustic, optic, hydrodynamic and particle cavitation. Acoustic cavitation leads to higher collapse temperature as compared to hydrodynamic cavitation.[71] In addition, cavitation could also be classified as transient and stable cavitation.[72] The classification depends on resonant size, cavity life time (which could form be a basis for the level of collapse) in the bulk liquid. Transient cavitation occurs as a result of vapor-filled cavities generated at an ultrasonic intensity higher than 10 W/cm^2 and this process involves larger variation in the bubble sizes. The lifetime of the transient bubble is approximately 30 μs, whereas the bubble formed during stable cavitation results in ultrasonic intensity in the range of 1–3 W/cm^2. The power or acoustic intensity (29.01 W/cm^2) was obtained using the following expression[73]

$$Power\ intensity\ (W/cm^2) = \frac{Power\ dissipated\ into\ the\ solvent}{\pi r^2} \quad (26)$$

The energy dissipated during the cavitation can affect the crystalline nature of cellulose due to the generation of hot spots.[69] The increase in surface area during sonication could lead to cleaving of the hydrogen bond between the cellulose layers resulting in the disruption of the ordered packing of cellulose molecules. This enhances the interaction of the zirconium metal ion onto the surface of the cellulose biopolymer. Due to the high-speed microjets that are produced during sonication, the frequency of collision between $Zr(OH)_2^{2+}$ particles and cellulose increases. The mode of binding of the zirconium oxy chloride on cellulose could be visualized with a part of the molecule binding to the surface of cellulose containing primary and secondary hydroxyl group as well as the glycosidic linkages of the cellulose biopolymer. Since primary OH group is more reactive, zirconium ion could interact more effectively with primary hydroxyl group rather than other secondary hydroxyl groups which is present in the cellulose biopolymer. Ultrasonication could also influence the degradation of cellulose which enhances the interaction between the zirconium ions to the glycosidic linkages present in the cellulose. A schematic representation of the mechanism is given in Figure 3.14. Since the adsorbent was prepared in methanol medium, it is probable that the alkoxy hydroxides can be hydrolyzed to the cationic zirconium hydroxide.[74] The zirconium ion could interact with the cellulose primary hydroxyl group resulting in the formation of Zr-O bond.[75] The cationic zirconium hydroxide would also interact well with fluoride through electrostatic interaction. The hydrogen bonding between the cellulose hydroxyl groups and fluoride also aids the effective interaction.

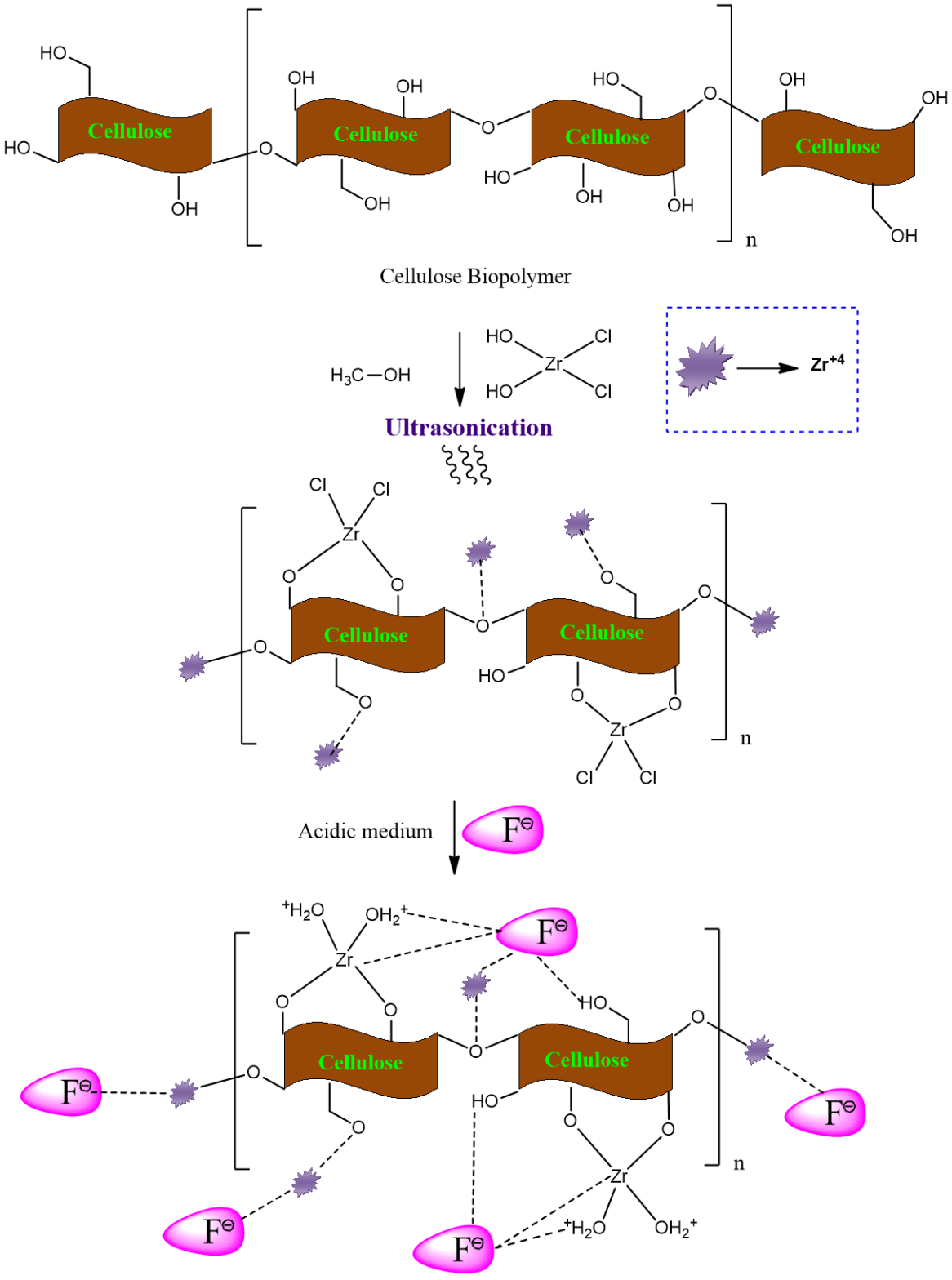

Figure 3.14. Schematic diagram depicting the interaction of fluoride ion with Zr impregnated cellulose biopolymer surface

c) Comparison of ultrasonication and conventional method of adsorbent preparation

A 4.0 g weight of cellulose biopolymer was dispersed in 30 mL of methanol and 2.0 g of zirconium oxychloride was added to the solution at ambient temperature. The resulting solution was stirred magnetically at 300 rpm for 8 h. The procedure was also repeated using ultrasonication over a period of 20 min, with a 5 min time interval and the amount of zirconium-loaded onto the cellulose biopolymer surface was determined by heating 0.3 g of the prepared adsorbent at 900 ^{0}C for 2 h, with the residue[75] being weighed as ZrO_2. When compared to conventional method, the same weight of zirconium loading onto the biopolymer surface (0.12 g ZrO_2 in 0.3 g of cellulose biopolymer) was obtained within 20 min ultrasonication. This shows that ultrasonication greatly enhances the efficacy of the adsorbent preparation as compared to the time consuming conventional method.

(iii)*Optimization of pH*

The adsorption of fluoride onto the surface of the biopolymer sorbent is quite effective in weakly acidic pH 4.5-5.5. At lower pH values, the small size and the high electronegativity of fluoride make it solvated thereby leading to a decrease in the percentage adsorption.[25] In the pH range 4.5-5.5, there is no turbidity in the aqueous solution that emerges after adsorption and this shows that the cationic zirconium hydroxide binds well with the cellulose biopolymer and effectively interacts with fluoride. The concentration of fluoride remaining in the solution was found to be less than the permissible limit of 1.0 mg L^{-1} in the above pH range. Statistically, three replicate analyses gave a reduction of fluoride in the aqueous solution to 0.6 ± 0.02 mg L^{-1}, which is considerably lower than the toxic limit. In the pH range 2.5-3.5, the cationic zirconium hydroxide would also interact well with fluoride, but considerable turbidity was observed in the aqueous phase after adsorption. In weakly acidic medium, the fluoride ion could also interact with the positively charged surface hydroxyl groups of cellulose and furthermore the hard-hard interaction[29] between zirconium and fluoride augments this interaction. Above pH 5.5, the deprotonation of the surface hydroxyl groups in the ZrIC adsorbent and the competition of the hydroxide anion with the fluoride anion for the active adsorption sites could also reduce the percentage adsorption of fluoride.

(iv)Amount of adsorbent

The amount of adsorbent used in the batch study with 5 mg L^{-1} fluoride was varied in the range 0.3-0.6 g. The removal of fluoride was effective in the range 0.5-0.6 g in 50 mL sample volume. The initial rise in adsorption is attributed to the strong electrostatic attraction between the fluoride anion and the ZrIC biopolymer adsorbent. Beyond 0.6 g, the active adsorption sites are saturated and there is no appreciable change in the percentage adsorption.

(v) Adsorption Isotherm and Kinetic studies

The adsorption of fluoride onto zirconium impregnated cellulose adsorbent was subjected to isotherm plots and their respective parameters are given in a Figure 3.15A-D and Table 3.4. The maximum Langmuir adsorption capacity (q_o), the constant (b) and dimensionless parameter (R_L) were found to be 4.95 mg g^{-1} and 0.3863 respectively. R_L values between 0 to1[76] reflect good adsorption and for the present adsorption system the value of R_L was found to be 0.3236 and this indicates the effectiveness of affinity between F^- ion and the Zr impregnated cellulose adsorbent surface for the optimized experimental conditions. The Freundlich constant n value[33] is in the range 1-10 ($0.1 < 1/n < 1.0$) and this shows the constructive adsorption of fluoride onto the ZrIC biopolymer adsorbent surface. The plot of $\ln q_e$ against ε^2 (Figure 3.15C) gives the respective D-R isotherm parameters (Table 3.4). The adsorption energy, E given as $-(2\beta)^{-0.5}$ was found to be -3.9417 kJ mol^{-1} and this indicates that the interaction between the fluoride anion and ZrIC adsorbent is exothermic. The value of Temkin constant, b was found to 2.243 kJ mol^{-1} and this illustrates the electrostatic interaction between fluoride ion and ZrIC biopolymer surface.[35]

The kinetic and intra particle diffusion plots for different fluoride concentrations are shown in Figure 3.16A-D and Table 3.5 lists the respective kinetic rate constants. The percentage of fluoride adsorbed increased with time (Figure 3.16A) and good removal efficiency was attained within 50 min. The high correlation coefficient obtained in the second order model shows that this is more appropriate to describe the adsorption kinetics of fluoride onto ZrIC biopolymer adsorbent. The plot of q_t versus $t^{0.5}$ is linear with a finite intercept value (Figure 3.16D) and this indicates that diffusion is not the only

process that could explain the adsorption of the fluoride ion on the ZrIC biopolymer adsorbent.

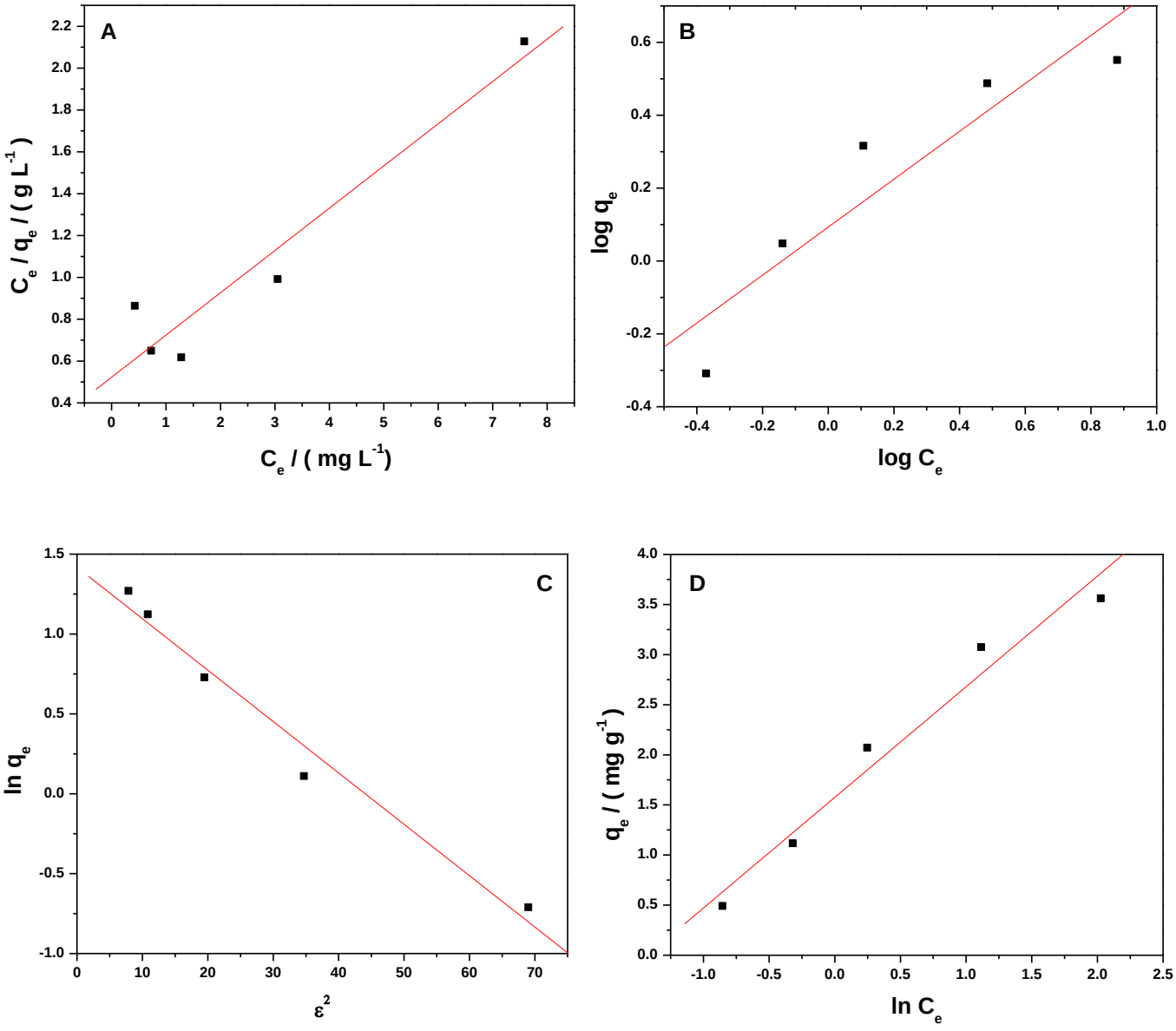

Figure 3.15. (A) Langmuir isotherm (B) Freundlich isotherm (C) D-R isotherm (D) Temkin isotherm.

Table 3.4. Adsorption isotherm parameters

Isotherm	Parameters				
Langmuir	q_o (mg g^{-1})	b (L mg^{-1})	R_L	r^2	χ^2
	4.9512	0.3863	0.3236	0.92	0.0480
Freundlich	K_F (mg $^{1-1/n}$ g^{-1} $L^{1/n}$)	n	r^2	χ^2	
	1.2381	1.5205	0.85	0.1411	
Dubinin Radushkevich	q_m (mg g^{-1})	β (mol^2 kJ^{-2})	E (kJ mol^{-1})	r^2	χ^2
	4.1266	0.0322	-3.9417	0.97	0.0203
Temkin	K_T	B	r^2	χ^2	
	4.1627	1.1044	0.96	0.2703	

Table 3.5. Kinetic parameters and intra-particle rate constant for fluoride ion adsorption

Conc. of F^- ion (mg L^{-1})	q_e mg g^{-1}	Pseudo first order kinetic model			Pseudo second order kinetic model			Intraparticular diffusion model	
		k_1 min^{-1} x 10^{-3}	q_1 mg g^{-1}	R^2	k_2 g mg min^{-1}	q_2 mg g^{-1}	R^2	k_{int} g mg^{-1} $(min^{0.5})^{-1}$	R^2
10.0	0.9684	2.832	0.1722	0.884	4.320	0.9709	0.999	0.0048	0.951
20.0	1.9371	3.086	0.1681	0.814	2.528	1.9373	0.999	0.0043	0.720

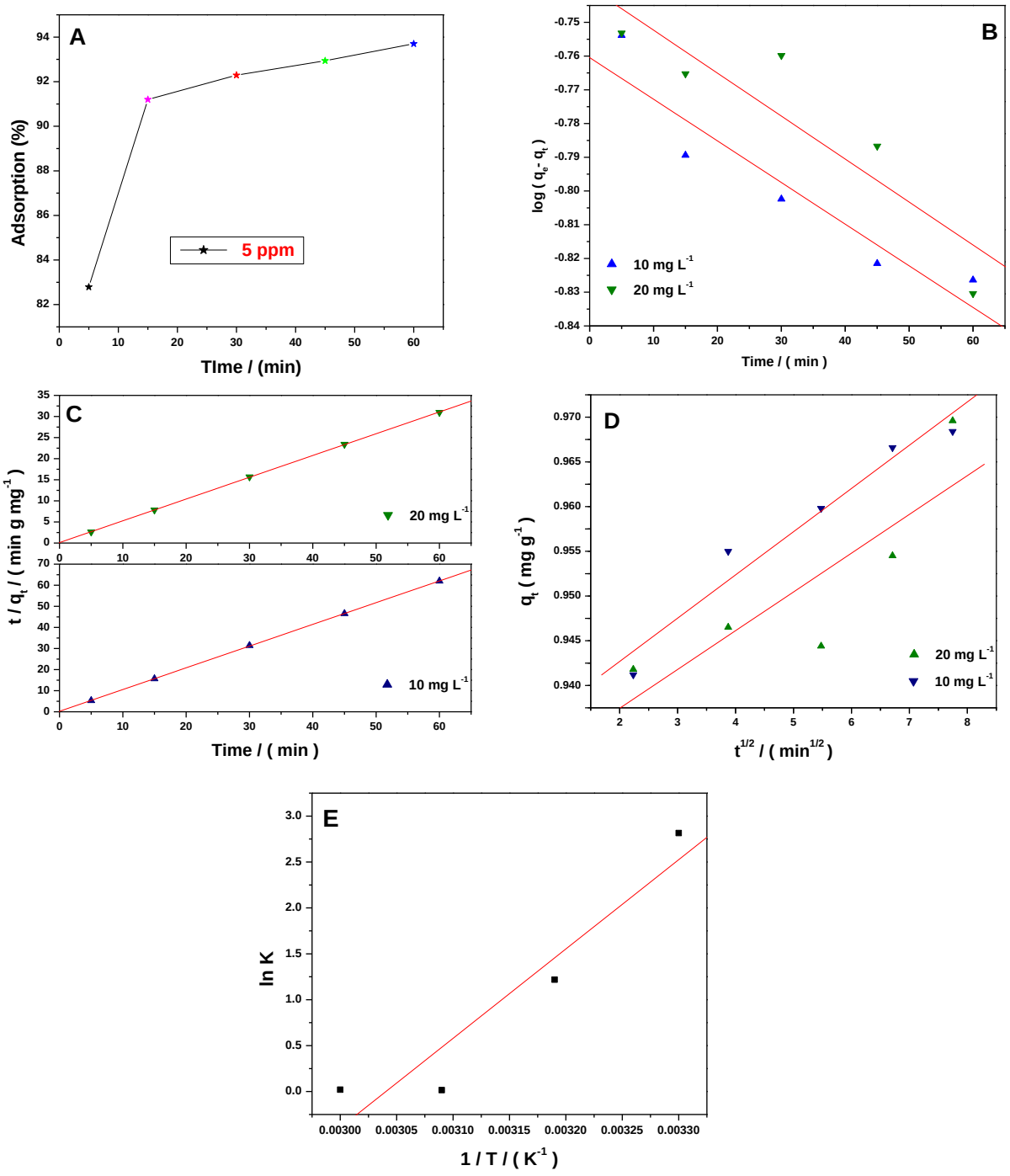

Figure 3.16. (A) Effect of time on adsorption (B) Pseudo first order kinetic plot (C) Pseudo second order kinetic plot (D) Plot of q_t versus square root of time (E) Variation of lnK with temperature

(vi) Adsorption Thermodynamics

The thermodynamic parameters for the adsorption of fluoride onto the zirconium impregnated cellulose adsorbent is obtained using the Van't Hoff equations. The equilibrium constant K is obtained from the fluoride ion concentration adsorbed on the ZrIC biopolymer adsorbent to that in the solution. The values of ΔH^0 and ΔS^0 were obtained from the lnK against 1/ T plot (Figure 3.16E) and the spontaneity of adsorption process is obvious from the negative Gibb's free energy values (Table 3.6) obtained at the various temperatures studied with 10 mg L^{-1} fluoride.[40] The average activation energy of adsorption,[41] $E_a = \Delta H^0_{ads} + RT$ was found to be -78.235 kJ mol^{-1} in accordance with the exothermic nature of interaction between fluoride and ZrIC adsorbent. The negative value of calculated ΔH^0 (-80.88 kJ mol^{-1}) also shows that the adsorption is exothermic. The ΔS_{total} involves the entropy changes due to the Zr-cellulose and the Zr-cellulose---F interaction. This can be expressed as $\Delta S_{total} = \Delta S_{Zr\text{-}cellulose} + \Delta S_{Zr\text{-}cellulose\text{---}F}$. Since, entropy is an extensive thermodynamic property, the overall entropy change is obtained from the summation of the individual entropy changes. The negative ΔS^0 (-245.93 J $mol^{-1}K^{-1}$) reflects the decreased randomness at the Zr impregnated cellulose adsorbent- solution interface.

Table 3.6. Thermodynamic parameters ΔH°, ΔS° and ΔG° and E_a for adsorption of fluoride at various temperatures.

T/ K	ΔG^o / kJ mol^{-1}	ΔH^o / kJ mol^{-1}	ΔS^o / J K^{-1} mol^{-1}	E_a / kJ mol^{-1}
303	-7.092	-80.88	-245.93	-78.23
313	-3.171			
323	-0.042			
333	-0.055			

3.3.4. Conclusions

The ultrasound assisted preparation of ZrIC adsorbent has shown good potential for the adsorption of fluoride. The conventional method of adsorbent preparation takes 8 hours as compared to the quick ultrasonication. The novel Zr impregnated cellulose adsorbent exhibits an adsorption capacity of 4.95 mg g^{-1} with the experimental data showing a good fit to Langmuir isotherm model. Electrostatic interaction of cationic zirconium hydroxide with fluoride supports the adsorption mechanism. The second order kinetics describes the adsorption process very well. The study of thermodynamics indicates a spontaneous, exothermic adsorption process and a decreased randomness at the adsorbent-solution interface.

References

1. Guo, X; Chen, F. *Environ. Sci. Technol.* **2005**, 39, 6808.
2. Klemm, D.; Heublein, B.; Fink, H. P.; Bohn, A. *Angew. Chem. Int. Ed.* **2005**, 44, 3358.
3. Loganathan, P.; Vigneswaran, S.; Kandasamy, J.; Naidu, R. *J. Hazard. Mater.* **2013**, 248-249, 1.
4. Ghorai, S.; Pant, K. K. *Chem. Eng. J.* **2004**, 98, 165.
5. Maliyekkal, S. M.; Shukla, S.; Philip, L.; Nambi, I. M. *Chem. Eng. J.* **2008**, 140, 183.
6. Viswanathan, N.; Meenakshi, S. *J. Hazard. Mater.* **2010**, 178, 226.
7. Sundaram, C. S.; Viswanathan, N.; Meenakshi, S. *Bioresour. Technol.* **2008**, 99, 8226.
8. Sundaram, C. S.; Viswanathan, N.; Meenakshi, S. *J. Hazard. Mater.* **2009**, 163, 618.
9. Viswanathan, N.; Meenakshi, S. *J. Colloid. Interface. Sci.* **2008**, 322, 375.
10. Viswanathan, N.; Meenakshi, S. *J. Hazard. Mater.* **2010**, 176, 459.
11. Alagamuthu, G.; Rajan, M. *Chem. Eng. J.* **2010**, 158, 451.
12. Liao, X. P.; Shi, B. I. *Environ. Sci. Technol.* **2005**, 39, 4628.
13. Anirudhan, T. S.; Suchitra, P. S. *Ind. Eng. Chem. Res.* 2010, 49, 12254.
14. Goswami, A.; Purkait, M. K. *Chem. Eng. Res. Des.* **2012**, 90, 2316.
15. Anirudhan, T. S.; Rauf, T. A.; Rejeena, S. R. *Desalination* **2012**, 285, 277.
16. Tian, Y.; Wu, M.; Liu, R.; Wang, D.; Lin, X.; Liu, W.; Ma, L.; Lie, Y.; Huang, Y. *J. Hazard. Mater.* **2011**, 185, 93.
17. Choudhuri, A. R.; Takoudis, C. G. *Thin Solid Films* 2004, 446, 155.
18. Jagtap, S.; Yenkie, M. K. N.; Labhsetwar, N.; Rayalu, S. *Microporous Mesoporous Mater.* **2011**, 142, 454.
19. Sundaram, S. C.; Viswanathan, N.; Meenakshi, S. *J. Hazard. Mater.* **2008**, 155, 206.
20. Lojewska, J.; Miskowiec, P.; Lojewski, T.; Proniewicz, L. M. *Polym. Degrad. Stab.* **2005**, 88, 512.
21. Dongre, R.; Ghugal, D. N.; Meshram, J. S.; Ramteke, D. S. *Afr. J. Environ. Sci. Technol.* **2012**, 6, 130.
22. Ghorai, S.; Pant, K. K. *Sep. Purif. Technol.* **2005**, 42, 265.
23. Kumar, A. S. K.; Kalidhasan, S.; Rajesh. V.; Rajesh, N. *Ind. Eng. Chem. Res.***2013**, 52 (34), 11838.
24. Ma, C.; Chang, Y.; Ye, W.; Shang, W.; Wang, C. *J. Colloid. Interface. Sci* . **2008**, 317, 148.
25. Raichur, A. M.; Basu, M. J. *Sep. Purif. Technol.* 2001, 24, 121.
26. Oladoja, N. A.; Ololade, I. A.; Alimi, O. A.; Akinnifesi, T. A.; Olaremu, G. A. *Chem. Eng. Res. Des.* **2013**, 91, 2691.
27. Oladoja, N. A.; Aliu, Y. D. *J. Hazard. Mater.* **2009**, 164, 1496.
28. Liu, R.; Gong, W.; Lan, H.; Yang, T.; Liu, H.; Qu, J. *Sep. Purif. Technol.* **2012**, 92, 100.
29. Pearson, R. G. *J. Am. Chem. Soc.* 1963, 85, 3533.
30. Kappe, C. O. *Angew. Chem. Int. Ed.* **2004**, 43, 6250.

31. Galema, S. A. *Chem. Soc. Rev.*1997, 26, 233.
32. I. Langmuir, *J. Am. Chem. Soc.* **1918**, 40, 1361.
33. Ru-Ling, T.; Feng-Chin, W.; *J. Hazard. Mater.* **2008**, 155, 277.
34. Foo, K. Y.; Hameed, B. H. *Chem. Eng. J.* **2010**, 156, 2.
35. Nigussie, W.; Zewgeb, F.; Chandravanshib, B. S. *J. Hazard. Mater.* **2007**, 147, 954.
36. Redlich, O.; Peterson, D. L.; *J. Phys. Chem.* **1959**, 63, 1024.
37. Weber, W. J.; Morris, J. C. *J. Sanit. Eng. Div. Am. Soc. Civ. Eng.***1963**, 89, 3.
38. Yu, Z.; Qi, T.; Qu, J.; Wang, L.; Chu, J. *J. Hazard. Mater.* **2009**, 167, 406.
39. Mittal, A.; Kurup, L.; Mittal, J. *J. Hazard. Mater.* **2007**, 146, 243.
40. Tang, X.; Li, Z.; Chen, Y. *J. Hazard. Mater.* **2009**, 161, 824.
41. Kumar, A. S. K.; Kalidhasan, S.; Rajesh. V.; Rajesh, N. *Ind. Eng. Chem. Res.* **2012**, 51, 58.
42. Gubbuk, I. H.; *J. Hazard. Mater.* **2011**, 186, 416.
43. Nawlakhe, W. G.; Paramasivam, R. *Curr. Sci.* **1993**, 65, 743.
44. Ku, Y.; Chiou, H. *Water, Air, Soil Pollut.* **2002**, 133, 349.
45. Ramos, R. L.; Ovalle-turrubiartes, J.; Sanchez-castillo, M. A. *Carbon* **1999**, 37, 609.
46. Tchomgui-Kamga, E.; Alonzo, V.; Nanseu-Njiki, C.P.; Audebrand, N.; Ngameni, E.; Darchen, A. *Carbon* **2010**, 48, 333.
47. Viswanathan, J. N.; Meenakshi, S. *J. Hazard. Mater.* **2010**, 178, 226.
48. Sundaram, C. S.; Viswanathan, J. N.; Meenakshi, S. *J. Hazard. Mater.* **2009**, 163, 618.
49. Viswanathan, J. N.; Sundaram, C. S.; Meenakshi, S. *J. Hazard. Mater.* **2009**, 161, 423.
50. Zhang, D.; Luo, H.; Zheng, L.; Wang, K.; Li, H.; Wang, Y.; Feng, H. *J. Hazard. Mater.***2012**, 241-242, 418.
51. Pradip, K. G.; Baruah, R. *Ind. J. Chem. Tech.* **2008**, 15, 500.
52. Swain, S. K.; Patnaik, T.; Patnaik, P. C.; Jha, U.; Dey, R. K. *Chem. Eng. J.* **2013**, 215-216, 763.
53. Swain, S. K.; Mishra, S.; Patnaik, T.; Patel, R. K.; Jha, U.; Dey, R. K. *Chem. Eng. J.* **2012**, 184, 72.
54. Janardhana, C.; Nageswara rao, G.; Sai satish, R.; Sunil kumar, P.; Anilkumar, V.; Vijay madhav, M. *Indian J. Chem. Technol.* **2007**, 14, 350.
55. Liao, X. P.; Shi, B. I. *Environ. Sci. Technol.* **2005**, 39, 4628.
56. Poursaberi, T.; Hassanisadi, M.; Torkestani, K.; Zare, M. *Chem. Eng. J.* **2012**, 189-190, 117.
57. Luo, F.; Inoue, K. *Solv. Extr. Ion Exch.* **2004**, 22, 305.
58. Hosseini, M.S.; Rahiminegad, H. *J. Anal. Chem.* **2006**, 61, 166.
59. Gupta, V. K.; Pathania, D.; Singh, P.; Rathore, B. S.; Chauhan, P. *Carbohydr. Polym.* **2013**, 95, 434.
60. Prasad, K.; Pinjari, D. V.; Pandit, A. B.; Mhaske, S. T. *Ultrason. Sonochem.* **2011**, 18, 1128.
61. Mohandes, F.; Salavati-Niasari, M. *Ultrason. Sonochem.* **2013**, 20, 354.
62. Anirudhan, T. S.; Noeline, B. F.; Manohar, D. M. *Desalination* **2012**, 285, 277.

63. Shishmakov, A. B.; Mikushina, Y. V.; Valova, M. S.; Koryakova, O. V.; Parshina, E. V.; Etrov, L. A. *Russ. J. Appl. Chem.* **2009**, 82, 2113.
64. Lojewska, J.; Miskowiec, P.; Lojewski, T.; Proniewicz, L. M. *Polym. Degrad. Stab.***2005**, 88, 512.
65. Dongre, R.; Ghugal, D. N.; Meshram, J. S.; Ramteke, D. S. *Afr. J. Environ. Sci. Technol.* **2012**, 6, 130.
66. Barathi, M.; Kumar, A. S. K.; Rajesh, N.; *J. Environ. Chem. Eng.* **2013**, 1, 1325.
67. Zhanga, G.; He, Z.; Xu, W. *Chem. Eng. J.* **2012**, 183, 315.
68. Mulinari, D. R.; Cruz, T. G.; Cioffi, M. O. H.; Voorwald, H. J. C.; Da Silva, M. L. C. P.; Rocha, G. J. M. Carbohydr Res. **2010**, 345, 1865.
69. Pinjari, D. V.; Pandit, A. B. *Ultrason. Sonochem.* **2010**, 17, 845.
70. Sawant, S. S.; Anil, A. C.; Krishnamurthy, V.; Gaonkar, C.; Kolwalkar, J.; Khandeparker, L.; Desai, D.; Mahulkar, A. V.; Ranade, V. V.; Pandit, A. B. *Biochem. Eng. J.* **2008**, 42, 320.
71. Gogate, P. R.; Pandit, A. B. *Rev. Chem. Eng.* **2001**, 17, 1.
72. Iskalieva, A.; Yimmou, B. M.; Gogate, P. R.; Horvath, M.; Horvath, P. G.; Csoka, L. *Ultrason. Sonochem.* **2012**, 19, 984.
73. Sun, Y. J.; Ma, G. P.; Ye, X. Q.; Kakuda, Y.; Meng, R. F. *Ultrason. Sonochem.* **2010**, 17, 654.
74. Rodrigues Filho, U. P.; Gushikem, Y.; Fujiwara, F. Y. *Langmuir* **1994**, 10, 435.
75. Muxel, A. A.; Gimenez, S. M. N.; De Souza Almeida, F.A.; Alfaya, R. V. S.; Alfay, A. A. S. *Clean – Soil, Air, Water* **2011**, 39, 289.
76. Moradi, O.; Fakhri, A.; Adami, S.; Adami, S. *J. Colloid Interface Sci.* **2013**, 395, 224.

CHAPTER 4

4. Aluminium hydroxide impregnated macroreticular aromatic polymeric resin as a sustainable option for defluoridation

4.1.1. Introduction

Most of the adsorbents used to remove fluoride utilize the incorporation of Al (III), Zr (IV) or La (III) in the matrix[1] since these hard cations can strengthen the interaction with the hard fluoride anion. The utility of Al (III) as aluminium oxy hydroxide-chitosan composite impregnated with MnO_2 nano particles are also known for their good potential to purify water by sequestering heavy metals and other contaminants.[2]

Polymeric resins belong to a versatile category of adsorbents that serve as an anchor to capture several metal ions.[3] Over the years, the most widely used polymeric sorbents are styrene–divinyl benzene (DVB) copolymers (Amberlite XAD resins) for removal of heavy metals and other pollutants. It is mainly due to their hydrophobic nature and good stability.[4,5] Amylose based polymeric resin as solid support for proteins have excellent ability to sequester uranyl ions from sea water.[6] Impregnation of chelating agents offers more selectivity in adsorption.[7] Chelating resin (CR) and anion exchange resin (AER),[8] Metal (III)-loaded Amberlite resin,[9] Al-Amberlite resin,[10] Ion exchange fibre,[11] Zr immobilized resin,[12] Al-chelating porous anion exchanger[13] have proved their efficacy in fluoride removal from aqueous solutions. Very recently, Ca-Zr-polyvinyl alcohol composite reported as a pH independent adsorbent with high adsorption capacity (12.72 mg g^{-1}) for defluoridation of water.[14] In this chapter, the potential application of aluminum hydroxide impregnated macroporous polymeric resin is explored as a sustainable option for fluoride removal from aqueous solution. The high surface area, good stability under diverse pH conditions and attainment of high adsorption capacity make the macroporous polymeric resins as excellent adsorbents for various applications. Functionalized polymeric resins also possess distinct advantages and recently, iminodiacetic acid functionalized cation exchange resin and amine functionalized copolymeric resins were reported for fluoride adsorption.[15,16,17,18] Against this backdrop, the application of polystyrene divinyl benzene resins by impregnation with metal ions would be more gainful keeping in view the prospective extension to practical field applications without compromising on the adsorption capacity. Hence, with hindsight on

the above benefits, the objective of this work was to devise an uncomplicated novel approach by direct impregnation of a macroreticular polystyrene divinyl benzene resin with Al^{3+} for defluoridation. In accordance with the HSAB concept, Al(III) being a typical hard acid, shows good ability to complex with the hard anion fluoride. Considering the above mentioned advantages of PSDVB (Polystyrene divinyl benzene resins), the loading of aluminium onto this polymeric support would offer effective solution to defluoridation. The first part of this work deals with the comprehensive characterization of the resin. The subsequent portion is devoted towards understanding the mechanism of interaction of fluoride ion with the polymeric resin, study of kinetics, thermodynamics and preliminary column studies.

4.1.2. Experimental Section

(i) Preparation of Aluminum hydroxide impregnated polymeric resin adsorbent

Aluminium hydroxide was freshly prepared by the treatment of aluminium sulphate and sodium hydroxide as reported previously.[18] A known weight of the polymeric resin (2.0 g) was dispersed in 30 mL acetone and 2.0 g of freshly prepared aluminium hydroxide was added into the dispersed macroporous polymeric resin and stirred for 8 hours in order to obtain a homogeneous mixture. The Al^{3+} impregnated resin adsorbent was separated by filtration, washed with acetone, dried at 50 °C in a vacuum oven (Biotechnics, India) for 2 hours and characterized using various techniques.

(ii) Adsorption studies through batch experiments

The batch adsorption experiments were conducted by equilibrating 0.1 g of aluminum hydroxide impregnated macroporous polymeric resin adsorbent with 50 mL of 5 mg L^{-1} fluoride ion solution at pH 3.0 and 7.0 in an orbital incubator shaker (Biotechnics, India). The concentration of fluoride in the aqueous phase was determined using the fluoride ion meter. The percentage of fluoride adsorbed increased with time and attained maximum efficiency at 60 min, wherein concentration remaining in solution was well within the permissible limit.

(iii) Column Study

The applicability of the aluminium hydroxide impregnated macroporous polymeric resin adsorbent material on a laboratory scale was checked for the defluoridation of water from a higher sample volume by packing 2.0 g of the sorbent (glass column (2.5 cm dia, 30 cm (length). A fixed volume (1.5 litres) of laboratory tap water spiked with 5 mg L^{-1} fluoride ion was delivered to the column at a flow rate of 5 mL min^{-1} and the concentration of fluoride was measured in the out coming solution using the ion meter. The concentration of fluoride was found to be less than 0.6 mg L^{-1} suggesting excellent removal efficiency and further the column could be re-used by desorption with 10mL of 0.05 mol L^{-1} sodium hydroxide as the eluent.

4.1.3. Results and Discussion

(i) Characterization of the adsorbent

The macroporous polymeric resin adsorbent was characterized at length using diverse techniques and the first amongst them was FT-IR analysis. The FT-IR spectrum (Figure 4.1) shows peaks relevant to the different functional groups in the polymeric resin, aluminum hydroxide impregnated macroporous polymeric resin adsorbent prior and subsequent to fluoride adsorption (Figure 4.1). Peaks around 1630 cm^{-1} indicate the aromatic C=C vibrational frequency. The broad peaks around 400-900 $cm^{-1}$and 3200 - 3700 cm^{-1} are related to the Al-O [AlO_6 & AlO_4] and O-H stretching vibrations [19,20,21] and this is an indication to the successful impregnation of amorphous aluminium hydroxide onto the macroporous polymeric resin matrix. Furthermore, a strong peak at 1117 cm^{-1} could be assigned to the C-OH stretching vibration which corresponds to the secondary alcohol C-O stretching frequency. After the impregnation of aluminium hydroxide, the disappearance of peak was observed at 3027 cm^{-1} corresponding to vinyl (= CH_2) group present in the macroporous polymeric resin and the characteristic Al-O characteristic peaks were observed at 983 cm^{-1}, 707 cm^{-1} and 551 cm^{-1} respectively.[22] In addition to this, the peak observed at 907 cm^{-1} could be attributed to the Al-OH and O-Al-O bending vibrations.[23,24]

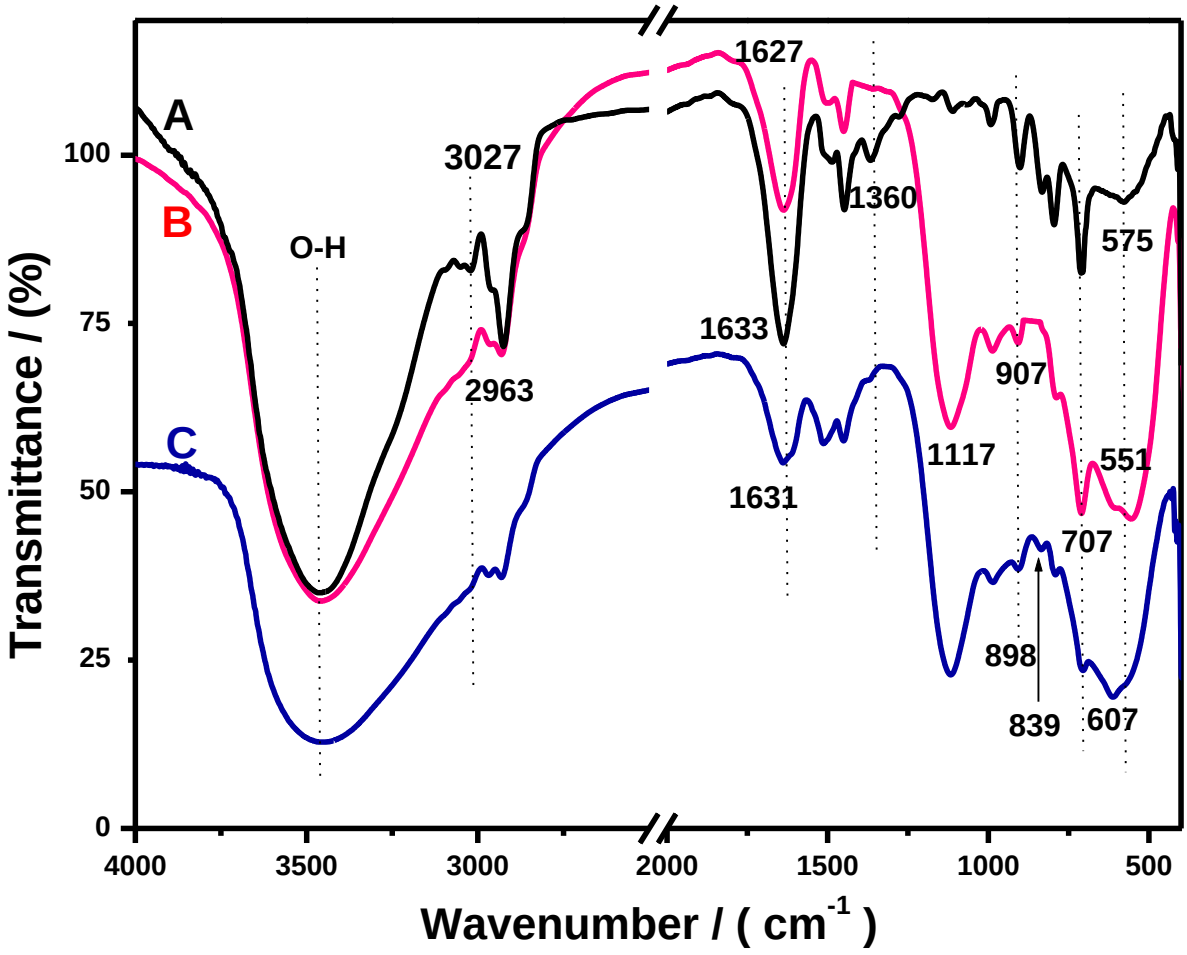

Figure 4.1. FT-IR spectrum of XAD 1180 polymeric resin (A) and Aluminum hydroxide impregnated macroporous polymeric resin adsorbent (B) and the fluoride adsorbed (C).

The interaction of fluoride ion onto the aluminium hydroxide impregnated macroporous polymeric resin adsorbent resulted in the decrease in the peak intensities at 907 cm^{-1} and 707 cm^{-1} thereby confirming the hydroxide groups (Al-OH) present at the adsorbent surface could be replaced by F^- ions in aqueous solutions. Generally, the metal-fluoride interactions[1] are observed typically in the region 500-900 cm^{-1}. A new peak observed at 839 cm^{-1}, could be attributed to the plausible anchoring of fluoride ion onto the adsorbent surface through ligand exchange or hydrogen bonding interactions**.** The significant peaks

observed in the polymeric adsorbent were retained after fluoride adsorption and this authenticates the stability of aluminium hydroxide impregnated macroporous polymeric resin adsorbent. The O-H peak also broadens after fluoride adsorption and the mode of fluoride ion interaction onto the aluminium hydroxide impregnated macroporous polymeric resin adsorbent is shown in Figure 4.2. The schematic representation illustrates that in aqueous solution, Al (III) could exist as cationic hydroxides interact with fluoride through electrostatic interaction. Furthermore, the hydrogen bonding interaction between the metal hydroxyl groups (Al-OH) and F^- would also enhance the interaction with the macroreticular resin matrix.

The scanning electron microscope (SEM) and optical images show certain typical morphological changes in the aluminum hydroxide impregnated macroporous polymeric resin surface before and after fluoride adsorption (Figure 4.3). The images were obtained by applying 20 kV voltage with 5000 x magnification for the intensification of surface. The polymeric resin is a cross-linked aromatic polymer and after impregnation the surface has a rough appearance and irregular shape with bright white particles (presumably due to aluminium hydroxide) adhering to the adsorbent surface. These features also testify that aluminium hydroxide is tethered onto the polymeric resin matrix. The adsorption of fluoride was also confirmed through the distinct features observed through the optical images. The addition of a spot test reagent (Kit WT-012 for fluoride testing supplied by Himedia Laboratories, India) shows a distinct red color on the aluminium impregnated polymeric resin surface. The disappearance of color with considerable decrease in the intensity of the images (Figure 4.4) after fluoride adsorption validates the interaction of metal ion with fluoride. Moreover, the corresponding EDS spectrum (Figure 4.5) confirms the presence of Al peaks at 1.486 keV thereby indicating the successful impregnation of aluminum hydroxide onto the macroreticular aromatic cross-linked polymeric matrix. The adsorption of fluoride on the surface of the macroporous resin adsorbent was evident from the characteristic fluorine peak at 0.677 keV besides the other major peaks such as C, O and Al respectively.

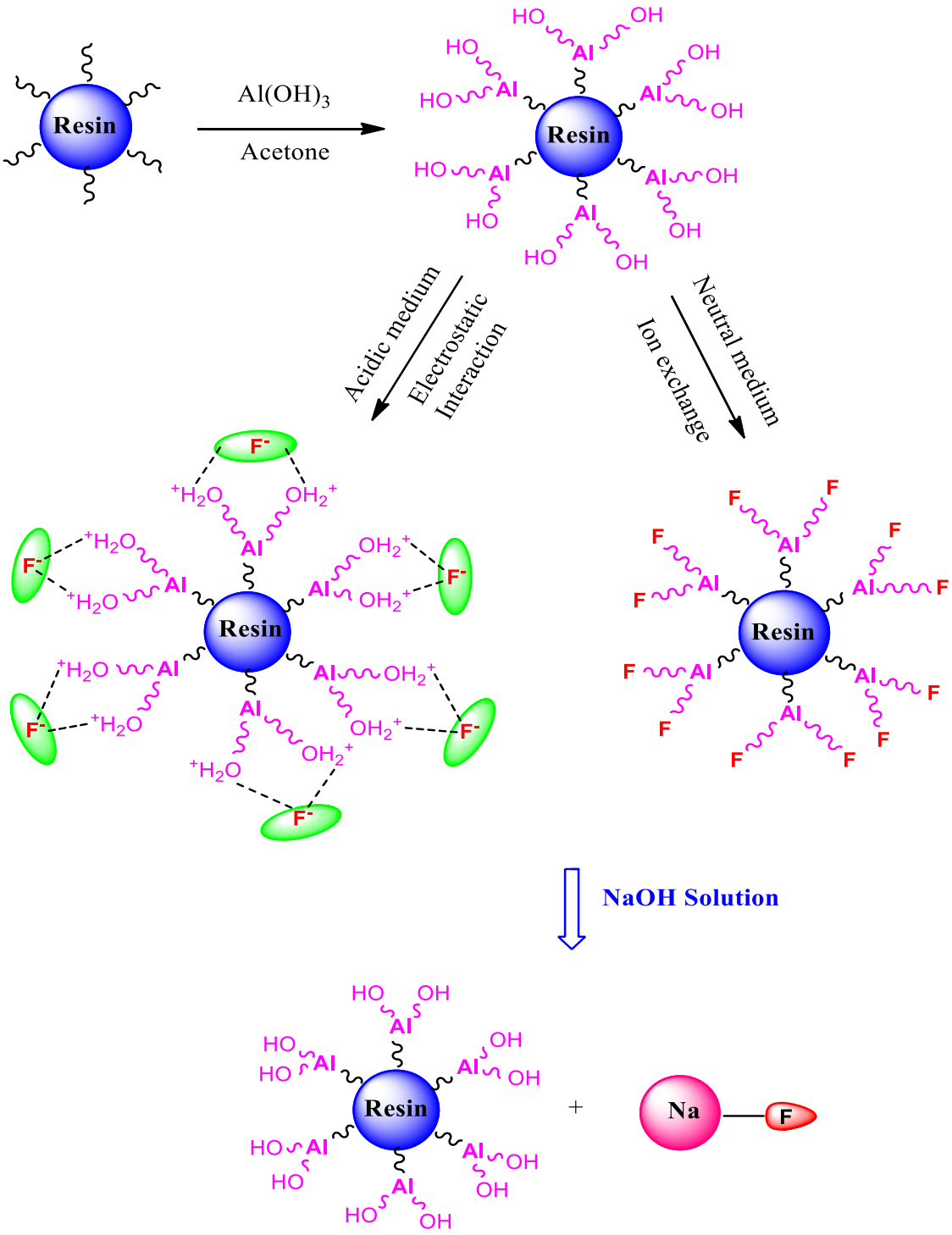

Figure 4.2. Schematic diagram depicting the interaction of fluoride with Aluminum hydroxide impregnated macroporous polymeric resin adsorbent

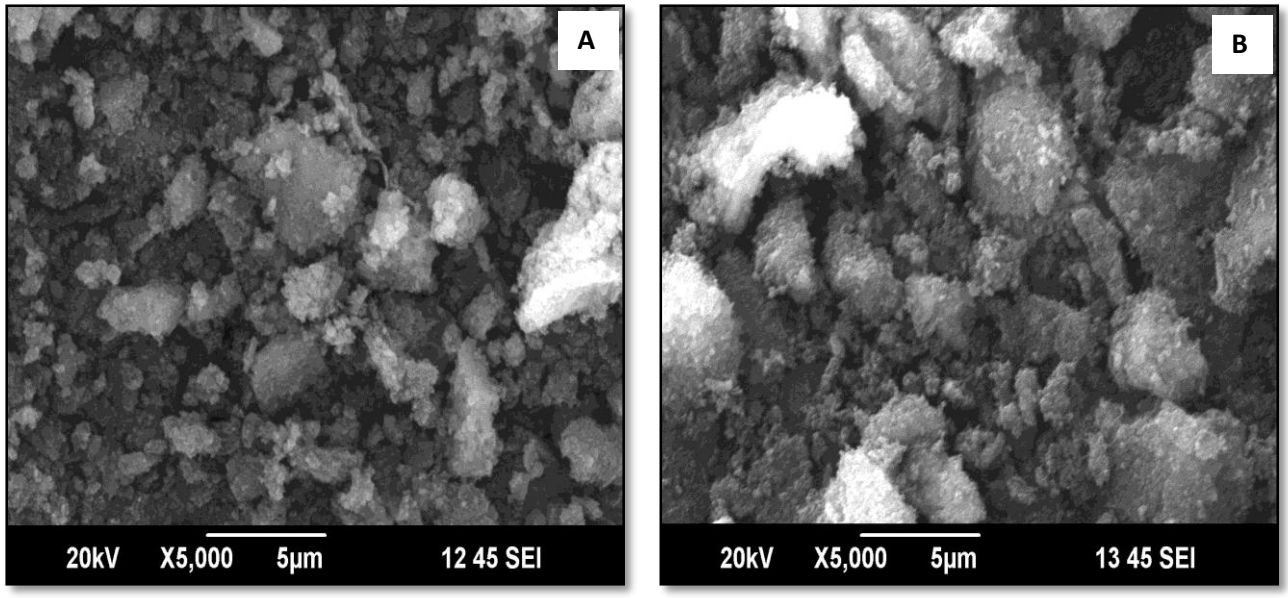

Figure 4.3. SEM and EDS images of aluminum hydroxide impregnated macroporous polymeric resin adsorbent (A) and fluoride ion adsorbed (B) onto the adsorbent surface.

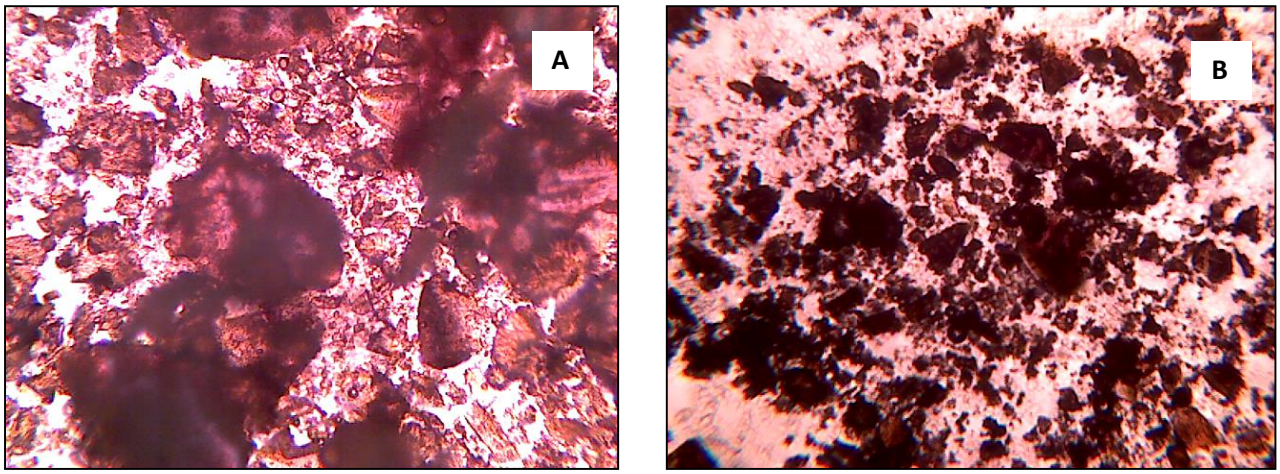

Figure 4.4. Optical images of adsorbent (Spot test reagent added) (E) and fluoride adsorbed onto adsorbent (F)

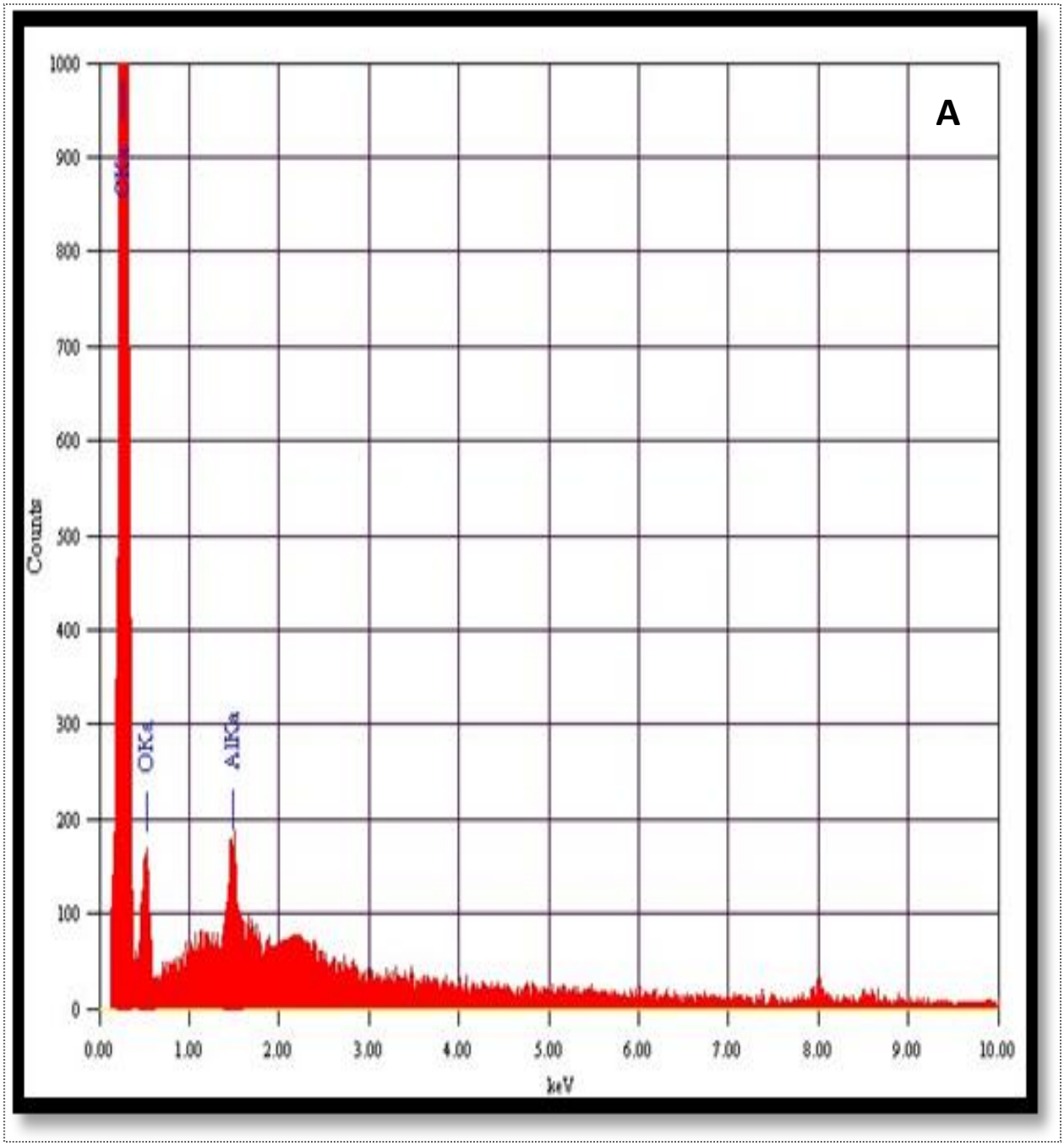

Figure 4.5a. EDS spectrum of aluminum hydroxide impregnated macroporous polymeric resin adsorbent

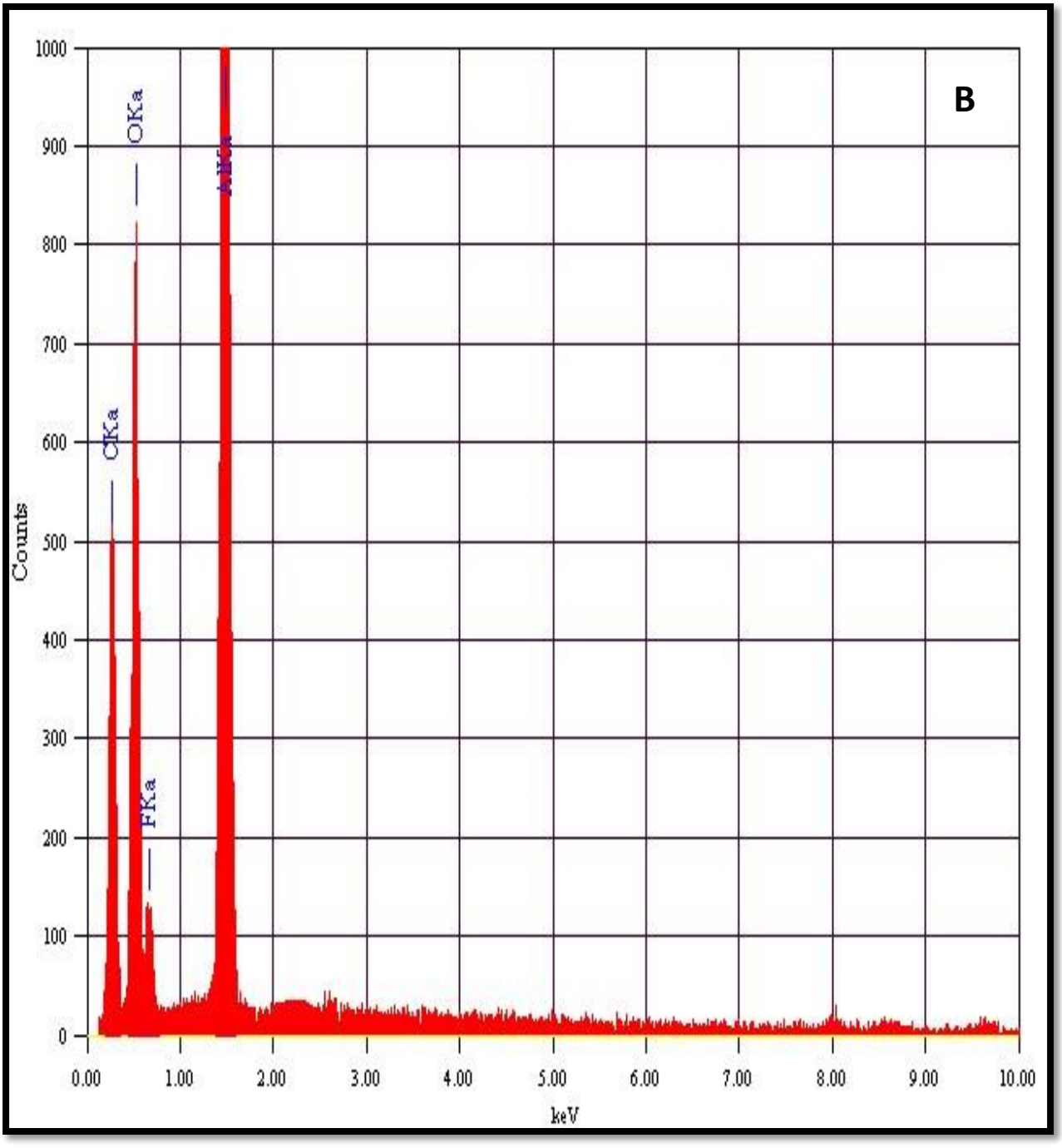

Figure 4.5b. EDS spectrum of aluminum hydroxide impregnated macroporous polymeric resin adsorbent after fluoride ion adsorbed onto the adsorbent surface.

The XRD profiles (Figure 4.6) before and after fluoride adsorption onto aluminum hydroxide impregnated macroporous polymeric resin shows interesting features. The bayerite phase [α-Al (OH) $_3$] corresponding to the diffraction peaks at 2θ=18.67° for (001) and 40.87° for (201) indicates the formation of the amorphous aluminum hydroxide onto the porous polymeric resin.[21] After fluoride adsorption onto the metal hydroxide impregnated macroporous polymeric resin, the characteristic peaks shifted form 18.67° to 17.41° and additional peaks were observed at 2θ=38.2°, 47.8° and 65.0° indicating the exchange of hydroxyl group by fluoride ion in aqueous solution to form aluminium fluoride (JCPDS no: 76-2058) adsorbed onto the resin matrix.

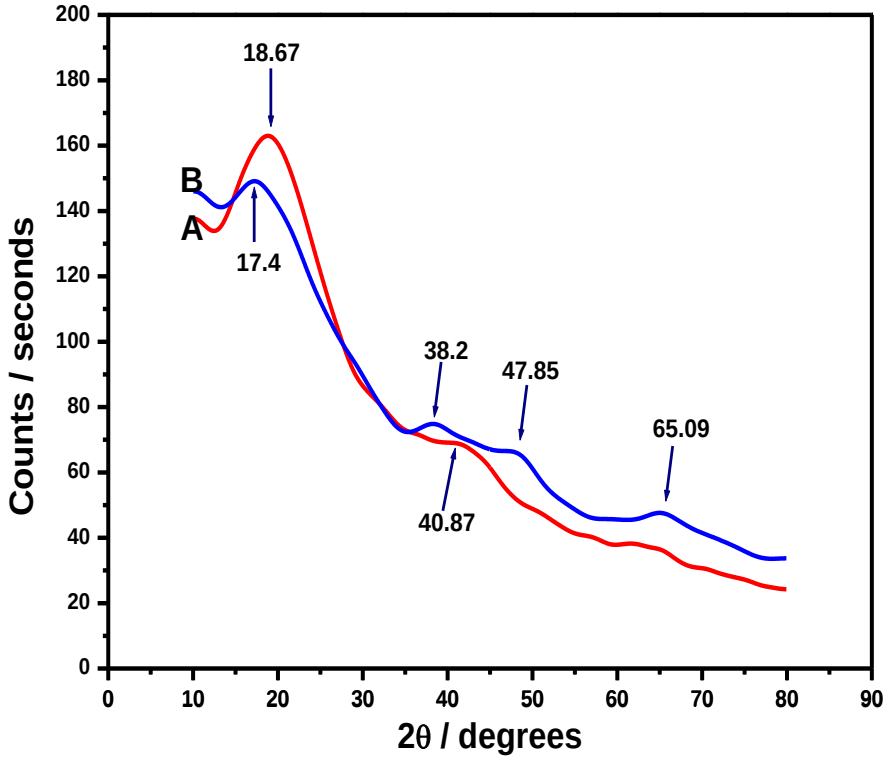

Figure 4.6. XRD pattern of Aluminum hydroxide impregnated macroporous polymeric resin adsorbent (A) and after fluoride ion adsorption (B)

The BET surface area of the Al $(OH)_3$ incorporated polymeric resin adsorbent obtained from N_2 adsorption-desorption isotherm plot (Figure 4.7a) and BET isotherm plot (Figure 4.7b) was found to be 373.73 $m^2\ g^{-1}$. There is a decrease in the surface area of resin matrix after the impregnation of $Al(OH)_3$. This could be ascribed to the fact that Al^{3+} resides favorably at the entry to the resin pores, resulting in considerable obstruction thereby inhibiting the flow of nitrogen into the resin surface. Consequently, the void space available for nitrogen adsorption is reduced, resulting in lower surface area values after metal impregnation onto resin matrix. However, even after the incorporation of Al(III) ion, the surface area of the polymeric resin is still large enough (330 $m^2\ g^{-1}$) to foster effective interaction of fluoride. The type IV isotherm plots indicate the mesoporous nature of the adsorbent. At lower pressure ($P/P_0 < 0.4$), the isotherm shape is similar to type II indicating the macroporous nature of the adsorbent. At high pressure ($P/P_0 > 0.4$), monolayer adsorption is evident and overall the nature of the metal ion impregnated adsorbent shows transition from multilayer to monolayer depending on the relative pressure ranges. The Barrett-Joyner-Halenda (BJH) pore size distribution curve (Figure 4.7c) provides a pore specific surface area of 300.38 $m^2\ g^{-1}$ and a pore size of 1.22 nm at a maximum pore volume of 0.997$cm^3\ g^{-1}$. Moreover, BJH distribution curves exhibit pore size in the range 2 to 16 nm confirming the presence of mesopores at the adsorbent surface. This indicates that Al^{3+} ions are strongly bound to the surface of the resin matrix, thereby enhancing the effective adsorption of fluoride ions from aqueous solution.

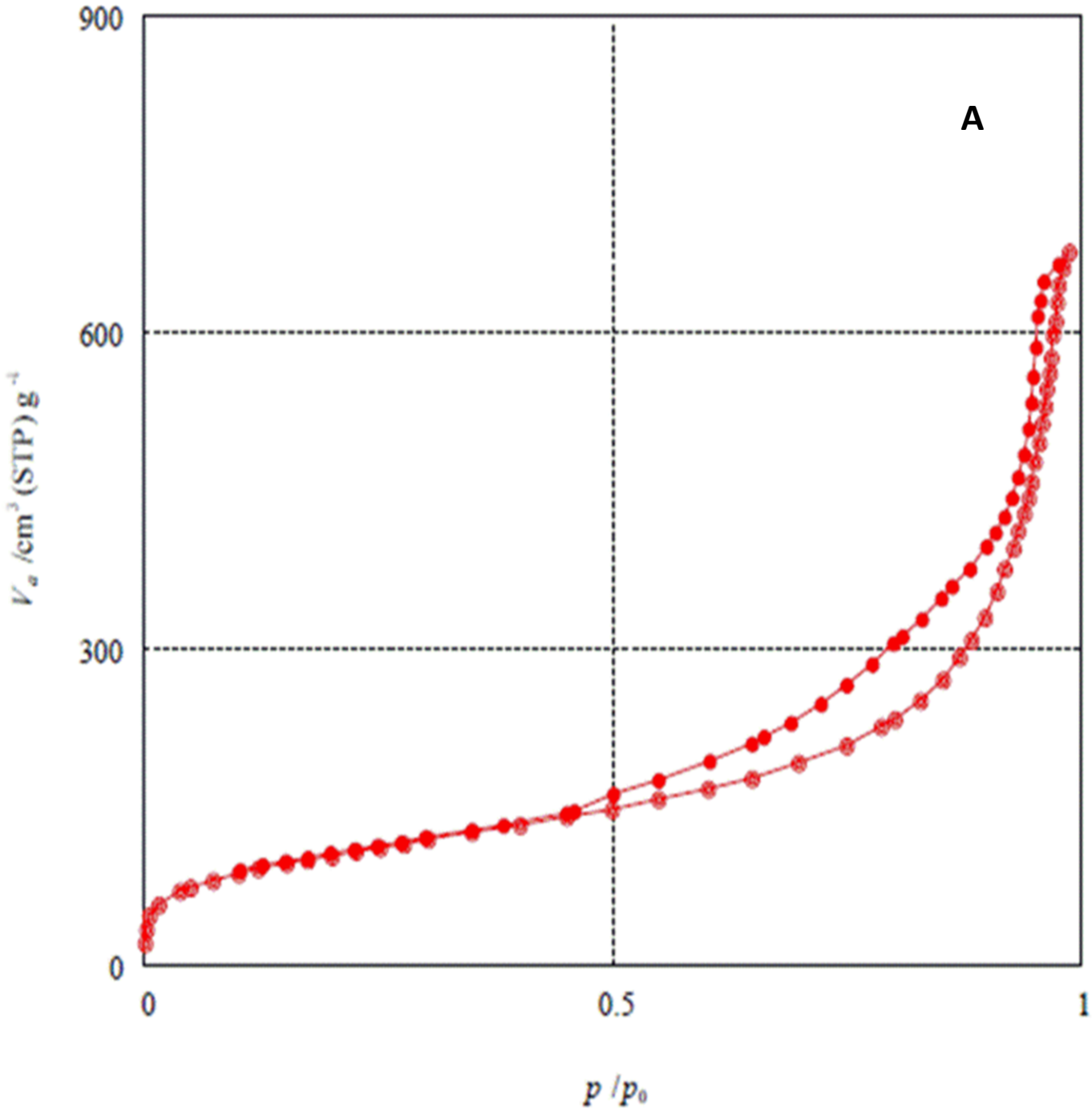

Figure 4.7a. N_2 adsorption-desorption isotherm plot of $Al(OH)_3$ impregnated macroporous polymeric adsorbent

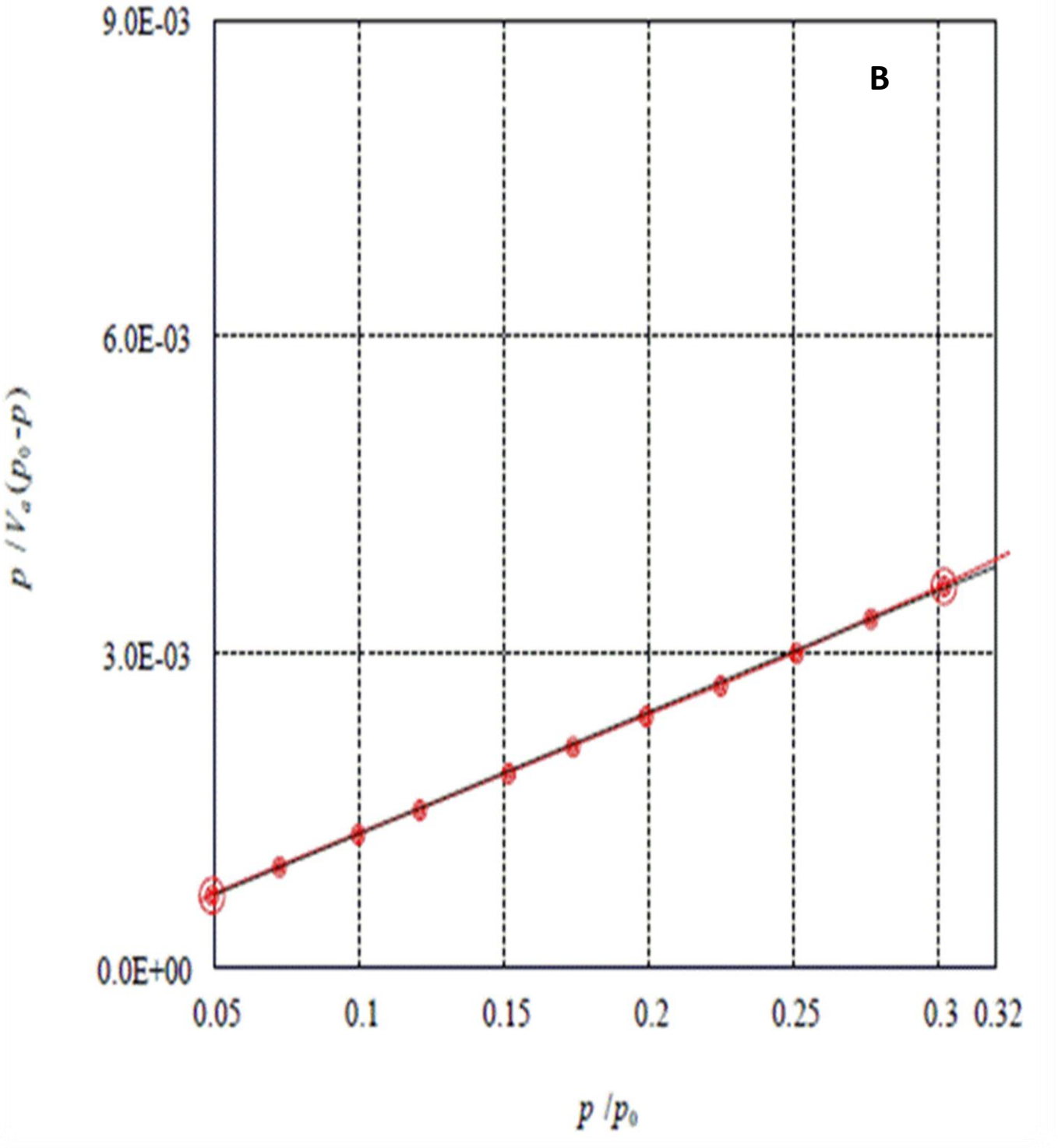

Figure 4.7b. BET isotherm plot of $Al(OH)_3$ impregnated macroporous polymeric adsorbent

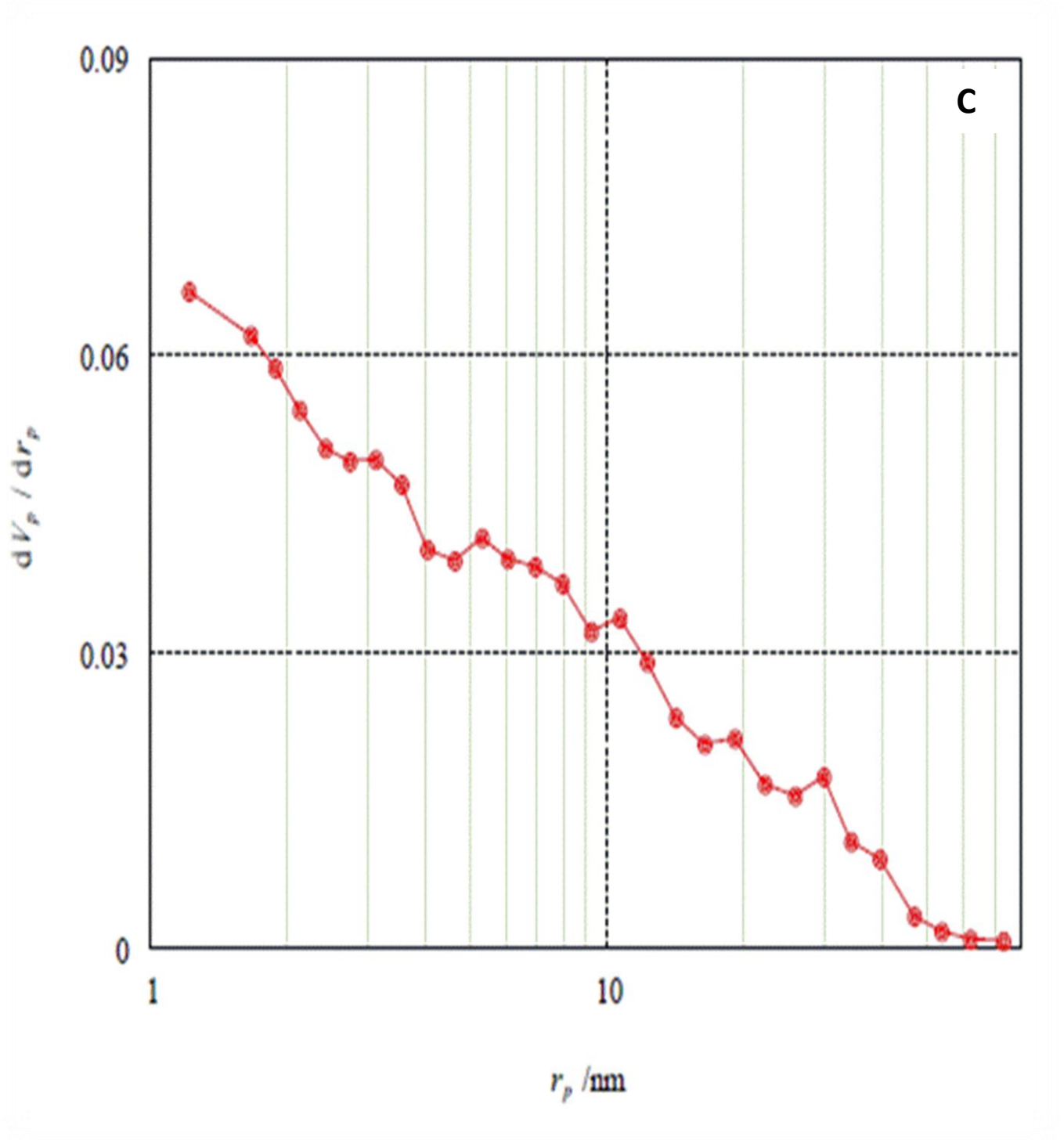

Figure 4.7c. BJH distribution curve of $Al(OH)_3$ impregnated macroporous polymeric adsorbent.

(ii) Mechanism for interaction between Al $(OH)_3$ and the resin

Amberlite XAD resins have a remarkably high surface area and it has been reported by Hubbard et al[25] [30] that the repeat units of XAD resins have a pendant or residual vinyl group depending on the degree of functionalization and cross linking of the vinyl benzene groups. They have also reported that XAD 1180 resin has a residual vinyl content of 1.6-1.8 mmol g^{-1}. Yang et al[26] have also proved that osmium (as its tetraoxide) could be anchored on to the residual or pendant vinyl groups in XAD resins by a process called as osmylation. In the same manner, the impregnation of aluminium hydroxide on to the residual vinyl groups (within the pores of the XAD1180 resin matrix) could be referred to as '*alumylation'*. The mechanism of impregnation of aluminium hydroxide onto the macroporous polymeric resin matrix is shown in three steps (Figure 4.8). In accordance with the familiar Fajan's rule, the Al^{3+} ion due to its high charge and small size has a high ionic potential and hence can polarize the hydroxide ion. A peak observed at 3027 cm^{-1} corresponds to the C-H stretching frequency of the residual vinyl groups present in the polymeric resin matrix. Hence, the π electrons in the residual vinyl group can foster the attack on the electrophilic aluminium ion to give a cyclic aluminium cation. Herein, the positive charge is shared between the more stable secondary carbon and aluminium. The charge on this carbon is sufficiently large enough to favor a Markonikov orientation of addition. The absence of this peak after impregnation indicates that Al^{3+} is anchored on the pendant vinyl groups in the XAD resin matrix. It is now more probable for the OH^- ion to attack the carbon on the bridged aluminium cation that is well suited to accommodate the positive charge. This results in the formation of a C-OH bond as evident from FT-IR spectrum through the appearance of a peak at 1117 cm^{-1}. This is quite typical for a secondary alcohol C-O stretching frequency. Furthermore, the peak observed at 907 cm^{-1} could be attributed to the Al-OH and O-Al-O bending vibrations[23,24] confirming that Al $(OH)_3$ is anchored onto the macroporous polymeric resin effectively.

Step 1

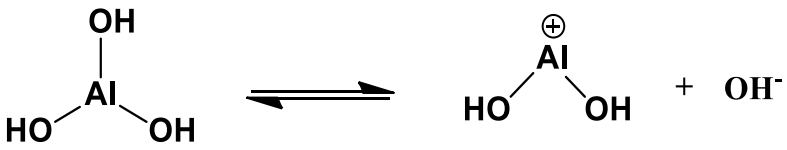

Step 2

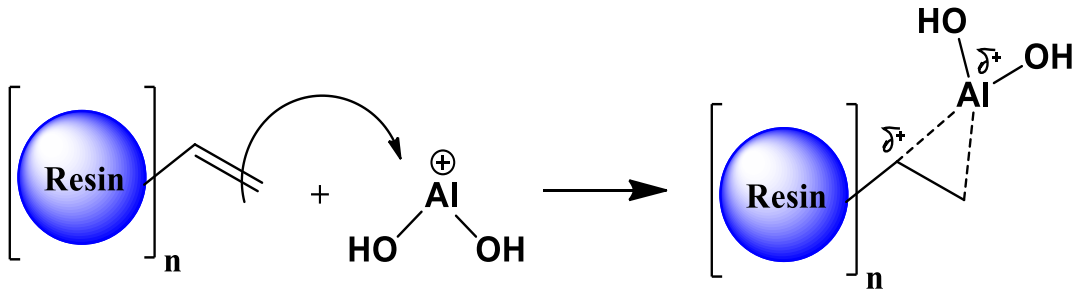

Step 3

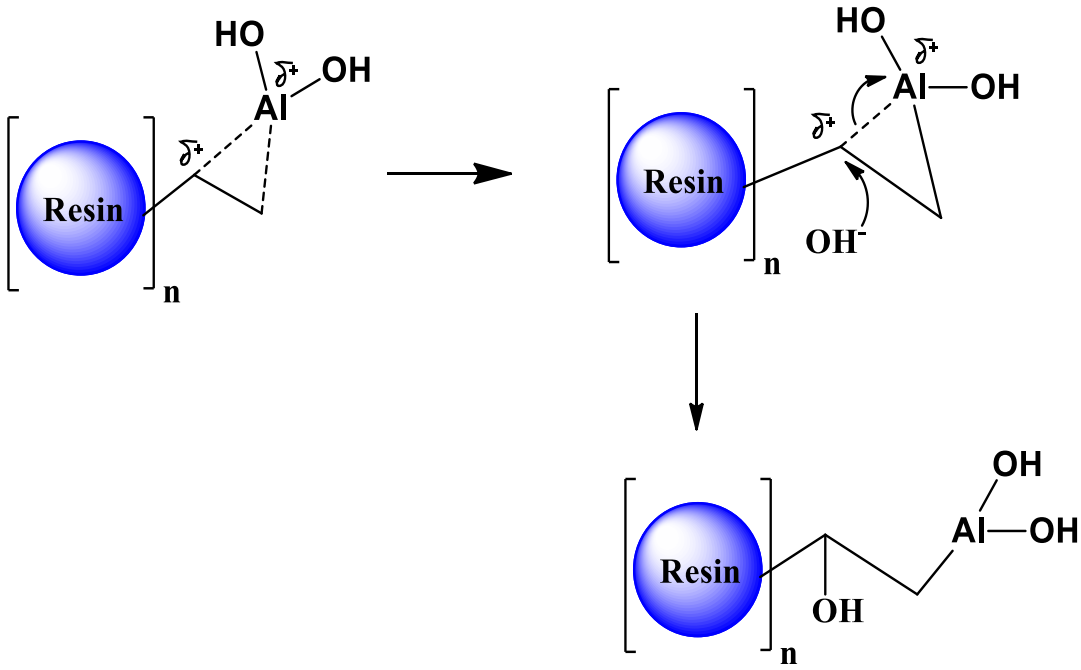

Figure 4.8. Proposed mechanism for preparation of aluminum hydroxide impregnated macroporous polymeric resin adsorbent.

(iii) Effect of pH

The removal of fluoride ions from aqueous medium is pH dependent. Hence, the fluoride sorption onto the polymeric resin matrix was studied at varying pH (3.0-9.0) using 0.1 g of the adsorbent at 303 K. The pH at the zero point charge of aluminum hydroxide impregnated macroporous polymeric resin adsorbent was determined by batch equilibration technique.[1] About 0.1g of the $Al(OH)_3$ impregnated adsorbent was added to 50 mL of 0.1 mol L^{-1} KNO_3 solution. The initial pH was regulated using 0.1mol L^{-1} HNO_3 or NaOH solution, in the range 3.0 - 9.0 and kept in a thermostat shaker at 27 ◦C for 24 h. The final pH of the solutions was recorded after 24 h. The pH_{zpc} of the aluminum hydroxide impregnated macroporous polymeric resin adsorbent was determined from the plot of [$pH_{initial} - pH_{final}$] versus $pH_{initial}$.

Figure 4.8 shows the percentage of fluoride adsorption as a function of pH as well as the plot of [$pH_{initial} - pH_{final}$] versus $pH_{initial}$. The pH_{zpc} was found to be 5.01 and typically, the adsorbent surface would be positively charged below the pH_{zpc} and negatively charged above pH_{zpc}. Hence, with 5.0 mg L^{-1} initial fluoride concentration below pH 5.01, the percentage of F^- ion adsorption is relatively higher as evident from Figure 4.9. Al^{3+} usually forms $[Al_{13}O_4(OH)_{24}(OH_2)_{12}]^{7+}$, $[Al_4O(OH)_{10}(OH_2)_5]^0$, and $[Al_6(OH)_{14}(OH)_7]^{2-}$ complexes in acidic, neutral, and alkaline conditions[27,28] respectively. The isoelectric point of $Al(OH)_3$ lies in the pH range of 7.5–8.5.[29] At pH 3.0, the metal hydroxyl groups present in the aluminium impregnated resin matrix would be protonated and hence facilitates the adsorption of fluoride through electrostatic interactions. Further, ion exchange is also plausible at neutral pH thereby enhancing the adsorption. The protonation of AlOH, followed by electrostatic interaction and ion exchange[30] are possible (Figure 4.2) depending on the solution pH.

When the pH is less than the isoelectric point of $Al(OH)_3$, the cationic aluminum hydroxides would be attracted to negatively charged fluoride ion. The increase in the negative charge on the surface of aluminum hydroxide above pH 8.5 results in surface electrostatic repulsion thereby decreasing the removal efficiency of fluoride. The possibility of the formation of soluble aluminates ($[Al(OH)_4]^-$) at sufficiently alkaline pH is also inherent and leads to the decrease in the percentage adsorption. The formation of

these soluble ionic constituents also affects the effective interaction of the cationic hydroxides of aluminium with fluoride. As a consequence, weakly acidic pH favors effective adsorption of fluoride.

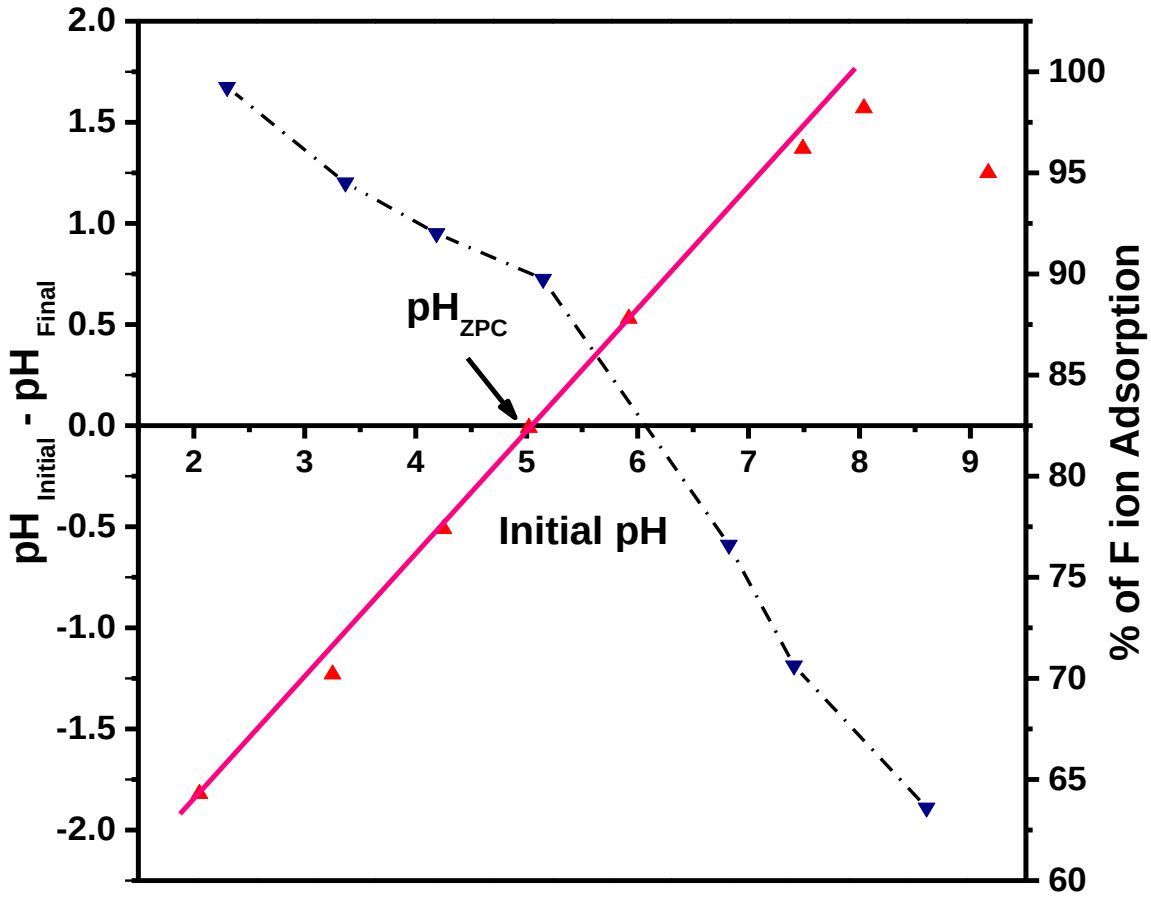

Figure 4.9. Zero point charge of the adsorbent and Impact of pH towards the F^- ion adsorption

(iv) Adsorption Isotherm studies

A variety of empirical isotherm models were used to review the experimental fluoride adsorption data. These isotherms feature some valuable parameters and the most popular among them are the Langmuir[31] and Freundlich isotherms.[32] Linear isotherms have been widely employed in several adsorption studies. However, in the present study, since some

of the experimental data points deviate from linearity, the nonlinear model would give a better fit to the data. Accordingly, the Langmuir and Freundlich isotherm data were studied by means of the non-linear model and the relevant plots (Figure 4.10) as well as the isotherm parameters were acquired using the Origin 9.0 software. The various isotherm parameters are given in Table 4.1. The q_{max} obtained from the nonlinear Langmuir model was found to be 92.39 mg g^{-1}. Although, the coefficient of determination R square has been used in many isotherm studies, the adjusted R square is usually considered to be a better way of expressing the fitting of data since it also takes into account the degrees of freedom involved with the sum of the squares. The coefficient of determination for the above isotherms was close to unity. A still better method to compare the models was obtained through the Akaike's Information Criterion (AIC) statistical methodology.[33] The AIC values were obtained through the equations

$$AIC = N\ ln\frac{SSE}{N} + 2N_p + \frac{2\mathrm{N_p}\left(N_p + 1\right)}{N - N_p - 1} \quad (27)$$

where N is the number of data points, and Np refers to the number of parameters in the corresponding models. Furthermore, the AIC values could also be compared using another parameter called as evidence ratio which is defined as

$$Evidence\ Ratio = e^{0.5\Delta_0} \quad (28)$$

where Δ is the difference in the AIC values between the two models. This comparison method ideally suits several two or three parameter isotherm models. The AIC values for the Langmuir and Freundlich models at different pH values are shown in Table 4.1. At pH 3.0, the evidence ratio of 2,282 means that the Freundlich model is 2.28 x 10^3 times more likely to be appropriate than the Langmuir isotherm. But Langmuir isotherm fits approximately 24 times more than that Freundlich isotherm at pH 7.0. The AIC value reduces from 24.5 to 15.6 when the experiments were repeated with fluoride spiked tap water at pH 7.0. This could be ascribed to the fact that at pH 3.0, the adsorption would be more random, fast and multilayer.

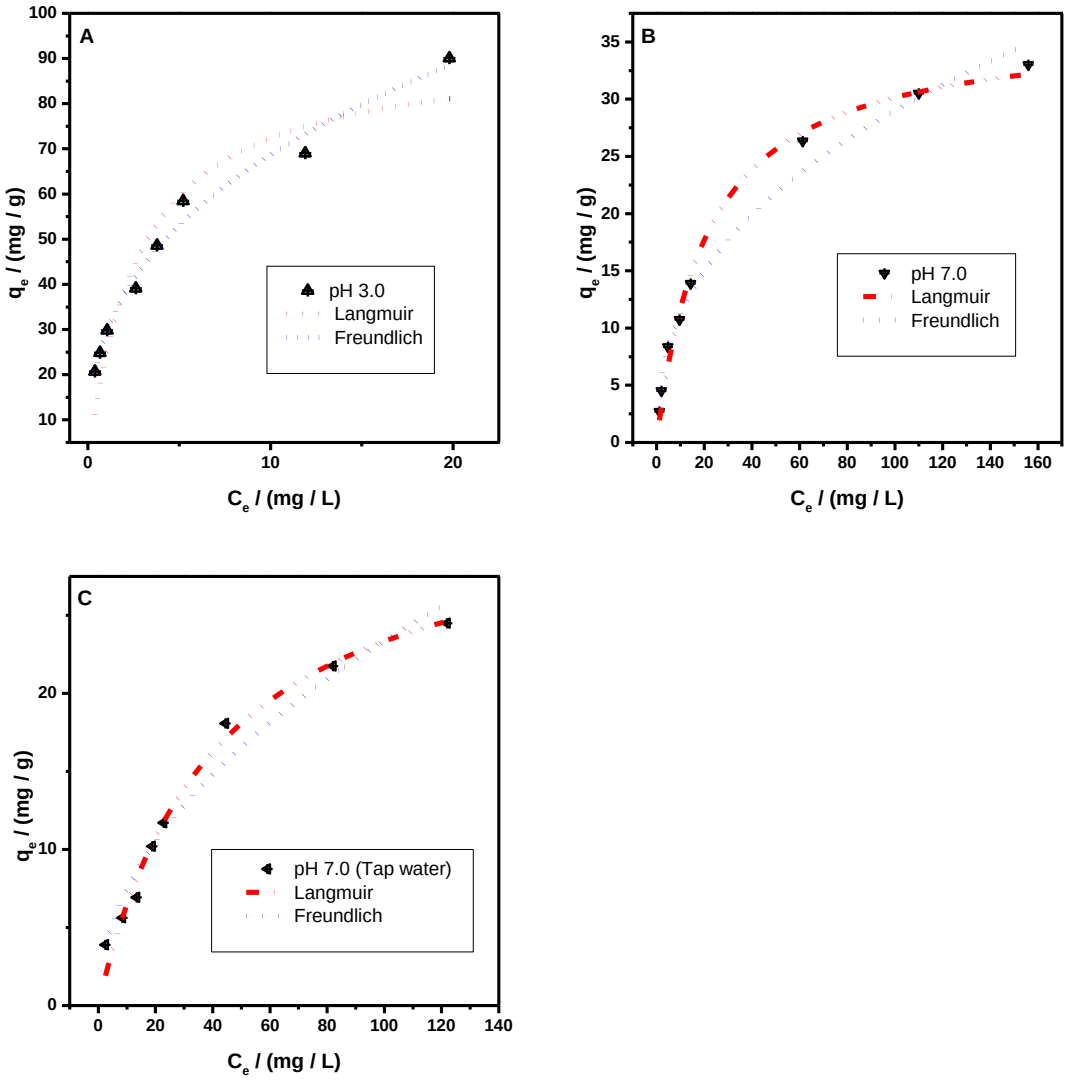

Figure 4.10. Non-linear Langmuir and Freundlich Isotherm plots obtained at pH 3.0 (A), pH 7.0 (B) and pH 7.0 (C, Tap water)

However, at higher pH, when the surface begins to acquire a net negative charge, the adsorption would favor a more ordered monolayer Langmuir model. Hence, at the natural pH of drinking water, the Langmuir model gives a better fit to the experimental data. Furthermore, a dimensionless parameter (R_L = 1 / 1 + b C_o) is used to link the energy of adsorption (b) for the Langmuir isotherm in describing the adsorption F ion onto the polymeric matrix. The value of R_L for the adsorption of fluoride ion on the aluminium hydroxide impregnated macroporous polymeric resin adsorbent was found to

be 0.052 and 0.7641 at pH 3.0 and pH 7.0 respectively which indicates the applicability of Langmuir isotherm[34] in describing the adsorption process.

Table 4.1. Adsorption isotherm parameters

Non-linear Isotherm Parameters	Non-linear Equation	pH		
		3.0	7.0	7.0 (Tap water)
Langmuir				
q_{max} (mg g^{-1})	$q_e = \frac{q_m b C_e}{1 + b C_e}$	92.393	36.610	32.927
b (L mg^{-1})		0.3614	0.0466	0.0243
R_L		0.052	0.7641	0.7994
Adj.R^2		0.902	0.991	0.982
SSE		334.71	7.5932	6.3321
χ^2_{red}		55.785	1.2655	1.0553
AIC		36.270	5.9825	4.5296
Freundlich				
K_F (mg $^{1-1/n}$ g^{-1} $L^{1/n}$)	$q_e = K_F C_e^{1/n}$	29.236	4.3672	2.3687
n		2.6960	2.4324	2.0117
Adj.R^2		0.986	0.980	0.965
SSE		48.342	16.893	12.587
χ^2_{red}		8.0571	2.8155	2.0979
AIC		20.8047	12.3798	10.026

The nonlinear isotherm plots at different pH (Figure 4.10) and the distinct isotherm parameters given in Table 4.1 indicate good affinity of the fluoride anion towards the aluminium hydroxide impregnated macroporous polymeric resin adsorbent. The nonlinear Freundlich isotherm plot (Figure 4.10) gives the adsorption intensity (n) in the range 1-10, showing the favorable[35] adsorption of fluoride onto aluminium hydroxide

impregnated macroporous polymeric resin surface. The adsorption capacity was also checked for drinking water sample. The drinking water (0.7 mg L^{-1} Fluoride) sample was spiked with varying fluoride concentrations (10, 20, 30, 40, 50, 80, 120 and 160 mg L^{-1}) in order to find out the maximum Langmuir adsorption capacity from the Langmuir isotherm plot (Figure 4.10). The q_{max} was found to be 31.27 mg g^{-1} for drinking water at pH 7.0.

(v) Adsorption kinetic studies

The nonlinear pseudo-first and second order models were used to evaluate the kinetics fluoride adsorption (Figure 4.11A and B). The Weber–Morris[36] intraparticle diffusion plot (Figure 4.11C and D) also gave an intercept suggesting that diffusion is not the only phenomenon that controls the adsorption of the fluoride ion on the aluminium hydroxide impregnated macroporous polymeric resin adsorbent. The kinetic parameters for the three kinetic models are listed in Table 4.2. The q_e (experimental and calculated) values match well with the second order model. Furthermore, the adjusted R square and the reduced chi square value also illustrate the applicability of the second order model in explaining the adsorption kinetics.The rate of adsorption of F^- ion on the surface of the aluminium hydroxide impregnated macroporous polymeric resin adsorbent could be influenced by a) external mass transfer where the halide is transported from the bulk solution to the external resin surface. b) intraparticle or pore diffusion, in which the adsorbate (fluoride) could enter the interior of the resin particles and c) adsorption. Amidst these three processes, adsorption is quicker and therefore surface or pore diffusion could influence the adsorption kinetics of fluoride. Adsorption step happens relatively fast and hence it is assumed that it does not have considerable influence on the overall kinetics of adsorption. The fluoride adsorption process exhibited three stages and the first linear portion could be attributed to the process of the diffusion of fluoride onto to the adsorbent surface. The second portion could be ascribed to intra-particle diffusion, which is a relatively slow process. The third stage accounts for diffusion through the pores of resin surface, followed by the attainment of equilibrium.

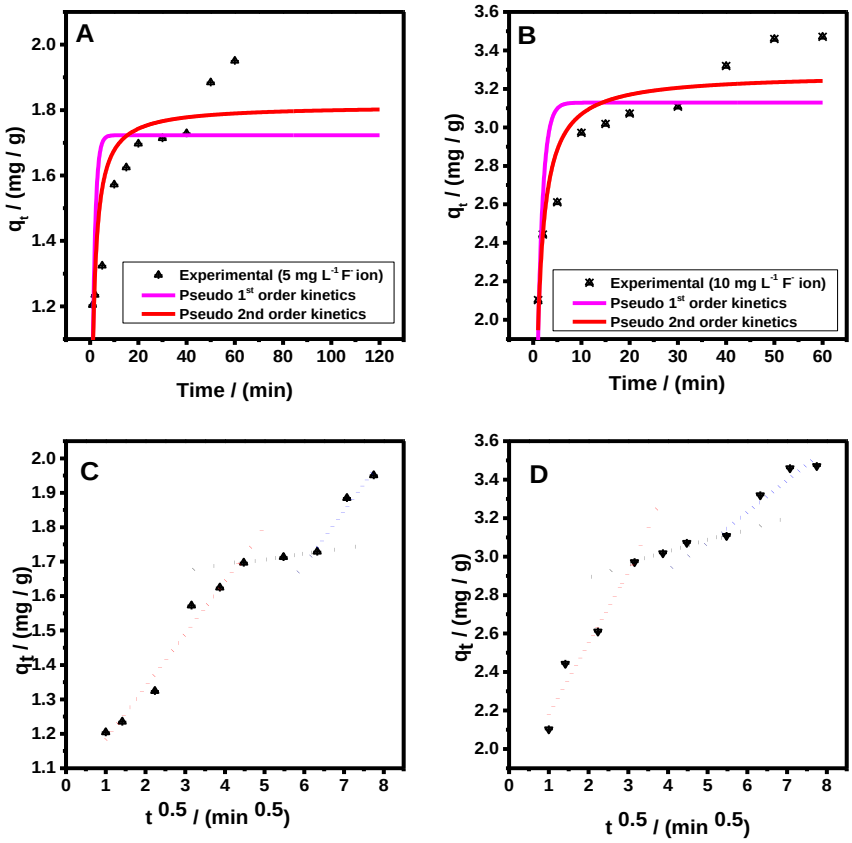

Figure 4.11. Plot of q_t against t at different fluoride concentrations (A and B) and Plot of q_t against $t^{1/2}$ at different fluoride concentrations (C and D)

Table 4.2. Kinetic parameters and intra-particle rate constant for fluoride ion adsorption

Conc. of F^- ion ($mg\ L^{-1}$)	q_e $mg\ g^{-1}$	Pseudo first order kinetic model			Pseudo second order kinetic model			Intraparticular diffusion model	
		k_1 min^{-1}	q_1 $mg\ g^{-1}$	R^2	k_2 $g\ mg\ min^{-1}$	q_2 $mg\ g^{-1}$	R^2	k_{int} $g\ mg^{-1}\ (min^{0.5})^{-1}$	R^2
4.806	2.0065	0.7556	1.8246	0.746	0.4839	2.0935	0.897	1.6196	0.998
10.461	3.471	0.9252	3.1286	0.609	0.4453	0.7088	0.841	2.7863	0.951

(vi) Adsorption Thermodynamics

The equilibrium between the fluoride ion in the solution and solid phase could be expressed as

$$[F^-_{solution}] \rightleftharpoons [F^-_{Solid}] \qquad (29)$$

So,

$$K_a = \frac{aF^-_{solution}}{aF^-_{solid}} \qquad (30)$$

Where K_a = Thermodynamic equilibrium constant. The Gibbs standard free energy expressed as

$$\Delta G = \Delta G^0 - RT ln \frac{aF^-_{solid}}{aF^-_{solution}} \quad (31)$$

Furthermore,

$$a_{\pm} = \gamma_{\pm} C \qquad (32)$$

Where $\gamma_{\pm}$ is activity coefficient, C is concentration of the active species. For a dilute solution, (40 mg F^- ion or 9 x 10^{-4}M NaF) the activity coefficient is very close to unity, so that the activity is equal to the concentration of the active species.

Now,

$$K_a = \frac{C^-_{Faq}}{C^-_{FSolid}} = \frac{C_{ads}}{C_e} = K_c \qquad (\therefore a = C) \qquad (33)$$

Hence at equilibrium $\Delta G = 0$ and therefore,

$$\Delta G^o = -RT \ln K c \qquad (34)$$

The equilibrium constant K_c was therefore obtained from the ratio of solid phase fluoride ion concentration at equilibrium (mg L^{-1}) to the concentration in solution (mg L^{-1}). The Gibb's free energy (ΔG^0) was obtained through above equation for the respective temperatures and the corresponding K_c values. The aluminium hydroxide impregnated macroporous polymeric resin adsorbent was subjected to adsorption of fluoride at different and the graphical connectivity between $\ln K_c$ and 1/T gives the enthalpy and entropy changes. The values of $\Delta H^0$and ΔS^0 were calculated from the $\ln K_c$ against 1/ T plot (Figure.4.12) The interaction between $Al(OH)_3$ impregnated resin and the F^- ion is crucial to comprehend the thermodynamics of adsorption.

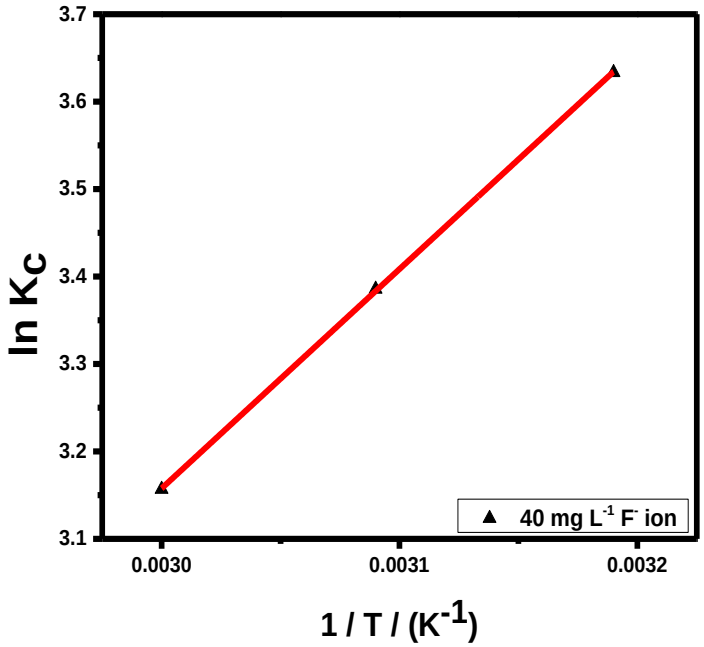

Figure 4.12. Variation of $\ln K_c$ with 1/T

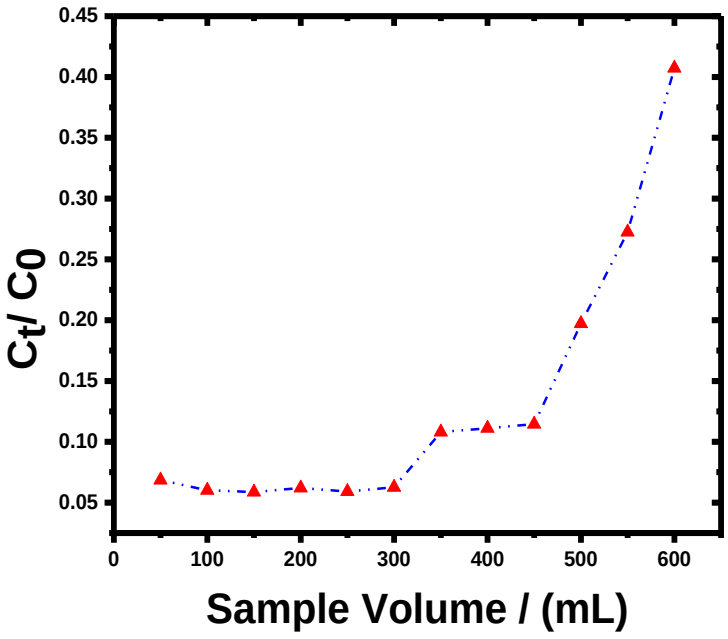

Figure 4.13. Plot of C_t/C_0 against the sample volume

The spontaneity of adsorption process is obvious from the Gibb's free energy values (Table 4.3) which are negative at the temperatures studied for 40, 50 and 60 mg L^{-1} of fluoride.[37] The negative enthalpy values obtained for all three concentrations shows that the adsorption is exothermic process. For a physical adsorption phenomenon, then ΔH^0 is typically lower than 80 kJ mol^{-1}, and a broad range of 80 - 400 kJ mol^{-1} is possible[38] for chemical adsorption. So the fluoride adsorption onto adsorbent surface is exothermic, favourable to the physical adsorption (since ΔH^0 = -20.845 $kJmol^{-1}$) which confirms by the experimental data is leading to obeying Freundlich isotherm at pH 3.0. The negative ΔS^0 values also suggest decreased randomness at the aluminium hydroxide impregnated macroporous polymeric resin adsorbent-solution interface.

Table 4.3. Thermodynamic parameters for adsorption of fluoride ion at different temperatures

Conc. of F^- ion (mg L^{-1})	Temperature (K)	ΔG^o (kJ mol^{-1})	ΔH^o (kJ mol^{-1})	ΔS^o (J K^{-1} mol^{-1})	Adj.R^2
40.0	313	-9.45	-20.845	-36.283	0.999
	323	-9.09			
	333	-8.74			

(vii) Preliminary column studies

The applicability of the aluminium hydroxide impregnated macroporous polymeric resin adsorbent material on a laboratory scale was checked for the defluoridation of water from a higher sample volume by loading 0.75 g of the sorbent in a glass column (2.5 cm dia, 30 cm (length). With the preliminary lab scale column study, we could bring down the level of fluoride to less than 1.5 ppm with 0.75 g of the adsorbent (with C_o= 5.43 mg L^{-1} F^-) up to a sample volume of 550 mL. Beyond 550 mL, the level of fluoride in the solution phase exceeded 1.5 ppm. Hence, the sample volume that could be tolerated effectively is taken as that in which the fluoride levels are within the permissible limit.

The plot of C_t/C_o against the sample volume is shown in Figure 4.13 and further studies are ongoing to optimize the various column parameters. A fixed volume of laboratory tap water was also spiked with 5 mg L^{-1} fluoride ion was delivered to the column at a flow rate of 5 mL min^{-1} and the concentration of fluoride was measured in the out coming solution using the ion meter. The concentration of fluoride was found to be less than 0.6 mg L^{-1} suggesting good removal efficiency.

4.1.4. Conclusions

The interaction between the aluminium hydroxide impregnated macroporous polymeric resin adsorbent and fluoride has demonstrated the potential application for defluoridation. Various characterization techniques supported the adsorption of fluoride through electrostatic, ion exchange and hydrogen bonding mechanism. The second order kinetics and the exothermic, spontaneous adsorption are other characteristic features associated with this method. A sample volume of 1500 mL on a laboratory scale column containing 5.0 mg L^{-1} of fluoride could be brought down to less than 1.0 mg L^{-1}. The robust polymeric resin adsorbent exhibits an adsorption capacity of 36.37 mg g^{-1} at pH 7.0. The q_{max} was found to be 31.27 mg g^{-1} for drinking water and this is attainable at the natural pH range prevalent in water and hence the method could pave way to develop a prototype and extend it to remediate fluoride in field applications.

References

1. Barathi, M.; Kumar, A. S. K.; Rajesh, N. *J. Environ. Chem. Eng.* **2013**, 1, 1325.
2. Udhaya Sankar, M.; Aigal, S.; Maliyekkal, S. M.; Chaudhary, A.; Anshup, Anil Kumar, A.; Chaudhari, K.; Pradeep, T. *Proc. Natl. Acad. Sci. U. S. A.* **2013**, 110, 8459.
3. Alexandratos, S. D. *Ind. Eng. Chem. Res.* **2009**, 48, 388.
4. Kumar, A. S. K. PhD Thesis, **2014**, BITS-Pilani Hyderabad, India.
5. SivaKesavaRaju, CH. PhD Thesis, **2006,** IIT Madras, India.
6. Zhou, L.; Bosscher, M.; Zhang, C.; Ozcubukcu, S.; Zhang, L.; Zhang, W.; Li, J. Liu, C. J.; Jensen, M. P.; Lai, L.; He, C. *Nature Chem.* **2014**, 6, 236.
7. Warshawsky, A.; *Talanta* **1974**, 21, 624.
8. Meenakshi, S.; Viswanathan, N. *J. Colloid Interface Sci.* **2007**, 308, 438.
9. Luo, F.; Inoue, K. *Solvent Extract. Ion Exch.* **2004**, 22, 305.
10. Ku, Y.; Chiou, H.; Wang, W. *Sep. Sci. Technol.* **2002**, 37, 89.
11. Ruixia, L.; Jinlong, G.; Hongxiao, T. *J. Colloid Interface Sci.* **2002**, 248, 268.
12. Mizuki, H.; Ito, Y.; Samatya, S.; Harada, H.; Kawakita, H.; Uezu, K. *Solvent Extract. Ion Exch.* **2011**, 29:1, 146.
13. Popat, K.M.; Anand, P.S.; Dasare, B.D. *React. Polym.* **1994**, 23, 23
14. Bhandari, R.; Janardhana, C. *Desalination and Water Treatment* **2016**, 57, 9437
15. Solangi, I.B.; Memon, S.; Bhanger, M.I. *J. Hazard. Mater.* **2010**, 176, 186.
16. Prabhu, S.M.; Meenakshi, S. Desalin. Water Treat. **2013**, 52, 1.
17. Luo, F.; Inoue, K. *Solvent Extract. Ion Exch.* **2004**, 22, 305.
18. Jain, S.; Jayaram, R.V. *Sep. Sci. Technol.***2009**, 44, 1436.
19. Barroso, M. N.; Gomez, M. F.; Arrua, L. A.; Abello, M. C. *Catal. Letters.* **2006**, 109, 13.
20. Qi, X.; Wang, Z.; Li, S.; Li, B.; Liu, X.; Lin, B. *Acta Phys. Sin.* **2006**, 22, 198.
21. Meher, T.; Basu, A. K.; Ghatak, S. *Ceram. Int.* **2005**, 31, 831.
22. Du, X.; Wang, Y.; Su, X.; Li, J. *Powder Technol.* **2009**, 192, 40.
23. Ma, C.; Chang, Y.; Ye, W.; Shang, W.; Wang, C. *J. Colloid Interface Sci.* **2008**, 317, 148.
24. Mozgawa, W.; Krol, M.; Bajda, T. *J. Mol. Struct.* **2009**, 924-926, 427.
25. Hubbard, K. L.; Finch, J. A.; Darling, G. D. *React. Func. Polym.***1998**, 36, 17.
26. Yang, J. W.; Han, H.; Roh, E. J.; Lee, S. G.; Song, C. E. *Org. Lett.* **2002**, 4, 4685.
27. Meher, T.; Basu, A. K.; Ghatak, S. *Ceram. Int.* **2005**, 31, 831.
28. Mahe, M.; Reynders, P.; Demourgues, A.; Heintz, J. *J. Am. Ceram. Soc.* **2007**, 90, 217.
29. Elmasry, M. H.; Sadek, O. M.; Mekhemer, W. K. *Water Air Soil Pollut.* **2004**, 158, 373.
30. Salifu, A.; Petrusevski, B.; Ghebremichael, K.; Modestus, L.; Buamah, R.; Aubry, C.; Amya, G. L. *Chem. Eng. J.* **2013**, 228, 63.
    I. Langmuir, *J. Am. Chem. Soc.* **1918**, 40, 1361.
31. Freundlich, H. M. F. *Z. Phys. Chem.* **1906**, 57, 385.

32. El-Khaiary, M. I.; Malash, G.F. *Hydrometallurgy* **2011**, 105, 314.
33. Sundaram, C. S.; Viswanathan, N.; Meenakshi, S. *J. Hazard. Mater.* **2008**, 155, 206.
34. Haghseresht, F.; La, G. *Energy Fuels* **1998**, 12, 1100.
35. Weber, W. J.; Morris, J. C. *J. Sanit. Eng. Div. Am. Soc. Civ. Eng.***1963**, 89, 3.
36. Swain, S. K.; Dey, R. K.; Islam, M.; Patel, R. K.; Jha, U.; Patnaik, T.; Airoldi, C. *Sep. Sci. Technol.* **2009**, 44, 2096.
37. Salifu, A.; Petrusevski, B.; Ghebremichael, K.; Modestus, L.; Buamah, R.; Aubry, C. Amy, G. L. *Chem. Eng. J.* **2013**, 228, 63-74.

CHAPTER 5

5. Preparation and characterization of Graphene oxide-Aluminium oxyhydroxide adsorbent for the effective defluoridation of water

5.1.1. Introduction

This chapter deals with the studies involved in the adsorption of fluoride onto the surface of Graphene oxide-Aluminium oxyhydroxide adsorbent followed by its application to real field water samples. Several techniques such as precipitation, coagulation, oxidation, solvent extraction, evaporation, distillation, reverse osmosis, ion exchange and electro dialysis are reported for fluoride removal. The inherent lacunae such as cost factor, stability of the resin and leaching of toxic aluminum are a major concern. These aspects have been brought out in numerous papers pertaining to fluoride adsorption. To circumvent the problem associated with the other techniques, adsorption is the most viable option and in this regard carbonaceous materials prove to be very effective. Variety of adsorbents are known for the remediation of fluoride from drinking water.[1] Among these, carbonaceous materials such as carbon nanotubes[2] and activated carbon[3] are quite effective for facile defluoridation of water by virtue of their high specific surface area, surface functional groups and adequate pore size distribution. Over the years, activated carbon[4] (AC) is universally used as an adsorbent for water treatment to remove a wide range of aquatic pollutants. Recently, Graphene oxide has emerged as an attractive member of carbon family in the same view of its high surface area and presence of various functional groups (hydroxyl, epoxy groups and carboxylic).[5,6] Graphene[7] has also proven to be an effective adsorbent for the adsorption of F^- ion in aqueous solution with an adsorption capacity of 17.65 mg g^{-1}. A novel metalloporphyrin grafted-graphene oxide[8] has been utilized as a sensor for F^- ion in aqueous solution and hence it is possible that suitable modification of graphene oxide could also assist in the adsorption of F^- ion with good adsorption capacity. The incorporation of Zr-hydroxide into graphene oxide can significantly increase the adsorption capacity of negatively charged ionic pollutants.[9,10] Furthermore, manganese oxide coated graphene oxide (MOGO)[11] studied recently for fluoride ion adsorption as a new hybrid material shows an adsorption capacity of 11.63 mg g^{-1}. Basic aluminum sulfate@ graphene hydrogel has been reported to possess an adsorption capacity of 33.4 mg g^{-1} at pH 7.2 towards F^- ion adsorption.[12]

A careful inspection of the literature shows that graphene oxide has not been explored to its full potential for enhanced fluoride adsorption. Taking advantage of the inherent properties of graphene oxide, aluminium oxy hydroxide [Al-O (OH)] incorporated graphene oxide was tested for potential application towards defluoridation. GO-Al $(OH)_3$ composites are fairly easy to synthesize[13] and chitosan reinforced with nano AlOOH composite[14] and chitosan–GO hydrogel composite[15] show good capacity to purify water free from microbial contaminants and toxic dyes respectively. Till date, there are no reports on the use of [Al-O (OH)] incorporated graphene oxide for defluoridation. Since, Al^{3+} is a hard acid, and F^- ion is a typical hard base, it is envisaged that the interaction between these two oppositely charged ionic species onto the GO surface would enhance the removal of fluoride. The objective of this work was to explore the mechanism of F^- ion adsorption onto [Al-O (OH)] incorporated graphene oxide adsorbent surface and its application in the real field water samples.

5.1.2. Experimental Section

(i) Preparation of Graphene oxide from graphite

An improved method was used for the synthesis of graphene oxide as reported earlier.[16] This procedure has considerable advantages in terms of more hydrophilic oxidized graphene, less toxicity and easy temperature control over the commonly followed Hummer's method of preparation. About 1.5 g of graphite powder was taken and gradually added to 9:1 mixture of concentrated H_2SO_4/H_3PO_4. The reaction was gently warmed to 35-40 ^oC followed by heating to 60 ^oC and constantly stirred for 12h. The above reaction mixture was cooled to room temperature and slowly poured in ice cold peroxide solution, where the brown colour entirely turned to yellow. Subsequently, the mixture was centrifuged at 4000 rpm for 4h and the supernatant was decanted away. The solid material obtained after centrifugation was thoroughly washed with 200 mL of water followed by 200 mL of 30% HCl and 200 mL of ethanol. After each wash, the filtrate was centrifuged at 4000 rpm for 2 h and the supernatant was discarded. The solid material was kept for drying at 30 ^0C in vacuum oven (Biotechnics, India) for 48 h.

(ii) Preparation of [Al-O(OH)] incorporated graphene oxide

About 0.2 g of graphene oxide was dispersed in 100 mL of Milli-Q water. The exfoliation was done by sonication (Ultrasonic bath, Biotechnics, India) for 1 h at a 15 min intermittent time interval. Subsequently, 6.30 g of aluminium sulfate was added to the exfoliated graphene oxide solution and stirred for 2 h. The pH was adjusted to 7.0 using 1.0 mol L^{-1} sodium hydroxide solution and stirred for an extended time interval of 16 h. The reaction mixture was filtered, washed with Millipore water several times to remove sulfate ions (tested using $BaCl_2$ solution) thoroughly. The adsorbent was dried overnight at 30 ^oC in a vacuum oven.

(iii)Adsorption studies through batch experiments

For the batch adsorption studies, about 50 mg of the GO-Al-O (OH) adsorbent was added to 100 mL of 5 mg L^{-1} fluoride ion solution in the pH range 6.5-7.5 and equilibrated in an orbital incubator shaker (Biotechnics, India) at different time intervals. The initial and final (equilibrium) concentrations of fluoride present in the solution phase were estimated using the F^- ion selective electrode. The adsorption percentage of fluoride increased with time and good removal efficiency occurs within 60 min thereby bringing the fluoride ion concentration to the allowable limits as per the WHO guidelines. The experimental data were analyzed by equilibrating varying initial concentrations of fluoride ion (5, 10, 20, 30, 40, 50 and 60 mg L^{-1}) with a known weight (50 mg) of the adsorbent and fitted using various adsorption isotherms.

(iv)Column study

This novel GO-Al-O(OH) adsorbent material shows very good potential toward extending to fluoride containing ground water as evident from the batch adsorption studies. Preliminary column studies were conducted on a laboratory scale glass column. About 2.0 g of GO-Al-O (OH) adsorbent was packed into a short glass column for checking the applicability on a laboratory scale. A known volume (2.0 L) of 5 mg L^{-1} F^- ion solution prepared in Milli Q water was fed to the column. The fluoridated solution passed through the adsorbent column at a flow rate of 6 mL min^{-1}, the out coming F^- ion concentration present in water was monitored frequently. The concentration of fluoride after treatment was found to be within the permissible limits (1.0- 1.5 mg L^{-1}). Fluoride

could adsorb effectively and the regeneration was effective for 3 adsorption-desorption cycles (with fluoride levels well within the permissible limits) using 30 mL of 1.0 mol L^{-1} NH_4OH as ammonium fluoride in the eluate. The percentage of desorption was calculated as

$$\text{Desorption Ratio (\%)} = \frac{\text{Amount of fluoride desorbed into the eluate}}{\text{Amount of fluoride adsorbed onto adsorbent surface}} \times 100 \quad (35)$$

The regeneration percentage of cycles 1, 2 and 3 were observed to be 76.85, 75.75 and 73.21 % respectively.

4.1.3. Results and Discussion

(i) Characterization of the adsorbent

a) Electronic (UV-Visible)spectroscopy

Figure 5.1A shows the UV-Vis spectrum of synthesized graphene oxide which was dispersed with Milli-Q water by ultrasonication. The absorption around 225 nm along with a shoulder peak around 300 nm corresponds to π-π* transition of C-C bonds[17] and C=O bonds of graphene oxide.[18]

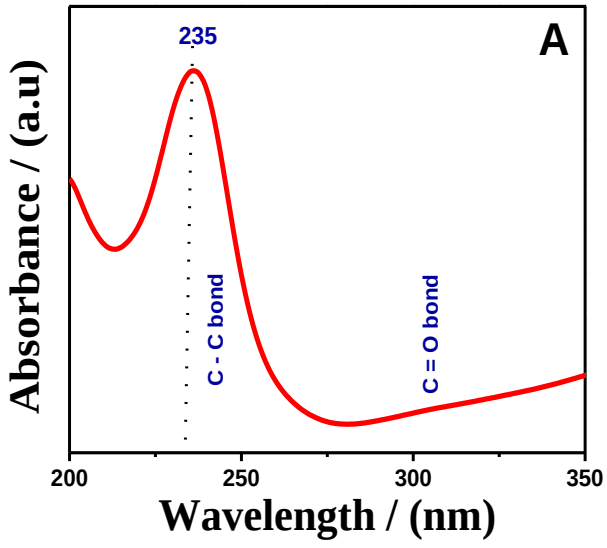

Figure 5.1. A) UV-Vis spectrum of graphene oxide

b) FT-IR Spectrum Analysis

The FT-IR spectrum of native graphite (Figure not shown) yields two peaks around 1672 cm^{-1} and 1536 cm^{-1} corresponding to C=C stretching vibrations as reported previously.[20] In addition, the peaks at 3152 cm^{-1} and 1401 cm^{-1} correspond to aromatic C–H stretching and C–H bending respectively.[21] Graphene oxide, a single layer of graphite oxide has various functional groups such as carboxyl, carbonyl, epoxy, hydroxyl[19] and these were identified using FT-IR spectroscopy. Figure 5.1B shows the FT-IR spectrum of Graphene oxide, [Al-O (OH)] incorporated graphene oxide adsorbent and after the adsorption of fluoride. The peaks observed at 3414 cm^{-1} and 1387 cm^{-1} could be ascribed to C-OH groups that are introduced in the graphite matrix during oxidation.[21] The absorption bands around 2856 cm^{-1} and 2923 cm^{-1} corresponds to ν_{sym} and ν_{asym} stretching vibrations of CH_2.[22] The broadness of peak at 3414 cm^{-1} could be attributed to the OH stretching vibrations.[23] The peaks around 1725 cm^{-1} and 1627 cm^{-1} correspond to C=O stretching of carboxylic/carbonyl functional groups while the peaks at 1215 cm^{-1} and 1050 cm^{-1} correspond to C-O bond[24,25] stretching vibrations confirming the formation of graphene oxide. After the impregnation of aluminium ion onto the surface of graphene oxide, the band at 3414 cm^{-1} was shifted to 3431 cm^{-1} and the peak broadened, indicating the interaction of metal ion with O-H groups of graphene oxide thereby increasing the proximity of Al–OH groups towards the surface of graphene oxide. In addition to this, the strong band at 609 cm^{-1} is assigned to the vibrational mode of AlO_6 while another two bands at 1116 and 1637 cm^{-1} can be attributed to Al–OH stretching and bending vibrations in the boehmite lattice.[26,27] With the adsorption of fluoride onto the adsorbent surface, the peak intensities are modified and the peak at 535 cm^{-1} could be related to the Al-F interaction.[28]

c) FT-Raman spectrum Analysis

Raman spectroscopy is yet another valuable non-destructive spectroscopic tool used to acquire valuable evidence for carbonaceous materials such as graphene.[29,30] Earlier reports[31,32] suggest that two distinct bands (G and D) are observable in the Raman spectra of graphitic materials.

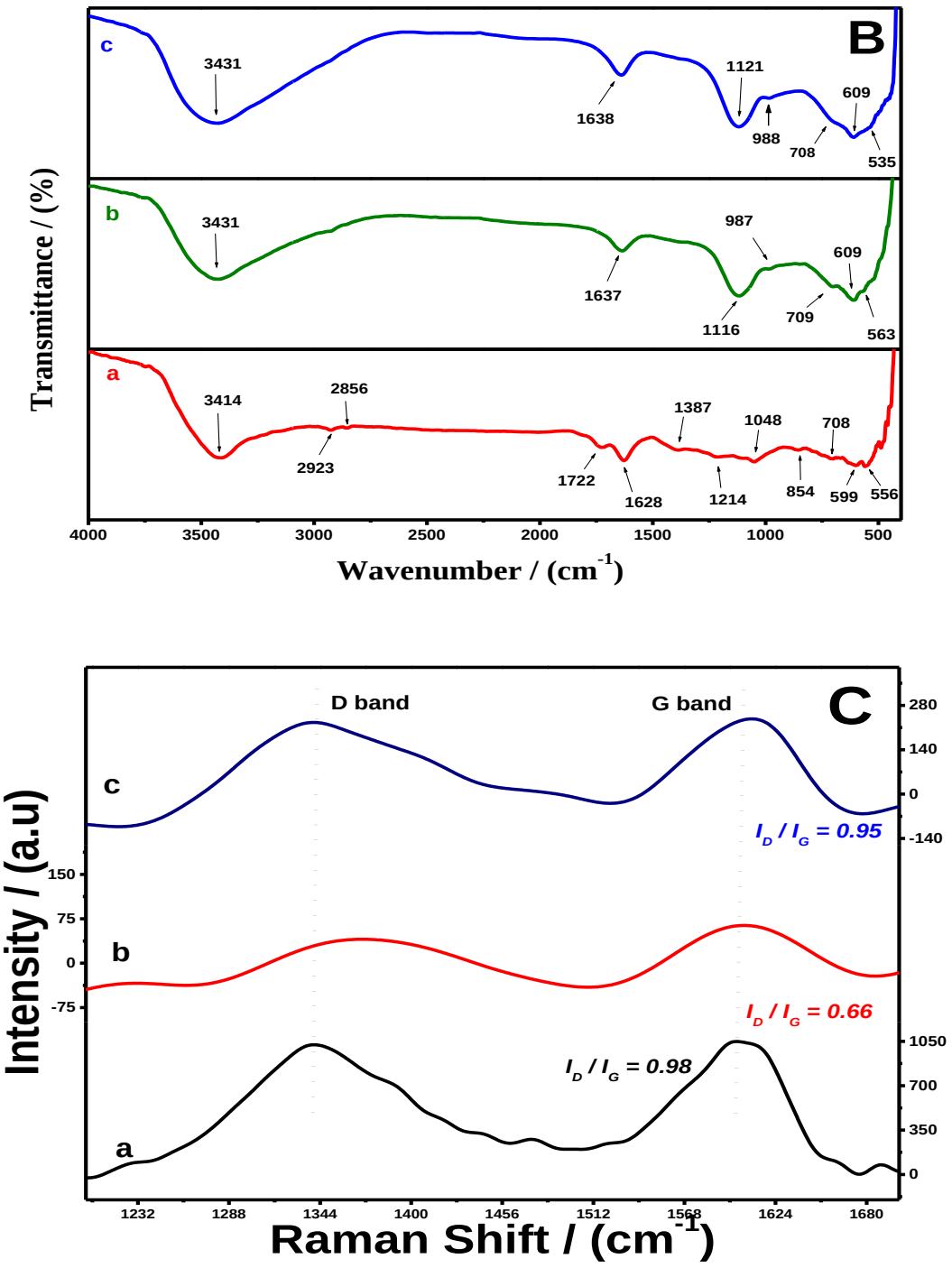

Figure 5.1. B) FT-IR spectra C) Raman spectra of synthesized GO (a), GO-Al-O(OH) adsorbent before (b) and after fluoride ion adsorption (c).

In case of pristine graphite, these bands are obvious at 1351 cm^{-1} and 1582 cm^{-1}. The D band is quite distinct for sp^3 domains in carbon layers and the G band provides reliable

information about the sp^2 in-plane vibrations.[29,33] Figure 5.1C shows the Raman spectra of GO showing a strong band at 1601 cm^{-1} (G band) for the optical E_{2g} in plane vibration at the Brillouin zone center and a weak band around 1340 cm^{-1} (D band) ascribed to A_{1g} breathing mode of vibrations.[34] Generally, in plane vibrations attributed to E_{2g} would be Raman active for carbonaceous materials possessing sp^2 hybridized carbon atoms. Nevertheless, the A_{1g} mode of vibrations are normally activated, when some defects appear at near k-point of Brillouin zone through an inter-valley double-resonance Raman phenomenon.[35] The intensity of D band is often used as a yardstick to quantify the extent of disorder in carbon-based materials. When the Al^{3+} ion interacts with GO, the intensity ratio I_D/I_G decreases from 0.98 to 0.66 and also the D band shows a shift from 1340 cm^{-1} to 1365 cm^{-1} which reveals the reduction of the oxidized molecular defects.[35] Further, I_D/I_G ratio is inversely related to the average crystallite size in graphitic materials.[36] After the fluoride adsorption, the intensity of I_D/I_G increases to 0.95 which implies that the level of disorder increases at surface as compared to the adsorbent thus leading to an increase in the ratio of I_D/I_G.

d) Powder XRD Analysis

Earlier literature reports suggest[31,37] the distinct diffraction peaks for graphite at 2θ = 26.38^o and 54.54^o corresponding to the planes (002) and (004) planes respectively in accordance with JCPDS No. 00-041-1487. In case of GO (Figure 5.1D) we observed the diffraction peaks (002) and (004), to be displaced by approximately 16^o and 12^o as a result of exfoliation of the graphite layers. The other diffraction peaks (100), (101), (102) and (103) characteristics of graphite were not observed and this indicates the presence of carbonyl, hydroxyl and carboxyl functional groups in GO during the exfoliation. The contributions to the reflection of other planes in graphite are negligible due to the exfoliation resulting from the oxidation of the graphite layers.[38] Further, the interlayer distance of the (002) peak plane[38] for GO is 9.10 Å (2θ = 9.709^o) which is larger than the native graphite (3.37Å), thereby confirming the expansion and exfoliation of graphite layers. The interlayer distance of GO increases to 9.24Å in ethanolic medium compared to approximately 6.6Å for a solvent free medium and this could be attributed to the intercalation of a solvent monolayer in the GO structure.[39]

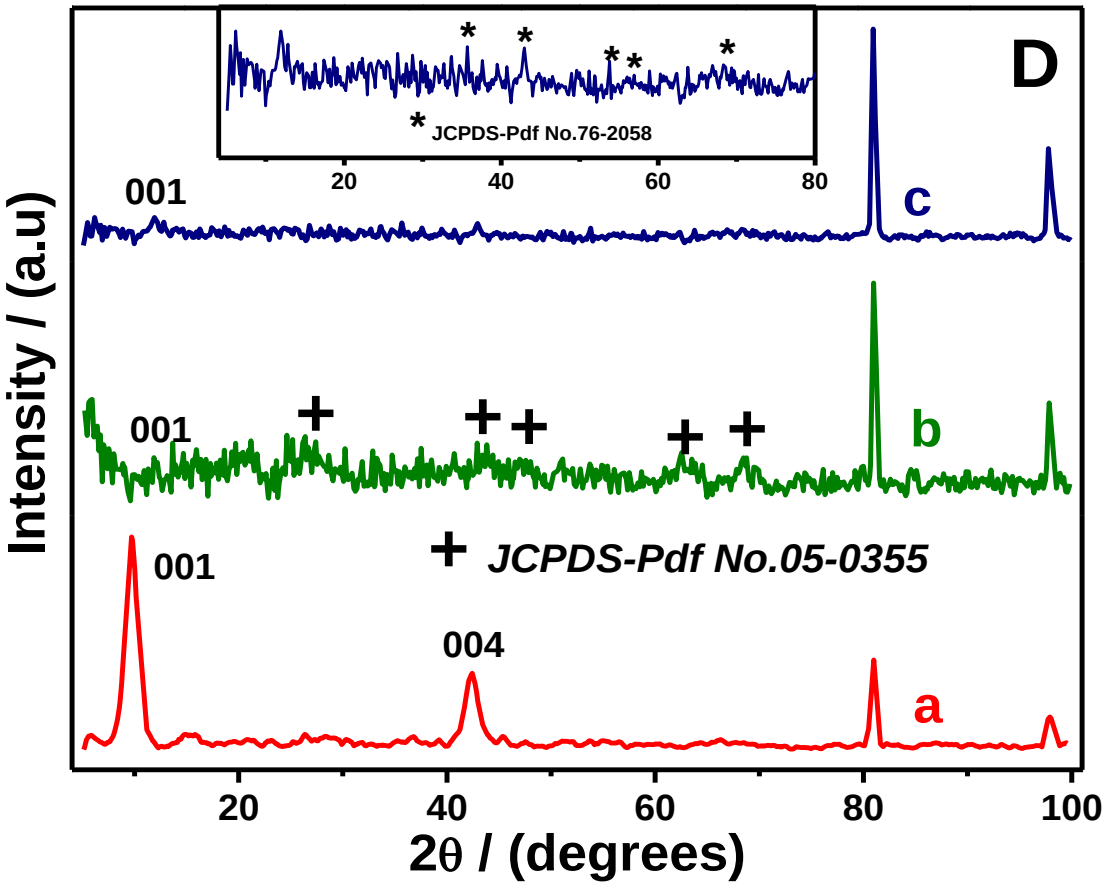

Figure 5.1. D) XRD spectra of synthesized GO (a), GO-Al-O(OH) adsorbent before (b) and after fluoride ion adsorption (c).

The XRD pattern of GO-Al-O (OH) adsorbent (Figure 5.1D) clearly shows that (002) and (004) planes of graphene oxide completely disappeared and shifted to around 2θ = 12° due to the interaction of Al^{3+} ions with the surface functional groups of GO. Since graphite is c-axis oriented, during oxidation process the functional groups are primarily introduced in the (002) and (004) planes only. Due to the amorphous nature of metal hydroxide, new peaks appear with small intensities at 2θ = 27.05°, 43.44°, 47.17°, 62.89° and 68.03° corresponding to the (120), (140), (131), (151) and (061) planes and these could be attributed to the presence of aluminium oxy hydroxide on the surface of graphene oxide (JCPDS No. 05-0355). After the adsorption of fluoride ion, the peaks were observed at 35.65°,42.92°,53.99°,56.38° and 68.45° corresponding to the (101), (210), (211), (220) and (301) planes of aluminium oxy fluoride (JCPDS No. 76-2058) indicating the replacement of O-H groups by fluoride ions to enhance the adsorption.

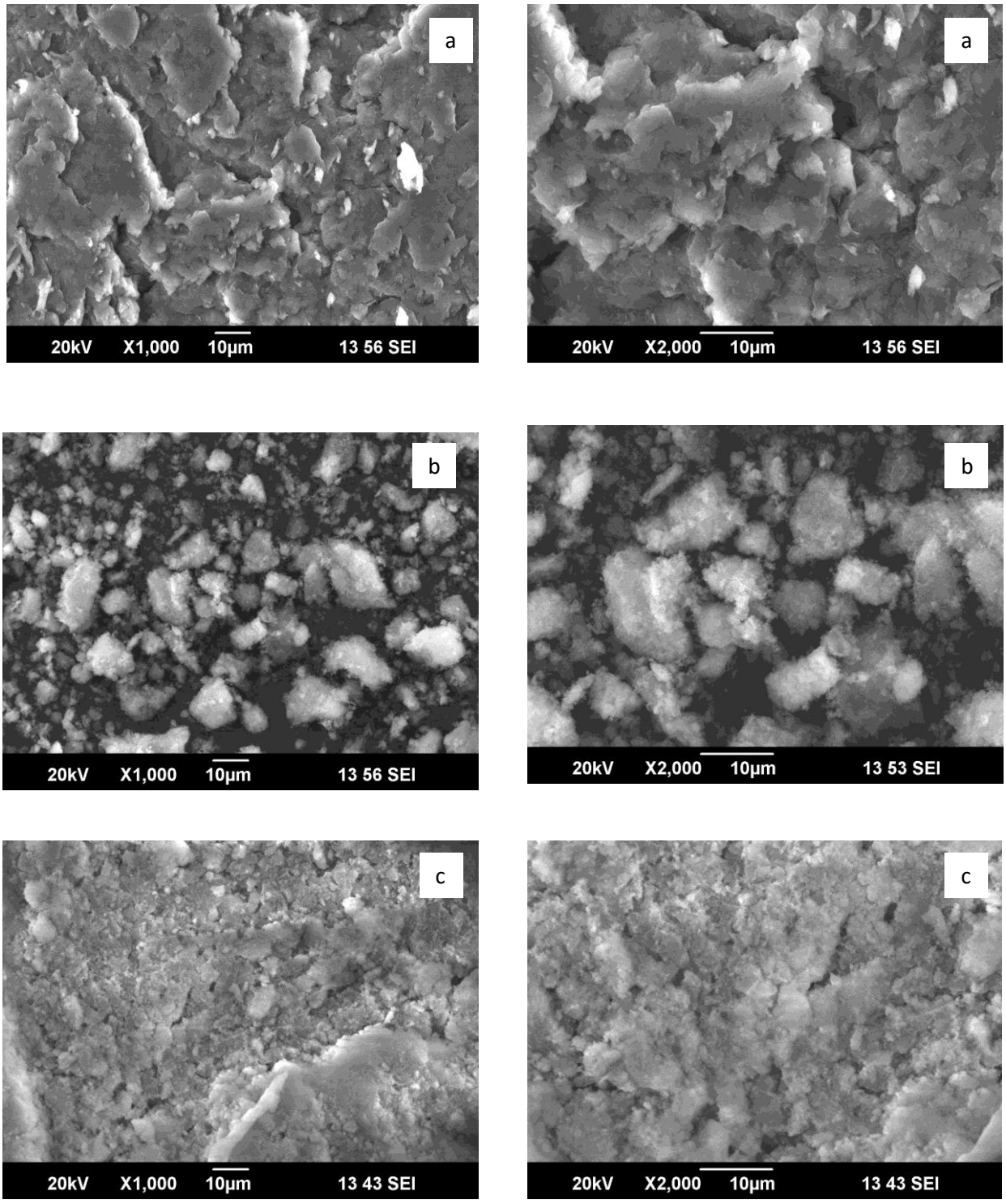

Figure 5.2. SEM images of GO (a), Aluminium oxy hydroxide incorporated GO (b) and after adsorption of fluoride (c) at different magnifications.

e) SEM & EDS Analysis

Certain marked differences in the SEM micrographs along with the EDS spectra (Figure 5.2 and 5.3) of graphene oxide and metal hydroxide incorporated graphene oxide were observed. The SEM micrographs of GO show crumpled morphology with stacked layers. However, the adsorbent surface is adorned with some bright spots showing the presence of aluminium oxy hydroxide onto GO surface. After adsorption of fluoride ion, the surface of adsorbent appears more congested with some small weak spots attributed to the interaction of fluoride onto the adsorbent surface. Moreover, the SEM image of graphene oxide showed trace impurities on its surface due to the presence of Cl and S which was also confirmed through the EDS peaks at 2.62keV and 2.31keV respectively. The amorphous nature of Al-O (OH) is also visible in the SEM micrograph of the adsorbent.

It is quite predictable from these images that Al-O (OH) is anchored on the surface of graphene oxide effectively. After fluoride adsorption, the surface of the adsorbent becomes almost homogeneous due to the agglomeration of Al-O (F) particles. The EDS spectrum (Figure 5.3) confirms the presence of Al, O, Na and C elemental peaks at 1.486, 0.525, 1.041 and 0.277keV and this clearly indicates that aluminium oxy hydroxide was loaded successfully onto the surface of GO.

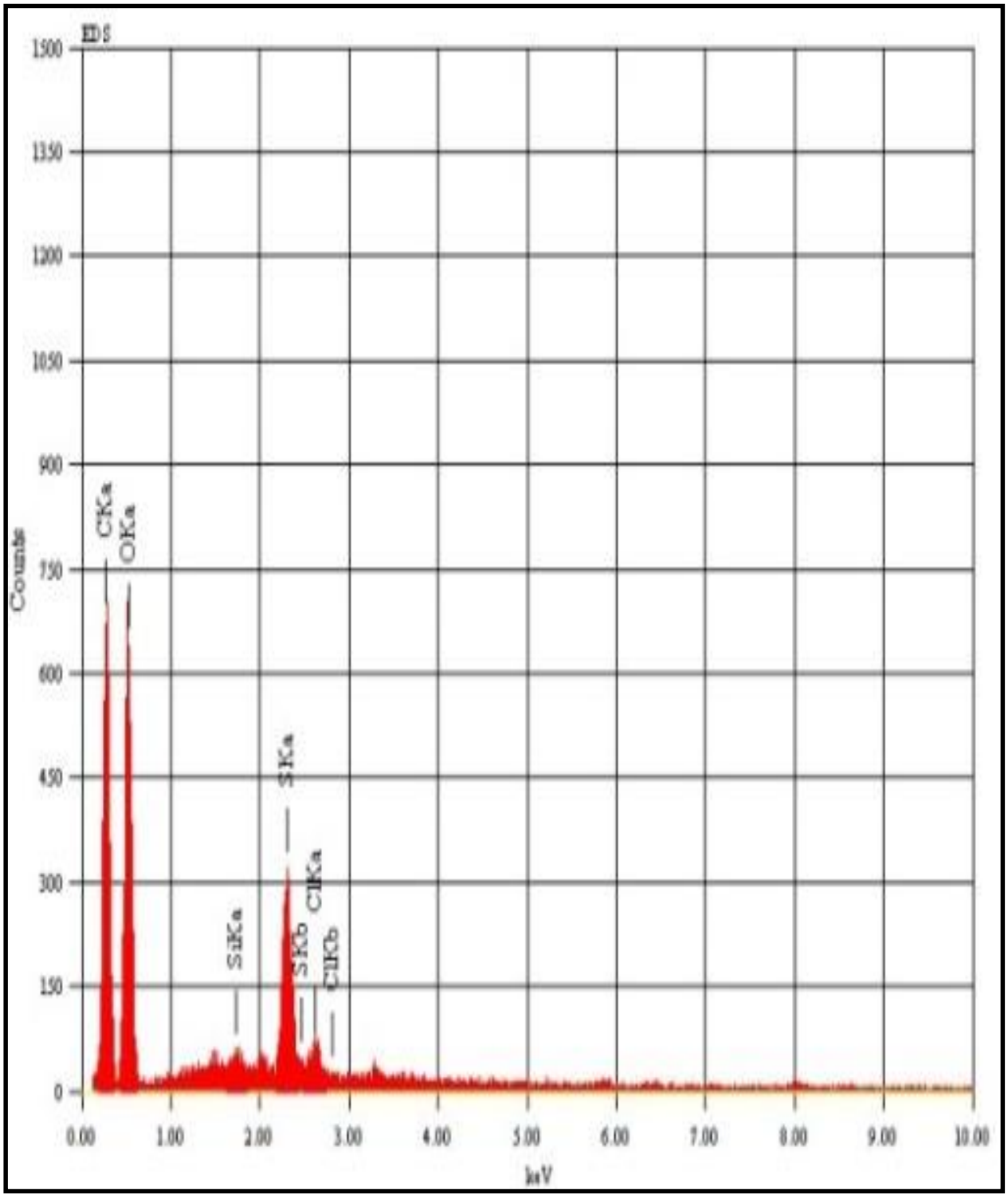

Figure 5.3a. EDS spectra of prepared graphene oxide.

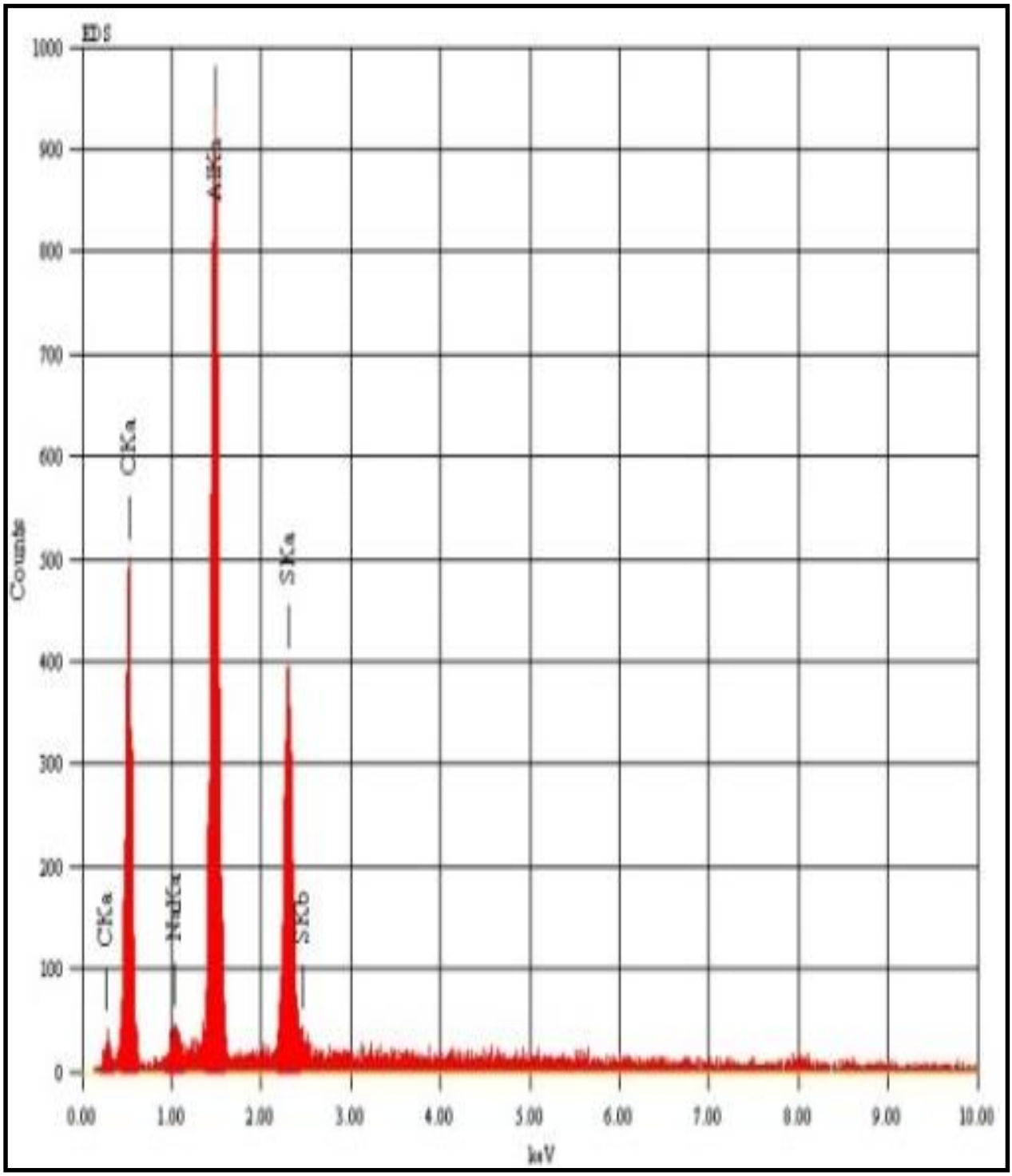

Figure 5.3b. EDS spectra of Aluminium oxyhydroxide incorporated graphene oxide adsorbent

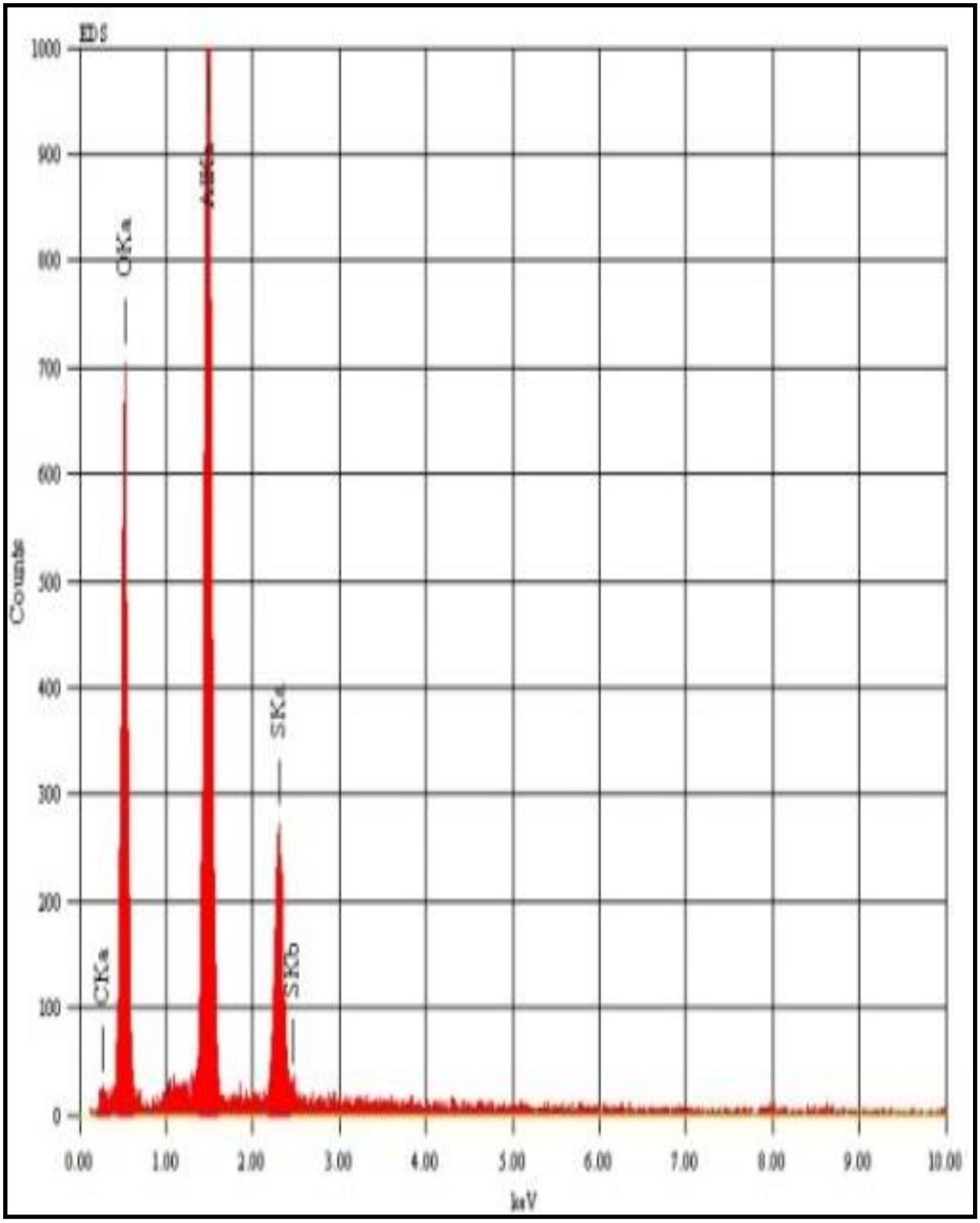

Figure 5.3c. EDS spectra of Aluminium oxyhydroxide incorporated graphene oxide adsorbent after adsorption of fluoride.

f) XPS Analysis

The XPS analysis was carried out to obtain valuable information about the surface changes during the preparation of graphene oxide from native graphite, GO-Al-O (OH) and to recognize the adsorbent surface changes before and after the adsorption of fluoride (Figure 5.4). The full survey XPS spectra (Figure 5.4A) shows the photoelectron lines at binding energy (B.E) values 285, 530, 74 and 685eV attributed to C1s, O1s, Al2p and F1s respectively. The C1s XPS spectrum (Figure 5.4B and Table 5.1) studies for graphite shows diverse peaks corresponding to non-oxygenated carbon (284.6eV, 59.9 %), in addition to the C–C (285.5eV, 17.29 %) bonding present in hexagonal graphite (284.1eV, 17.5 %)[40] The assignment of peaks for the O1s spectra of graphite reveals that the B.E. at 530.5 (1.92 %), 531.7(1.47 %), 533(1.29 %) and 534.5eV (0.63 %) could be the result of contributions from C=O or O=C–OH groups, surface chemisorbed oxygen species, C–OH groups and water respectively.[41,42] This could probably emanate from the nature of fluid (CO, CO_2 and CH_4)-deposited onto graphite from the atmosphere.[40] Also, the % C/O ratio (Table 5.1) for graphite was found to be 17.83 and for graphene oxide it decreased to 1.64 %, confirming the oxidation of graphite. The high resolution C1s XPS spectrum of graphene oxide (Figure 5.4B and table 5.1) distinctly indicates considerable degree of oxidation with diverse functional groups including C=C (282.61eV, 19.66%) C-OH (284.6eV, 30.59%), and C-O-C or C=O bonds (286.12eV, 8.89%).[43,44] The XPS results are in good agreement with the FT-IR spectroscopic data discussed earlier. The O1s spectrum is more surface specific compared to C1s and the peaks present at 530.29, 529.19 and 531.4eV in the O1s data of graphene oxide can be assigned to C-OH, C-O-C (O^{2-} oxidation state[45]) and C=O groups respectively.

Table 5.1. Elemental composition of various atoms present on the adsorbent surface

Materials	XPS Analysis								
	At.% of C					At.% of O	C/O ratio	At.% of Al	At.% of F
	Sp^3 C	Sp^2 C	C-OH	C=O or C-O	Total				
Graphite	17.29	77.74	-	-	94.69	5.31	17.83	-	-
Graphene oxide	2.99 (C^{2-})	19.66	30.59	8.89	62.13	37.88	1.64	-	-
GO-Al-O(OH)	-	13.97	4.80	1.50	20.27	60.27	0.34	19.46	Nil
GO-Al-O(F)	8.62	7.78	5.54	0.63	22.57	47.90	0.47	20.82	8.72

After the incorporation of aluminum oxy hydroxide, C/O ratio decreased from 1.64 to 0.34% which confirms the interaction between the graphene oxide and Al-O (OH). Furthermore, the high resolution C 1s XPS spectrum of GO-Al-O (OH) clearly indicates that the Al-metal hydroxide interacts with hydroxyl, epoxy groups and carbonyl groups of graphene oxide. The decrease in intensity was apparent corresponding to the carbon atoms in different functional group environment such as C-OH (284.5eV, 13.97%), and C-O-C or C=O bonds (286.54eV, 4.8%), O=C-OH bond (289.14eV, 1.5%). As shown in Figure 5.4C, the O1s spectrum confirms that the Al-O (OH) could be anchored to graphene oxide by three different oxygen species namely, Al-O-Al at 531.0eV (14.17%), Al-OH at 532.0eV (31.11%) and adsorbed water (H-O-H) or C-OH of GO at 533.4eV (14.99%). In addition, a distinct Al 2p transition was observed at 74.7eV, characteristic of Al-O (OH) or pseudoboehmite.[46,47,48] In order to corroborate the interactions between fluoride and GO-Al-O (OH), XPS studies of the adsorbent before and after F^- ion adsorption at pH 7.0 were conducted. After the fluoride adsorption, the high resolution O1s XPS spectra showed peaks at 531.6eV (30.44%) which corresponds to the Al-OH formation and the peak at 532.7eV (9.13%) suggests that the hydroxyl groups might be involved in the fluoride adsorption process (ligand exchange) and also the experimental Al 2p peak maximum is shifted from 74.7 to 74.2eV. Usually, the binding energies of organic fluoride (688.0 to 689.0eV) are presumably higher than the metal fluoride (684.0 to 685.5eV) and thus the adsorption of fluoride was confirmed through the high

resolution F1s XPS spectra peak at 684.8eV.[49] This indicates the interaction of fluoride ion with Al^{3+} ions immobilized onto the surface of graphene oxide.

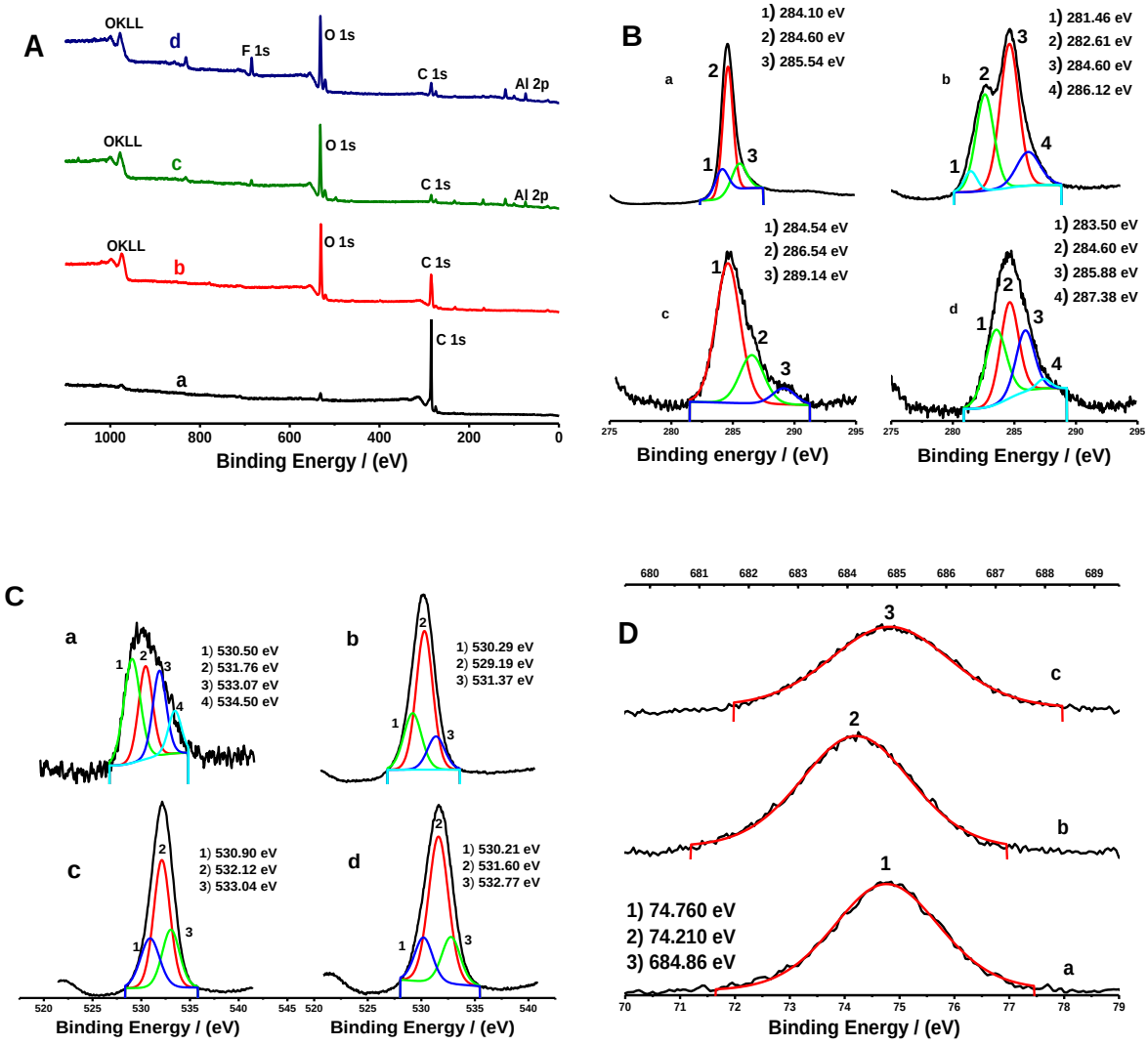

Figure 5.4. A) Total survey of XPS spectra B) C1s spectrum C) O 1s spectrum of graphite (a), prepared GO (b), GO-Al-O-(OH) adsorbent (c) and after adsorption fluoride (d). D) Al 2p spectrum of GO-Al-O-(OH) adsorbent (a) and fluoride adsorbed onto the adsorbent surface (b), F 1s spectrum of F^- ion adsorbed onto the adsorbent surface (c).

Trace silicon impurities are surfaced in the EDS and XPS analysis. This could arise from the graphite or other reagents used in the preparation of GO. Trace amount of Si

impurities (Confirmed by EDS and XPS) would form SiC (C^{2-} state of carbon was confirmed by XPS spectra around 3% at 281.46 eV). The small intensity peak in the adsorbent surface could emanate from the trace fluorine impurity in graphite. This is probable since in the purification of carbonaceous material such as graphite, fluorine processes are adopted to remove the metallic and other impurities as soluble fluorides.[50] Normally, it is not observed, but with a high resolution technique such as XPS the very trace fluorine impurity in the adsorbent could originate during stirring with $Al_2(SO_4)_3$ solution, where in the aluminium oxy hydroxide after being formed leaves behind the SiC surface with hydroxyl groups. These hydroxyl groups can be replaced by the trace fluorine impurity to form Si-F bond[51] (Observed at 685.3 eV). After fluoride adsorption, this peak shifted to 684.8 eV with a very high intensity which confirms the fluoride adsorption onto the adsorbent surface. This peak intensity is a combination of Al-F resulting primarily after fluoride adsorption and Si-F as a trace impurity.

(ii) Probable Mechanism

The probable mechanism for the adsorption of fluoride ion onto the surface of GO-Al-O (OH) adsorbent is shown in Figure 5.5. According to the HSAB principle,[52] Al^{3+} is a hard acid with small ionic radius (0.5 Å) and it could interact effectively with hard base F^- to enhance the adsorption. In aqueous solution, Al^{3+} could exist as cationic hydroxides such as $Al(OH)_2^+$, $Al(OH)^{2+}$ etc. and these species could interact with fluoride ions by electrostatic attractive forces. The XPS surveys of O 1s for GO-Al-O (OH) adsorbent and spent adsorbents were used to explain clearly the fluoride ion adsorption mechanism. The high resolution O1s spectrum of adsorbent (prior and after fluoride ion adsorption) showed that the adsorption of fluoride would enhance by the surface hydroxyl groups present in the adsorbent. Figure 5.4C shows the XPS peaks of Al-OH at 532.5eV (31.11%) and Al-O^{2-} at 530.9eV (14.17%) respectively.[46] The loss of Al–OH (almost 22%) content is due to the formation of Al–F bonds (Table 5.1) which indicates the adsorption process to involve ligand exchange between hydroxyl groups and fluoride ions. The presence of Al-F fluoride was confirmed by the XPS peak observed at 684.8eV.[49] Moreover, hydrogen bonding and electrostatic interaction would also enhance

the adsorption of fluoride at different pH levels onto the surface of GO-Al-O (OH) material.

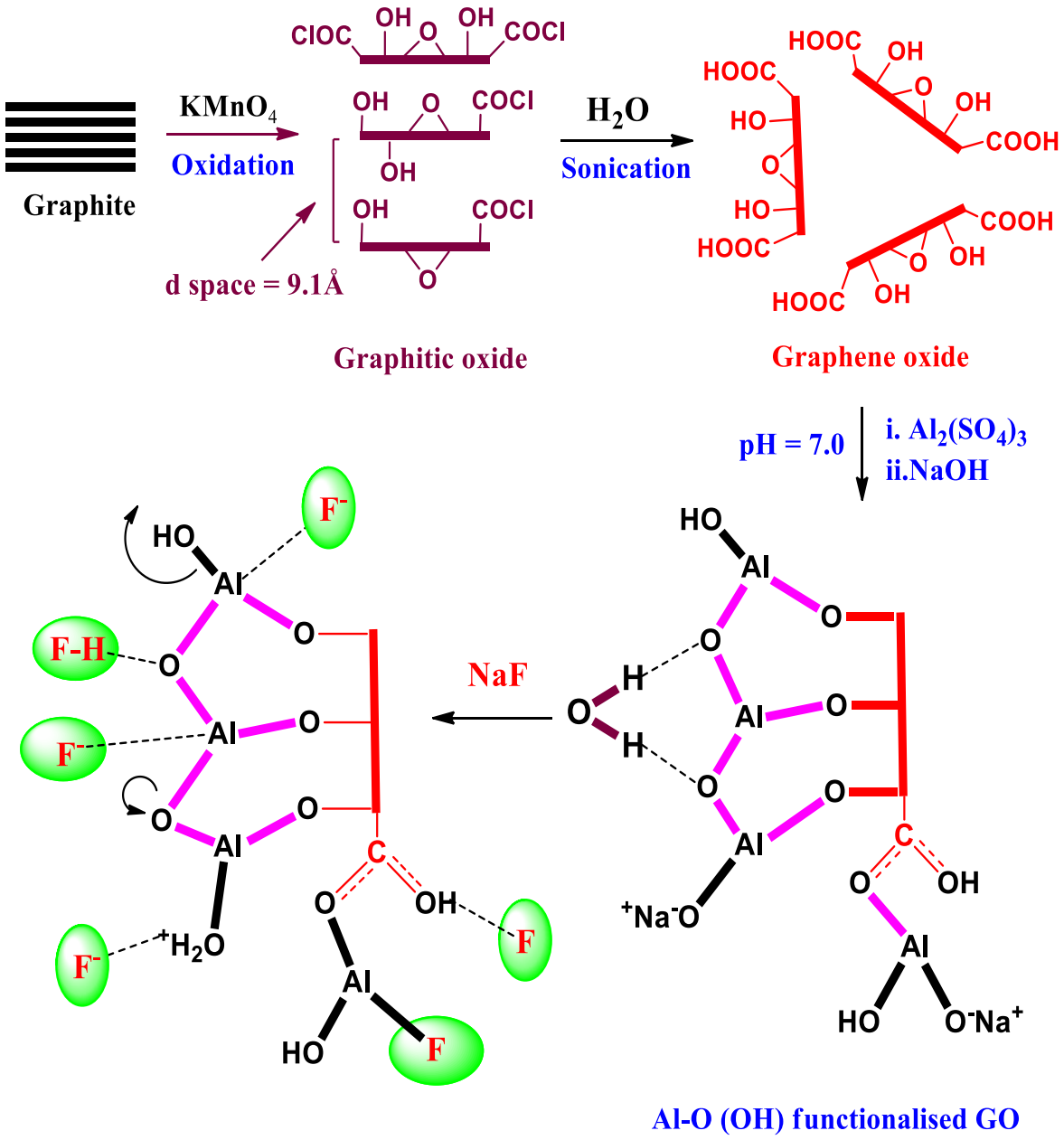

Figure 5.5. Preparation of GO and GO-Al-O-(OH) adsorbent and the possible mechanism towards the fluoride ion adsorption.

(iii) Effect of pH

The interaction of fluoride ions onto the GO-Al-O (OH) adsorbent surface depends on the solution pH, existence of fluoride in different forms (HF, F^-, and HF_2^-) and zero-point charge or isoelectric point of the adsorbent surface. The pH at which the adsorbent surface acquires a neutral charge is referred to as zero-point charge and this could be easily determined by batch equilibrium technique.[53] About 100 mg of GO-Al-O (OH) adsorbent was added to 100 mL F^- ion solution (100 mg L^{-1}) at different initial pH (3.0-9.0) by addition of 0.1mol L^{-1} HCl or NaOH. The experiments were carried out in a thermostat shaker at 27 ˚C for 24 h. After a time period of 24 h, the final pH and F^- ion concentration in the supernatant solutions was measured. The zero-point charge (pH_{zpc}) of GO-Al-O (OH) adsorbent was determined from the plot of ΔpH [$pH_{initial} - pH_{final}$] versus $pH_{initial}$ (Figure 5.6).

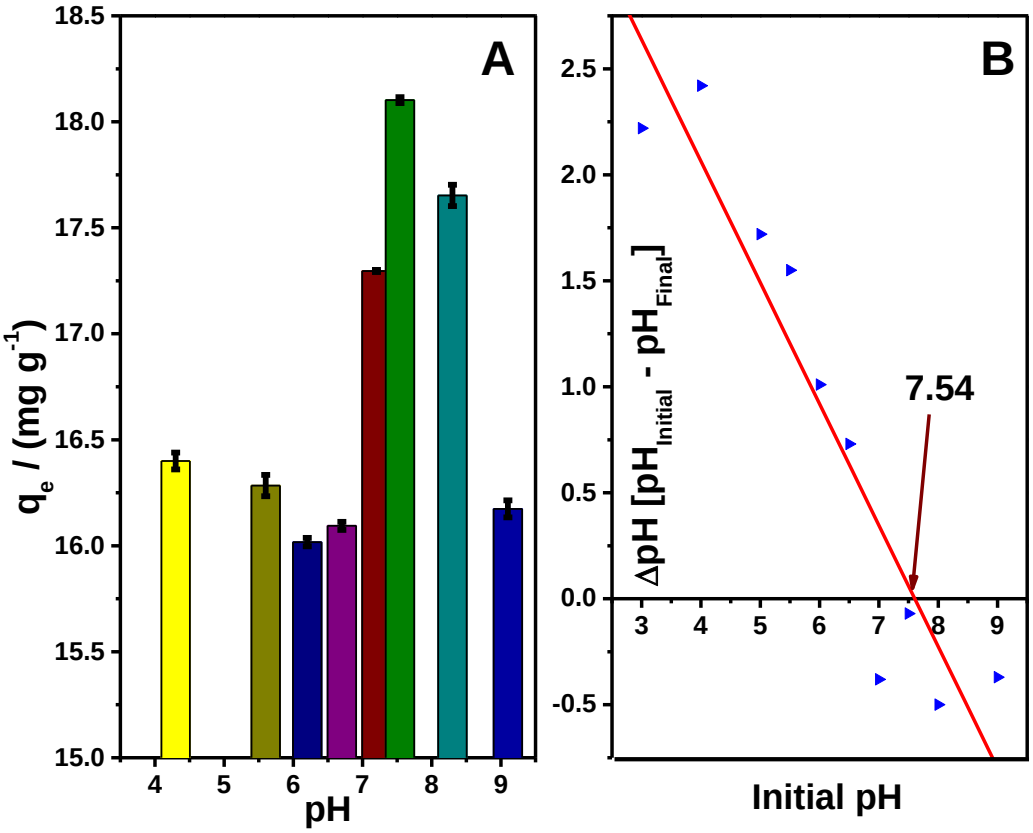

Figure 5.6. Adsorption of fluoride ion influenced by pH and zero point charge onto the adsorbent surface

The resultant zero-point charge of GO-Al-O (OH) adsorbent was found to be 7.54 which implies that the adsorbent surface is positive below pH $_{zpc}$ and negative above pH $_{zpc}$. The influence of pH on the adsorbent is shown in Figure 5.6. The maximum equilibrium adsorption capacity of fluoride was observed at pH 7.5-8.3 (18.10 mg g^{-1} at pH 7.5 and 17.65 mg g^{-1} at pH 8.3) but at pH below 6.0 or above 8.5, the adsorption capacity also reduced marginally owing to the solubility of aluminium fluoride and Al $(OH)_4^-$ in aqueous phase. Al^{3+} ion anchors onto surface of graphene oxide effectively (%Al present in the adsorbent is almost same before and after adsorption of fluoride). Indeed, with an initial concentration of 10 mg L^{-1} of F^- ion, over the pH range 7.0-8.5, the level of fluoride in the solution phase was within the permissible limits.

"Al^{3+} ion anchors onto surface of graphene oxide effectively (%Al present in the adsorbent is almost same before and after adsorption of fluoride). Indeed, with an initial concentration of 10 mg L^{-1} of F^- ion, over the pH range 7.0-8.5, the level of fluoride in the solution phase was within the permissible limits." The leaching of Al^{3+} was very marginal as evident from the XPS data at pH 7.0. However, we have checked the leaching of Al^{3+} using ICP-OES at varying initial fluoride concentrations (Table 5.2). In the pH range 7.0-8.0, the leached aluminum content in aqueous solution is very less (3.0-5.0 ppb) even at different initial fluoride concentrations than below pH 7.0 or above pH 8.0. It might be due to the formation of soluble Al-F complexes at higher pH ranges. In pH 5.0 - 6.0 range, the aluminum content in the aqueous solution is less than 200 ppb. Hence, the leaching of aluminium is well within the permissible limit (0.2 ppm) in the pH range 5.0-8.0, thereby making the adsorbent good for practical applications.

(iv)Adsorption Isotherm studies

Figure 5.7A-F shows the different isotherm models that were applied to study adsorption behavior by measuring the amount of fluoride at equilibrium and concentration left in solution after adsorption onto GO-Al-O (OH) adsorbent surface. The various isotherm equations and parameters are given in Table 5.2. Generally, Langmuir[54] and Freundlich isotherms[55] are widely used to study adsorption. Various other empirical models (Table 5.3) also add considerable insight into the nature or mechanism of adsorption. The plot of

C_e/q_e against C_e, corresponding to Langmuir isotherm model gave a maximum adsorption capacity (q_o) of 51.42 mg g^{-1}.

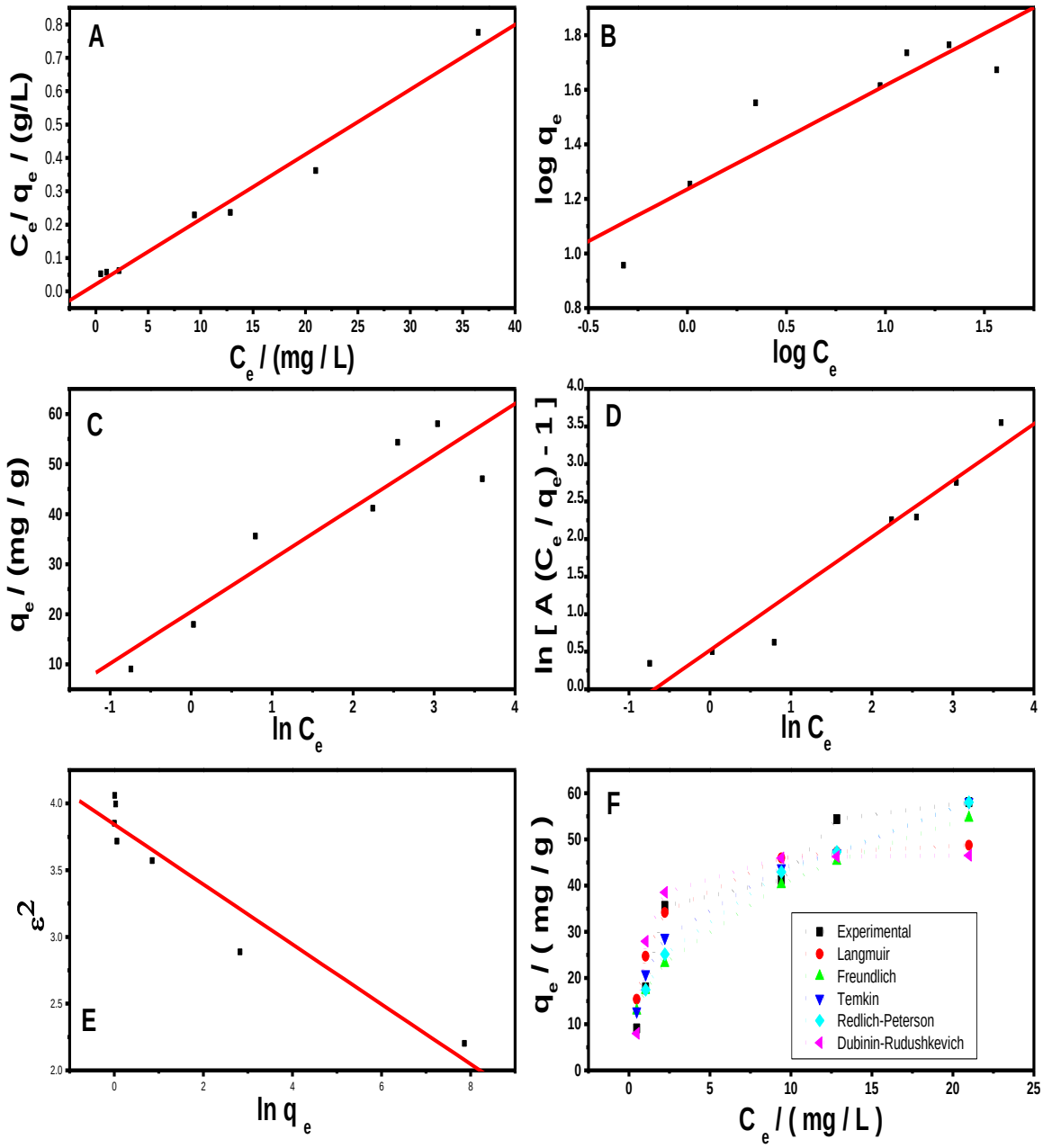

Figure 5.7. Isotherm models A) Langmuir plot B) Freundlich plot C) Temkin plot D) Redlich-peterson (R-P) plot E) Dubinin-Radushkevich (D-R) plot F) Plot of q_e Vs C_e

The change in the concentration of aluminium sulphate did not cause any significant change in the adsorption capacity of fluoride. Hence, we did not include the variation of composition in the manuscript. However, the data for three different concentrations of Aluminium sulphate given below shows that beyond 100 mM, saturation is almost reached.

GO-Al-O-(OH)	[50 mM of aluminium sulfate]	= 42.69 mg g^{-1}
GO-Al-O-(OH)	[100 mM of aluminium sulfate]	= 51.42 mg g^{-1}
GO-Al-O-(OH)	[200 mM of aluminium sulfate]	= 56.75 mg g^{-1}

This indicates the admirable capability of GO-Al-O (OH) adsorbent towards F^- ion adsorption. In addition to this, the separation factor ($R_L = 1 / 1 + b\ C_o$) found to be less than unity showing the applicability of Langmuir model to fit the data. For the Freundlich isotherm model, the intensity of adsorption (n) and the adsorption capacity (K_F) were obtained from the plot of log q_e against log C_e and if Freundlich constant n lies between 1and10, it indicates the favourable adsorption of F^- ion onto the Al-O (OH) modified GO adsorbent. The high values of n and K_F as shown in Table 5.3 signify the effective uptake of F^- ion onto the GO-Al-O (OH) adsorbent surface. The Dubinin–Radushkevich isotherm (D-R)[56] has similarity to Langmuir model and it gives the adsorption energy (β) and adsorption mechanism involved in the interaction between fluoride ion and the GO-Al-O (OH) adsorbent surface. The adsorption energy, E can also be expressed as $-(2\beta)^{-0.5}$ and the positive value of E (+1.4924 kJ mol^{-1}) indicates that the interaction between the fluoride anion and GO-Al-O (OH) adsorbent is endothermic and hence higher temperatures are favourable for adsorption. In addition to this, Temkin[57] isotherm obtained from the plot of q_e against lnC_e accounts that the heat of adsorption decreases linearly with coverage due to F^- - GO-Al-O (OH) interactions with uniform binding energy distribution. The value of b (kJ mol^{-1}) was found to 0.243 which shows the electrostatic interaction between fluoride ion and GO-Al-O (OH) adsorbent. The exponent g obtained from Redlich-Peterson (R-P) isotherm model[58] was found to be 0.75 and this explains the fact that adsorption of fluoride could be described satisfactorily

through the Langmuir model. Comparing the regression coefficient values, the adsorption of fluoride onto the surface of GO-Al-O-(OH) adsorbent follows the order, Langmuir = D-R > R-P > Temkin> Freundlich model.

Table 5.2. Isotherm parameters for the adsorption of fluoride

Isotherm models	Parameters				
Langmuir	q_o (mg g^{-1})	b (L mg^{-1})	R_L	r^2	χ^2
	51.41	0.8971	0.1003	0.9	1.1905
Freundlich	K_F (mg $^{1-1/n}$ g^{-1} $L^{1/n}$)	n	r^2	χ^2	
	17.18	2.6305	0.79	2.3679	
Dubinin Radushkevich	q_m (mg g^{-1})	β (mol^2 kJ^{-2})	E (kJ mol^{-1})	r^2	χ^2
	46.67	0.2245	1.4924	0.97	1.4287
Temkin	K_T	B	r^2	b (kJ mol^{-1})	χ^2
	7.2095	10.3819	0.83	0.243	1.0835
Redlich-Peterson	g	A (L g^{-1})	r^2	χ^2	
	0.7537	46.1255	0.93	1.4562	

Table 5.3. Kinetic parameters for the adsorption of fluoride onto Al-O (OH) incorporated graphene oxide

Conc. of F^- ion (mg L^{-1})	q_e mg g^{-1}	Pseudo first order kinetic model			Pseudo second order kinetic model			Intraparticular diffusion model	
		k_1 min^{-1}	q_1 mg g^{-1}	R^2	k_2 g mg min^{-1}	q_2 mg g^{-1}	R^2	k_{int} g mg^{-1} $(min^{0.5})^{-1}$	R^2
5.0	9.048	0.0445	2.9117	0.78	0.0178	10.521	0.99	0.7897	0.86
10.0	17.940	1.7960	0.9722	0.88	0.0200	17.141	0.99	0.8064	0.92

(v) Adsorption kinetic and thermodynamic studies

The kinetics were analyzed through the pseudo first order,[59] second order,[60] and intraparticle diffusion rate equations[61] (Table 5.3) for the adsorption of F^- ion onto the GO-Al-O-(OH) adsorbent. The various kinetic plots applied for F^- ion adsorption and the corresponding kinetic parameters are shown in Figure 5.8A-C and Table 5.4. In Weber–Morris[61] intraparticle diffusion model, a plot of q_t versus t 0.5 would be linear and if the plot passes through the origin then we could infer that intraparticle diffusion is the only rate-determining step. The plot was linear in this adsorption process giving the intraparticle rate constant (k_{int}) and a non-zero intercept (Figure 5.8C) pointing to the fact that boundary layer phenomenon could also direct the adsorption of F^- ion onto the GO-Al-O-(OH) adsorbent surface. The value of regression coefficient (r^2) for the pseudo-second-order adsorption model was almost unity. Also, the calculated q_e value through this model matched well with experimental (q_e) value. Hence, the pseudo second-order kinetic model is more suitable to describe the kinetic behavior of F^- ion adsorption onto GO-Al-O-(OH) adsorbent surface.

The F^- ion adsorption was tested at different temperatures using 10 mg L^{-1} of fluoride to ascertain the spontaneity from the equilibrium constant (K) values. Adsorption free energy (ΔG^0), adsorption enthalpy (ΔH^0) and adsorption entropy (ΔS^0) were calculated from the classic Van't Hoff plot of lnK against 1/ T (Figure 5.8D). Also, the activation energy (E_a) required for favourable F^- ion adsorption was obtained using the expression $E_a = \Delta H^o_{ads} + RT$. The adsorption free energy shows negative values (-6.094 kJ mol^{-1}) which elucidates the spontaneity of F^- ion adsorption process onto the GO-Al-O (OH) adsorbent surface. Adsorption enthalpy (ΔH^0) is normally lower than 80 kJ mol^{-1} for physical adsorption process and Table 5.4 shows the adsorption enthalpy (+21.384 kJ mol^{-1}) and the average activation energy (+23.986 kJ mol^{-1}) as positive thereby supporting the fact the adsorption of F^- ion could involve ligand exchange by physical adsorption process. Entropy is an extensive thermodynamic property and the positive value of ΔS^0 (87.71J $mol^{-1}K^{-1}$) also testifies the feasibility and favorable adsorption of F^- ion onto GO-Al-O (OH) adsorbent surface.

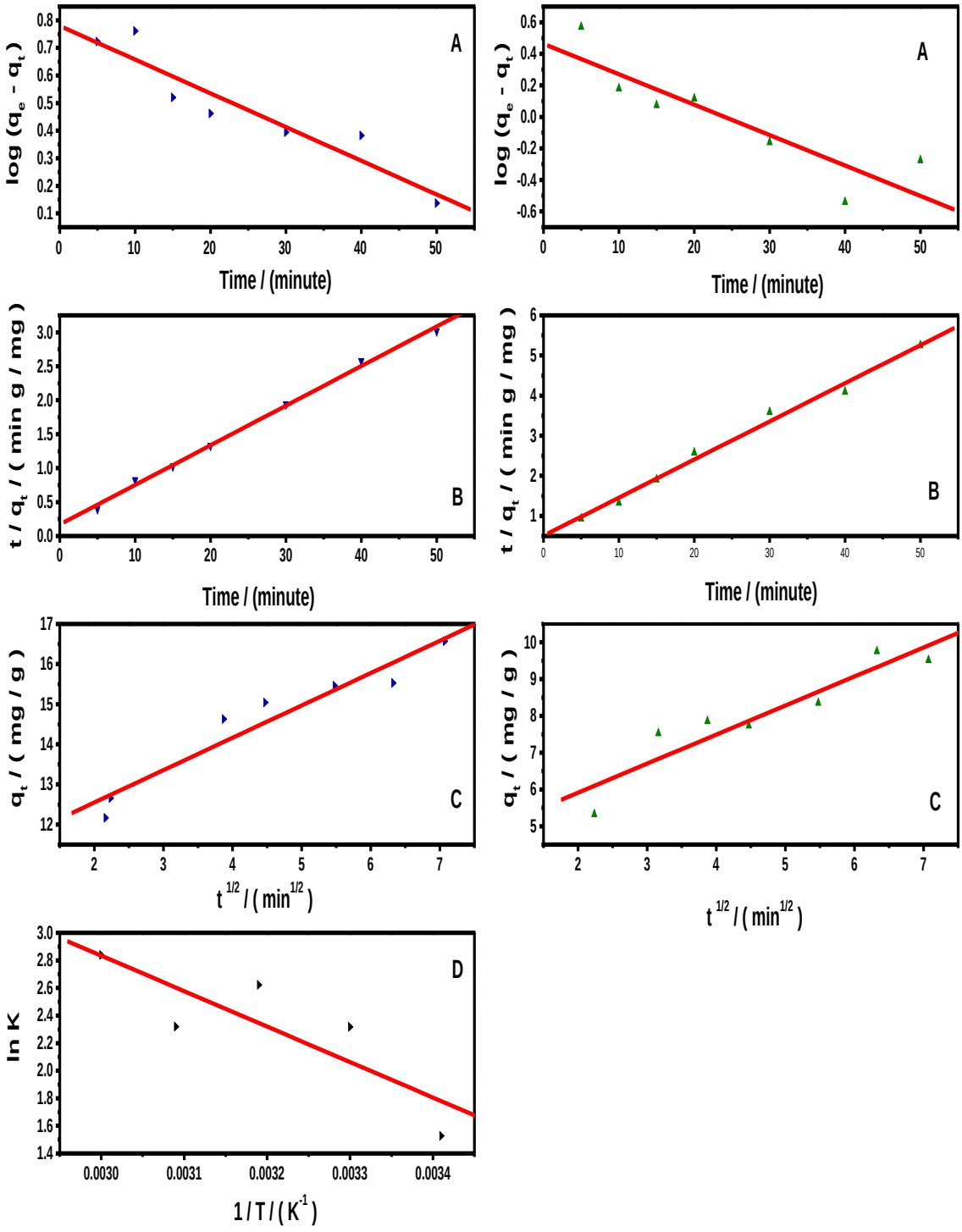

Figure 5.8. Kinetic plots obtained from the A) pseudo first-order equation B) pseudo second-order equation C) Intra-particle diffusion kinetics equation with 5.0 mg L^{-1} and 10.0 mg L^{-1} F^- ion concentrations D) Van't Hoff isotherm plot obtained for the adsorption of F^- ion onto GO-Al-O- (OH) adsorbent surface.

Table 5.4. Adsorption thermodynamic parameters

T/ K	ΔG^o / kJ mol^{-1}	ΔH^o / kJ mol^{-1}	ΔS^o / J K^{-1} mol^{-1}	E_a / kJ mol^{-1}
293	-3.72			
303	-5.84			
313	-6.82	+21.384	+87.71	+23.986
323	-6.23			
333	-7.86			

(vi) Application to Field study

The scientific basis of the results obtained in batch process was quite encouraging and hence the method has good potential to be scaled up to the column process at the natural pH prevalent in drinking water.

(a) Bulk synthesis

About 1.0 g of laboratory synthesized or commercial graphene oxide was dispersed in 1.0 L of Milli-Q water. Sonication is an important parameter for the exfoliation of graphene oxide. So, the exfoliation was done by extended sonication (Ultrasonic bath, Biotechnics, India) for 6 h at a 15 min intermittent time interval. Subsequently, 63.0 g of aluminium sulfate was added to the exfoliated graphene oxide solution and sonicated further for 2 h with 15 minutes time interval. After sonication, the solution was kept for constant stirring for 24 hours. The pH was adjusted to 7.0 using 1.0 mol L^{-1} sodium hydroxide solution and stirred for an extended time interval of 48 h. About 550-560 mL of sodium hydroxide (1.0 mol L^{-1}) solution was used to prevent the agglomeration of adsorbent particles. The reaction mixture was filtered, washed with 3.0 L of Millipore water several times to remove sulfate ions (tested using $BaCl_2$ solution) thoroughly. The adsorbent was centrifuged after each wash and dried at 30 ^oC in a vacuum oven for 48h. The dried material was ground well to get a homogeneous mixture and used for field applications.

(b) Application to the real water samples and prototype development

- A known volume of tap water was collected and spiked with 5.0 mg L^{-1} fluoride. About 8.0 g of the prepared GO-Al-O(OH) adsorbent was packed into water filter which was purchased from a local market (Figure 5.9). A volume of 8.0 L containing 5.0 mg L^{-1} fluoride solution could be treated with 8.0 g of prepared adsorbent at ambient pH conditions and bringing down fluoride to WHO permissible limits.

Figure 5.9. A simple water purification filter system packed with GO-Al-O-(OH) adsorbent

- Furthermore, the real water samples were also collected at five different places (Yedavelly, Yellareddy gudam, Narkatpalley) in Nalagonda district, Telangana. About 1.0 g of prepared GO-Al-O(OH) adsorbent was added into 1.0 L of collected real water samples and stirred well for 60 minutes. The solution was filtered through Whatmann 42 filter paper and submitted for water analysis to NABL (National Accredited Board for Laboratories) Accredited Laboratory. The collected real water samples were analyzed before and after treatment at Intertek Private Limited, Hyderabad (NABL Accredited Lab) and the results obtained in these studies are given in Table 5.5.

Table 5.5. Defluoridation results of collected real water samples with GO-Al-O(OH) adsorbent at ambient pH conditions, **Note:** A*- Agreeable and DA*- Disagreeable

Parameters (Units)	Results obtained								
	Collected samples before treatment				After treatment with GO-Al-O-(OH) adsorbent				
	1	2	3	4	Commercial GO				Synthesized GO
					1	2	3	4	4
Colour (Hazan)	<1.0	<1.0	<1.0	<1.0	<1.0	<1.0	<1.0	<1.0	<1.0
Odour	A*	DA*	DA*	A*	A*	A*	A*	A*	A*
pH Value	8.0	8.4	8.2	8.3	8.0	8.26	8.1	8.4	8.28
Turbidity (NTU)	<1.0	<1.0	<1.0	<1.0	<1.0	<1.0	<1.0	<1.0	<1.0
Total dissolved Solids (mg L^{-1})	3746	556	2362	1090	3576	702	2126	2188	826
Total Hardness as $CaCO_3$ (mg L^{-1})	1256	379	805	566	1029	315	630	630	546
Chloride (mg L^{-1})	1168	97	1742	200	959	142	551	693	123
Fluoride (mg L^{-1})	5.4	5.1	5.8	4.4	1.1	1.1	1.2	1.1	1.1
Nitrate (mg L^{-1})	63.9	13.2	70.0	52.3	701	25	211	199	62
Sulphate (mg L^{-1})	37.4	25.4	31.4	228.8	115	33	167	144	69
Aluminium (mg L^{-1})	**	**	**	**	0.05	0.07	0.06	0.10	0.07
Total Arsenic (mg L^{-1})	**	**	**	**	**	**	**	**	**
Iron (mg L^{-1})	0.14	**	0.03	**	**	**	**	**	**
Lead (mg L^{-1})	**	**	**	**	**	**	**	**	**
Chromium (mg L^{-1})	**	**	**	**	**	**	**	**	**
Total Coloiforms and E.Coli (Per 100 mL)	--	--	--	--	--	--	--	--	--

♣ A known weight of NaF was spiked with 50.0 L of tap water to get 5 mg L^{-1} F^- ion solution. This fluoride spiked water can be treated either in a simple bucket system or packed column prototype. A known amount of prepared adsorbent was added to the water samples at ambient pH conditions and stirred for 5-10 minutes vigorously in a plastic bucket and allowed to settle down for overnight. This is called as bucket system (Figure 5.10). The fluoride spiked water used in a bucket system was analyzed before and after treatment with GO-Al-O-(OH) adsorbent and results are given in Table 5.6. The leaching of aluminium in the residual water is negligible.

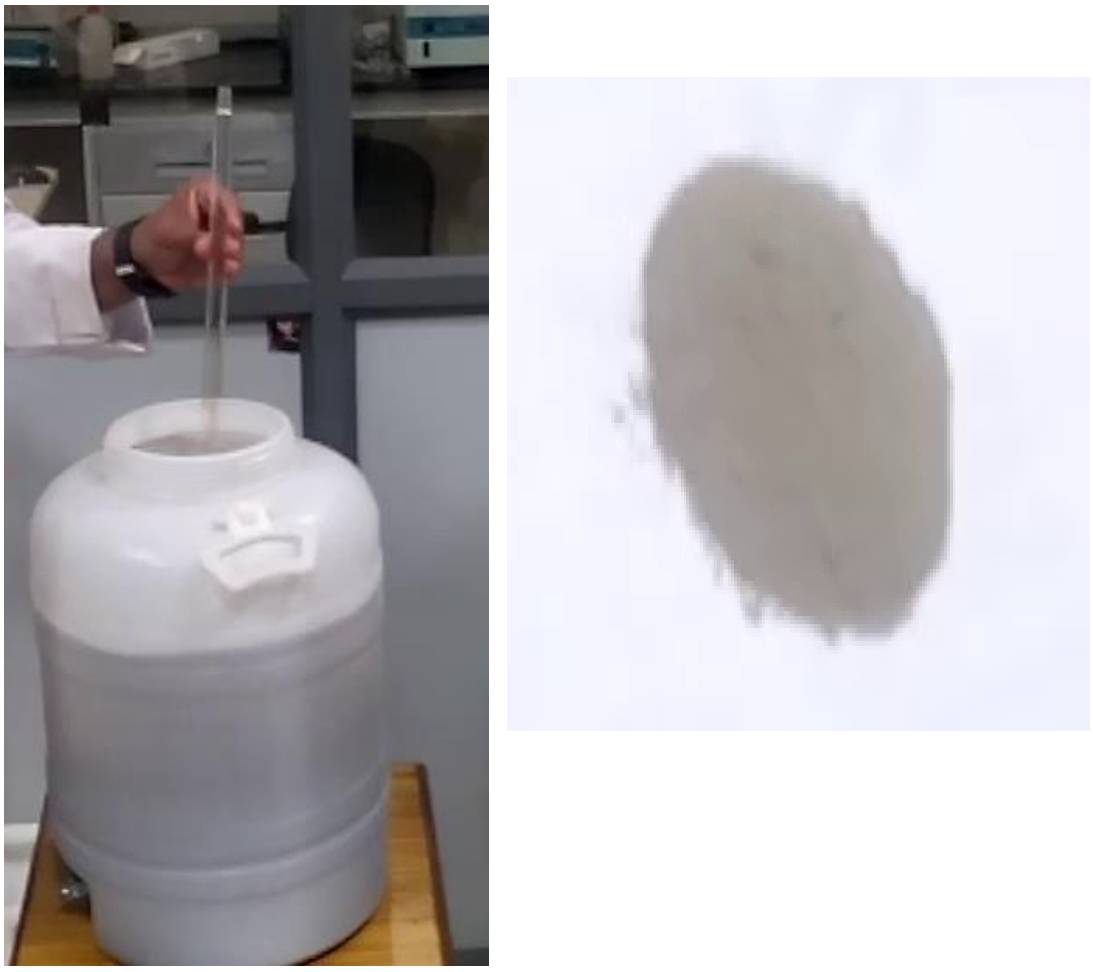

Figure 5.10. A simple bucket system (A) with GO-Al-O-(OH) adsorbent (B) for defluoridation of water.

♣ About 50.0 g of prepared GO-Al-O(OH) adsorbent was mixed with 150.0 g of sand (approximately 1mm size) and packed (Figure 5.11) in a stainless steel column (25 cm length and 3 cm dia). This is called packed column prototype model. The prepared fluoridated solution (5 mg L^{-1}) passed through the stainless column at the flow rate of 40 mL min^{-1} and the out coming water was collected at the end of 25.0, 45.0 and 50.0 L respectively. The collected water samples were analyzed for various parameters in NABL accredited Lab and results shown in Table 5.6. The packed column could be regenerated with 4.0 L of 1.0 mol L^{-1} NH_4OH as ammonium fluoride in the eluate.

Figure 5.11. A prototype model with GO-Al-O-(OH) adsorbent packed column

Table 5.6. Defluoridation results of samples collected from simple bucket and prototype column system at ambient pH conditions, **Note:** A*- Agreeable and DA*- Disagreeable.

Parameters (contains same units as in Table 5.5)	Results obtained					
	Simple Bucket system		Prototype column system			
	Before treatment (20.0 L)	After treatment (20.0 L)	Before treatment	After treatment with adsorbent		
				Sample 1 (25.0L)	Sample 2 (45.0L)	Sample 3 (50.0 L)
Colour	<1.0	<1.0	<1.0	<1.0	<1.0	<1.0
Odour	DA*	A*	A*	A*	A*	A*
pH Value	8.35	7.66	8.23	7.44	7.33	7.56
Turbidity	1.89	<1.0	<1.0	<1.0	<1.0	<1.0
Total dissolved Solids	330	470	326	470	434	404
Total Hardness as $CaCO_3$	133	133	131	180	141	133
Chloride (as Cl^-)	72.2	68.4	72.2	71.2	70.30	69.35
Fluoride (as F^-)	4.9	0.8	4.9	<0.1	0.85	1.09
Nitrate (as NO_3^-)	1.02					
Sulphate (as SO_4^{2-})	33.8	135	26	124	86	41
Aluminium (as Al)	<0.01	<0.01	0.03	<0.01	<0.01	<0.01
Total Arsenic (as As)	<0.01	<0.01	<0.01	<0.01	<0.01	<0.01
Iron (as Fe)	<0.01	<0.01	<0.01	<0.01	<0.01	<0.01
Lead (as Pb)	<0.01	<0.01	<0.01	<0.01	<0.01	<0.01
Chromium (as Cr)	<0.01	<0.01	<0.01	<0.01	<0.01	<0.01
Total Coloiforms	Absent	Absent	Absent	Absent	Absent	Absent
E.Coli	Absent	Absent	Absent	Absent	Absent	Absent

The results show that 50 g of the GO-Al-O-(OH) adsorbent has potential to defluoridate 50 L of 5.0 mg L^{-1} F^- contaminated water. The leaching of aluminium is also negligible. This indicates that GO-Al-O-(OH) adsorbent has good potential in field applications.

4.1.4. Conclusions

This work has described well the interaction between the graphene oxide modified Al-O (OH) adsorbent and fluoride. The maximum adsorption capacity (q_{max}) of this novel GO-Al-O (OH) adsorbent is 51.42 mg g^{-1} and the adsorption could be explained satisfactorily through Langmuir and Dubinin-Radushkevich isotherm models. FT-IR and Raman spectroscopic techniques proved to be a valuable tool to comprehend the adsorption mechanism. Ligand exchange and physical adsorption are mostly favored for the adsorption of fluoride and this was corroborated from the XPS studies. In addition to this, the thermodynamic feasibility and pseudo second order kinetic model augurs this adsorption process. With 2.0 g of the adsorbent packed on laboratory scale column, it is possible to treat 2000 mL of 5.0 mg L^{-1} fluoride solution at pH 7.0 thereby bringing the concentration within the permissible limits. This is possible at the normal pH existing in water and hence the Al-O (OH) impregnated graphene oxide adsorbent could demonstrate its efficacy for field applications.

References

1. Jagtap, S.; Yenkie, M. K.; Labhsetwar N.; Rayalu, S. *Chem. Rev.* **2012**, 112, 2454.
2. Li, Y. H.; Wang, S.; Zhang, X.; Wei, J.; Xu, C.; Luan, Z.; Wu, D. *Mater. Res. Bull.* **2003**, 38, 469.
3. Chingombe, P.; Saha, B.; Wakeman, R. J. *Carbon* **2005**, 43, 3132.
4. Yin, C. Y.; Aroua, M. K.; Daud, W. M. A. W. *Sep. Purif. Technol.* **2007**, 52, 403.
5. Dreyer, D. R.; Park, S.; Bielawski, C. W.; Ruoff, R. S. *Chem. Soc. Rev.* **2010**, 39, 228.
6. Subrahmanyam, K. S.; Vivekchand, S. R. C.; Govindaraj, A.; Rao, C. N. R. *J. Mater. Chem.* **2008**, 18, 1517.
7. Li, Y.; Zhang, P.; Du, Q.; Peng, X.; Liu, T.; Wang, Z.; Xia, Y.; Zhang, W.; Wang, K.; Zhu, H.; Wu, D. *J. Colloid Interface. Sci.* **2011**, 363, 348.
8. Poursaberi, T.; Ganjali, M. R.; Hassanisadi, M. *Talanta* **2012**, 101, 128.
9. Luo, X.; Wang, C.; Wang, L.; Deng, F.; Luo, S.; Tu, X.; Au, C. *Chem. Eng. J.* **2013**, 220, 98.
10. Zong, E.; Wei, D.; Wan, H.; Zheng, S.; Xu, Z.; Zhu, D. *Chem. Eng. J.* **2013**, 221, 193.
11. Li, Y.; Du, Q.; Wang, J.; Liu, T.; Sun, J.; Wang, Y.; Wang, Z.; Xia, Y.; Xia, L. *J. Fluorine. Chem.* **2013**, 148, 67.
12. Chen, Y.; Zhang, Q.; Chen, L.; Bai, H.; Li, L. *J. Mater. Chem. A* **2013**, 1, 13101.
13. Bai, M.; Wang, J.; Wu, W.; Zeng, X.; Chen, J. *Mater. Lett*. **2014**, 116, 178.
14. Sankar, M. U.; Aigal, S.; Maliyekkal, S. M.; Chaudhary, A.; Anshup, Kumar, A. A.; Chaudhari, K.; Pradeep, T. *Proc. Natl. Acad. Sci. U.S.A.* **2013**, 110, 8459.
15. Chen, Y.; Chen, L.; Bai, H.; Li, L. *J. Mater. Chem. A* **2013**, 1, 1992.
16. Marcano, D. C.; Kosynkin, D. V.; Berlin, J. M.; Sinitskii, A.; Sun, Z.; Slesarev, A.; Alemany, L. B.; Lu, W.; Tour, J. M. *ACS Nano* **2010**, 4, 4806.
17. Pham, V. H.; Cuong, T. V.; Hur, S. H.; Shin, E. W.; Kim, J. S.; Chung, J. S.; Kim, E. J. *Carbon* **2010**, 48, 1945.
18. Sun, X.; Liu, Z.; Welsher, K.; Robinson, J.; Goodwin, A.; Zaric, S.; Dai, H. *Nano Res.* **2008**, 1, 203.
19. Eigler, S.; Grimm, S.; Enzelberger-Heim, M.; Muller, P.; Hirsch, A. *Chem. Commun.* **2013**, 49, 7391.
20. Kumar, A. S. K.; Rajesh, N. *RSC. Adv.* **2013**, 3, 2697.
21. Li, X.; Zhang, G.; Bai, X.; Sun, X.; Wang, X.; Wang, E.; Dai, H. *Nat. Nanotechnol.* **2008**, 3, 538.
22. Lin, Y.; Xu, S.; Li, J. *Chem. Eng. J.* **2013**, 225, 679.
23. Yeh, T. F.; Syu, J. M.; Cheng, C.; Chang, T. H.; Teng, H. *Adv. Funct. Mater.* **2010**, 20, 2255.
24. Xu, Y.; Bai, H.; Lu, G.; Li, C.; Shi, G. *J. Am. Chem. Soc.* **2008**, 130, 5856.
25. Rattana, Chaiyakun, S.; Witit-anun, N.; Nuntawong, N.; Chindaudom, P.; Oaew, S.; Kedkeaw, C.; Limsuwan, P. *Procedia Eng.* **2012**, 32, 759.
26. Kiss, A. B.; Keresztury, G.; Farkas, L. *Spectrochim Acta A-M.* **1980**, *36*, 653.
27. Feng, Y.; Lu, W.; Zhang, L.; Bao, X.; Yue, B.; lv, Y.; Shang, X. *Cryst. Growth Des.* **2008**, 8, 1426.

28. Barathi, M.; Santhana Krishna Kumar, A.; Rajesh, N. *J. Environ. Chem. Eng.* **2013**, 1, 1325.
29. Ferrari, A. C.; Meyer, J. C.; Scardaci, V.; Casiraghi, C.; Lazzeri, M.; Mauri, F.; Piscanec, S.; Jiang, D.; Novoselov, K. S.; Roth, S.; Geim, A. K. *Phy. Rev. Lett.* **2006**, 97, 187401.
30. Calizo, I.; Balandin, A. A.; Bao, W.; Miao, F.; Lau, C. N. *Nano Lett.* **2007**, 7, 2645.
31. Sun, G.; Li, X.; Qu, Y.; Wang, X.; Yan, H.; Zhang, Y. *Mater. Lett.* **2008**, 62, 703.
32. Ferrari, A. C. *Solid State Commun.* **2007**, 143, 47.
33. Tuinstra, F.; Koenig, J. L. *J. Chem. Phys.* **1970**, 53, 1126.
34. Pimenta, M. A.; Dresselhaus, G.; Dresselhaus, M. S.; Cancado, L. G.; Jorio, A.; Saito, R. *Phys. Chem. Chem. Phys.* **2007**, 9, 1276.
35. Zhu, C.; Guo, S.; Fang, Y.; Dong, S. *ACS Nano*, **2010**, 4, 2429.
36. Martínez-Orozco, R. D.; Rosu, H. C.; Lee, S.W.; Rodríguez-González, V. *J. Hazard. Mater.* **2013**, 263, 52.
37. Li, Z. Q.; Lu, C. J.; Xia, Z. P.; Zhou, Y.; Luo, Z. *Carbon*, **2007**, 45, 1686.
38. Sun, H.; Liu, S.; Zhou, G.; Ang, H. M.; Tadé, M. O.; Wang, S. *ACS Appl. Mater. Interfaces* **2012**, 4, 5466.
39. You, S.; Luzan, S.; Yu, J.; Sundqvist, B.; Talyzin, A. V. *J. Phys. Chem. Lett.* **2012**, 3, 812.
40. Parthasarathy, G.; Sreedhar, B.; Chetty, T. R. K. *Curr. Sci.* **2006**, 90, 995.
41. Yang, D.; Velamakanni, A.; Bozoklu, G.; Park, S.; Stoller, M.; Piner, R. D.; Stankovich, S.; Jung, I.; Field, D. A.; Ventrice Jr, C. A.; Ruoff, R. S. *Carbon* **2009**, 47, 145.
42. Filik, J.; May, P. W.; Pearce, S. R. J.; Wild, R. K.; Hallam, K. R. *Diam. Relat. Mater.* **2003**, 12, 974.
43. Venugopal, G.; Krishnamoorthy, K.; Mohan, R.; Kim, S.-J. *Mater. Chem. Phys.* **2012**, 132, 29.
44. Wan, W.; Zhao, Z.; Hu, H.; Gogotsi, Y.; Qiu, J. *Mater. Res. Bull.* **2013**, 48, 4797.
45. Kuznetsov, M. V.; Zhuravlev, J. F.; Gubanov, V. A. *J. Electron. Spectrosc. Relat. Phenom.* **1992**, 58, 169.
46. Kloprogge, J. T.; Duong, L. V.; Wood, B. J.; Frost, R. L. *J. Colloid Interface. Sci.* **2006**, 296, 572.
47. Balchev, I.; Minkovski, N.; Marinova, T.; Shipochka, M.; Sabotinov, N. *Mater. Sci. Eng. B* **2006**, 135, 108.
48. Thomas, S.; Sherwood, P. M. A. *Anal. Chem.* **1992**, 64, 2488.
49. Wu, X.; Zhang, Y.; Dou, X.; Zhao, B.; Yang, M. *Chem. Eng. J.* **2013**, 223, 364.
50. Dorenfeld, A.C. Process for purifying Graphite, **1957**, Patent No. US2787528 A
    a. http://www.google.com/patents/US2787528
51. Shufan, N. I. N. G.; Hongyan, L. I.;. Wei, C. H. E. N.; Bin, L. I. U.; Shoutian, C. H. E. N. *Rare Metals* **2005**, 24, 240.
52. Pearson, R. G. *J. Am. Chem. Soc.***1963**, 85, 3533.
53. Ofomaja, A. E.; Ho, Y.-S. *Bioresource Technol.* **2008**, 99, 5411.
54. I. Langmuir, *J. Am. Chem. Soc.* **1918**, 40, 1361.
55. Freundlich, H. M. F. *Z. Phys. Chem.* **1906**, 57, 385.

56. Dubinin, M. M. *Chem. Rev.* **1960**, 60, 235.
57. Temkin, M. I. *Zh. Fiz. Chim*. **1941,** *15*, 296
58. Redlich, O.; Peterson, D. L.; *J. Phys. Chem.* **1959**, 63, 1024.
59. Lagergren, S. *K. Sven.Vetenskapsakad. Handl.* 1898, **24**, 1.
60. Nie, Y.; Hu, C.; Kong, C. *J. Hazard. Mater.* **2012**, 233–234, 194.
61. Weber, W. J.; Morris, J. C. *J. Sanit. Eng. Div. Am. Soc. Civ. Eng.***1963**, 89, 3.

CHAPTER 6

6. Summary and Conclusion

6.1. Summary and Conclusion

The removal of excess fluoride from water requires the development of novel methods. In order to accomplish this, cellulose, polymeric resins and graphene oxide based adsorbents were tested for defluoridation. Adsorbents were prepared using microwave and ultrasonication methods.

The first method presented in the thesis deals with a novel microwave assisted preparation of Al-Zr impregnated cellulose biopolymer adsorbent and its application for defluoridation. The adsorbent prior and subsequent to the adsorption of fluoride was characterized comprehensively using Fourier transform infrared spectroscopy (FT-IR), Energy dispersive X-ray spectrometry (EDX) and X-ray diffraction (XRD) studies. The adsorption of fluoride is favored by the interaction of cationic aluminium and zirconium hydroxides through electrostatic, hydrogen bonding and complexation mechanism. The novel Al-Zr impregnated cellulose adsorbent exhibits an adsorption capacity of 5.76 mg g^{-1} and the experimental data showed a good fit to the Freundlich and Langmuir isotherm models. The spontaneity of adsorption and second order kinetic model describes the adsorption process. The adsorbent exhibits excellent adsorption up to 5 mg L^{-1} fluoride and shows good potential towards practical application.

The second method illustrates the utility of an ultrasound assisted methodology approach in the impregnation of zirconium in a cellulose matrix and application for fluoride removal in aqueous solutions. The ultrasound assisted preparation of zirconium impregnated cellulose adsorbent has shown good potential for the adsorption of fluoride. The conventional method of adsorbent preparation takes 8 hours as compared to the quick ultrasonication. Fluoride from aqueous solution interacts with the cellulose hydroxyl groups and the cationic zirconium hydroxide. The effectiveness of this process was confirmed by comprehensive characterization of zirconium impregnated cellulose (ZrIC) adsorbent using Fourier transform infrared spectroscopy (FT-IR), Energy dispersive X-ray spectrometry (EDX) and X-ray diffraction (XRD) studies. The novel Zr impregnated cellulose adsorbent exhibits an adsorption capacity of 4.95 mg g^{-1} with the

experimental data showing a good fit to Langmuir isotherm model. The second order kinetics describes the adsorption process very well. The study of thermodynamics indicates a spontaneous, exothermic adsorption process and a decreased randomness at the adsorbent-solution interface.

The potential application of aluminum hydroxide impregnated macroporous polymeric resin was explored as a sustainable option for defluoridation of water. Various characterization techniques supported the adsorption of fluoride through electrostatic, ion exchange and hydrogen bonding mechanism. The zero point charge of prepared adsorbent was found to be 5.01. The second order kinetics and the exothermic, spontaneous adsorption are other characteristic features associated with this method. The q_{max} obtained from the nonlinear Langmuir model was found to be 92.39 mg g^{-1} and 36.61 mg g^{-1} at pH 3.0 and 7.0 respectively. However, it was found to be 32.92 mg g^{-1} for drinking water and a sample volume of 1500 mL on a laboratory scale column containing 5.0 mg L^{-1} of fluoride could be brought down to less than 1.0 mg L^{-1}. This is attainable at the natural pH range prevalent in water and hence the method could pave way to develop a prototype and extend it to remediate fluoride in field applications. The adsorbent could be regenerated with sodium hydroxide.

The novel aluminium oxy hydroxide [Al-O (OH)] modified graphene oxide by chemical precipitation method shows effective application for fluoride removal in real water samples. XPS analysis reveals that a distinct Al 2p transition was observed at 74.7eV, characteristic of Al-O (OH) or pseudoboehmite. The zero-point charge of GO-Al-O (OH) adsorbent was found to be 7.54. Ligand exchange and physical adsorption are mostly favored for the adsorption of fluoride and this was corroborated from the XPS studies. The thermodynamically feasible adsorption is supported by the pseudo second order kinetics and a high Langmuir maximum adsorption capacity (51.42 mg/g) for GO-Al-O (OH) adsorbent. Furthermore, it is possible to treat 2.0 L of 5.0 mg L^{-1} fluoride ion solution to bring the level within the permissible limits and the regeneration of the adsorbent was done using ammonium hydroxide.

Grapheneoxide-aluminium oxyhydroxide adsorbent has high adsorption capacity as compared to other modified adsorbents in the wide range of pH. The leaching of aluminium in the residual water is negligible and the prepared GO-Al-O(OH) adsorbent has good potential for defluoridation in real field water samples. The prototype model was developed and demonstrated successfully for the defluoridation of 50.0 L of water containing 5.0 mg L^{-1} F^- using 50.0 g of the adsorbent. The summary of methods are given in Table 6.1.

Table 6.1. Summary of methods

Adsorbent	**Suitable pH**	**Q_{max} (mg g^{-1})**	**Isotherm**	**Kinetics**
Al-Zr-cellulose	4.5-5.5	5.76	Freundlich	Pseudo second order
Zr-Cellulose	4.5-5.5	4.95	Langmuir	Pseudo second order
$Al(OH)_3$-Resin	3.0-7.0	36.37	Freundlich and Langmuir	Pseudo second order
GO-Al-O-(OH)	6.5-8.0	51.42	Langmuir	Pseudo second order

6.2. Scope for Future Work

The results obtained in this study offered many new and interesting possibilities for future research. Some of them are listed below-

1. Metal ions (Al, Zr and La) loaded onto biopolymers using microwave and ultrasound assisted preparation would open up the scope for the better selectivity and enhancement in adsorption of fluoride.
2. Metal ions (Al, Zr and La) loaded onto Graphene oxide-biopolymer (cellulose, chitosan) composite opens up further exciting possibilities for defluoridation towards field application in real water samples.

LIST OF PUBLICATIONS

Publications relevant to thesis work

1. ***M. Barathi,*** A. Santhana Krishna Kumar, N. Rajesh**,** Aluminium hydroxide impregnated macroreticular aromatic polymeric resin as a sustainable option for defluoridation**, *J. Environ. Chem. Eng. 3 (2015) 630-641.***
2. ***M. Barathi,*** A. Santhana Krishna Kumar, Chinta Uday Kumar, N. Rajesh, Graphene oxide-aluminium oxy hydroxide interaction and its application for the effective adsorption of fluoride, ***RSC advances 4 (2014) 53711-53721.***
3. ***M. Barathi,*** A. Santhana Krishna Kumar, N. Rajesh, A novel ultrasonication method in the preparation of zirconium impregnated cellulose for effective fluoride adsorption, ***Ultrason. Sonochem. 21 (2014) 1090-1099.***
4. ***M. Barathi,*** A. Santhana Krishna Kumar, N. Rajesh, Efficacy of novel Al–Zr impregnated cellulose adsorbent prepared using microwave irradiation for the facile defluoridation of water, ***J. Environ. Chem. Eng. 1 (2013) 1325-1335.***

Contributions related to adsorption

1. Shivani Sharma, ***M. Barathi,*** N. Rajesh, Efficacy of a heterocyclic ligand anchored biopolymer adsorbent for the sequestration of palladium**, *Chem. Eng. J. 259 (2015) 457-466.***
2. *A.* Santhana Krishna Kumar, Shivani Sharma, R. Sudheer Reddy, ***M. Barathi,*** N. Rajesh, Comprehending the interaction between chitosan and ionic liquid for the adsorption of palladium, ***Int. J. Biol. Macromol. 72 (2015) 633-639.***
3. A. Santhana Krishna Kumar, ***M. Barathi,*** Swetha Puvvada, N. Rajesh, Microwave assisted preparation of glycidyl methacrylate grafted cellulose adsorbent for the effective adsorption of mercury from a coal fly ash sample, ***J. Environ. Chem. Eng. 1 (2013) 1359-1367.***

Abstract presented in Conferences

1. ***M. Barathi,*** A. Santhana Krishna Kumar, N. Rajesh, Zirconium impregnated cellulose biopolymer for the effective defluoridation of drinking water, **15th CRSI-National Symposium in Chemistry,** Banaras Hindu University, Varnasi, held on Feb 1-3, 2013.
2. ***M. Barathi,*** A. Santhana Krishna Kumar, N. Rajesh, A macroporous polymeric adsorbent impregnated with Al^{3+} for effective fluoride adsorption, **International conference on Green chemistry: Catalysis, Energy and Environment (ICGC-2015),** Goa University, Goa held on January 22-24, 2015.

BIOGRAPHY OF Prof. N. RAJESH

Prof. N. Rajesh Department of Chemistry, Birla Institute of Technology and Science, Pilani, Hyderabad Campus, India obtained his Master's degree and Ph. D from Indian Institute of Technology (IIT), Madras, India. He is involved in teaching and research for the past 20 years. He is a fellow member of the Royal Society of Chemistry (FRSC) London. His research interests include development of greener sorbents for the effective detoxification of heavy metals and dyes from industrial effluents. He has several research publications in peer reviewed journals and is also an expert reviewer for various international journals. He has been recognized by Elsevier as an outstanding reviewer for 2015 for his reviewing contributions to the Journal of Environmental Chemical Engineering. Currently, his group is engaged in the development of novel biopolymer, graphene and clay based sorbents for heavy metal remediation. He has collaborative interaction with the department of chemistry, University of South Dakota, USA. He is a member of American Chemical Society (ACS) and a life member of Chemical research society of India (CRSI) and Indian Science Congress (ISC). He has several ongoing funded projects and also successfully completed projects sponsored by UGC and DST, India.

BIOGRAPHY OF Mr. M. BARATHI

Mr. M. Barathi obtained his Master's degree in Chemistry from Saraswathy Narayanan College, Madurai, India, in 2009 and started his work as junior research fellow in the Department of Chemistry at BITS Pilani, Hyderabad campus, India. He is well versed in various analytical separation methods and has good number of publications to his credit and presented his work in national and international conferences. Currently, his research interests focus on the development of suitably customized polymeric composites by modifying with metal ions for defluoridation of water at community level.